Institut für Erd- und Umweltwissenschaften
Mathematisch-Naturwissenschaftliche Fakultät
Universität Potsdam

Closure of the Neotethys Ocean in Anatolia: structural, petrologic & geochronologic insights from low-grade high-pressure metasediments, Afyon Zone

Amaury Pourteau

Kumulative Dissertation
zur Erlangung des akademischen Grades
Doktor der Naturwissenschaften (Dr. rer. nat.)

eingereicht an der Mathematisch-Naturwissenschaftliche Fakultät
Universität Potsdam

Potsdam, Oktober 2011

Published online at the
Institutional Repository of the University of Potsdam:
URL http://opus.kobv.de/ubp/volltexte/2012/5780/
URN urn:nbn:de:kobv:517-opus-57803
http://nbn-resolving.de/urn:nbn:de:kobv:517-opus-57803

Abstract

In the last past years, subduction-related metamorphism has been documented in three tectono-sedimentary units of Western Anatolia (namely the Afyon Zone, the Lycian Nappes and the Menderes Massif), which were previously supposed to have undergone only greenschist-facies metamorphism, related to obduction and collision. These discoveries of high-pressure relicts reopened the discussion on the number and position of Neotethyan oceanic branches that once existed before the assembly of the present-day Anatolian microcontinent, as well as the validity of the regional tectonic nomenclature. In the Afyon Zone, representing a complete stratigraphic sequence of a Mesozoic continental passive margin and its pre-Mesozoic substratum, Alpine high-pressure metamorphism was previously evidenced locally, whereas it is continuous from Northwestern to southern Central Anatolia, over more than 700km.

In the present study, low-grade high-pressure mineral assemblages (Fe-Mg-carpholite and glaucophane) are reported from the Afyon Zone, which is re-interpreted as a continuous blueschist-facies metamorphic belt. Well-preserved carpholite-chloritoid assemblages are useful to improve our understanding of prograde phase relations and transitions in the FeO-MgO-Al_2O_3-SiO_2-H_2O system and reconstruct the metamorphic evolution of subduction of continental units. Inspection of petrographic textures, minute variations in mineral composition and Mg-Fe distribution among carpholite-chloritoid assemblages documents multistage mineral growth, accompanied by a progressive enrichment in Mg, and strong element partitioning. Using an updated thermodynamic database, including the first data for ferro-carpholite, I modelled the pressure and temperature conditions that are consistent with textural and chemical observations. Carpholite-bearing assemblages in the Afyon Zone account for a temperature increase from 280 to 380°C between 0.9 and 1.1 GPa.

^{40}Ar-^{39}Ar geochronology on white mica and multi-equilibrium thermobarometric calculations based on chlorite-mica and chlorite-chloritoid parageneses are combined in order to provide the first accurate metamorphic ages for the Afyon Zone, the Lycian Nappes and the Menderes Massif. This reveals that a) in the Afyon Zone and the Lycian Nappes early medium-pressure retrograde assemblages formed about 65-60 Ma ago, and in the southern Menderes cover b) high-pressure metamorphism occurred about 45 Ma ago and c) post-Barrovian mica cooling about 26 Ma ago. The Afyon Zone and the metamorphosed Lycian Nappe belong to a continuous Maastrichtian high-pressure belt, and the southern Menderes cover represents the eastern ending of the Eocene high-pressure belt exposed in the Aegean.

The shape of the Anatolian high-pressure metamorphic belts was reconstructed by restoring post-accretionary tectonics (mainly extensional and strike-slip deformation from the Oligocene onwards). This reconstruction, based on existing structural and palaeomagnetic data, indicates that Western Anatolia was shaped mainly during post-collisional tectonics, while the bending of the accretionary zone in Central Anatolian was acquired during Eocene continental accretion.

I use structural, petrologic and geochronologic constraints provided in this study and by previously published data to refine regional tectonic nomenclature and reconstruct the progressive assembly of Western and Central Anatolia since the Late Cretaceous. I demonstrate that in Western Anatolia at least two branches of the Neotethys were successively sutured in the Palaeocene and the Oligocene, while in southern Central Anatolia continental amalgamation ended by the Eocene.

This regional-scale study illustrates that the petrology of metasediments along established, or even supposed, former continental margins can be used to reconstruct the palaeotectonic evolution of long-lived accretionary zones such as the Eastern Mediterranean realm.

Zusammenfassung

In den letzten Jahren konnten in drei tektonisch-sedimentären Einheiten West-Anatoliens (Afyon Zone, Lykische Decken und Menderes Massif) Beweise für subduktionsbezogene Metamorphosen gefunden werden. Ursprünglich vermutete man, dass diese Einheiten durch Obduktion und Kollision lediglich grünschieferfaziell überprägt seien. Deshalb eröffneten die jüngsten Entdeckungen von Hochdruck Relikten neuen Raum für Diskussionen, nicht nur über Anzahl und Position der neotethyschen Meeresarme vor der Bildung des heutigen anatolischen Mikrokontinents, sondern auch über die Gültigkeit der regionalen tektonischen Nomenklatur. In der Afyon Zone, die eine vollständige stratigraphische Sequenz des mesozoischen passiven Kontinentalhanges sowie prä-mesozoischen Substrats repräsentiert, konnten beispielsweise alpine Hochdruck-Metamorphosen bis dahin nur lokal nachgewiesen werden. Dabei erstreckt sich die gesamte Einheit kontinuierlich über 700 km vom nordwestlichen zum südlichen Teil Zentral-Anatoliens.

Die vorliegende Studie berichtet von niedrig-gradigen Hochdruck Mineralvergesellschaftungen (Fe-Mg-Karpholit und Glaukophan) in der Afyon Zone, die deshalb als zusammenhängender blauschieferfazieller Gürtel neu interpretiert werden kann. Dabei dienen gut erhaltene Karpholit-Chloritoid Vergesellschaftungen der Verbesserung unseres Verständnisses prograder Phasenbeziehungen und -übergänge im FeO-MgO-Al_2O_3-SiO_2-H_2O-System und sind außerdem ein hilfreiches Werkzeug für die Rekonstruktion der metamorphen Entwicklung subduzierter kontinentaler Einheiten. Untersuchungen petrographischer Strukturen, minimale Variationen der Mineralzusammensetzungen und Mg-Fe Verteilung zwischen Karpholith-Chloritoid Vergesellschaftungen beweisen ein mehrstufiges Mineralwachstum, begleitet von progressiver Anreicherung in Mg und starker Elementpartitionierung. Die Anwendung einer aktualisierten thermodynamischen Datenbank (inklusive erster Daten für Fe-Karpholith) erlaubt es, Druck und Temperatur Bedingungen zu modellieren, die maßgeblich für texturelle und chemische Beobachtungen sind. Mineralvergesellschaftungen mit Karpholith in der Afyon Zone zeigen einen Temperaturanstieg von 280 bis 380 °C zwischen 0.9 und 1.1 GPa.

Die Kombination von ^{40}Ar-^{39}Ar Geochronologie an Hellglimmern und thermobarometrische Gleichgewichtsberechnungen von Chlorit-Glimmer und Chlorit-Chloritoid Paragenensen liefern erste genaue Metamorphosealter für die Afyon Zone, die Lykischen Decken und das Menderes Massif. Dies beweist, dass in der Afyon Zone und den Lykischen Decken frühe retrograde Mitteldruck Vergesellschaftungen sich vor ungefähr 65-60 Ma bildeten und in der Bedeckung des südlichen Menderes Massifs Hochdruck Metamorphosen vor 45 Ma ereigneten, mit anschließender post-grünschieferfaziellen Abkühlung der Glimmer vor ungefähr 26 Ma. Die Afyon und die metamorphisierten Lykischen Decken gehören daher zu einem zusammenhängenden maastrichtischen Hochdruck Gürtel, während das Menderes Massif das östliche Ende des Eozänen Hochdruck Gürtels in der Ägäis repräsentiert.

Das Streichen des anatolischen Hochdruck Gürtels konnte durch die Rekonstruktion post-akkretionärer tektonischer Ereignisse (hauptsächlich entlang von Deformationsstrukturen mit Extensions- und Seitenverschiebungscharakter) wieder hergestellt werden. Diese Rekonstruktion basiert auf existierenden strukturellen und paläomagnetischen Daten und zeigt, dass sich das westliche Anatolien zum großen Teil nach der Kollisions-Tektonik formierte, während sich die Umbiegung der Akkretionszone in Zentral-Anatolien durch die kontinentale Akkretion im Eozän herausbildete.

Strukturelle, petrologische und geochronologische Limitierungen dieser Studie und bereits früher publizierte Daten der Literatur erlauben eine detailliertere regionale tektonische Nomenklatur und Rekonstruktion des progressiven Zusammenschlusses von West und Zentral-Anatolien seit der späten Kreide. Es wird gezeigt, dass in West-Anatolien mindestens zwei Meeresarme der Neotethys sukzessive im Paläozän und Oligozän geschlossen wurden, während die kontinentale Verschweißung im südlichen Anatolien erst im Eozän abgeschlossen war.

Diese regionale Studie zeigt, dass es durch die petrologische Untersuchung von Metasedimenten entlang etablierter oder sogar vermuteter früherer Kontinentalränder möglich ist, die paläotektonische Entwicklung langlebiger Akkretionszonen im östlichen Mittelmeerraum zu bestimmen.

Contents

List of figures

List of tables

Acknowledgements

First of all, I would like to thank my supervisor Roland Oberhänsli for enrolling me in this scientific journey, supporting my research and encouraging me to follow my interests, although he had been the initial architect of this DFG-funded research project. During the last four years, I reaped considerable benefits of Roli's multidisciplinary erudition, every-day energy and innumerable anecdotes. I am also deeply grateful to him for letting me time to write my own research proposal for further investigations in Anatolia at the same time as my PhD thesis, and for offering me to stay in Potsdam University for some years more.

I am particularly indebted to Osman Candan for sharing his extensive knowledge of Anatolian geology and for his kindness and generosity in the field, as well as during our visits in Izmir. Thanks go also to his assistants at Izmir University, Cüney Akal and Mete Çetinkaplan, for keeping me aware about the advances of their investigations. I would like to thank Romain Bousquet for his broad-mindedness, consistent support (albeit lastly discontinuous!) and friendship, which greatly helped me throughout my PhD study. My work benefited from the keenness and expertise of Olivier Vidal and Pierre Lanari, who helped me to comprehend the sensitivity of thermodynamic models to the parameters they are based on. Masafumi Sudo is greatly thanked for helping me to perform Ar geochronology in Potsdam and striving to solve chronic lab issues.

The two external reviewers of this dissertation, Aral Okay and Christian Chopin, are deeply thanked for their help and willingness to evaluate and comment my work within a very tight time lapse.

Along these last years, I have been honoured by Stefan Schmid's enthusiasm for Anatolian geology in general, and the results of my work in particular. Thanks to his continuous flow of questions, he encouraged me to justify, often revise and always refine my own concepts. Gwenaëlle Salaün is warmly thanked for sharing and discussing her tomographic results and for explaining me how she did it better than the others! Thanks go also to Côme Lefebvre for sharing his work in Central Anatolia and to Mélody Philippon for frequent discussions on the Aegean and Anatolian geology and her supply of Aegean literature. I am also particularly indebted to Erik Düsterhöft, who in the last past months has always been willing to help and advise me.

In various stages of my thesis, I strongly appreciated constructive discussions with Douwe van Hinsbergen, Kamil Ustaszewski, Donna Whitney, Alastair Robertson, Laurent Beccaletto, Pierre Gautier, Erdin Bozkurt, Jean-Luc Régnier, Osman Parlak, Erkan Toraman, Thomas Zack and Cemal Göncüoğlu among others.

I am grateful to the technical staff, as well as my officemates, colleagues and friends from the Institute für Erd- und Umweltwissenschaften at Potsdam University for help of any kind. Among them, I thank Henry Wichura for translating the abstract of this thesis into German and Ed Sobel for English corrections. Dieter Rhede and Oona Appelt are also acknowledged for their assistance on the GFZ electron microprobe.

Finally, I am profoundly grateful to my wife Aurélie and my daughter Soledad for supporting me every single day with love and patience. I also thank all my family and friends for their continuous confidence in my choices.

Chapter 1

Introduction

Context and challenges

The blueschist metamorphic facies was defined by the occurrence of index minerals like glaucophane, lawsonite or jadeite in metabasalts (e.g., Eskola, 1921; Miyashiro and Banno, 1958; Evans, 1990). In contrast, metasediments intercalated with blueschist-facies metabasites commonly encompass the low-variance assemblage chlorite-mica-chloritoid-quartz, which is also stable under greenschist-facies conditions. Metapelites were therefore long thought to lack any diagnostic mineral for low-grade high-pressure metamorphism (Miyashiro, 1973; Winkler, 1974; Turner, 1981). From the 1970s onwards, an increasing number of petrologists demonstrated that Fe-Mg-carpholite, $(Fe,Mg)Al_2Si_2O_6(OH)_4$), is an index mineral for blueschist-facies metamorphism in the FeO-MgO-Al_2O_3-SiO_2-H_2O system (typically metapelites and metabauxites; e.g., Goffé et al., 1973; de Roever, 1977; Goffé, 1982; Chopin and Schreyer, 1983; Vidal et al., 1992; Agard et al., 2001; Verlaguet et al., 2011).

In passive margin sequences, mafic volcanic rocks often occur scarcely, if at all, while siliciclastic sediments are generally abundant and well exposed over large areas. Low-grade high-pressure metasediments therefore are more appropriate to help to reconstruct continental accretion scenarios at a regional scale (see Bousquet et al., 2008). Because Fe-Mg-carpholite appearance is restricted to certain bulk rock compositions (metasediments rich in Al, poor in Ca and Na), it might occur only in specific stratigraphic levels. Therefore, deciphering the exact metamorphic history of low-grade metasediments requires thorough field exploration. However, the exact phase relations and Mg-Fe partitioning in carpholite-bearing assemblages remain a key challenge to address in order to retrieve accurate pressure and temperature conditions experienced by low-grade high-pressure metasediments.

Because thermodynamic data for ferro-carpholite are lacking, several studies were devoted to estimating metamorphic conditions recorded by low-variance assemblages of metasediments by calibrating the dependency of chlorite and white mica compositions on pressure and temperature (e.g., Cathelineau and Nieva, 1986; Hillier and Velde, 1991; Massonne and Szpurka, 1997; Leoni et al., 1998; Vidal et al., 2001; Dubacq et al., 2010). In the last decade, multi-equilibrium thermobarometry has been developed and refined for assemblages with few phases such as quartz-chlorite-mica, allowing the reconstruction of accurate pressure-temperature metamorphic paths (Vidal and Parra, 2000; Parra et al., 2002; De Andrade et al., 2006; Malasoma and Marroni, 2007; Yamato et al., 2007). These advances suggest new perspectives to combine ^{40}Ar-^{39}Ar geochronology and multi-equilibrium thermobarometry on mica-bearing assemblages in order to place metamorphic paths of metasediments into a time frame.

Metasediments therefore promise to be useful for unravelling the evolution of complex accretionary regions, such as Western and Central Anatolia in the Eastern Mediterranean, where crucial issues such as the exact number and position of Neotethyan oceanic branches that once existed in the region remain highly debated (Ricou et al., 1986; Okay and Tüysüz, 1999; Ring et al., 1999; Dercourt et al., 2000; Jolivet et al., 2004; Şengün, 2006; Stampfli and Kozur, 2006; Göncüoğlu et al., 2007; Moix et al., 2008). In the literature, it seems to be commonly accepted that the Anatolian microplate was finally assembled between the latest Cretaceous and the early Cenozoic after the accretion of the southern composition margin of Eurasia and a continental fragment that had drifted apart from the northern margin of Gondwana (e.g., Şengör and Yılmaz, 1981; Okay et al., 2001; Candan et al., 2005). Over the last decades, this accretionary history has been addressed by numerous metamorphic petrology works that mostly focused only on a few units: the late Cretaceous lawsonite blueschists and eclogites of the Tavşanlı Zone (e.g., Çoğulu**,** 1967; Okay, 1980a; Gautier, 1984; Okay et al., 1998; Sherlock et al., 1999; Okay, 2002; Davis and Whitney, 2006; Çetinkaplan et al., 2008; Seaton et al., 2009), the Oligocene Barrovian history of the Menderes Massif (Dürr, 1975; Akkök, 1983; Şengör et al., 1984a; Ashworth and Evirgen, 1985; Satır and Friedrichsen, 1986; Hetzel et al., 1998; Bozkurt and Satır, 2000; Whitney and Bozkurt, 2002; Régnier et al., 2003) and the late Cretaceous metamorphic soles of the wide-scattered remnants of obducted Neotethyan ophiolites (e.g., Thuizat et al., 1981; Önen and Hall, 1993; Parlak et al., 1996; Robertson et al., 1996; Dilek and Whitney, 1997; Yalınız et al., 2000; Çelik et al., 2006). In the last past years, widespread occurrences of rock-forming Fe-Mg-carpholite were reported from three tectono-sedimentary units from Western Anatolia (Oberhänsli et al., 2001; Rimmelé et al., 2003a, 2003b, 2006; Candan et al., 2005), which were long considered to have suffered only greenschist-facies metamorphism (Dürr, 1975; Bingöl, 1974; Şengör et al., 1984a; Ashworth and Evirgen, 1984; Göncüoğlu et al., 1992; Okay et al., 1996). These recent findings shattered previous conceptions on the tectono-metamorphic evolution of the units in particular, and of the entire region in general, and shed light on the necessity to revise the regional extent of subduction-related metamorphism by re-inspecting the petrology of poorly-studied metasediments.

The present study focuses on re-evaluating the metamorphic history of a Mesozoic passive margin sedimentary sequence in Western and Central Turkey, which was thought to be restricted to the greenschist-facies, but was recently reconsidered based on the discovery of blueschist-facies (Candan et al., 2005). This tectono-sedimentary unit, named the Afyon Zone, runs continuously along a possible suture zone from Northwestern to Central Anatolia, i.e., over more than 700 km, and constitutes a key region for deciphering the final amalgamation of Western and Central Anatolia. The metamorphic evolution of the unit in particular and of the region in general is addressed from several approaches: i) revising the structural distribution of index metamorphic minerals, ii) evaluating the pressure-temperature conditions accounting for the observed mineral assemblages, iii) determining the timing of metamorphism, iv) restoring the post-accretionary deformation, and v) reconstructing regional geodynamics.

Organisation of the thesis

The results of the present thesis are distributed into three distinct manuscripts that have been submitted for publication in peer-reviewed journals.

In Chapter 2, I re-evaluate the metamorphic evolution of the entire Afyon Zone all along from North-western to Central Anatolia. The shape of the Anatolian metamorphic belts was restored from late- to post-collisional deformation from the Oligocene onwards. My findings have immediate impact on the palaeotectonic evolution of Central Anatolia related to the closure of the Neotethyan oceanic domain and the amalgamation of Gondwana-derived continental fragments.

Chapter 3 is devoted to petrologic investigations. Well-preserved carpholite and carpholite-chloritoid assemblages from the Afyon Zone are thoroughly inspected in order to retrieve exact paragenetic successions. Emphasis is on Fe and Mg distribution between coexisting carpholite and chloritoid, and the use of Mg-Fe partitioning coefficients to evaluate thermodynamic equilibrium. Using an updated thermodynamic database, with new thermodynamic data for ferro-carpholite, I evaluate pressure-temperature variations accounting for petrographic and chemical observations.

In Chapter 4, I employ ^{40}Ar-^{39}Ar geochronology on white mica and multi-equilibrium thermobarometry in order to place the metamorphic evolution of the Afyon Zone and adjacents units lacking accurate time constraints into a pressure-temperature-time frame. Providing the first isotopic ages for the metamorphism of these passive margin sequences strongly helps to better understand regional geology and leads me to propose a comprehensive geodynamic reconstruction for the late Cretaceous to Neogene times.

Chapters 2 to 4 have been submitted for publications in international peer-reviewed journals. Chapter 2, entitled "*High-pressure metasediments in central Turkey: Constraints on the Neotethyan closure history*", was published by Amaury Pourteau, Osman Candan and Roland Oberhänsli in Tectonics, 29, TC5004, doi:10.1029/2009TC002650. It is cited below as Pourteau et al. (2010). Chapter 3, entitled "*Multistage growth of Fe-Mg-carpholite and chloritoid, from field evidence to thermodynamic modelling*", was submitted in October 2011 by Amaury Pourteau, Romain Bousquet, Olivier Vidal, Roland Oberhänsli and Osman Candan to the Journal of Petrology. It is cited below as Pourteau et al. (2011a). Chapter 4, entitled "*Final amalgamation of the Anatolian microcontinent: Insight from ^{40}Ar-^{39}Ar geochronology and* P-T *estimation in high-pressure metasediments from Western and Central Anatolia*" was submitted in September 2011 by Amaury Pourteau, Masafumi Sudo, Osman Candan, Pierre Lanari, Olivier Vidal and Roland Oberhänsli to the Journal of Metamorphic Geology. It is cited below as Pourteau et al. (2011b).

Chapter 2

High-pressure metasediments in central Turkey: Constraints on the Neotethyan closure history

Abstract

The distribution of oceanic domains and continental blocks in Central Anatolia remains a challenge in understanding the Alpine geodynamic evolution of the Tethys realm. The consumption of a Neotethys oceanic branch at the Mesozoic-Cenozoic boundary welded the Central Anatolian Crystalline Complex in Central Turkey, and the Anatolide-Tauride Block in Western Turkey, with the northerly Eurasian margin. Whether those two regions constituted a single or two distinct continental masses is still matter of debate. High-pressure metamorphism has been locally evidenced in the Afyon Zone, which was however defined as a greenschist-facies metamorphic zone of the Anatolide-Tauride Block. Since the Afyon Zone composes a metamorphic equivalent of a continental margin exposed far south of the Izmir-Ankara suture zone, this encouraged us to reevaluate its metamorphic evolution in order to better understand the relation between Western and Central Turkey. Our investigations reveal that the high-pressure minerals Fe-Mg-carpholite and glaucophane are present in the entire Afyon Zone, which we reconsider as a blueschist-facies zone. We additionally present a tectonic reconstruction, stripping off the post-collisional tectonics. It reveals that today's bending of the high-pressure belt is consistent with an Eocene collision of the Anatolide-Tauride Block around the southern edge of the Central Anatolian Crystalline Complex. We argue that the Central Anatolian Crystalline Complex and the Anatolide-Tauride Block were two distinct continental masses separated by a Neotethyan oceanic stripe, the closure of which engendered subduction-related metamorphism in the latter, and arc volcanism and high-grade metamorphism in the former by late Cretaceous to early Cenozoic.

2.1. Introduction

Throughout Mesozoic to Cenozoic times, the present-day Turkish landmass was built by the accretion of several small-scale continental blocks that were associated with the closure of several Tethyan oceanic basins (e.g., Şengör and Yılmaz, 1981; Okay, 1986; Sengör, 1990; Stampfli and Borel, 2002; Moix et al., 2008; Oberhänsli et al., 2010a). Northern Turkey exposes a polystage fold-thrust belt known as the Pontides. A large part of this region is occupied by the Sakarya Zone, which consists of a Precambrian to Palaeozoic crystalline basement, late Triassic blueschists and eclogites and a non-metamorphosed Jurassic to Eocene sedimentary cover (Tekeli, 1981; Okay and Monié, 1997). Considering the Alpine evolution of the region, the Pontides represented the southern Eurasian margin (Şengör and Yılmaz, 1981). Western and Southern Turkey consist of metamorphosed and non-metamorphosed Precambrian to Eocene rocks, known as the Anatolide-Tauride Block (Okay and Tüysüz, 1999) (also referred to as 'Menderes-Taurus Block' by Şengör (1990); and 'Tauride-Anatolide Composite Terrane' by Göncüoğlu et al. (1997)) (Figure 2.1). The term 'Anatolides' is used to designate the metamorphosed rocks at the northern edge of the Anatolide-Tauride Block, whereas the term 'Taurides' designates the non-metamorphosed thrust and folded sediments, more to the south (Okay, 1984). Central Turkey is largely occupied by the Central Anatolian Crystalline Complex

(Figure 2.1) (Göncüoğlu et al., 1997) made of late Cretaceous intrusions and Barrovian-type metamorphic rocks. Protolithic ages of these high-temperature low- to medium-pressure rocks are inferred as early Palaeozoic to Mesozoic, based on correlation with lithostratigraphic similarities to the Anatolide-Tauride Block (Göncüoğlu et al., 1997).

In Western Turkey, the Pontides and the Anatolide-Tauride Block are separated by an ophiolitic belt, known as the Izmir-Ankara suture zone, thrust southwards onto the Anatolides and Taurides (Şengör and Yılmaz, 1981). The ophiolites from the Izmir-Ankara suture zone are also recognized in dismembered bodies, widespread on top of the Anatolide-Tauride Block (Figure 2.1). Metamorphic sole ages of these ophiolites indicate that northward subduction in the northern Neotethys Ocean was initiated sometime between 95 and 90 Ma (e.g., Thuizat et al., 1981; Parlak and Delaloye, 1999; Önen and Hall, 2000; Çelik et al., 2006). Most of these ophiolites display geochemical signatures typical of a supra-subduction environment (Parlak et al., 1996; Collins and Robertson, 1998; Parlak et al., 2002; Çelik and Delaloye, 2006). This intra-oceanic subduction led then to tectonic burial and metamorphism of the northern part of the Anatolide-Tauride Block in upper Cretaceous to early Cenozoic times. Intrusion of Eocene granodiorites in these ophiolites as well as in the underlying blueschists postdates the ophiolite emplacement (Harris et al., 1994).

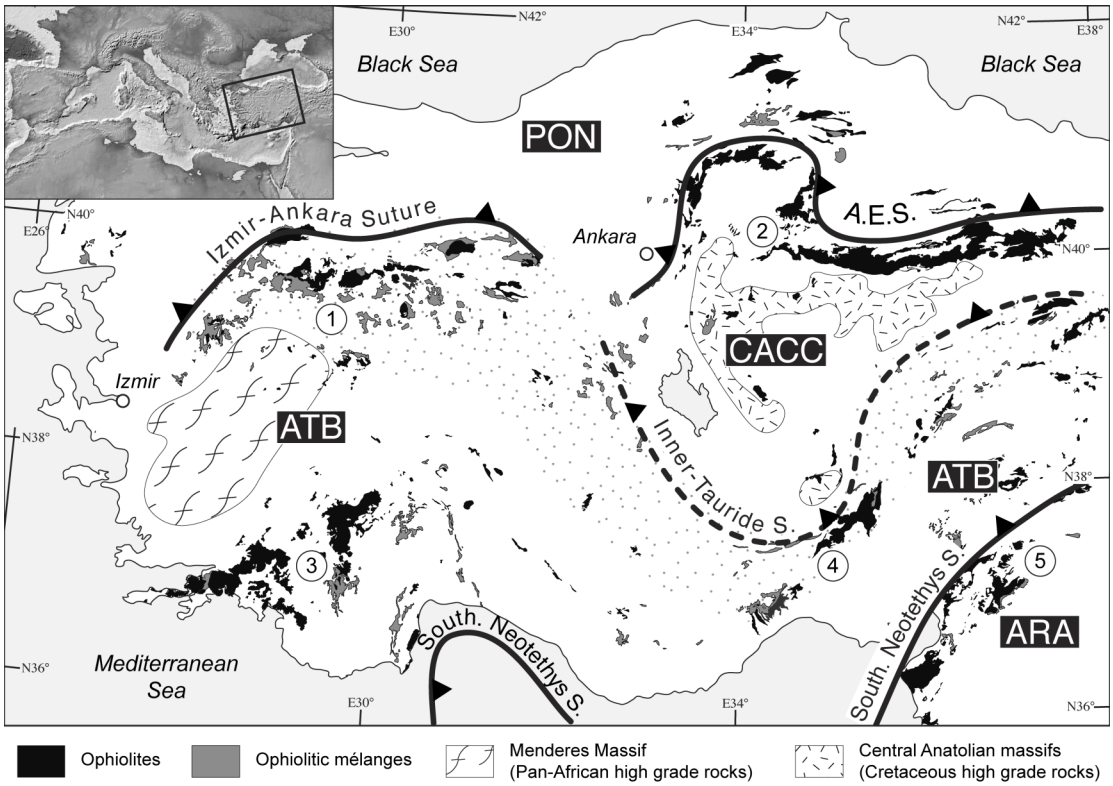

Figure 2.1: Ophiolites, sutures and continental blocks in Western-Central Turkey: (1) Kütahya Ophiolites; (2) Ankara-Erzincan Ophiolites; (3) Lycian Ophiolites; (4) Tauride Ophiolites; (5) Hatay-Malatya Ophiolites. Abbreviations: A.E.S., Ankara-Erzincan suture; ATB, Anatolide-Tauride Block; CACC, Central Anatolian Crystalline Complex; PON: Pontides; ARA, Arabian Block. Dotted area for the study area (Figure 2.2). Contours modified after MTA (2002).

In northern Central Turkey, the Pontides and the Central Anatolian Crystalline Complex are separated by an ophiolitic belt, known as the Ankara-Erzincan suture zone (Figure 2.1). Mafic and ultramafic bodies occur in the Central Anatolian Crystalline Complex and are interpreted as remnants of a large ophiolitic slab that once covered this region (e.g., Yalınız et al., 1996; Floyd et al., 1998). The timing of obduction is predated by middle Turonian to early Santonian epi-ophiolitic pelagic sediments preserved on top of these Central Anatolian ophiolites and postdated by late Maastrichtian and younger non-metamorphosed cover sediments on top of the Central Anatolian Crystalline Complex (Yalınız and Göncüoğlu, 1998). However it was argued that some so-called ophiolites may be intrusive into late Cretaceous granitoids and high-grade metamorphic rocks (Kadioğlu et al., 1998; Whitney and Dilek, 1998).

Between the Anatolide-Tauride Block and the Central Anatolian Crystalline Complex, no ophiolitic belt is exposed but Cenozoic to Quaternary sedimentary basins. Some authors thus considered the Central Anatolian Crystalline Complex as a northern promontory of the Anatolide-Tauride "composite terrane" (Göncüoğlu et al., 1997). This model is based on lithostratigraphic similarities between the Central Anatolian Crystalline Complex and the Anatolide-Tauride Block. Alternatively, other authors suggested that the Anatolide-Tauride Block was once separated from the Central Anatolian Crystalline Complex by an oceanic branch, referred to as the Inner Tauride Ocean (Görür et al., 1984; Dilek et al., 1999; Okay and Tüysüz, 1999) (Figure 2.1). It was proposed that this narrow oceanic domain was consumed along a northwards-dipping subduction and closed in latest Cretaceous to early Cenozoic times. This model is mainly based on the following arguments. (i) Cenozoic to Quaternary sedimentary basins at the southwestern and southeastern edges of the Central Anatolian Crystalline Complex include upper Maastrichtian to middle Eocene marine slope sequences, thought to reflect arc-related environments (Görür et al., 1984; Gökten and Floyd, 1987; Gökten, 1993; Görür et al., 1998). In addition, Eocene volcanic and intrusive rocks in the southernmost of these basins (Ulukışla Basin) present inherited subduction-related geochemical features, suggesting supra-subduction mantle wedge as a source (Clark and Robertson, 2002). However, the upper Maastrichtian to early Palaeocene lowermost levels of the Ulukışla basin and the Şarkişla basin (south and east of the Central Anatolian Crystalline Complex, respectively) lie unconformably over ophiolitic mélanges (Görür et al., 1998; Clark and Robertson, 2002), suggesting that they might postdate the exhumation of the southerly metamorphosed Anatolide-Tauride platform carbonates and the ophiolitic mélange (Bolkar Mountains). (ii) Late Cretaceous calc-alkaline granitoids from the southwestern edge of the Central Anatolian Crystalline Complex display geochemical features, suggesting a mantle source with significant subduction-related components (Ilbeyli et al., 2004; Ilbeyli, 2005; Boztuğ et al., 2007), and belong to the group of volcanic-arc granitoids (Aydın et al., 1998; Kadioğlu et al., 2003). But, most of the geochemical studies on the Central Anatolian intrusive rocks led to classify them as syn- to post-collisional granitoids, rather related to the collision between the Central Anatolian Crystalline Complex and the Pontides (e.g., Akıman et al., 1993; Aydın et al., 1998; Boztuğ, 1998; Boztuğ, 2000; Köksal et al., 2004). (iii) It was shown that the Lycian, Kütahya and Tauride ophiolites (Figure 2.1) were derived from a single oceanic basin, as evidenced by uniform metamorphic sole ages (around 90-100 Ma), comparable lithologic and geochemical features, and lateral continuity along smaller bodies in the

central Taurides (Juteau, 1980; Şengör and Yılmaz, 1981; Thuizat et al., 1981; Lytwyn and Casey, 1995; Parlak and Delaloye, 1999; Robertson, 2002; Önen, 2003; Çelik et al., 2006). Dismembered ophiolites lying on top of the Central Anatolian Crystalline Complex (Floyd et al., 1998, 2000; Yalınız et al., 2000) differ significantly from the Lycian, Kütahya and Tauride ophiolites in terms of lithostratigraphy (Parlak et al., 2002; Robertson, 2002). In addition, blueschist blocks are widely reported from the non-metamorphosed mélange associated with the Lycian, Kütahya and Tauride ophiolites (van der Kaaden, 1966; Okay, 1982; Göncüoğlu et al., 1992; Rimmelé, 2003; Droop et al., 2005). In contrast, no high-pressure (H*P*) material has been reported in the metamorphosed ophiolitic mélanges of the Central Anatolian ophiolites or below the Ankara-Erzincan ophiolites (Floyd et al., 2000; Yalınız et al., 2000; Rice et al., 2006) (Figure 2.1). It was thus put forward that the Anatolide-Tauride ophiolites differ from the Central Anatolian ophiolites because they did not derive from the northerly Ankara-Erzincan Zone but rather from an oceanic branch once located between the Central Anatolian Crystalline Complex and the Anatolide-Tauride Block (e.g., Knipper et al., 1986; Ricou et al., 1986). (iv) Aeromagnetic anomaly maps (Ateş et al., 1999; MTA, 2007) show a linear, strongly positive anomaly along the southwestern edge of the Central Anatolian Crystalline Complex suggesting a limit between two continental blocks. Today's position of the anomaly does not fit exactly the expected location of a hypothetical Inner Tauride suture, and any similar magnetic anomaly is not depicted either along the Izmir-Ankara suture in Western Turkey or along the Ankara-Erzincan suture in northern Central Turkey.

Although many studies recently put forward various arguments in favor of a sutured Inner Tauride oceanic branch, this model has not been yet equivocally accepted. Therefore we addressed this key issue studying the metamorphic evolution of the Anatolide metamorphic zones, particularly towards Central Turkey. If any oceanic branch was closed as Inner Tauride suture, subduction-related metamorphism should be recorded in the Anatolides in Central Turkey. Here we provide new metamorphic data from the northern Anatolide-Tauride Block, related to the late Cretaceous to Palaeogene evolution of Western to Central Turkey. In addition, we present a reconstruction model restoring the Alpine tectonic setting at the early post-collisional stage (by the Eocene-Oligocene boundary). The model allows us to consider the subduction- and collision-related structures and geometries despite the overprint of Neogene to Recent strike-slip and extensional tectonics. Combining these new petrologic data and tectonic reconstruction contributes to better understand the Alpine geodynamic evolution of Western and Central Turkey.

2.2. Geological setting

2.2.1. The Anatolide metamorphic zones

The lithostratigraphy of the Anatolide-Tauride Block is best described in Western Turkey. Therefore we summarize the main characteristics and nomenclature for Western Turkey, and expand this tectono-stratigraphy. The lithostratigraphy of the Anatolide-Tauride Block is classically separated into two rock groups: a Precambrian to early Palaeozoic basement (referred to as core series) and unconformably-overlying Ordovician to Eocene sediments and volcanics (referred to as cover series).

The lower Triassic to upper Cretaceous stratigraphic cover sequence represents the northern continental passive margin of the Anatolide-Tauride Block developed during the opening of the northern Neotethys oceanic branch (Şengör and Yılmaz, 1981; Okay, 1984).

The term 'Anatolides' is used to designate the Alpine metamorphic rocks at the northern edge of the Anatolide-Tauride Block, whereas the term 'Taurides' designates the non-metamorphosed early Palaeozoic to early Cenozoic sediments, to the south (Okay, 1984). In Western Turkey, the Anatolides were subdivided into several metamorphic zones according to their Alpine metamorphic grade (Okay, 1984, 1986). From north to south these are: the Tavşanlı Zone, the Afyon Zone, the Menderes Massif and the Lycian Nappes. Alternatively, Göncüoğlu and co-workers (Özcan et al., 1988; Göncüoğlu et al., 1992, 1997), based on lithostratigraphic similarities, refer to a 'Kütahya-Bolkardağ Belt', which includes all the zones of the Anatolides, except for the Menderes core series. This nomenclature, however, does not account for variations of metamorphic grade within the Anatolides, so we use the nomenclature of Okay.

The Tavşanlı Zone is composed of cover series metamorphosed under high-pressure-blueschist- to low-temperature-eclogite-facies conditions (e.g., Okay, 2002; Whitney and Davis, 2006; Çetinkaplan et al., 2008). Late Cretaceous dates ranging between 88 and 80 Ma are interpreted as ages of the high-pressure peak of these blueschists (Ar-Ar and Rb-Sr on phengite and glaucophane) (Harris et al., 1994; Okay et al., 1998; Sherlock et al., 1999; Seaton et al., 2009). Additionally the Tavşanlı Zone comprises an ophiolitic mélange containing blueschists blocks (Droop et al., 2005; Çetinkaplan et al., 2008). South of and structurally below the Tavşanlı Zone, the Afyon Zone consists of a polymetamorphic Precambrian basement and a monometamorphic Palaeozoic to Mesozoic cover (Candan et al., 2005). The Afyon Zone was thought to have undergone only greenschist-facies metamorphism (Okay, 1984; Özgül, 1984; Okay et al., 1996). However, recent findings of glaucophane, in both basement and cover, and Fe-Mg-carpholite, in the cover (Figure 2.2), are local evidence for an Alpine blueschist-facies metamorphic event in the central part of the Afyon Zone (Candan et al., 2005). The time interval between the age of the oldest metamorphic rocks and the age of the youngest non-metamorphosed rocks suggests a Palaeocene metamorphic age for the Afyon Zone (Candan et al., 2005).

Southwest of and structurally below the Afyon Zone, the Menderes Massif is characterized by Alpine Barrovian metamorphism in both core and cover series, which is believed to be Eocene in age (Satır and Friedrichsen, 1986). The core series underwent a polymetamorphic evolution with Precambrian metamorphism up to eclogite- and granulite-facies conditions (Candan et al., 2001; Oberhänsli et al., 2010b). A Fe-Mg-carpholite-kyanite assemblage recovered from the cover series of the southern Menderes Massif shows that at least the metamorphosed Triassic clastics of the southern part of the Menderes Massif were affected by Alpine high-pressure low-temperature (H*P*-L*T*) metamorphism (Rimmelé et al., 2003b; Rimmelé et al., 2005; Whitney et al., 2008a). Along its southern and eastern edges, the Menderes Massif is structurally overlain by the Lycian Nappes, consisting of a pile of thrust sheets of Carboniferous to Oligocene sediments and ophiolites (de Graciansky, 1972; Monod, 1977; Collins and Robertson, 1998). The Lycian Nappes were transported southwards over the Menderes Massif and emplaced over the Tauride autochthonous units between late

Eocene and late Miocene times (Poisson, 1977; Collins and Robertson, 1998). Firstly, greenschist-facies metamorphism was evidenced by the presence of chloritoid in the Lycian Nappes along their contact with the Menderes Massif (Ashworth and Evirgen, 1984). Recently, the metamorphic grade of this region was reevaluated as blueschist facies as evidenced by the widespread occurrence of Fe-Mg-carpholite (Oberhänsli et al., 2001; Rimmelé et al., 2003a, 2003b, 2006). According to Ar-Ar radiochronologic results on phengite, this H*P* metamorphic event happened sometimes between 90 and 70 Ma (Ring and Layer, 2003). In contrast, the other parts of the Lycian Nappes are non-metamorphic (Oberhänsli et al., 2001). Therefore, we propose that these H*P* metamorphic rocks, occurring as klippen on top of the Menderes Massif and on its southern and eastern edges (Rimmelé et al., 2006), should be separated from the non-metamorphic Lycian Nappes (*sensu* de Graciansky, 1972) and distinguished as the Ören Unit.

West of and structurally above the Menderes Massif, the easternmost edge of the Cycladic Blueschist Unit of the Aegean region, which was metamorphosed under epidote-blueschist- to eclogite-facies conditions in middle Eocene times (e.g., Candan et al., 1997; Oberhänsli et al., 1998; Ring et al., 1999), crops out in Western Turkey. In the present paper, we focus on the eastward continuation of the Anatolides, therefore the controversial tectonic imbrication of the Anatolide zones with the Cycladic Blueschist Unit and other units of the Aegean Domain is out of the scope of this study. Hence the Cycladic Blueschist Unit is not treated in the model we propose here for the evolution of Western-Central Turkey.

2.2.2. The Afyon Zone

2.2.2.1. Lithostratigraphy

Originally, the Afyon Zone was defined as a passive margin sequence metamorphosed under greenschist-facies conditions, extending from Western to Central Turkey (Okay, 1984, 1986). It was recognized in the areas of Simav, Kütahya, Afyon, Konya, Yahyalı and Kayseri, and in the Bolkar Mountains. The Afyon Zone presents a lithostratigraphic sequence made of Precambrian core, a Palaeozoic cover and a Mesozoic cover, similarly to the Menderes Massif (Candan et al., 2005).

Precambrian basement rocks

The area of Afyon exposes upper-greenschist- to amphibolite-facies rocks as the lowermost stratigraphic level of the Afyon Zone (Figure 2.2). These rocks consist of garnet-biotite micaschists, chlorite-albite schists, quartzites, glaucophane-bearing metamorphosed gabbroic stocks and leucocratic metagranite. High-grade mineral assemblages in the schists and glaucophane growth in the metagabbros evidence a polymetamorphic history of the basement of the Afyon Zone. Such a polyphased metamorphic evolution, the uniformity of thick metaclastic series, the existence of widespread metamorphosed gabbroic stocks and the absence of any marble layer are the features supporting a lithostratigraphic correlation with the metamorphosed Precambrian clastics of the Menderes Massif core (Candan et al., 2005). However, due to differing Alpine metamorphic evolution, these basements are considered as parts of two distinct metamorphic units (see below).

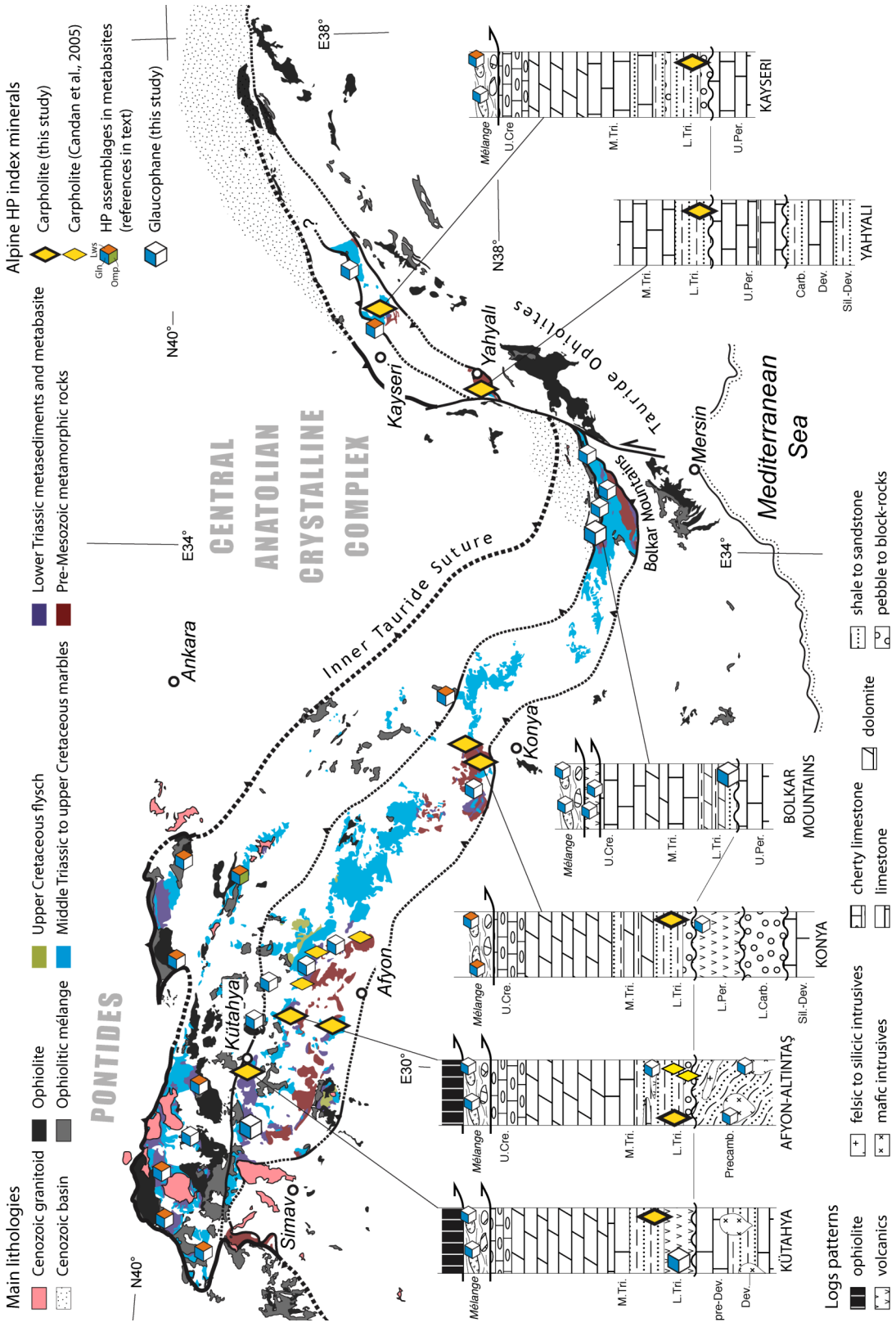

Figure 2.2: Localities of high-pressure minerals in the Tavşanlı and Afyon Zones (map) and their lithostratigraphic position in the Afyon Zone (logs). Contours modified after MTA (2002). Note that carpholite is found in most of the occurrences of the Lower Triassic clastics of the Afyon Zone.

Palaeozoic cover rocks

Like the Menderes Massif, the Afyon Zone includes metamorphosed Palaeozoic sediments and volcanics. Near Simav, they consist of low-grade metamorphic pre-Devonian clastics and carbonates that were intruded by Devonian orthogneisses (395-385 Ma Pb-Pb zircon ages, C. Akal, unpublished data, 2006) (Figure 2.2). Near Konya, the Palaeozoic sequence consists of metamorphosed Silurian to Devonian neritic carbonates, a lower Carboniferous blocky unit (Göncüoğlu et al., 2007; Robertson and Ustaömer, 2009), and metamorphosed early Permian volcanics (284-280 Ma Pb-Pb zircon ages, C. Akal, manuscript in preparation, 2010). The occurrence of blue amphibole was widely reported in these metavolcanics (Bayiç, 1968; Bingöl, 1974; Kurt, 1996). In the Bolkar Mountains (Figure 2.2), recrystallized upper Permian platform-type dark limestones represent the local lowermost levels of the Afyon Zone (Demirtaşlı et al., 1984). Further east, near Yahyalı, the Afyon Zone exposes Silurian to Devonian phyllites, Devonian coral marbles, Carboniferous phyllites and upper Permian platform marbles (Ayhan and Lengeranli, 1986; Gençalioğlu-Kuşcu et al., 2001).

Mesozoic cover rocks

In the Afyon Zone, metamorphosed Mesozoic sediments and volcanics rest unconformably on either the polymetamorphic basement (near Afyon) or Palaeozoic sequences (near Simav, Konya and Yahyalı). This regional unconformity (Figure 2.2) is represented by lower Triassic continental basal carbonate- and/or quartz-conglomerates. They are widespread in the Afyon Zone: near Afyon (Göncüoğlu et al., 1992; Tolluoğlu et al., 1997; Gürsu et al., 2004; Candan et al., 2005), near Konya (C. Akal, manuscript in preparation, 2009), near Yahyalı (Ayhan and Lengeranli, 1986) and near Kayseri (Dirik et al., 1999, and references therein). A thick volcanic sequence consisting of rhyolitic and dacitic lava flows and associated volcaniclastics occurs near Simav (ca. 241 Ma U-Pb zircon age, C. Akal, unpublished work, 2007). In these areas, the metaconglomerates are overlain by metaclastics, including yellowish and/or reddish phyllites, metasandstones, marbles as well as mafic metavolcanic lenses. In contrast, in the Bolkar Mountains, Permian limestones are overlain by lower Triassic varicolored shales, calc-schists and clayey limestones, with local layers of slates and mafic metavolcanics (Demirtaşlı et al., 1984). Throughout the Afyon Zone, the lower Triassic siliciclastic sequence turns gradually into a thick recrystallized upper Triassic to upper Cretaceous dolomitic platform with a transition zone consisting of varicolored shales, yellowish dolomites and quartz arenites. The uppermost levels of the carbonate sequence are characterized by Maastrichtian pelagic marbles with chert interlayers (Göncüoğlu et al., 1992; MTA, 2002; Candan et al., 2005). The Mesozoic cover stratigraphy as a whole is interpreted as a rift- to passive-margin sequence (Göncüoğlu et al., 1992).

2.2.2.2. Early reports of H*P* minerals in the Afyon Zone

In van der Kaaden's (1966) compilation of the blue amphibole occurrences in Turkey, some localities concern the Afyon Zone as later defined by Okay (1984). Indeed van der Kaaden (1966), and later Bayiç (1968), reported blue amphibole in metavolcanics of the Konya area. He also found blue amphibole in the region of the Bolkar Mountains and farther east, with lawsonite, in the Kayseri area (Figure 2.2). Bingöl (1974) then published a metamorphic map of Turkey, in which he depicted a belt

of 'high pressure greenschist glaucophanic facies' running from Konya to Kayseri via the Bolkar Mountains. Later, Okay (1984) extended this metamorphic zone westwards and defined it as the Afyon Zone, characterized by greenschist facies. Chemical analyses on the blue amphiboles from andesitic metabasalts of Konya area showed ferroglaucophane compositions, indicating a H*P*- L*T* metamorphic overprint of the magmatic mineral assemblages (Kurt, 1996). Recently, Candan et al. (2005) showed that, near Afyon, Fe-Mg-carpholite occurs in quartz-metaconglomerates, and yellowish and reddish phyllites attributed to lower Triassic times (Figure 2.2). In addition, they found glaucophane in metagabbros of the basement and metavolcanics at the base of the upper Triassic to upper Cretaceous carbonate platform. Similar to the Ören Unit (Rimmelé et al., 2003a), fibrous calcite crystals in so-called rosetta-marbles from the Afyon Zone were interpreted as textural relics of aragonite by these authors. Fe-Mg-carpholite, glaucophane and calcite pseudomorphs after aragonite in the Mesozoic cover are evidence for Alpine H*P*-L*T* metamorphism in this part of the Afyon Zone. Based on carpholite-bearing assemblages, *P-T* conditions were estimated as minimum 6-9 kbar for ca. 350°C (Candan et al., 2005).

In the Afyon area, non-metamorphic uppermost Palaeocene to lower Eocene limestones unconformably overlie upper Maastrichtian cherty marbles and point to a Palaeocene age of the H*P* metamorphic event. So far it remained unclear whether this blueschist-facies metamorphism is characteristic of the whole Afyon Zone.

Since, in contrast with the Afyon Zone basement, no Alpine H*P* metamorphism was detected in the Menderes Massif core, these basement series are considered as parts of different metamorphic zones.

2.2.3. Elements for reconstruction

As shown on geological maps the present-day strike of the Anatolide continental margin sediments is characterized by two curvatures: (i) one in Western Turkey, referred to as the Isparta Angle in the Tauride units (e.g., Blumenthal, 1963; Monod, 1977; Robertson et al., 2003), and (ii) the other in Central Turkey around the south edge of the Central Anatolian Crystalline Complex (Figure 2.4a). In the same way as Özgül (1984) divided the Taurides, we may thus consider three sectors for the Anatolides: (a) the western Anatolides around the Menderes Massif, (b) the central Anatolides including the areas of Afyon and Konya, and (c) the eastern Anatolides, from the Bolkar Mountains to the Kayseri area.

Whether the curvature reflects the primary outline of the Anatolide continental passive margin, or was acquired during late Cretaceous to early Cenozoic subduction-collision stage, or even later due to post-collisional tectonics, remains unclear. This isssue can be addressed when restoring the well-studied, intense post-collisional extensional and strike-slip tectonics. Therefore, in order to restore the pre-Neogene shape of the Anatolides, we compiled published quantitative information concerning the post-collisional deformation in Western to Central Turkey, i.e., strike-slip faults, normal faults and detachments offsets, and block rotations (Tables 2.1, 2.2; Figure 2.4).

2.2.3.1. Western Anatolides

Since late Oligocene times (Seyitoğlu and Scott, 1992), Western Turkey has been affected by extensional tectonics related to the collapse of the Alpine orogen (Collins and Robertson, 1998). Two extensional phases are generally distinguished: a first phase dominated by detachment systems and a second phase related to the formation of grabens bounded by brittle, high-angle normal faults (Figure 2.4b).

The Menderes detachments

The exhumation of the southern Menderes sub-massif is matter of intense debate (e.g., Bozkur and Park, 1994; Hetzel and Reischmann, 1996; Collins and Robertson, 1998; Bozkurt and Satır, 2000; Gessner et al., 2001b; Régnier et al., 2003; Ring et al., 2003; Seyitoğlu et al., 2004; Régnier et al., 2007). Since quantitative evaluation of the extension in this sector has not yet been published, this debate is out of the scope of our paper.

To the north, the Simav detachment (Figure 4b) is a top-to-the-NNE shallow-angle normal fault (Işık and Tekeli, 2001; Işık et al., 2003; Ring et al., 2003; Işık et al., 2004; Ring and Collins, 2005; Thomson and Ring, 2006) developed between the northern Menderes Massif and the Afyon Zone. It is responsible for the exhumation of the northern Menderes sub-massif and early Miocene syn-kinematic granitoids between the late Oligocene and the middle Miocene (Işık et al., 2004).

Seyitoğlu et al. (2004) argued that most of the exhumation of the entire Menderes Massif was achieved along a single top-to-the-NNE detachment, rooting as the Simav detachment. Their single-detachment model 'requires a stretching factor of 2' (p. 361) for the first phase of extension, whereas the second phase, accommodated along the Menderes grabens, is considered as relatively negligible. Keeping in mind that along a NNE-SSW transect (direction of extension) the Menderes Massif is about 300 km long (Bozkurt and Oberhänsli, 2001; MTA, 2002) (Figure 4a), the estimate of Seyitoğlu et al. (2004) implies a total offset of 150 km along the detachments. In contrast, based on geological markers, Ring et al. (2003) suggested that the Simav detachment accommodated at least 50 km horizontal stretching. Since this is based on geological observations, we prefer the estimate of Ring.

A bivergent detachment system is considered to be responsible for episodic exhumation of the central Menderes sub-massif (Hetzel et al., 1995b; Gessner et al., 2001b; Ring et al., 2003). The northerly Alaşehir detachment (Emre and Sözbilir, 1997; Koçyiğit et al., 1999; Gessner et al., 2001b; Işık et al., 2003) and the southerly Büyük Menderes detachment (Figure 2.4b) (Emre and Sözbilir, 1997; Gessner et al., 2001b; Lips et al., 2001) present rather symmetrical structural features, with top-to-the-NNE and top-to-the-S fabrics, respectively. Both detachments were likely active between early to middle Miocene and Pliocene (Seyitoğlu and Scott, 1992; Hetzel et al., 1995a; Emre and Sözbilir, 1997; Gessner et al., 2001b; Lips et al., 2001; Glodny and Hetzel, 2007). Total offsets were estimated as ca. 12 km (Gessner et al., 2001b) and > 7.5 km (Glodny and Hetzel, 2007) along the Alaşehir detachment, and as ca. 10 km (Gessner et al., 2001b) along the Büyük Menderes detachment. Palaeomagnetism suggests that the extension along these detachments engendered a differential anticlockwise rotation of the southern Menderes sub-massif according to the northern Menderes sub-massif (van Hinsbergen et al., 2010).

The Menderes grabens

From late Miocene, a second extensional phase in Western Turkey resulted in forming numerous grabens bounded by high-angle normal faults. The Simav graben, the Alaşehir graben, the Küçük Menderes graben and the Büyük Menderes graben are the main Neogene extension-related basins developed since the late Miocene (Figure 2.4b).

On either side of the central Menderes sub-massif, the activity of the Alaşehir and Büyük Menderes detachments was accompanied by the development of rolling-hinge half-graben, the Alaşehir and the Büyük Menderes grabens, as evidenced by L*T*-thermochronology (Gessner et al., 2001b) and structural and sedimentological data (Seyitoğlu et al., 2002). Concerning the still-active Alaşehir graben, Glodny and Hetzel (2007) recently suggested that, since 16 Ma, continuous extension evolved from detachments (ductile-brittle deformation) to graben systems (brittle deformation). Bozkurt (2000) estimated as 5 km the extension accommodated by the Büyük Menderes graben, while, based on recently published seismic lines (Çiftçi and Bozkurt, 2009), we have calculated a total offset of ca. 10 km for the Alaşehir graben.

2.2.3.2. Central Anatolides

Post-Alpine tectonics in the central Anatolides are evidenced by still-active, southeast-striking grabens: the Afyon-Akşehir graben and the Tuz Gölü basin (Figure 2.4b), which are thought to have started opening in the Maastrichtian and early Miocene, respectively (Çemen et al., 1999; Koçyiğit et al., 2000). An estimate of the extension amount has never been suggested.

In the central Taurides, the Beyşehir-Hoyran-Hadim nappes are a non-metamorphic allochthonous unit and were emplaced southwards over the autochthonous units between latest Cretaceous and Eocene (Özgül, 1984; Andrew and Robertson, 2002; Elitok and Drüppel, 2008). Subsequently, between the middle Eocene and the Oligocene, these Tauride nappes experienced a ~40° clockwise rotation during the formation of the Isparta Angle (Figure 2.4b), as shown by palaeomagnetic results (Kissel et al., 1993).

2.2.3.3. Eastern Anatolides

The Ecemiş Fault is a major structure that affects the Anatolide-Tauride Block in southern Central Turkey (Figures 2.2, 2.4a, 2.4b). It is the southern segment of the Central Anatolian Fault Zone that consists of a sinistral strike-slip fault, at least 700 km long (Koçyiğit and Beyhan, 1998). Despite the fact that the timing of the tectonic activity of the Ecemiş Fault is disputed (Yetiş, 1984; Koçyiğit and Beyhan, 1998, 1999; Westaway, 1999; Jaffey and Robertson, 2001; Umhoefer et al., 2007), at least some of the fault displacement clearly postdates the imbrication of the Anatolides and Taurides. The Ecemiş Fault offsets the Bolkar Mountains units from their eastern continuation and a large sheet of the Tauride ophiolites into two smaller bodies (Figures 2.2, 2.4a, 2.4b). The total sinistral offset along the Ecemiş fault was estimated as between 60 and 80 km (Yetiş, 1984; Koçyiğit and Beyhan, 1998; Westaway, 1999; Jaffey and Robertson, 2001). Near Sariz, in the eastern Taurides (Figure 2.4b), Kissel et al. (2003) evidenced a 40° anticlockwise rotation in Eocene volcanic rocks.

Table 2.1: Estimates of the post-collisional extension in the western Anatolides (see Figure 2.4b).

Detachments	Location	Kinematics	Time	Offset	References
Simav detachment	northern Menderes sub-massif	top-NNE to top-NE	late Oligocene to early Miocene	>50 km	Ring et al. (2003)
Alaşehir detachment	central Menderes sub-massif (northern edge)	top-NE	late Miocene to early Pliocene	~12 km >7.5 km	Gessner et al. (2001b) Glodny and Hetzel (2007)
Büyük Menderes detachment	central Menderes sub-massif (southern edge)	top-S	late Miocene to early Pliocene	~10 km	Gessner et al. (2001b)
Grabens	**Location**	**Kinematics**	**Time**	**Offset**	**References**
Alaşehir graben	between northern and central Menderes sub-massifs	top-NE ?	since early Miocene	~10 km	calculted from Çiftçi and Bozkurt (2009)
Büyük Menderes graben	between central and southern Menderes sub-massifs	top-S ?	since early-middle Miocene	5 km	Bozkurt (2000)

Table 2.2: Post-collisional rotations from palaeomagnetic studies in the Anatolide-Tauride Block (see Figure 2.4b).

Unit	Sample age	Time	Horizontal rotation	α95	References
western Taurides	Eocene-Miocene	middle Miocene	-32°	12.0°	Kissel and Poisson (1987)
central Taurides (BHH Nappes)	lower Eocene	middle Eocene to Oligocene	+39°	13.8°	Kissel et al. (1993)
	Palaeocene-lower Eocene		+40°	11.6°	Kissel et al. (1993)
	Miocene		0°	8.4°	Kissel et al. (1993)
eastern Taurides (near Sariz)	Eocene	since Miocene?	-46°	7.3°	Kissel et al. (2003)
	Eocene	since Miocene?	-36°	12.0°	Kissel et al. (2003)
	Eocene	since Miocene?	-37°	7.5°	Kissel et al. (2003)

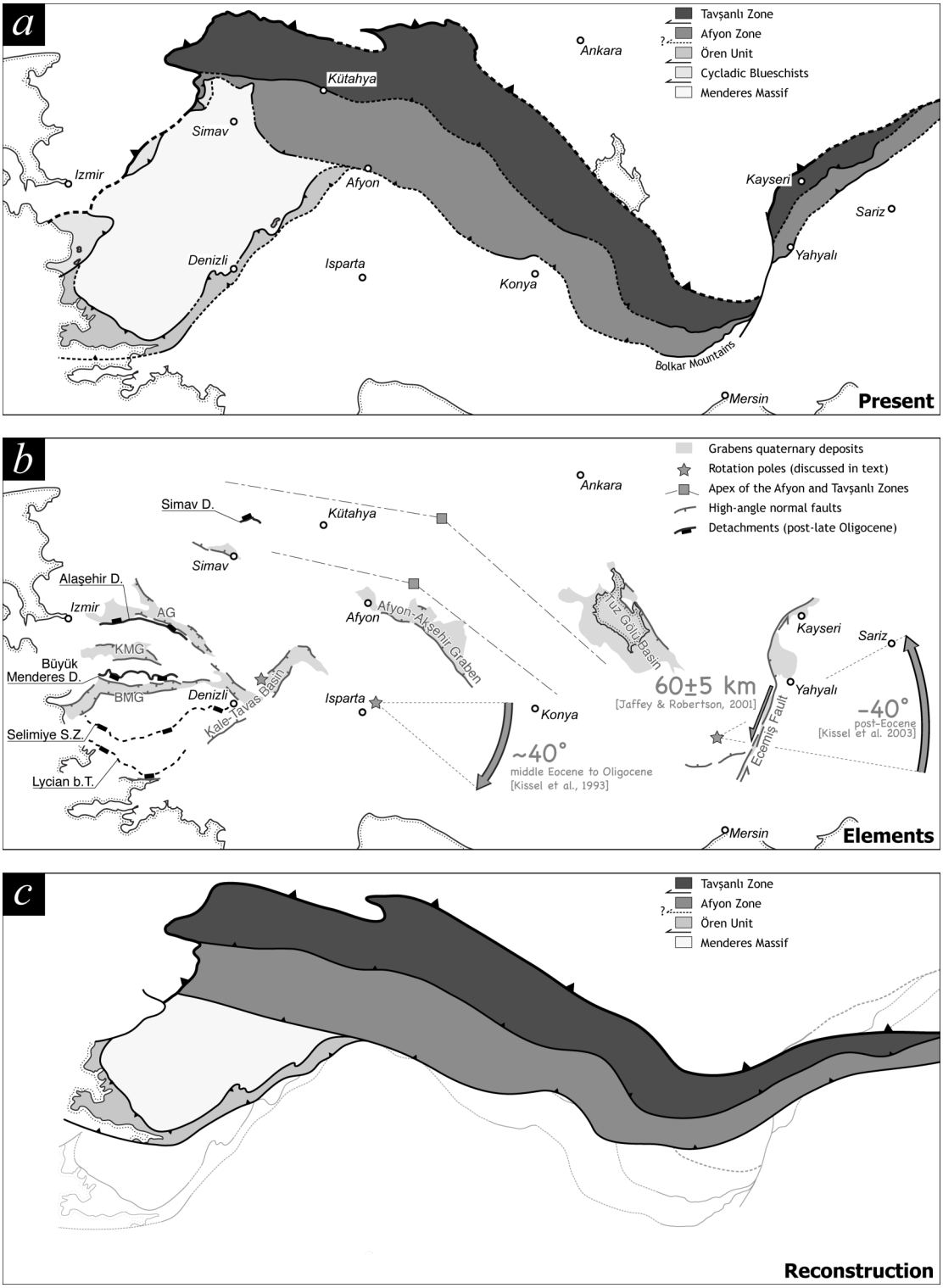

Figure 2.3: Tectonic reconstruction of the Anatolides at the post-orogenic stage. a, present-day Anatolides. b, elements of post-collisional deformation of the Anatolides. c, reconstructed Anatolides using the available data (reconstruction not isochronous!). Abbreviations: AG: Alaşehir graben; KMG: Küçük Menderes graben; BMG: Büyük Menderes graben. See references and discussion in text and Tables 2.1 and 2.2.

2.3. New HP mineral localities

We investigated the entire Afyon Zone, prospecting for potential H*P*-L*T* minerals, and found new localities of carpholite and glaucophane.

2.3.1. Carpholite

All along the Afyon Zone, except the Bolkar Mountains, we observed that the lower most levels of the Mesozoic cover series, which are attributed to early Triassic times, systematically include fine-grained, reddish phyllites. In these rocks, we found carpholite-bearing quartz segregations from Kütahya to Afyon, in the Konya area (near Meydan and Sizma), near Yahyalı and in the Kayseri area, that is all along the Afyon Zone (Figure 2.2). These carpholite occurrences are very similar to those observed elsewhere in the Tethyan realm (e.g., Goffé and Chopin, 1986; Azañón and Goffé, 1997; Oberhänsli et al., 2001; Bousquet et al., 2002; Rimmelé et al., 2003a; Oberhänsli et al., 2010a). In the areas of Kütahya and Konya, it is found as well-preserved fibrous crystals, reaching locally 15 cm in length (Figure 2.3a, 2.3b). In the areas of Yahyalı and Kayseri, we found tiny carpholite relics, consisting of 10- to 100-µm-long fibres isolated within quartz grains (Figure 2.3e, 2.3f). There, chlorite-white mica assemblages correspond to pseudomorphs after larger, inter-connected carpholite crystals. Near Afyon (Figure 2.3c), carpholite occurs as centimetric, rosetta-shaped crystals in pyrophyllite-rich quartz metaconglomerates, pyrophyllitites (most probably derived from altered rhyolites) and reddish metapelites (Candan et al., 2005) (Figure 2.2). No carpholite was found so far in the Bolkar Mountains. Electron microprobe analyses show that carpholite is systematically ferromagnesian and Mn-free ($X_{Mn} < 0.07$), and therefore an index mineral for H*P*-L*T* metamorphism (Chopin and Schreyer, 1983).

2.3.2. Glaucophane

Glaucophane occurs scarcely in the coherent sequence of the Afyon Zone. But we found glaucophane in metamorphosed lower Triassic volcanics between Simav and Kütahya and in metamorphosed impure mafic volcanic layers within the lower Triassic coherent serie of the Bolkar Mountains (Figure 2.2). In the Bolkar Mountains, we observed two additional types of glaucophane localities, already mentioned by van der Kaaden (1966) and Bingöl (1974) (Figure 2.2): on the one hand blueschist blocks in the ophiolitic mélange, particularly at the northern types like massive lavas (glaucophanites), metasediments (glaucophane-bearing quartzites), variolites and pillow breccias. We found these blueschist lenses to be overlain by an ophiolitic metamorphic sole for which a blueschist-facies overprint was evidenced (Dilek and Whitney, 1997). Such blueschist-facies lithologies are common in the Tavşanlı Zone (e.g., Okay, 1982) and absent from the Afyon Zone. In addition, similar blueschists occur in an identical structural position as the Tavşanlı blueschists in Western Turkey (Önen and Hall, 2000). Therefore we consider the Kızıltepe blueschists as remnants of the Tavşanlı Zone.

In the Afyon Zone, the occurrence of glaucophane at different levels (basement and cover) of the coherent sequence is further proof that the entire unit underwent Alpine H*P* metamorphism.

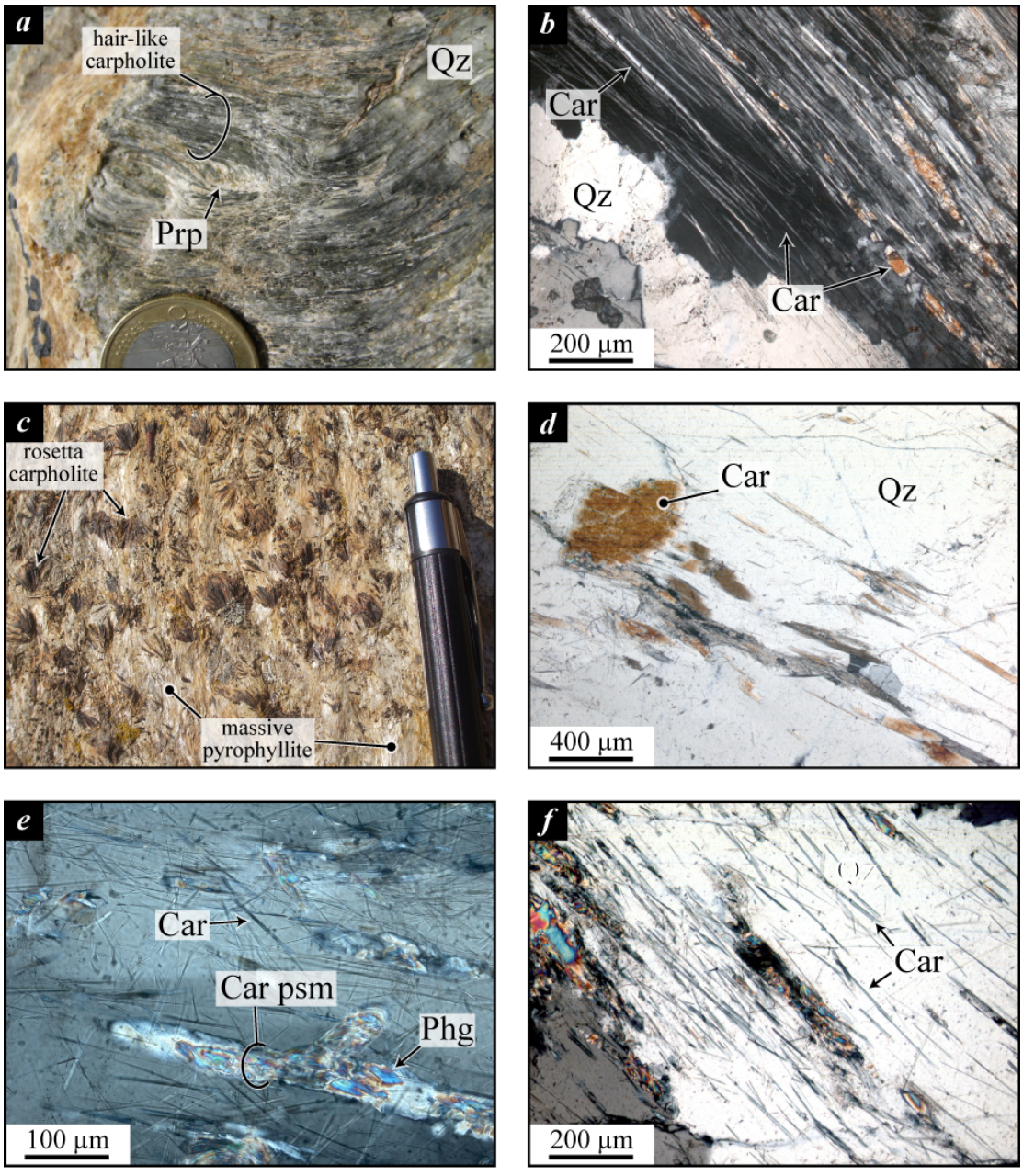

Figure 2.4: Examples of typical carpholite occurrences along the Afyon Zone: a) near Kütahya; b) near Altıntaş (crossed polars); c) near Afyon; d) near Konya (crossed polars); e) near Yahyalı (crossed polars); f) near Kayseri (crossed polars). Abbreviations: Car, carpholite; Car psm, pseudomorph after carpholite; Phg, phengite; Prp, pyrophyllite; Qz, quartz. Note that everywhere except near Afyon carpholite is found in quartz segregations.

2.4. Interpretations

2.4.1. Metamorphic zones

Afyon Zone

The Afyon Zone represents the northern continental passive margin of the Anatolide-Tauride Block. Our observations show that it was metamorphosed under blueschist-facies conditions as indicated by widespread occurrence of Fe-Mg-carpholite and associated glaucophane. Although Fe-Mg-carpholite was found nowhere in the Bolkar Mountains (Figure 2.2), several points attest that the northern Bolkar Mountains do belong to the H*P* metamorphic Afyon Zone.

(1) *High pressure minerals*. The northern Bolkar Mountains lower Triassic series is made up of low-grade shales, calc-schists and clayey limestones (Demirtaşlı et al., 1984), i.e., Ca-rich, Si-poor rocks. Fe-Mg-carpholite growth is only possible in Si-, Al-, Fe-rich and Na-free rocks, i.e., in the system KFMASH (Theye et al., 1992). Hence the lack of carpholite in the Bolkar Mountains can be attributed to compositional variations in the metapelites of the lower Triassic stratigraphy of the Afyon Zone. However, mafic volcanic layers within this low-grade sequence contain glaucophane and the upper Permian black marbles and Mesozoic platform marbles contain fibrous calcite crystals, like in the Ören Unit (Rimmelé et al., 2003a) and in other parts of the Afyon Zone (Candan et al., 2005), where they are interpreted as calcite pseudomorphs after aragonite.

(2) *Thrust tectonics.* In the Bolkar Mountains, the metamorphosed Mesozoic cover series (Northern Bolkar units) lie under the non-metamorphosed Tauride Permian carbonates (Southern Bolkar units) along an upper Eocene south-facing thrust (Demirtaşlı et al., 1984). On the eastern side of the Ecemiş Fault (Figure 2.2), the Fe-Mg-carpholite-bearing Yahyalı Nappe is overthrust from the south by the non-metamorphic Tauride units, referred to as the Aladağ Nappes (Tekeli et al., 1984; Jaffey and Robertson, 2001). As the Southern Bolkar units are correlated with the Aladağ Nappes (Yetiş, 1984), based on their structural positions, the Northern Bolkar units can be correlated with the carpholite-bearing Yahyalı Nappe.

(3) *Lithostratigraphy.* The lower Triassic sequence of the Yahyalı Nappe, east of the Ecemiş Fault, is stratigraphically correlated with the lower Triassic sequence of the Northern Bolkar units (Ayhan and Lengeranli, 1986). Moreover, in almost all papers, the Bolkar Mountains are classically considered as part of the Afyon Zone (Özgül, 1976; Okay, 1984, 1986).

Combined with previous reports by Kurt (1996) and Candan et al. (2005), our observations show that all along its extent the Afyon Zone includes H*P*-L*T* index minerals such as Fe-Mg-carpholite and glaucophane. The entire Afyon Zone thus constitutes a continental passive margin metamorphosed under blueschist-facies conditions that runs continuously from north of the Menderes Massif in the west to south and east of the Central Anatolian Crystalline Complex (Figure 2.4a). The terminology of the Anatolide metamorphic zones introduced by Okay (1984) remains relevant, although the Afyon Zone was initially considered as a greenschist-facies unit. However the coherence of H*P*-L*T* metamorphic conditions throughout the Afyon Zone reflects a subduction-related setting and has strong geodynamic implications.

Tavsanlı Zone

From Western to Central Turkey, lawsonite-bearing blueschists typical of the Tavşanlı Zone are reported, either within a coherent stratigraphic sequence or as blocks within the ophiolitic mélange (van der Kaaden, 1966; Çoğulu, 1967; Bingöl, 1974; Okay, 1980a, 1980b; Okay et al., 1998; Droop et al., 2005; Whitney and Davis, 2006; Çetinkaplan et al., 2008) (Figure 2.2). We thus consider that the Tavşanlı Zone also extends from north of the Menderes Massif in the west to east of the Central Anatolian Crystalline Complex (Figure 2.4a), most probably concealed under the Cenozoic sediments of the Tuz Gölü, Ulukışla and Sivas Basins.

We therefore track the H*P* Afyon Zone, and possibly the Tavşanlı Zone, all along the hypothetical border between the Anatolide-Tauride Block and the Central Anatolian Crystalline Complex. Together with the Ören Unit and the Menderes Massif cover in southwestern Turkey, the Afyon Zone and the Tavşanlı Zone constitute the Anatolide H*P* metamorphic belt, at least 700 km in length.

2.4.2. Post-collisional tectonics

2.4.2.1. Western Anatolides

Concerning the first phase of extension, we restored the detachment activity following the kinematic direction indicated by structural field indicators, i.e., top-to-the-NNE for the Simav and Alaşehir detachments, and top-to-the-S for the Büyük Menderes detachment (see references above).

Concerning the second phase of extension, the Alaşehir and Büyük grabens are strikingly decreasing in width from the coast inland. Van Hinsbergen et al. (2010) show that the exhumation of the northern and southern Menderes sub-massifs was not accompanied by rotation. Consequently the shift in direction of the detachment-related mineral lineation originates from rotation during the exhumation of the central Menderes sub-massif. These features indicate a scissor-like opening around a common rotation pole located in the area of Denizli (van Hinsbergen et al., 2010) (Figure 2.4b). Contrasting extension factors between the Aegean Sea and the Menderes region (about 2 and between 1.2 and 1.6, respectively) (Yılmaz et al., 2000) are coherent with this gradient of extension, decreasing eastwards. Both grabens present some changes in their strike (see in particular the westernmost Büyük Menderes graben; Figure 2.4b). Le Pichon et al. (1973) used similar features to localize a rotation pole in the northern Aegean Sea. However the superposition of several sets of normal faults since Miocene (Seyitoğlu et al., 2002) hampers the use of their method in the Menderes Massif.

2.4.2.2. Central Anatolides

Clockwise rotation evidenced in the central Taurides likely also occurred in the central Anatolides. The restoration of the 40° clockwise rotation of the Beyşehir-Hoyran-Hadim Nappes around the Isparta Angle apex shows that, before bending, the units had a strike towards WNW. This direction is parallel to the western Anatolides north of the Menderes Massif. In addition, the Afyon and Tavşanlı Zones present a slight curvature north of the Isparta Angle that might be related to the

formation of the latter (Figure 2.4a), since these apexes are aligned with the one of the Isparta Angle (Figure 2.4b). We reconstructed the position of the Anatolides considering that distortion and amount of rotation decrease from the Isparta Angle s.s. towards north. Thus we restored the Beyşehir-Hoyran-Hadim Nappes by 40° (Kissel et al., 1993) and arbitrarily removed the curvature around the Isparta Angle from the Afyon Zone and the Tavşanlı Zone.

2.4.2.3. Eastern Anatolides

Concerning the offset of the Ecemiş fault, we used the minimal estimate of 60 ± 5 km calculated by Jaffey & Robertson (2001), in order to provide a minimal reconstruction model.

Kissel et al. (2003) considered that palaeomagnetic results in Central Turkey indicate a total offset of ca. 500 km along the North Anatolian Fault. However, local geological studies rather suggest 35 to 100 km (Şengör et al., 1985; Koçyiğit, 1989; Westaway, 1994; Armijo et al., 1999; Hubert-Ferrari et al., 2002). Therefore, regarding that the eastern Anatolide-Tauride Block is clearly bent northwards around the southern edge of the Central Anatolian Crystalline Complex, we suggest that this post-Eocene anticlockwise rotation was achieved around a pivot point localized at the southern edge of the Central Anatolian Crystalline Complex (Kissel et al., 2003). We consider that the amount of anticlockwise rotation in the eastern Anatolide-Tauride Block increases from zero in the Bolkar Mountains area to 40° near Sariz (Kissel et al., 2003). This could be explained with the progressive influence of the Eastern Anatolian fault system.

2.4.2.4. Reconstruction: conclusion

Our reconstruction is presented in the Figure 2.4c. It is essential to note that this reconstruction is not isochronous. Indeed, in Western Turkey, post-collision tectonics started in late Oligocene, whereas Central Turkey experienced strike-slip tectonics and rotation starting by the Eocene-Oligocene boundary or even earlier (Umhoefer et al., 2007; Whitney et al., 2008b). Little is known about the evolution of Western Turkey during the Oligocene. Any isochronous reconstruction, at the Eocene-Oligocene boundary, cannot be suggested. Figure 2.4c should thus be regarded as the tectonic setting of the Anatolides not at any precise time, but after the exhumation of the H*P* passive margin and before post-orogenic deformation.

2.5. Discussion

2.5.1. Tectonic reconstruction of the Anatolides

Despite large uncertainties, our reconstruction clearly shows that, before the Neogene, the Anatolide metamorphosed continental margin had a rather linear and continuous strike, over at least 700 km (Figure 2.4c). The two curvatures of the Anatolides were acquired during post-collisional tectonic stages. In Western Turkey, extensional tectonics largely exaggerated the distance of southward transport of the Lycian Nappes over the Menderes Massif. According to our reconstruction, the migration of the Lycian Nappes due to the tectonic nappe stacking had a maximum amplitude of 150 km (Figure 2.4c).

2.5.2. Inner Tauride suture zone

The fact that a passive continental margin in the Anatolides underwent H*P*-L*T* metamorphism is a strong argument supporting the existence of an Inner Tauride suture between the Central Anatolian Crystalline Complex and the Anatolide-Tauride Block. Herein we present new arguments, which favor further the existence of an Inner Tauride suture.

A nappe system in Central Anatolia?

The model of the 'Anatolide nappes' of Göncüoğlu et al. (1997) is based on the idea that the central and eastern Anatolides rooted in the Ankara-Erzincan suture zone, north of the Central Anatolian Crystalline Complex (Figure 2.1), and were transported southwards to their present position, similarly to the emplacement of the Lycian Nappes over the Menderes Massif. In Western Turkey, such a scenario is supported by H*P* metamorphic zones along the Izmir-Ankara suture, the occurrence of klippen of Lycian Nappes over the Menderes Massif, top-to-the-south thrusting indicators (H*P* phase) and the south-facing position of the Ören Unit at the contact with the Menderes Massif (Güngör and Erdoğan, 2001; Rimmelé et al., 2003a, 2006). In Central Turkey, although Alpine blueschists and eclogites were documented in the Ankara-Erzincan suture zone (Kargı Massif) (Okay et al., 2006), differing metamorphic ages and tectonic relations with units of the Pontides preclude a close genetic link between these H*P* rocks (105 Ma, Kargı Massif (Okay et al., 2006)) and the Tavşanlı Zone (88-80 Ma (Harris et al., 1994; Okay et al., 1998; Sherlock et al., 1999; Seaton et al., 2009)). In addition, klippen of Anatolides are not reported on top of the Central Anatolian Crystalline Complex, and furthermore at regional scale bedding planes of the Anatolides dip northwards (MTA, 2002), that is the passive margin dips towards and likely below the Central Anatolian Crystalline Complex. Our first argument might be denied by assuming that the Anatolides are rootless nappes. Regarding our second argument, one might assume that all the Anatolide klippen were eroded. However, fragments of Central Anatolian ophiolites, which were derived from the Ankara-Erzincan suture zone, are preserved and lie directly on top of the Central Anatolian high grade rocks (Yalınız and Göncüoğlu, 1998). In contrast with the Menderes Massif, which is overlain by remnants of the H*P* Ören Unit (e.g., Rimmelé et al., 2006), slices of H*P* metamorphic series between the ophiolites and the high-grade rocks of the Central Anatolian Crystalline Complex are missing. These features, as well as the northward dip of the Anatolide passive margin sequences, argue against the model of 'Anatolide nappes' of Göncüoğlu et al. (1997).

Metamorphism and tectonic setting

During late Cretaceous times, the Central Anatolian Crystalline Complex and the Anatolides experienced very contrasting thermal histories. The Central Anatolian Crystalline Complex is characterized by high-temperature low- to medium-pressure metamorphism (Whitney et al., 2001) and associated late Cretaceous granitoid intrusions. Metamorphism is dated between ca. 91 Ma and 84 Ma (U-Pb zircon, monazite; Whitney et al., 2003; Whitney and Hamilton, 2004). In contrast, the Anatolide H*P* belt represents a subduction-related setting (Okay et al., 2001). The Tavşanlı Zone, at the northernmost part of the Anatolide-Tauride Block, was deeply buried and suffered H*P*-L*T* metamorphism sometimes between 88 and 80 Ma (Okay et al., 1998; Sherlock et al., 1999; Seaton et

al., 2009) while the Central Anatolian Crystalline Complex was undergoing high-temperature low-pressure metamorphism. The Afyon Zone was likely buried after early Palaeocene (Göncüoğlu et al., 1992) and suffered H*P*-L*T* metamorphism (Candan et al., 2005; this study). The Menderes Massif cover was affected by an Alpine H*P*-L*T* event during Cenozoic times (Rimmelé et al., 2003b, 2005). However, the Central Anatolian Crystalline Complex or any block of the ophiolitic mélange of the Ankara-Erzincan ophiolites and Central Anatolian ophiolites are completely free of these H*P*-L*T* events. Contrasting metamorphic evolutions, representing different tectonic setting, support the interpretation that the Central Anatolian Crystalline Complex and Anatolide-Tauride Block constituted two distinct continental blocks. The former constituting the upper plate with arc-related magmatism and the latter the subducted lower plate.

2.5.3. Geodynamics of the Anatolides

As shown by our reconstruction (Figure 2.4c), burial and exhumation of the Anatolides occurred along a linear, coherent subduction wedge related to the consumption of the Izmir-Ankara–Inner-Tauride Ocean. However two crucial questions, regarding the relation between the Ören Unit and the Afyon Zone, and the reason why nappes were formed over the Menderes Massif, remain to be answered.

Emplacement of the Lycian Nappes

Based on its metamorphism, we suggested that the blueschist-facies Ören Unit should be separated from the non-metamorphic Lycian Nappes (*sensu* Graciansky, 1972) (Figure 2.4a). The boundary between the Ören Unit and the non-metamorphic Lycian Nappes is either covered by the Lycian ophiolites (MTA, 2002) or reworked as a steep normal fault in the Kale-Tavas Basin (Seyitoğlu et al., 2004). As the contact represents a substantial metamorphic gap, juxtaposing rocks exhumed from a subduction zone to non-metamorphic passive margin platform sediments, we infer that the Ören Unit was thrust southwards over the Lycian Nappes (Figure 2.4a).

Numerous klippen of Lycian lithology were reported on top of the Menderes Massif and the Cycladic Blueschist Unit (Güngör and Erdoğan, 2001; Rimmelé et al., 2006). From each of these klippen, Fe-Mg-carpholite is reported in the lower Triassic metapelites (Rimmelé et al., 2006). There is no evidence for any slice of non-metamorphic Lycian Nappes on top of the Menderes Massif, nor north of it. It is hence likely that the Ören Unit represents a rootless blueschist-facies thrust sheet, transported from the suture zone over the Menderes Massif. In turn the non-metamorphic Lycian Nappes belong to the Taurides and correspond to their imbricated foreland (Figure 2.5). They were not thrust over the Menderes Massif.

Since our reconstruction bases only on quantified tectonic accidents, the pre-late Oligocene tectonic setting in Western Turkey displays the maximal distance (150 km) reached by the Ören Unit after its transport over the Menderes Massif. Figure 2.4c shows that extension in Western Turkey largely exaggerated the distance over which the Ören Unit was thrust.

Tectonics related to the burial and exhumation of the Cycladic Blueschist Unit and Menderes Massif have played a key role in the formation of the Ören Unit. In Western Turkey, the Cycladic

Blueschist Unit was buried to epidote-blueschist- to eclogite-facies conditions (Candan et al., 1997). Phengites yielded metamorphic ages of 40 Ma, suggesting that this H*P* unit was exhumed in Eocene times (Oberhänsli et al., 1998). In the Menderes Massif, H*P*-L*T* metamorphism, subsequently following Barrovian-type overprint and cooling-exhumation stage are thought to have occurred between early Palaeocene and late Eocene and between late Eocene and late Oligocene respectively (Satır and Friedrichsen, 1986; Bozkurt and Satır, 2000). H*P*-L*T* metamorphism of the Ören Unit happened sometime between late Cretaceous and early Tertiary (Rimmelé et al., 2003a; Ring and Layer, 2003; Candan et al., 2005). Therefore, the Ören Unit was unrooted and emplaced during exhumation of the Menderes Massif in Eocene to early Oligocene times. This is supported by the occurrence of an Eocene flysch between the Menderes cover and the Ören Unit.

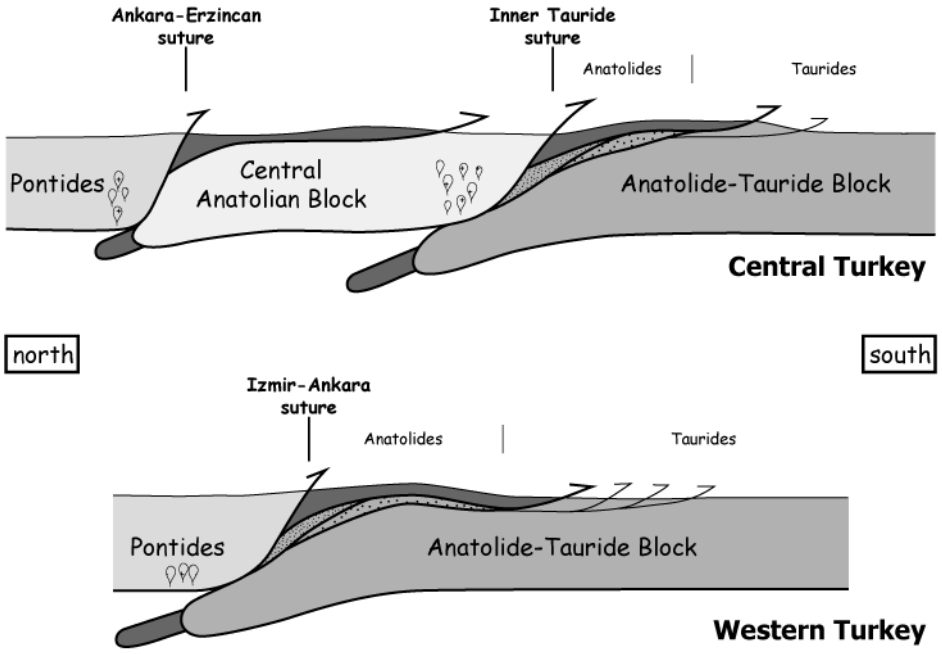

Figure 2.5: Schematic reconstructed cross-sections of Central and Western Turkey in early post-collisional times at crustal scale. See discussion in text.

Indentation of the Central Anatolian Crystalline Complex

Symmetric and possibly coeval rotations may have occurred in the central and the eastern Anatolide-Tauride Block (Kissel et al., 1993; Kissel et al., 2003) (Figure 2.4b). In the central Taurides, the timing of the rotation is well constrained between early middle Eocene and early Miocene (Kissel et al., 1993). However in the eastern Taurides, Kissel et al. (2003) provided very little information concerning the stratigraphic age of the samples they used for their palaeomagnetic study. Thus they considered the rotation to be 'post-Eocene'. This lack of information has a major impact on the understanding of the cause of the Anatolide bend around the Central Anatolian Block.

Based on the stratigraphy of Tertiary basins installed along the Inner Tauride suture, Görür et al. (1998) inferred that the Anatolide-Tauride Block collided with the Central Anatolian Crystalline Complex in upper Eocene times, coeval with the rotation recorded in the Beyşehir-Hoyran-Hadim Nappes. Consequently, the collision of the Anatolide-Tauride Block with the Central Anatolian

Crystalline Complex (acting as an indentor) could be responsible for rotation of the western and central Anatolide-Tauride Block. Such middle Eocene to Oligocene rotation was never evidenced in Western Turkey. Since the age of the rotation is vague in the eastern Taurides, the cause of rotation remains doubtful. We envisage two possibilities: (i) for an Eocene rotation, the indentation of the southern apex of the Central Anatolian Crystalline Complex, and (ii) for an Oligo-Miocene rotation, the indentation of the Arabian Block (Figure 2.1) during its collision with the Anatolide-Tauride Block (Şengör and Yılmaz, 1981; Robertson et al., 2006). The second model can be tested as following. We argued that the 40° counterclockwise rotation in the eastern Taurides (Kissel et al., 2003) happened around a rotation pole located at the southern apex of the Central Anatolian Crystalline Complex. The sample location where rotation was evidenced (near Sariz) is thus situated ca. 200 km away from this rotation pole. Therefore this 40° rotation is equivalent to a northward displacement of ca. 140 km according to this pivot point. A similar offset has been shown for the Dead Sea Fault that accommodated ca. 110 km of sinistral strike-slip displacement (Dubertret, 1932; Quennell, 1958; Freund et al., 1968; McKenzie et al., 1970; Ben-Avraham et al., 2008). Therefore it seems likely that the eastern Anatolides-Taurides underwent rotation due to their syntaxial position regarding the Arabian-Eurasia collision, as already evoked by Hempton (1987) and Koçyiğit and Beyhan (1998).

2.6. Conclusion

In the present paper, we demonstrate that the entire Afyon Zone, representing a coherent passive margin sequence, underwent subduction-related H*P*-L*T* metamorphism between late Cretaceous and early Cenozoic times. The Tavşanlı Zone and the Afyon Zone are both H*P* units running from north of the Menderes Massif to south and east of the Central Anatolian Crystalline Complex. The continuity of this Anatolide H*P* belt indicates that the northern passive margin of the Anatolide-Tauride Block was dragged into an intra-oceanic subduction zone, continuous from the Izmir-Ankara to the Inner-Tauride oceanic branches of the northern Neotethys. Suturing of this oceanic domain welded the Anatolide-Tauride Block to the Pontides in Western Turkey and to the Central Anatolian Crystalline Complex in Central Turkey (Figure 2.5). As a result of the Eocene collision, the Anatolides were bent around the southern apex of the Central Anatolian Crystalline Complex, leading to the formation of the eastern limb of the Isparta Angle. In Western Turkey, syn-compressional uplift of the Menderes Massif as a dome led to the transport of the H*P* metamorphic Ören Unit towards south and to the imbrication of the Lycian Nappes, up to Miocene times. Then Neogene extensional tectonics triggered by the opening of the Aegean Domain contributed to the rotation of the western limb of the Isparta Angle.

Chapter 3

Multistage growth of Fe-Mg-carpholite and chloritoid, from field evidence to thermodynamic modelling

Abstract

Low-grade high-pressure metasediments from western Anatolia contain well-preserved carpholite-chloritoid assemblages that offer a great opportunity to improve our understanding of prograde phase relations in the FMASH system. We led a thorough inspection of petrographic texture, minute variations in mineral compositions and Mg-Fe distribution among carpholite-chloritoid assemblages. Our observations bring evidence of multistage growth of Fe-Mg-carpholite and chloritoid, which display a progressive enrichment in Mg. This compositional changes and the partial transition from Fe-rich carpholite to Fe-Mg-carpholite with Fe-rich chloritoid represent a prograde succession of assemblages of the low-grade blueschist facies. Then, using an updated thermodynamic database, including new data for ferro-carpholite, we calculated phase diagrams for theoretic and natural compositions in the FMASH system. This allows us to decipher the meaning of observed mineral assemblages and mineral compositions in terms of *P-T* changes.

3.1. Introduction

Given continuous exposure along former plate boundaries, high-pressure metasediments constitute key records of burial and exhumation of the continental margin in subduction zones. However, although greenschist, amphibolite, granulite and eclogite facies phase relations in the KFMASH system are rather well understood (e.g., Kons and Thompson, 1985; Spear, 1993; McDade and Harley, 2001; Wei et al., 2004), phase relations in blueschist-facies metasediments still needs significant improvements. Fe-Mg-carpholite (hereafter 'carpholite' or 'Car') was identified as the index mineral of the blueschist facies in the (K)FMASH system, which was long thought to lack any (Goffé et al., 1973; Chopin and Schreyer, 1983). Carpholite occurs generally in quartz segregations in aluminous metapelites, in many Tethyan belts, as well as Indonesian, New Caledonian and China, and more rarely as a rock-forming mineral in metabauxites, metasediments, quartz metaconglomerates and pelitic layers in marbles (e.g., Goffé, 1982; Goffé et al., 1988; Theye et al., 1992; Black et al., 1993; Agard et al., 2001; Rimmelé et al., 2003b; Candan et al., 2005; Trotet et al., 2006; Verlaguet et al., 2011).

Carpholite-bearing quartz veins derive from a fluid phase stemmed from the local country-rock itself (Henry et al., 1996) at the transition from middle- to high-pressure (at low temperature) conditions, by the breakdown reactions: chlorite + kaolinite or pyrophyllite = carpholite + quartz + water, or pyrophyllite + chlorite = carpholite + quartz + water (Chopin and Schreyer, 1983; Vidal et al., 1992). Early works showed that carpholite represents early grades of a high-pressure, low-temperature metamorphic mineral sequence (e.g., Chopin and Schreyer, 1983). Successive assemblages of the

FMASH system along a blueschist-facies path are: 1) Fe-rich-carpholite; 2) Fe-Mg-carpholite ± ferro-chloritoid; 3) Mg-rich carpholite + Fe-rich chloritoid; 4) magnesio-carpholite + Fe-Mg-chloritoid + kyanite; 5) Fe-Mg chloritoid + kyanite ± Fe-rich staurolite, where the prefixes "ferro-" and "magnesio--" refer to contents greater than 90 % in Fe and Mg, respectively, and the terms "Fe-rich", "Fe-Mg" and "Mg-rich" refer to the X_{Mg} (= $Mg/(Fe^{2+}+Mn+Mg)$) lesser than 0.3, between 0.3 and 0.7 and greater than 0.7, respectively. At fixed bulk rock composition, the Mg-content of ferromagnesian minerals thus increases with metamorphic conditions, as evidenced by experiments (Chopin and Schreyer, 1983) and natural cases from Crete (Theye et al., 1992) and the Betics (Azañón and Goffé, 1997).

Carpholite and carpholite-chloritoid assemblages thus are characteristic for blueschist-facies conditions. With increasing temperature, carpholite is replaced by chloritoid through the continuous reaction carpholite = chloritoid + quartz + water, which is switched towards higher temperatures as carpholite Mg/Fe ratio increases (Theye et al., 1992; Vidal et al., 1992). This reaction is strongly temperature-dependent, rendering the understanding of carpholite-chloritoid assemblages a key challenge for constraining the thermal evolution of high-pressure aluminous metapelites. Previous studies noticed that Mg and Fe are strongly partitioned between carpholite and chloritoid in textural equilibrium ($7 < KD < 9$; where $K_D(Car/Ctd) = (Mg/Fe^{2+})_{Car}/(Mg/Fe^{2+})_{Ctd}$) (Goffé, 1982; Theye et al., 1992; Vidal and Theye, 1996). Large variations of the (Fe,Mg)-substitution in carpholite reported by some studies (El-Shazly, 1995; Goffé, 1982) point out that calculating partitioning coefficient between coexisting phases requires a thorough petrographic inspection (see Vidal and Theye, 1996). Bearing in mind the common use of Mg-Fe exchange between ferromagnesian phases (e.g., garnet-clinopyroxene; Ellis and Green, 1979; garnet-biotite; Ferry and Spear, 1978; chlorite-chloritoid; Vidal et al., 1999) for geothermometry, it appears crucial to evaluate the sensitivity of $K_D(Car/Ctd)$ to *P* and *T* metamorphic conditions.

In Western Turkey, the good preservation of carpholite-chloritoid assemblages at the base of a metamorphosed Mesozoic passive margin sequence (Candan et al., 2005; Pourteau et al., 2010, 2011b) offers a great opportunity to improve our understanding of the prograde phase transitions in aluminous metasediments. We carry out detailed petrographic observations at macroscopic to microscopic scales. Based on the use of new and refined thermodynamic data, we further present results of thermodynamic phase modelling in order to interpret our petrographic observations and estimate metamorphic *P-T* conditions in the study area.

3.2. Petrography

We present here detailed descriptions of textural and compositional features at various scales observed in carpholite-bearing quartz veins, as well as beige and silvery carpholite-bearing phyllites from the Afyon Zone in western Turkey. Based on the close link between textures and changes in mineral compositions we present results of thermodynamic modelling reliably phase relations in the FMASH system.

3.2.1. Regional context

During the last decade, carpholite assemblages were found in various tectonic zones along the Anatolian segment of the Neotethyan closure realm. Widespread carpholite-bearing assemblages were discovered, from west to east, in the Ören Unit (Oberhänsli et al., 2001; Rimmelé et al., 2003a, 2006), the Menderes Massif (Rimmelé et al., 2003b), the Afyon Zone (Candan et al., 2005; Pourteau et al., 2010) and the Bitlis Massif (Oberhänsli et al., 2010, 2011). In these units, carpholite formed in Permo-Triassic metasediments like aluminous metapelites, metaconglomerates and impure marbles.

Among these units, the Afyon Zone (Figure 3.1) comprises the largest diversity of carpholite-bearing rock types. There, carpholite was reported as typical fibres in metamorphic quartz veins in dark reddish phyllites, and as fan- or rosette-shaped aggregates in aluminous metasediments from a clastic sequence ranging from conglomerates to sandstones and siltstones. Carpholite-bearing quartz veins occur all along the Afyon Zone, whereas the others are exclusively found in the Afyon area (Candan et al., 2005; Pourteau et al., 2010) (Figure 3.1). *P-T* estimation showed that carpholite rocks were retrogressed through 0.5-0.7 GPa and ca. 350°C in the westerly Kütahya region, and 0.85 GPa and 400°C in the easterly Yahyalı region (Pourteau et al., 2011b).

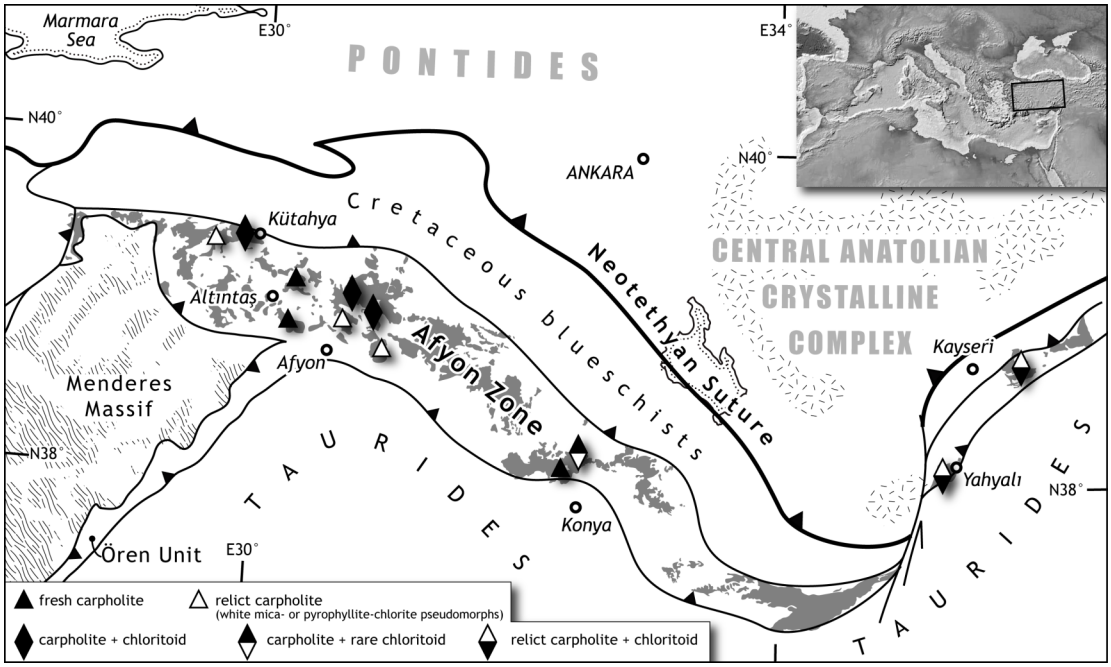

Figure 3.1: Distribution of the carpholite assemblages in the Afyon Zone (plain grey areas). The Pontides and the Central Anatolian Crystalline Complex were parts of the upper plate above the north-dipping subduction zone. The Taurides represent the fold-and-thrust foreland. Unit contours are from Pourteau et al. (2011b).

3.2.2. Analytical procedure

We inspected minute petrographic textures and mineral relations in carpholite-chloritoid bearing rocks from the Afyon Zone. Qualitative compositional variations of carpholite and chloritoid are first described by variation of molecular weight (back-scattered electron imaging; the terms 'light'

and 'heavy' designating Mg- and Fe-rich mineral compositions, respectively), and then quantified as ferromagnesian substitution (electron microprobe analysis). Mineral compositions were measured on an electron microprobe JEOL8500 (University of Potsdam), using the standards pyrope for Si and Al, rutile for Ti, hyperstene for Fe, fayalite for Mn, diopside for Mg and Ca, anorthite for Na and microcline for K. Operating conditions for spot analyses and element maps were 15 kV accelerating voltage, 1-5 µm beam size, 150 nA beam current, for 10 s on peak and 5 s on background.

Carpholite structural formula, $(Fe,Mn,Mg)Al_2Si_2O_6(OH)_4$, was calculated on the basis of 8 oxygens. Fe^{3+} (= 2 – Al) and Fe^{2+} (= Fe_{total} – Fe^{3+}) contents were calculated following Goffé and Oberhänsli (1992). Only analyses with oxide sum between 85 and 90 wt % were retained. The structural formula of chloritoid, $(Fe,Mn,Mg)_2Al_4Si_2O_{10}(OH)_4$, was calculated on the basis of 12 oxygens. Fe^{3+} (= 4 – Al) and Fe^{2+} contents were calculated following Chopin et al. (1992). Only analyses with oxide sum between 90 and 94 wt% were retained.

In the following, carpholite and chloritoid compositions are expressed in terms of X_{Mg} (=$Mg/(Fe^{2+}+Mg+Mn)$). The Mg-Fe distribution between carpholite and chloritoid is discussed in terms of an apparent partitioning coefficient (K_D) calculated as $(Mg/Fe^{2+})_{Car}/(Mg/Fe^{2+})_{Ctd}$.

3.2.3. Outcrop, sample and thin section observation

3.2.3.1. Quartz veins

Mesoscopic description. Quartz veins represent the most common carpholite-bearing rock type in the Afyon Zone. They are observed in fine-grained, dark reddish phyllites that exhibit tiny black dots of chloritoid, and scarce patches of beige phyllosilicates at mesoscopic scale. Carpholite is frequently recognized in the field as greyish-greenish hair-like fibres, which obviously grew coevally with quartz. At sample scale carpholite fibre bunches, which locally reach up to 15 cm in length, are generally parallel to each other, but may vary strongly in orientation on a single outcrop due to multistage vein crystallization, as well as late deformation (e.g., isoclinal folding; Bousquet et et al., 1998; Wiederkehr et al., 2008).

Microscopic description. Under the optical microscope, carpholite appears as typical bunches of long and thin fibres that are parallel with quartz sub-grains, and as isolated tiny needles within quartz. Carpholite preservation in quartz veins varies at the regional scale (Figure 3.1). Carpholite in quartz veins is well preserved in the Altıntaş and Konya areas, while it is moderately to strongly retrogressed in the Kütahya, Yahyalı and Kayseri areas. In such-highly retrogressed samples, tiny needles of carpholite are still preserved within quartz, while larger fibres were totally pseudomorphosed into retrograde assemblages: chlorite + pyrophyllite or, more rarely, chlorite + white mica ± chloritoid.

Several samples containing well-preserved carpholite (Table 3.1) exhibit textural evidence for two stages of carpholite growth (Figure 3.2a). Hair-like carpholite fibres grown parallel to elongated quartz subgrains represent a well-preserved, primary association. This is affected by discrete, brittle stretching that opened cracks filled with a second generation of carpholite and quartz (Figure 3.2a). This second generation consists of carpholite, which is oblique to the primary carpholite, and sub-

euhedral quartz grains. These two generations are therefore well distinguished texturally. The process responsible for opening a carpholite-quartz vein in micaschists was repeated to form these two textural generations of carpholite.

Chloritoid was only observed in one sample among those containing several textural generations of carpholite. This sample (Kon0305) contains very scarce chloritoid crystals (a few grains of 100 µm length per thin section), isolated or aggregated into rosette structures. It notably occurs in parts of the sample that are rich in iron oxide. The fact that chloritoid laths are oriented rather parallel to nearby carpholite fibres suggests coeval growth, i.e., textural equilibrium. Beside quartz, carpholite, chloritoid and iron oxide no other phase is observed.

Table 3.1: Mineral assemblages in investigated samples. Rock type abbreviations: S.Ph., silvery phyllite; B.Ph., beige phyllite.

Sample	Location	rock type	Qtz	Car	Ctd	Chl	Sud	Ck	Phg	Prg	Prl
AFY0212	Kütahya	vein	●	○	○	+	-	-	+	-	○
BAY0851	Afyon	S.Ph.	●	○	○	-	-	-	○	-	○
01-408/10	Afyon	S.Ph.	●	○	○	-	-	-	○	-	○
AFY0800	Afyon	B.Ph.	-	●	○	-	+	+	●	-	●
KON0305	Konya	vein	●	●	+	-	-	-	-	-	-
KON0803	Konya	vein	●	●	-	○	-	-	-	○	-
YAH04	Yahyalı	vein	●	+	○	○	-	-	○	-	-
KAY0801	Kayseri	vein	●	+	○	○	-	-	○	-	-

● > 20 vol. % ○ 2-20 vol. % + < 2 vol. % - not seen

The sample Afy0212 from the Kütahya area contains carpholite, chloritoid and pyrophyllite, and quartz (Figure 3.2b). Carpholite and bow-tie-shaped chloritoid are intimately associated. Pyrophyllite occurs as large crystals that wrap carpholite-chloritoid associations. Local textures suggest that elongated chloritoid-pyrophyllite associations might represent pseudomorphs after carpholite. However chlorite seems absent (Table 3.1). In other parts, well-preserved carpholite accompanied by chloritoid demonstrates that, at thin-section scale, carpholite can be variously preserved. Optical microscopy however does not allow deeper inspection of the phase relations.

The samples Kay0801 (Kayseri area) and Yah04 (Yahyalı area) only contain isolated tiny carpholite needles within quartz. Chlorite and white mica are abundant as complex intergrowths of 100-µm large crystals. In some parts of the samples, chloritoid laths are present within chlorite-mica complexes. Theses samples clearly exhibit carpholite and chloritoid in textural disequilibrium.

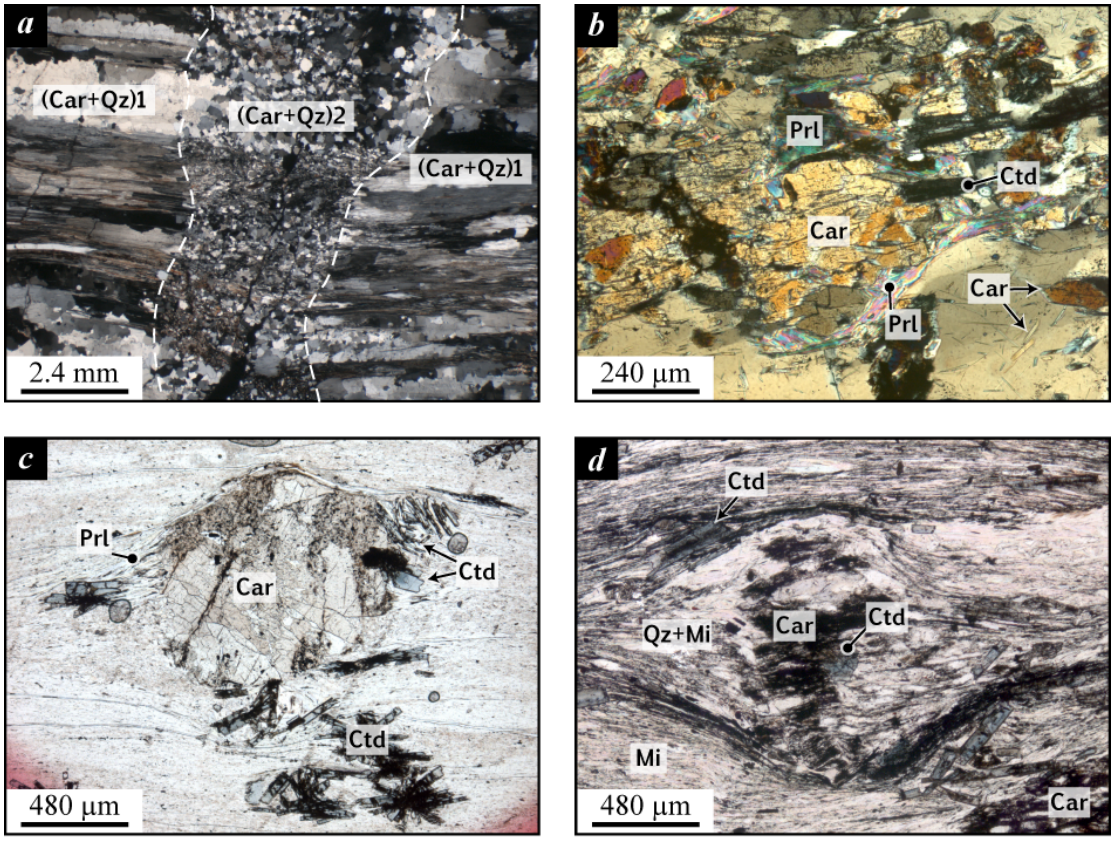

Figure 3.2: Microphotographs of carpholite-bearing assemblages. a) Vein displaying two textural generations of carpholite-quartz growth (Kon0305). b) Carpholite-chloritoid-pyrophyllite assemblage in a quartz vein (Afy0212). c) Typical occurrence of carpholite in the beige phyllite (Afy0800). Note the pressure shadows around carpholite porphyroblasts and the ubiquity of chloritoid in various textural positions. d) Coexisting carpholite and chloritoid in silvery phyllite (Bay0851). Note color variations in (001)-parallel chloritoid grain. Abbreviations: Car, carpholite; Ctd, chloritoid; Mi, white mica; Prl, pyrophyllite; Qz, quartz.

3.2.3.2. Beige phyllite

Mesoscopic description. Near Bayat, in the Afyon area, carpholite is found as a rock-forming mineral in kaolinite-rich rhyolitic tuffs (Candan et al., 2005). A carpholite-bearing beige phyllite is interlayered with horizons of massive beige phyllosilicates, and chloritoid-bearing micaschist. Carpholite occurs as dark green rosette aggregates that reach up to 10 mm across, while chloritoid is observed as tiny black laths. The carpholite abundance varies widely at mesoscopic scale. In some horizons it represents more than half the rock volume. This is evidence for the key role of bulk rock composition in metamorphic mineral assemblages formed.

Microscopic description. Carpholite from the beige phyllite is stained by iron oxide and contains inclusions of sheet silicates (abundant) and chloritoid (rare). Tabular and bow-tie chloritoid crystals, which are ubiquitous in carpholite-bearing horizons, occur (i) isolated in the matrix, (ii) in contact with carpholite aggregates, (iii) as inclusions in carpholite, and (iv) within pressure shadows developed around carpholite aggregates (Figure 3.2c). Chloritoid is wrapped by the matrix foliation and widely affected by weathering. The matrix is composed of fine-grained colourless phyllosilicates and tiny iron oxide grains. Around carpholite rosettes, asymmetric sigmoids of white phyllosilicates

formed coevally with the foliation, creating pressure shadows. These allowed the preservation of chloritoid with white phyllosilicates. These phyllosilicates are rather coarse-grained and elongated parallel to the main foliation at outer parts of the pressure shadows, and very fine-grained and unoriented in the inner parts, as well as between carpholite prisms.

Strikingly neither quartz nor chlorite were observed by optical microscopy.

3.2.3.3. Silvery phyllite

Mesoscopic description. Carpholite-bearing silvery phyllite crops out near Bayat, in the Afyon region, close to the beige phyllite. It also represents the matrix of coarser sediments like quartz conglomerates, in which carpholite rosettes can reach up to 10 cm across (Candan et al., 2005). In the phyllite, carpholite is seen as fan-shaped, dark-brown aggregrates (up to 1-2 mm in size) in a fine-grained matrix containing small patches of beige phyllosilicates and scarce, tiny chloritoid dots.

Microscopic description. Optical microscopy reveals that the silvery phyllite is a quartz micaschist, made of carpholite and chloritoid aggregates in a matrix of fine-grained white phyllosilicates, quartz, iron oxides, and detrital tourmaline. Carpholite aggregates, forming round-shaped complexes up to 5 mm across, are intimately associated with quartz, and accompanied by chloritoid at the rims. Carpholite is stained by abundant, dense nets of iron oxides, as described in samples from other regions (e.g., Theye et al., 1992). Locally, these nets delimitate round-shaped areas, free of iron oxides that can be regarded as relict nucleation sites of carpholite. Other inclusions in carpholite are scarce white phyllosilicates. Chloritoid is abundantly present in the schistous matrix and forms tabular, bow-tie, and rosette crystals. These are variously oriented in respect to main schistose, which is defined by white phyllosilicates. Late shear planes (C-type) are associated to phyllosilicates recrystallization.

3.2.4. Electron microscopy and mineral compositions

3.2.4.1. Quartz vein

Electron microscopy

Multistage carpholite growth. Samples showing two generations of carpholite were investigated using a back-scattered electron (BSE) imaging system of the electron microprobe. Microtextures and molecular weight variations reveal a multitude of carpholite growth stages. In some samples, BSE imaging shows that carpholite was affected by discrete cracks that were filled with consistently lighter carpholite, which was in turn cracked, allowing the growth of even lighter carpholite (Figure 3.3a). These structures are in line with observations by optical microscope (Figure 3.2a), but cracking is even evidenced in carpholite of the first textural generation. Carpholite was thus progressively enriched in Mg. The transition from rather ferrous to more magnesian carpholite was achieved through multiple discrete stages of intermediate compositions, which are barely distinguishable from each other. The sample Kon0305 illustrates that cracking can be diffusely distributed.

Coexisting carpholite-chloritoid. In the sample Kon0803, compositional variations indicate that cracking was accompanied by a progressive increase of Mg-content in carpholite, which occurred at the scale of some micrometres (Figure 3.3a), in contrast to the cracks of several millimetre width observed in Kon0305 (Figure 3.2a). More magnesian carpholite mostly grew parallel to pre-existing fibres. In Kon0305, chloritoid is observed as rare laths mostly among secondary carpholite, but it occasionally appears in textural equilibrium with carpholite of various compositions. Since in these cases it was not affected by stretching, chloritoid formed after the primary carpholite and likely coevally with the second generation. Moreover, BSE imaging displays that chloritoid composition varies between and among aggregated crystals.

In Afy0212, electron microscope discloses that the coexistence of carpholite and chloritoid clearly corresponds to a frozen reaction (Figure 3.3b). Carpholite is partly replaced by intimately associated quartz and bow-tie aggregates of chloritoid. Carpholite cores display a homogeneous molecular weight, but rims often consist of several overlapped fringes of lighter carpholite, suggesting a succession of abrupt enrichments in Mg (Figure 3.3b). Pyrophyllite and scarce white mica, which occurs as thin layers within pyrophyllite (Figure 3.3b), or as tiny (~10 µm long) single crystals, grew over carpholite zoning. Chlorite is observed in trace amount in contact with carpholite, or occasionally associated with pyrophyllite as pseudomorphs after chloritoid bow-tie crystals. The growth of mica and chlorite occurred during late retrograde stages likely as results from limited fluid circulation through the rock. Chlorite and pyrophyllite are therefore not part of the high-pressure metamorphic assemblage, which in the quartz veins is only composed of carpholite, chloritoid and quartz.

Mineral compositions

Mineral composition analysis with the electron microprobe might be biased by any eventual abrupt change in mineral composition immediately below the thin-section surface under observation. Therefore, we foresee the possibility to obtain intermediate compositions for carpholite and chloritoid exhibiting abrupt chemical changes at the scale of some micrometres. This analytical limit might also have attenuated extreme values.

In Kon0305, X_{Mg} ratios of primary and secondary carpholite range between 0.52 and 0.56, and between 0.60 and 0.67, respectively (see Table 3.2). In the same way, in Kon0803, they vary from 0.64 to 0.67, and 0.67 to 0.72, respectively. In Afy0212, X_{Mg} ratios of primary carpholite ranges between 0.27 and 0.35, with a frequency peak around 0.31, and that of secondary carpholite covers a distinct range between 0.39 and 0.54, with a frequency peak around 0.51. Microprobe analyses thus show that variations in carpholite composition are significant (difference in X_{Mg} up to 0.15) and consistently directed towards higher Mg-contents. It can be noted that carpholite from the Konya area is generally more Mg-rich than from the other areas of the Afyon Zone. Highly retrogressed carpholite from the samples Yah04 and Kay0801 has an X_{Mg} ranging from 0.34 to 0.39, and from 0.26 and 0.33, respectively.

X_{Mg} ratios in chloritoid range from 0.15 to 0.19 in Kon0305, from 0.07 to 0.11 in Afy0212, from 0.12 to 0.15 in Yah04, and from 0.08 to 0.14 in Kay0801. Concerning Afy0212, no link between the composition and the textural occurrence of chloritoid could be established.

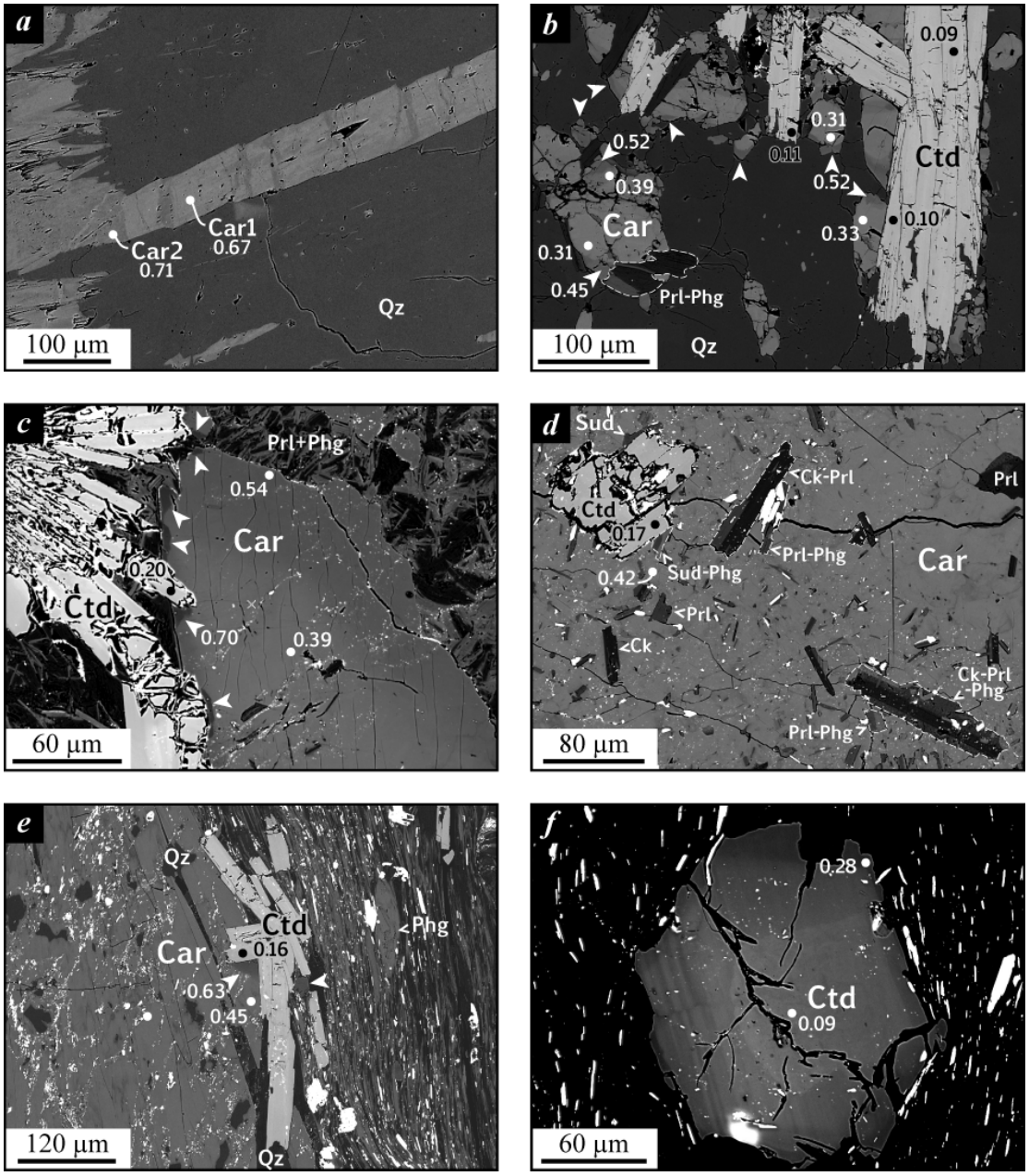

Figure 3.3: Back-scattered electron images of carpholite-bearing assemblages and X_{Mg}-values of carpholites and chloritoids measured locally (mineral analyses in Table 3.2). a) Cracking of carpholite in a quartz vein (Kon0803). b) Frozen state of the reaction carpholite = chloritoid + quartz + water in a vein (Afy0212). The arrows indicate discontinuous zoning. c) Continuously-zoned carpholite overgrown by chloritoid and Mg-rich carpholite fringes (arrows) in the beige phyllite (Afy0800). d) Mineral inclusions in carpholite of the beige phyllite (Afy0800). Note that chloritoid is associated with sudoite, and that phyllosilicate inclusions are made of interlayered pyrophyllite, cookeite, white mica and sudoite. e) Continuously zoned carpholite overgrown by chloritoid accompanied by Mg-rich carpholite (arrows) in silvery phyllite (01/408-10). f) Concentric zoning of chloritoid (same as in the Figure 3.4b) with progressive outward decrease of the molecular weight in silvery phyllite (Bay0851). Molecular weight increases following this order: Cookeite < pyrophyllite < quartz < sudoite < magnesio-carpholite < K-white mica < ferro-carpholite < chloritoid < iron oxides.

Table 3.2: Representative mineral analyses.

Sample	Kon0803		Afy0212			Afy0800				01-408/10			Bay0851	
Key feature	Discontinuous zoning		Discontinuous zoning			Discontinuous and continuous zoning			Inclusions in carpholite			Discontinuous zoning			Continuous zoning	
Mineral	Car1	Car2	Car1	Car2	Ctd	Car1 core	Car1 rim	Car2	Ctd	Car	Ctd	Sud	Car1	Car2	Ctd	Ctd core	Ctd rim
SiO2	38.664	39.014	37.489	37.937	24.342	37.806	38.306	40.658	24.567	37.78	24.137	33.046	37.576	38.321	24.505	24.279	24.968
TiO2	0.144	0.166	0.194	0.109	0.000	0.149	0.059	0.076	0.000	0.102	0.011	0.020	0.100	0.085	0.06	0.015	0.006
Al2O3	31.094	31.839	30.932	31.711	41.004	30.617	30.837	32.953	40.724	31.633	39.737	35.137	30.846	31.712	40.347	38.84	41.429
FeO	8.089	6.907	16.515	10.984	27.341	14.465	11.18	7.487	23.769	13.601	25.836	5.180	12.45	9.091	25.147	27.873	21.098
MnO	0.596	0.431	0.032	0.050	0.005	0.076	0.145	0.098	0.303	0.089	0.270	0.021	0.274	0.167	0.324	0.199	0.298
MgO	8.063	8.582	3.661	6.349	1.246	4.699	6.381	8.571	3.182	5.285	2.786	11.866	5.456	7.838	2.645	1.509	4.589
CaO	0.004	0.004	0.001	0.000	0.000	0.009	0.007	0.010	0.006	0.007	0.006	0.057	0.012	0.000	0.009	0.007	0.004
Na2O	0.026	0.004	0.028	0.054	0.033	0.021	0.000	0.024	0.015	0.000	0.014	0.008	0.020	0.015	0.01	0.000	0.037
K2O	0.035	0.029	0.006	0.014	0.005	0.007	0.017	0.026	0.002	0.053	0.013	0.022	0.014	0.028	0.007	0.011	0.033
Total	86.715	86.976	88.858	87.208	93.976	87.849	86.932	89.925	92.593	88.55	92.81	85.391	86.748	87.257	93.054	92.733	92.462
Si	2.04	2.03	2.01	2.01	2.00	2.03	2.04	2.05	2.02	2.00	2.00	3.08	2.02	2.01	2.02	2.04	2.02
Ti	0.01	0.01	0.01	0.00	0.00	0.01	0.00	0.00	0.00	0.00	0.00	0.00	0.00	0.00	0.00	0.00	0.00
Al total	1.93	1.96	1.95	1.98	3.97	1.94	1.94	1.96	3.94	1.98	3.89	3.86	1.96	1.96	3.92	3.84	3.96
Fe2+	0.28	0.25	0.69	0.46	1.85	0.58	0.43	0.27	1.58	0.57	1.68	0.40	0.51	0.36	1.65	1.80	1.39
Fe3+	0.08	0.05	0.05	0.02	0.03	0.07	0.07	0.05	0.06	0.03	0.11	0.00	0.05	0.04	0.08	0.16	0.04
Mn	0.03	0.02	0.00	0.00	0.00	0.00	0.01	0.00	0.02	0.00	0.02	0.00	0.01	0.01	0.02	0.01	0.02
Mg	0.63	0.67	0.29	0.50	0.15	0.38	0.51	0.64	0.39	0.42	0.34	1.65	0.44	0.61	0.32	0.19	0.55
XMg	0.67	0.71	0.30	0.52	0.08	0.39	0.54	0.70	0.20	0.42	0.17	0.80	0.45	0.63	0.16	0.09	0.28

3.2.4.2. Beige phyllite

Carpholite from the beige phyllite is strikingly zoned. Continuous zoning is observed as a unidirectional decrease of molecular weight from core to rim at the scale of carpholite needles (Figures 3.3c, 3.4). Fe-Mg profiles were measured from rim to rim along this chemical gradient (Figure 3.4a). The inner part of the carpholite crystal has a homogeneous composition with X_{Mg} around 0.42. Outwards, the Mg-content linearly increases and reaches a narrow plateau at 0.51. These profiles illustrate the existence of a continuous, unidirectional compositional zoning of carpholite. Throughout the thin-section, continuously zoned carpholite yielded X_{Mg} ranging from 0.35 in the innermost parts of fan-shaped aggregates, to 0.54 at crystal rims, with frequency peaks around 0.40-0.45 and 0.51-0.53. On the other hand, distinctively lighter fringes overgrow obliquely this continuous zoning gradient at crystal rims, constituting discontinuous zoning (Figure 3.3c). They account for a significant jump to X_{Mg}-values between 0.67 and 0.73. Carpholite thus grew along two successive zoning patterns, leading to its progressive enrichment in Mg.

Chloritoid rosette aggregates, in contact with carpholite, are locally so abundant that they overlap each other, resulting in complex textures. In such aggregates, compositional variations can cover the full range of X_{Mg} obtained at the thin-section scale. The overall chloritoid composition scatters widely between 0.09 and 0.23 in X_{Mg} with two frequency peaks around 0.11-0.14 and 0.20-0.23. Chloritoid locally grew over carpholite, in association with light Mg-rich carpholite fringes (> 0.69) (Figure 3.3c). In such site, compositions with among the highest X_{Mg}(Ctd) were measured (0.19-0.23). Chloritoid inclusions in carpholite, which are locally associated with sudoite, present a corroded aspect that indicates that chloritoid existed prior to carpholite formation (Figure 3.3d). Although chloritoid inclusions are rare, their composition is rather scattered, with $0.12 \leq X_{Mg} \leq 0.18$, and independent from surrounding carpholite X_{Mg}.

Fine-grained sheet silicates occur in the inner parts of the pressure shadows and between carpholite prisms as tiny, randomly oriented, intergrowth of pyrophyllite and white mica (Figure 3.3c). In contrast, larger phyllosilicates exposed to stronger shearing (i.e., at the edge of sigmoids; Figure 3.2c) are pyrophyllite, accompanied by smaller white mica crystals. While the former seem in equilibrium with carpholite, the latter likely grew as breakdown products (Figure 3.3c). Although white mica is generally too small for electron-microprobe analysis, a few reliable measurements could be performed. White mica compositions are commonly rich in muscovite (> 80%) and pyrophyllite (15-20%), and poor in celadonite (0-5 %). Micas occurring between prisms of carpholite rosette aggregates display significantly higher celadonite-content, with Tschermak substitution reaching up to 17%.

Phyllosilicate inclusions in carpholite are pyrophyllite, white mica, cookeite, and sudoite that consist of either monomineralic or composite grains. Composite grains are made of interstratified pyrophyllite-cookeite, pyrophyllite-cookeite-white mica, cookeite-sudoite and white mica-sudoite (Figure 3.3d). Included white mica compositions are mostly a mix of muscovite (> 80%) and pyrophyllite (15-20%) with very low celadonite-content (0-3 %). Cookeite ($LiAl_4AlSi_3O_{10}(OH)_8$), which was previously reported from many carpholite-bearing terranes (Goffé et al., 1996; Jullien et al., 1996), is widespread within carpholite and absent in the rock matrix. Cookeite represents the only Li-bearing phase of the rock. Rare sudoite, which is the only Fe-Mg chlorite representative in the beige

phyllite, is associated with chloritoid, or interlayered with cookeite or white mica. Sudoite analyses provide constant X_{Mg}-values of 0.80, similar to those commonly reported from carpholite-bearing rocks (Goffé et al., 1988; Theye et al., 1992; Azañón and Goffé, 1997; Rimmelé et al., 2003b). Iron oxides, also ubiquitous in the matrix, are distributed as "nets" that extend continuously across mineral boundaries. Iron oxides did not participate to the carpholite growth and breakdown reactions. Quartz and trioctahedral chlorite are strikingly absent in the beige phyllite.

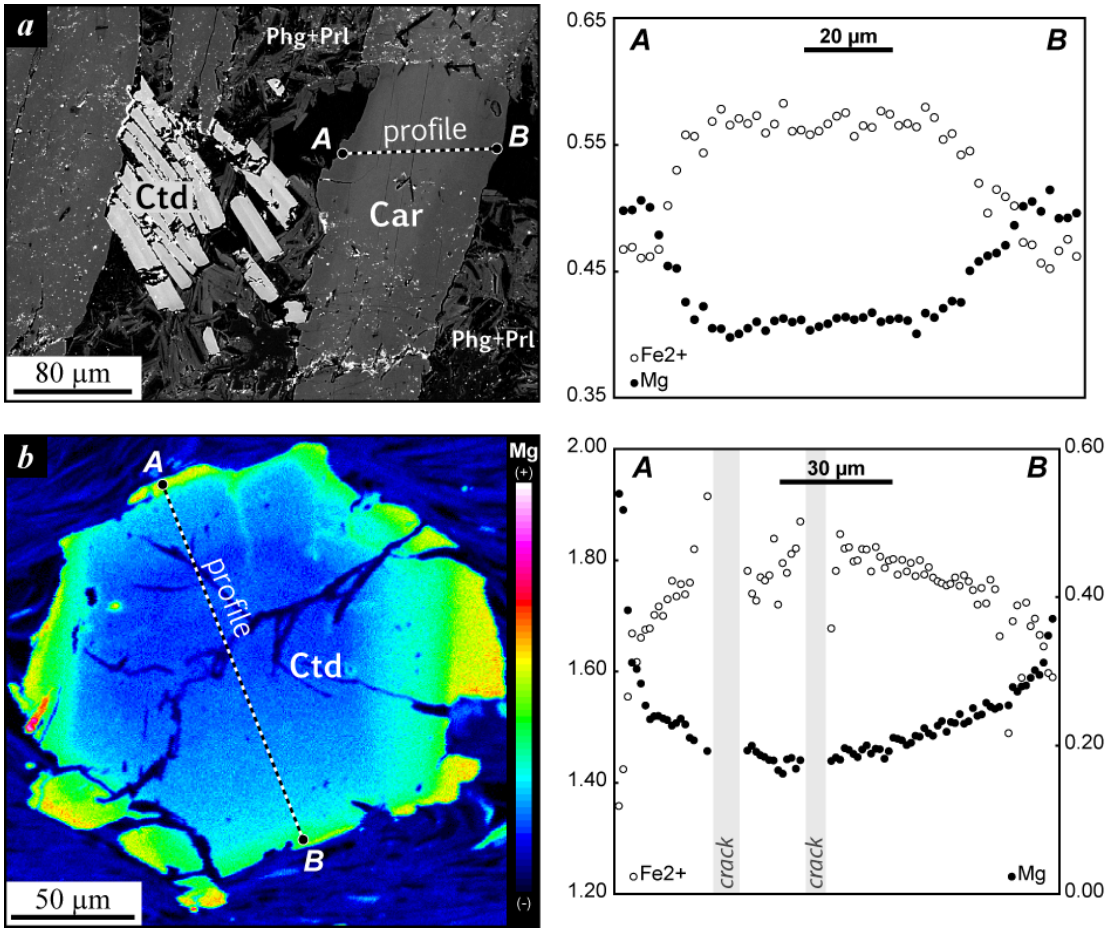

Figure 3.4: Compositional variations in a) carpholite: left, BSE image; right, Fe^{2+}- and Mg-profiles (beige phyllite, Afy0800) and b) chloritoid: left, Mg chemical map; Fe^{2+}- and Mg-profiles (silvery phyllite, Bay0851).

3.2.4.3. Silvery phyllite

In the silvery phyllite, both carpholite and chloritoid are significantly zoned.

On back-scattered electron images, carpholite generally presents a uniform molecular weight, confirmed by rather homogenous X_{Mg} (0.42-0.49 in 01-408/10; 0.52-0.55 in Bay0851). Pronounced increase of Mg-content at the rim of carpholite crystals (Figure 3.3e), similar to the beige phyllite, is also common in the silvery phyllite samples. These rims account for a jump of X_{Mg} to 0.63-0.70 in 01-408/10, and 0.73-0.75 in Bay0851. Primary and secondary carpholite generations therefore are clearly of distinct compositions.

Like in the beige phyllite, chloritoid also grew at the expense of carpholite, in association with discontinuous carpholite zoning (Figure 3.3e). In this setting, chloritoid generally yields $X_{Mg} \geq 0.15$. Chloritoid crystals are commonly zoned. Two significant zoning patterns are observed in chloritoid. On the one hand, chloritoid with crystal section perpendicular to (001) exhibit concentric zoning characterized by a unidirectional increase of Mg-content from core to rim (Figure 3.3f). This is not linear, nor strictly continuous, but rather displays abrupt transition between continuously zoned sectors. This onion-ring structure is perturbed by some discrete cracks filled by chloritoid of higher X_{Mg}. This concentric zoning accounts for a progressive X_{Mg}(Ctd) increase from 0.08 to 0.30. On the other hand, an abrupt enrichment in Mg is seen at the tip of numerous chloritoid laths (with crystal section oblique to (001)). This constitutes a significant outward jump from ca. 0.10 to ca. 0.20. In both silvery phyllite samples, overall chloritoid compositions range between 0.08 and 0.30.

The phyllosilicate matrix is composed of dominant white mica, as well as pyrophyllite. Both minerals are commonly intergrown. Layers of pyrophyllite in white mica are rather frequent in parts not affected by the deformation responsible for the main foliation. Pyrophyllite, which generally contains white mica interlayers, is observed as scarce inclusions in carpholite. In white mica, Tschermak substitution attains 8-17% in Bay0851 and 2-38% in 01-408/10, with a main cluster around 8-11%. In the latter sample, the celadonite-richest compositions were obtained from pre-foliation mica of the matrix. In white mica in apparent equilibrium with carpholite and quartz, Tschermak substitution amounts to 24-27 %.

Quartz, which is closely associated with carpholite, mainly formed from the breakdown of the latter. Spherical quartz “pockets” included in carpholite suggest that quartz was also present before and during carpholite growth (Figure 3.3e).

Iron oxide is ubiquitous: as dense nets of tiny grains included in carpholite and chloritoid, and as small laths in the white mica-pyrophyllite matrix. Locally, the continuity of "nets" of iron oxides through grain boundaries is preserved, though carpholite is partly replaced by chloritoid and quartz.

Detrital tourmaline and ilmenite are commonly seen as accessory phases that were not involved in the discussed metamorphic assemblages. A peculiar feature of the silvery phyllite is the absence of chlorite, already mentioned by Candan et al. (2005).

3.3. Phase relations

Element distribution within and among carpholite and chloritoid is used to decipher mineral growth and phase transition. Below, we discuss Mg-Fe distribution (“apparent K_D”) in comparison with equilibrium K_D-values established by previous studies (Goffé, 1982; Theye et al., 1992; Vidal and Theye, 1996; Vidal et al., 1999).

3.3.1. Carpholite growth and breakdown

3.3.1.1. Discontinuous X_{Mg} variations

Crack filling.

Multistage cracking of carpholite in quartz veins is associated with the growth of new carpholite grains with increasing Mg-content (Figure 3.3a). This feature probably results from the growth of carpholite from a fluid phase becoming enriched in Mg *vs.* Fe during stepwise deformation. The change of fluid composition may be related to the breakdown of a Mg-richer phase (likely chlorite) in the country rock.

Carpholite-chloritoid and Mg-Fe distribution

Discontinuous Mg-Fe zoning was observed at the rims of carpholite in quartz veins, beige phyllite and silvery phyllites. The abrupt increase of X_{Mg}(Car) is commonly associated with the growth of chloritoid at the expense of primary Fe-richer carpholite (Figures 3.3b, 3.3c, 3.3e). It represents an early stage of the progressive replacement of Fe-rich carpholite, through the reaction: Fe-Mg-Car = Mg-rich-Car + Fe-rich-Cld + Qz + H_2O (de Roover, 1977; Chopin and Schreyer, 1983).

In previous works, carpholite-chloritoid pairs in thermodynamic equilibrium were found to yield Mg-Fe partitioning coefficients around 7-8 (K_D(Car/Ctd)). Below, these values are compared with "apparent K_D-values" calculated for the carpholite-chloritoid samples from the Afyon Zone.

The sample Afy0212 (quartz vein) contains two groups of carpholite compositions with X_{Mg}(Car1) = 0.27-0.35 and X_{Mg}(Car2) = 0.39-0.54, which corresponds to two distinct growth generations. In contrast, a single generation of chloritoid with X_{Mg}(Ctd) = 0.07-0.11 was observed, suggesting a continuum for chloritoid growth. The frequent occurrence of several successive Fe-Mg fringes at carpholite rims (Figure 3.3b) hampers retrieving exact carpholite-chloritoid pairs for the calculation of partitioning coefficients. However, combining the Fe-richest secondary carpholite and chloritoid, on the one hand, and the Mg-richest carpholite and chloritoid on the other hand, yields apparent K_D-values of 8.5 and 9.5, respectively.

The quartz vein sample Kon0305 contains two groups of carpholite compositions with X_{Mg}(Car 1) = 0.52-0.56 and X_{Mg}(Car2) = 0.60-0.67, and one group of chloritoid compositions with X_{Mg}(Ctd) = 0.15-0.19. Although chloritoid occurs surrounded by both carpholite groups, it is mainly observed among the Mg-richer carpholite (Car2), suggesting equilibrium between Car2 and Ctd. Correlating in each site chloritoid with the Mg-richer carpholite provides apparent K_D-values of 7.4-7.9. In contrast, combining local chloritoid analyses with the Fe-richer carpholite gives lower K_D-values (4.6-5.7).

In Afy0800 (beige phyllite), Mg-rich carpholite and Fe-rich chloritoid in textural equilibrium yield K_D values of 8.1-9.7. In 01-408/10 (silvery phyllite), combining locally primary carpholite and Fe-richest chloritoid, and secondary carpholite and chloritoid provides K_D-values of 7.3 -7.6 and 8.5 and 9.7, respectively. In Bay0851, K_D-values of 8.5-8.8 were obtained from carpholite and chloritoid in textural equilibrium.

Apparent K_D-values between carpholite and chloritoid in textural equilibrium consistently range between 7.4 and 9.7. Within this range, the highest values were obtained from samples containing complex carpholite growth patterns and/or zoned chloritoid. The apparent K_D-value may thus be used as a rough test for thermodynamic equilibrium, though it strongly depends on the accuracy of mineral analyses and compositional homogeneity of the analyzed minerals (in particular of chloritoid). A precise range of acceptable values for thermodynamic equilibrium conditions is difficult to assess. Nevertheless, K_D-values below 5 consistently correlated textural disequilibrium, while values of 7-10 likely prevail for equilibrium. In the case of intermediate values (5-6), apparent K_D cannot be used as a univocal marker of the thermodynamic state. Very-high K_D-values (> 10) seem in turn to indicate that the carpholite considered formed at higher temperature than the chloritoid considered.

3.3.1.2. Continuous X_{Mg} variation

Continuous Mg-Fe zoning was documented in carpholite from the beige phyllite (Afy0800), and in chloritoid from the silvery phyllite (Bay0851) (Figures 3.3, 3.4). In the beige phyllite (Afy0800), the continuous increase of X_{Mg}(Car) extends from 0.35 to 0.54 from core to rim (Figure 3.4). Chloritoid composition covers a continuous range ($0.09 < X_{Mg}(Ctd) < 0.23$.), whereas the Mg-richest chloritoid (($X_{Mg} > 0.19$) is commonly (but not exclusively) associated with Mg-rich carpholite fringes (0.67-0.74). Chloritoid composition present complex variations within crystals and among aggregates and two composition groups can hardly be distinguished. Moreover, chloritoid inclusions in carpholite likely formed along the early low-pressure prograde path, before any carpholite. Due to these patterns, the thermodynamic equilibrium cannot here be tested by calculating the apparent K_D-values.

In the silvery phyllite samples, continuous Mg-Fe zoning in chloritoid contrasts with the bimodal distribution of carpholite analyses (related to discontinuous zoning). In contrast to the beige phyllite (Afy0800), chloritoid Mg-content clearly increased through time, as shown by the consistent element zoning. We evaluate the possibility of carpholite-chloritoid equilibrium by calculating apparent K_D-values. Combining the Mg-richest chloritoid ($X_{Mg} \sim 0.30$) and carpholite ($X_{Mg} \sim 0.75$) gives apparent K_D-values of 7.2. In turn, the compositions of Fe-richest carpholite ($X_{Mg} = 0.52$ in Bay0851 and 0.42 in 01-408/10) and chloritoid (0.08 and 0.09, respectively) yield high to very-high Mg-Fe partitioning coefficient ($K_D = 12.1$ and 7.4, respectively). These values may indicate that in Bay0851 the Fe-richest chloritoid formed before the Fe-richest carpholite. Because no chloritoid inclusions occur in carpholite, we infer that primary carpholite with $X_{Mg} < 0.52$ was not preserved (or analyzed), while its chloritoid affiliate was. Despite the limits of this test and obvious calculation uncertainties, due in particular to compositional heterogeneity of the chloritoid in these samples, we assume that carpholite and chloritoid mostly grew in equilibrium, evolving coevally towards higher Mg-contents.

3.3.2. Carpholite precursors

Inclusions of sheet silicates (interlayered pyrophyllite, K-white mica, cookeite and sudoite), as well as chloritoid, in carpholite of the beige phyllite provide information about the nature of the low-

pressure precursors. The very low celadonite-content of included white mica reveal that they constitute low-pressure, prograde relics. The abundance of pyrophyllite, white mica and cookeite preserved as inclusions in carpholite suggests that these phases were in large amount compared to rarely observed chloritoid and sudoite.

Here again, Mg-Fe distribution is used to test our assumptions based on textural criteria that chloritoid inclusions grew earlier than surrounding carpholite. Mineral compositions yield low apparent K_D-values (between 2.5 and 4.1), confirming thermodynamic disequilibrium among these pairs. Where previously reported (Oman, Crete), two explanations were put forward for the formation of chloritoid before carpholite. (i) During its prograde history, the rock may have followed a rather warm subduction thermal gradient through the low-pressure part of the chloritoid stability field, and undergone subsequently rapid burial into the carpholite stability field (Goffé et al., 1988). (ii) Along a typical subduction geotherm (~ 10°C/km), chloritoid can be produced instead of carpholite even at high-pressure conditions, if the water activity is low (Theye et al., 1992). At low-temperature high-pressure conditions, variations of water activity may thus control carpholite *vs.* chloritoid appearance. The growth of cookeite before carpholite indicates high water activity along the low-pressure prograde path (Vidal and Goffé, 1991), so that the formation of chloritoid before carpholite is indicative of a "warm" prograde subduction thermal gradient (12-15°C/km).

Abundant inclusions of cookeite in carpholite points out a significant amount of Li in the beige phyllite. The origin of Li in aluminous metasediments has been discussed in several studies (Goffé, 1982; Jullien and Goffé, 1993; Poinssot et al., 1993; Verlaguet et al., 2011), who demonstrated that Li originates from the sedimentary protolith itself. The lack of any other Li-bearing phase suggests that *P-T* conditions did not exceed the stability field of cookeite, which is stable under SiO_2 saturated conditions at pressures of 0.1-1.4 GPa and temperatures of 260-480°C (Vidal and Goffé, 1991; Jullien et al., 1996).

3.3.3. Why is there nearly no quartz in the beige phyllite?

To our knowledge, the beige phyllite from the Afyon area so far is the only documented case of quartz- and trioctahedral-chlorite-free carpholite-chloritoid-pyrophyllite-phengite assemblage. The absence of quartz and chlorite are singular features for a carpholite-bearing rock. Carpholite-bearing, quartz-free rocks usually contain diaspore that balances the excess in Al_2O_3 relatively to SiO_2 (Goffé, 1982). However, diaspore is absent from our samples in general, and from the beige phyllite in particular. Bearing in mind that the structural formula of chloritoid (+ SiO_2 + H_2O) is equivalent to carpholite, the coeval growth of carpholite and chloritoid in the beige phyllite may reflect SiO_2 undersaturated conditions. Reactions that produce no quartz must be envisaged to be responsible for the formation of carpholite. The reactions sudoite + quartz = carpholite and chlorite + pyrophyllite = carpholite + quartz (Vidal et al., 1992) can likely be excluded given the absence of quartz inclusions in carpholite. Instead, the reaction chloritoid + sudoite + pyrophyllite = carpholite (Theye et al., 1997) can be expected. Although it was mentioned for quartz-bearing assemblages, stoichiometry allows it to occur in absence of quartz. Measured mineral compositions imply that 1 chloritoid (X_{Mg} of 0.12-0.18)

+ 6 sudoite (X_{Mg} = 0.8) + 1 pyrophyllite would produce 6 carpholite (X_{Mg} of 0.57-0.59) if the reaction was isochemical. But this calculated carpholite composition differs from the measured lower X_{Mg}-values (0.35-0.45), which means that iron oxide may have taken part to the reaction (as a reactant) or the reaction was not isochemical.

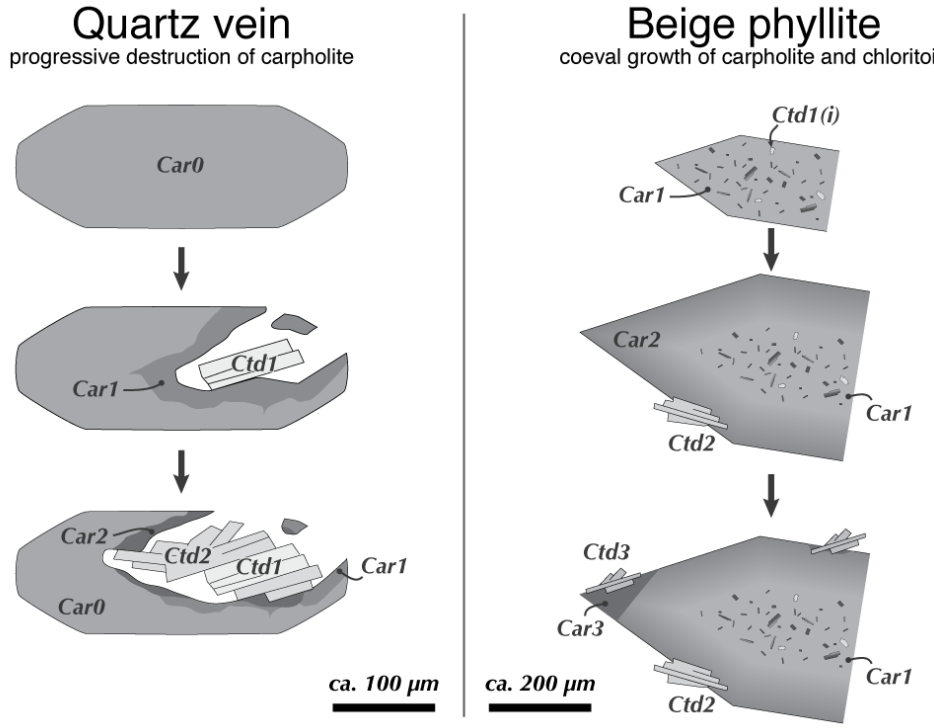

Figure 3.5: Schematic petrologic reconstruction of the successive assemblages observed in quartz vein and beige phyllite samples (Afy0212 and Afy0800, respectively). Grey level illustrates molecular weight changes as seen on back-scattered images (darker grey for Mg-richer compositions). Ctd1(i) designates chloritoid inclusions in carpholite. See text for description and discussion.

3.3.4. Summary

Our detailed inspection of carpholite-chloritoid-bearing samples allows us to better understand the relation between carpholite and chloritoid. The investigated samples encompass clear pieces of evidence for Mg-Fe growth zoning in carpholite and chloritoid, suggesting coeval growth along a prograde metamorphic path. In the beige phyllite, carpholite contains scarce, corroded chloritoid with various compositions, as hints of a rather "warm" prograde path. Primary carpholite (of Fe-rich to Fe-Mg-composition) is partially overgrown by Mg-richer, secondary carpholite and Fe-rich chloritoid (Figure 3.5), giving evidence for the progressive reaction carpholite = chloritoid + quartz + H_2O (de Roover, 1977). We showed that Mg-Fe distribution between coexisting carpholite and chloritoid can be used as a rough test of thermodynamic equilibrium, but strongly depends on the chemical homogeneity of the investigated crystals. Due to the consistent occurrence of small-scale chemical variations in carpholite and chloritoid from our samples, no exact K_D(Car/Ctd) could be measured. Nevertheless, Mg-Fe partitioning coefficients generally range between 7 and 10 between carpholite and chloritoid in textural equilibrium. Lower apparent K_D-values (< 5) are obtained between carpholite and chloritoid in clear textural disequilibrium, while very high values were obtained where chloritoid composition varies

at small scale. Mg-Fe distribution reveals that continuously zoned carpholite and chloritoid from silvery phyllites grew coevally in thermodynamic equilibrium. According to our observations in the silvery phyllite, carpholite and chloritoid equilibrated at the scale of several hundred of micrometres.

3.4. Modelling of phase relations

3.4.1. Thermodynamic data and boundary conditions

Phase diagrams for the FMASH system were calculated by Gibbs energy minimization (De Capitani and Brown, 1987) using the software TheriakDomino (De Capitani and Petrakakis, 2010). The updated JUN92.RGB thermodynamic database of Berman (1988) was used and completed with available data for magnesio-chloritoid (Vidal et al., 2001), magnesio-sudoite and magnesio-carpholite (Vidal et al., 1992) and chlorites (Vidal et al., 2006), as well as refined data for ferro-chloritoid (Vidal et al., 1999) (Table 3.3). Lack of thermodynamic data for ferro-carpholite due to too cold conditions for efficient experimental synthesis (Vidal, 1991) had so far precluded precise modelling of iron-rich phase assemblages in high-pressure aluminous metapelites. The third law standard state entropy of Fe-carpholite and its Cp(*T*) function were estimated according to the methods described by Holland (1989) and Berman and Brown (1985), respectively. The standard state formation enthalpy of Fe- and Mg carpholite, and Fe-chloritoid were then adjusted in order to reproduce the following natural data: stability of Fe-carpholite with ($0.14 \leq X_{Mg} \leq 0.97$) as reported in the literature under reasonable *T*/*P* ratios, phase relations as documented in natural examples, like the reactions Mg-rich carpholite = chlorite + kyanite + quartz in absence of chloritoid (Azañón and Goffé, 1997; Rimmelé et al., 2003b), and K_D(Car/Ctd)-values of ca. 8 at 10 kbar and 400°C (Western Crete; Theye et al., 1992). The enthalpy of Fe-chloritoid was increased by 1 kJ/mol compared to the value of Vidal et al. (1999) and that of Mg-carpholite was decreased by 3 kJ/mol compared to the values proposed by Vidal et al. (1992).

Table 3.3: Thermodynamic data used for ferro-chloritoid, magnesio-carpholite and ferro-carpholite.

		Ferro-chloritoid	Magnesio-carpholite	Ferro-carpholite
G°a	J/mol	0.00	0.00	0.00
H°f	J/mol	-3210200	-4774800	-4418010
S°	J/mol/K	162.0[(1)]	220.0[(2)]	246.7
V°	J/mol/bar	6.967[(1)]	10.590[(2)]	10.690
k1		444.369[(1)]	601.808[(2)]	620.648
k4		-3880.207[(1)]	-4505.050[(2)]	-4928.620
k3		-4869293[(1)]	-11153000[(2)]	-9748420
k8		-916326240[(1)]	-1661427000[(2)]	1554312000
v1.10^5	K^{-1}	2.618563	2.904000[(2)]	2.904000
v2.10^5	K^{-2}	0.001222	0.000000[(2)]	0.000000
v4.10^7	Pa^{-1}	-0.13053826	-0.17900000[(2)]	-0.17900000
v2.10^{12}	Pa^{-2}	0.0012584	0.0000000[(2)]	0.0000000

(1) Vidal et al. (1999); (2) Vidal et al. (1992)

The new thermodynamic data were used to calculate phase diagrams depicting the phase relations between carpholite, chloritoid, chlorite and aluminosilicates in water-saturated and quartz-saturated or –unsaturated conditions. *P-T* phase diagrams were calculated for 0.3 to 2.0 GPa, 200-550°C, and *T-X* phase diagrams were calculated for a similar temperature range at 1.0 GPa in order to model high-pressure phenomena. We hereafter use the terms "very low", "low" and "moderate" temperatures to refer to conditions below ca. 300°C (kaolinite domain), between 300 and 450°C (pyrophyllite domain) and above 450°C (kyanite domain), respectively. The term "high-pressure" refers to *T*/*P* ratios below 12°C/km (i.e., 375°C/GPa), i.e., above 0.8 GPa at 300°C and 1.3 GPa at 500°C.

3.4.2. Results

3.4.2.1. *P-T* diagram

P-T diagrams (Figure 3.6a-e) were calculated using bulk composition of carpholite-quartz vein with various X_{Mg}, following the general formula: Mg(x)Fe(1-x)Al(2)Si(12)O(48)H(40), where x is between 0 and 1.

Carpholite, chloritoid and chlorite are stable at L*T*-H*P*, M*T*-H*P* and L*T*- to M*T*-L*P* conditions, respectively. At low pressure, such a bulk composition is expected to form chlorite-kaolinite, chlorite-pyrophyllite ± chloritoid and chlorite-kyanite ± chloritoid assemblages with increasing temperature (Figure 3.6). The upper thermal stability of carpholite is shifted at higher temperature with increasing X_{Mg}(Car), and it is found to lie at 350-400°C at X_{Mg}(Car) > 0.7. Chloritoid stability closely depends on its composition: Ferro-chloritoid is stable between 200-250°C and ca. 500°C at any pressure, while Mg-rich chloritoid is stable at pressures and temperatures beyond the modelled conditions (eclogite facies). As its X_{Mg} increases, the chloritoid stability field slides towards higher pressure and temperatures, which is consistent with experimental data (Chopin and Schreyer, 1983) and its common occurrences in the greenschist, blueschist and eclogite facies. Chlorite from kaolinite and pyrophyllite stability fields is mostly composed of sudoite and Fe-amesite or amesite (depending on the X_{Mg}(bulk)). These results are similar to those obtained by Vidal et al. (1992).

3.4.2.2. Mg-Fe partitioning

In order to illustrate model predictions concerning element partitioning between carpholite and chloritoid, K_D-values were calculated and then plotted as K_D-isolines along with X_{Mg}(Car) isolines (Figure 3.6f). K_D(Car/Ctd) appears to depend strongly on temperature. It decreases from very-high values (> 10) for carpholite (X_{Mg}<0.5)-chloritoid assemblages to high values (8-5) for Mg-rich-carpholite-chloritoid assemblages, similar to values reported in the literature (Theye et al., 1992). Although the pressure dependency of Mg-Fe partitioning is much weaker, K_D(Car/Ctd) slightly decreases with increasing pressure. The calculated decrease of K_D(Car/Ctd) with increasing X_{Mg} is not correlated by natural data, but this is likely due to the difficulty to retrieve exact carpholite-chloritoid pairs (see above). It is noteworthy that K_D-values for Fe-rich carpholite compositions should be considered with the greatest care because they are directly not constrained by any natural data.

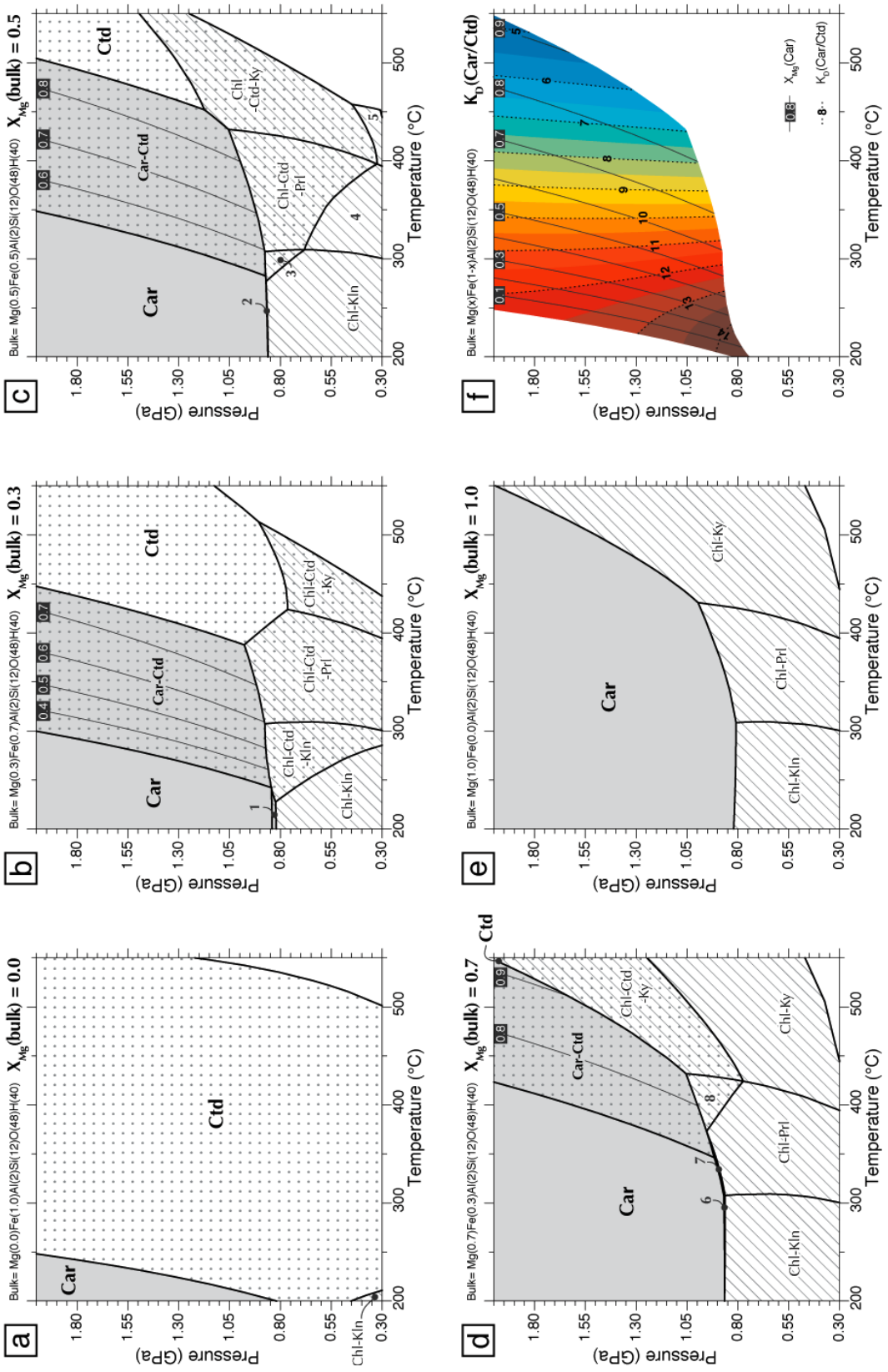

Figure 3.6: Pressure-temperature phase diagrams (a-e) using bulk compositions equivalent to carpholite + quartz + water, and K_D(Car/Ctd) and X_{Mg}(Car) isolines (f). Quartz and water are always present in excess although not specified. Unspecified plain-white fields represent andalusite-, sillimanite- and/or staurolite-bearing assemblages, which are not considered. Fields with number labels are: 1, 2, 6, Car-Chl-Kln-Qz-w; 3, Chl-Ctd-Kln-Qz-w; 4, Chl-Prl-Qz-w; 5, Chl-Ky-Qz-w; 7, Car-Chl-Prl-Qz-w; 8, Chl-Ctd-Prl-Qz-w. Mineral abbreviations like previous and: Chl, chlorite; Kln, kaolinite; w, water.

3.4.2.3. *T*-X_{Mg} diagram

A more detailed discussion of the carpholite replacement by chloritoid during the increase of temperature at high-pressure conditions (Figure 3.6) can be made on the basis of a T-X_{Mg} diagram (Figure 3.7) at constant pressure (1.0 GPa) using the same bulk composition as previously but with variable X_{Mg}(bulk), i.e., Mg(x)Fe(1-x)Al(2)Si(12)O(48)H(40). This diagram displays a (truncated) lens-shaped carpholite-chloritoid field, like in the conceptual T-X diagrams of de Roever (1977) and Theye et al. (1992).

Primary carpholite (Car1) forms from the precipitation of a silicate fluid under high-pressure conditions. When temperature exceeds the upper thermal limit of Car1 stability field, Car1 breaks down into more Mg-bearing carpholite (Car2) and Fe-rich chloritoid (Ctd2). In turn, as temperature keeps increasing, Car2 becomes unstable and breaks down into a carpholite even richer in Mg (Car3) and corresponding chloritoid (Ctd3), also richer in Mg than Ctd2. A crucial point is that chloritoid successively formed thus remains stable along the prograde path. Indeed, Ctd1 and Ctd2 are stable towards higher temperatures (Figure 3.7), so that at the third stage, even if reactions are assumed to be complete, the rock consists of the assemblage Car3-Ctd1-Ctd2-Ctd3 (with quartz and water). This results in a scatter of chloritoid compositions, as well evidenced in our all samples.

Therefore, the composition of a carpholite-chloritoid pair directly reflects a temperature, while relative modes, which can be determined graphically, depend on the bulk composition of precursory carpholite.

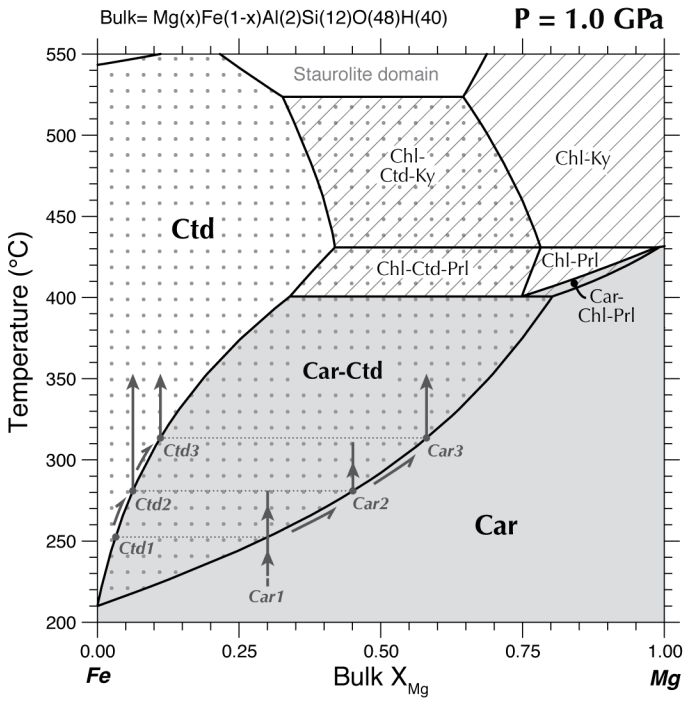

Figure 3.7: Binary temperature-composition (*T*-X) phase diagram at constant pressure (1.0 GPa) with excess H_2O and varying bulk composition. Bulk composition corresponds to carpholite of varying X_{Mg} with excess SiO_2. Note that Ctd1 represents the "*virtual equivalent*" of Car1. Unspecified plain-white fields represent staurolite-bearing assemblages, which are not considered. Mineral abbreviations like in Figure 3.3.6.

3.4.3. Application to natural systems

3.4.3.1. Beige phyllite sample Afy0800

In order to model the rather simple, but unique, phase assemblage observed in the beige phyllite sample Afy0800 (carpholite-chloritoid-pyrophyllite), a *P-T* phase diagram was calculated using a bulk composition measured by X-ray fluorescence (Table 3.4). Since white mica is the only K-bearing phase and likely plays a negligible role in the FMASH phase assemblage, we removed it from the bulk composition with respect to the total amount of K and the average composition of white mica (Table 3.4). Sample bulk composition reveales little amount of Ca, whereas no calcic phase occurs. Little Na mostly consists of paragonite in white mica. We consequently did not consider Ca and Na for thermodynamic modelling. The phase diagram produced using the bulk composition corrected from K, Ca and Na Mg(0.06)Fe(0.25)Al(1.44)Si(2.10)O(26.65)H(40) predicts the systematic occurrence of quartz. In this grid, the carpholite-chloritoid-pyrophyllite assemblage, which is the main association observed in the sample, comprises 0.10 moles of quartz, while the sample is obviously free of quartz. This amount of quartz was tentatively removed from the bulk composition (corrected Si = 2.00). Although the presence of quartz is still predicted for most of the modelled *P-T* space (Figure 3.8), the bulk composition with corrected Si-content reproduces the observed assemblage and allows further petrologic discussion.

Predicted phase assemblages correspond to one or two ferromagnesian phases among carpholite, chlorite and chloritoid, one phase among diaspore, kaolinite, pyrophyllite and kyanite, and generally quartz to accommodate excess in SiO_2. The grid predicts two quartz-free domains (Figure 3.8): one in the stability field of carpholite at 0.85-1.15 GPa and 305-360°C, the other in the stability field of chlorite at < 0.85 GPa and 300-310°C (up to 400°C below 0.4 GPa). Within the former field, the assemblage carpholite-chloritoid-pyrophyllite-water (in absence of diaspore and quartz), which is the main association observed in the sample, is stable in a narrow elongated field (with the label "9" in Figure 3.8), extending from 0.87 GPa/310°C to 1.07 GPa/320°C. Predicted compositions of carpholite (modal amount = 0.05) and chloritoid (modal amount = 0.26) are X_{Mg}(Car) = 0.59-0.60 and X_{Mg}(Ctd) = 0.12. In the low-pressure quartz-free domain, the possible early prograde assemblage retrieved from mineral inclusions in carpholite (chloritoid-pyrophyllite-sudoite considering the FMASH system) is stable in the field labelled as "3" in Figure 3.8. In this field, chlorite (modal amount = 0.02) composition mainly consists of sudoite (64-72 %) and Fe-amesite (20-30 %), while chloritoid (modal amount = 0.26) has a predicted X_{Mg} of 0.14.

This *P-T* diagram does not predict large compositional variations as they were observed in carpholite and chloritoid. As raised from modelling of quartz vein systems, an isochemical grid can hardly allow reconstructing an accurate *P-T* path. Nevertheless, keeping in mind that white mica and cookeite were not considered for modelling, the grid shown in Figure 3.8 is assumed to provide reliable *P-T* estimates for this sample.

Table 3.4.: Correction of the measured bulk composition of Afy0800 using the average phengite composition (based on 24 spot analyses).

	Phengite	AFY0800		
	average	measured	corrected 1	corrected 2
SiO_2	47.56	48.97		
TiO_2	0.04	0.22		
Al_2O_3	35.24	32.88		
Fe_2O_3	1.81	4.45		
MnO	0.01	0.02		
MgO	0.52	0.67		
CaO	0.63	0.04		
Na_2O	0.02	0.43		
K_2O	9.66	5.61		
P_2O5		0.08		
Loi		6.07		
Total	95.48	99.45		
Si	3.14	0.49	2.10	2.00
Ti	0.00	0.00	0.01	
Al	2.74	0.39	1.44	1.44
Fe	0.10	0.03	0.25	0.25
Mn	0.00	0.00	0.00	
Mg	0.05	0.01	0.06	0.06
Ca	0.00	0.00	0.00	
Na	0.08	0.01	0.01	
K	0.81	0.07	0.00	
Total		1.00		

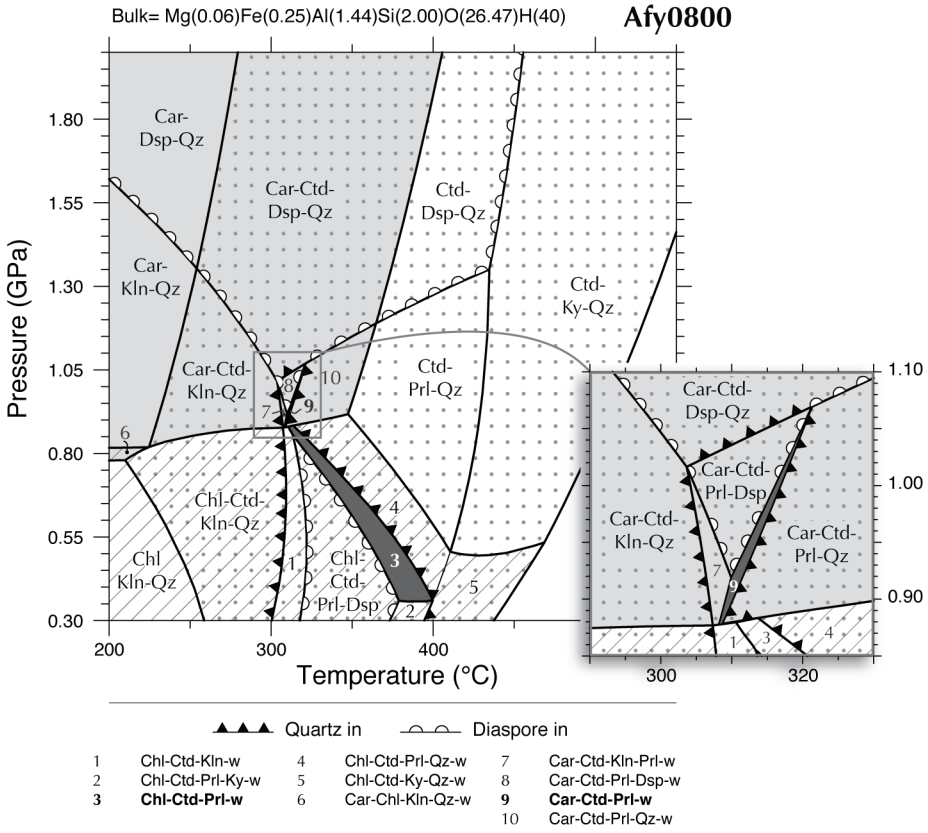

Figure 3.8: *P-T* phase diagram calculated for the beige phyllite sample Afy0800, using a corrected bulk composition (see text and Table 3.4).

3.4.3.2. Quartz vein sample Afy0212

In order to derive absolute temperature from mineral compositions (Figure 3.8), pressure conditions prevailing during the transition from carpholite to carpholite-chloritoid assemblage must be estimated. As indicated by the absence of diaspore in the beige phyllite, pressure can reasonably estimated to have attained 10 kbar (Figure 3.9). The textures observed in the sample Afy0212 clearly accounts for a temperature increase. Primary carpholite has an average X_{Mg} of 0.3, which means that the quartz vein initially precipitated at > 0.85 GPa and ≤ 250°C (Figures 3.6b, 3.8). This quartz vein thus formed while the country rock was buried along a thermal gradient ≤ 9°C/km. Primary carpholite is overgrown by secondary carpholite (X_{Mg} = 0.45-0.54) and chloritoid (0.07-0.11). These X_{Mg} ranges indicate continuous (at the scale of the sample) growth of carpholite and chloritoid in thermodynamic equilibrium as temperature increased from 280 to 310°C (Figure 3.8). The fresh aspect of chloritoid in this sample is consistent with the model prediction that chloritoid remains stable as temperature keeps increasing (Figure 3.7). This illustrate that the composition of coeval carpholite and chloritoid can be used to retrieve the prograde evolution of temperature at high-pressure conditions.

3.4.3.3. Pressure-temperature conditions in the western Afyon Zone

In the western Afyon Zone, the retrograde metamorphic evolution is constrained by *P-T* estimates of 0.6 GPa/350°C based on chlorite-mica (pseudomorphs after carpholite) multi-equilibrium in a quartz vein from the region of Kütahya (Pourteau et al., 2011b). According to the present thermodynamic model, the Mg-richest carpholite-chloritoid pairs (X_{Mg}(Car) = 0.75 – X_{Mg}(Ctd) = 0.30) (in the silvery phyllite sample Bay0851) indicate that temperature reached at least 380°C at high pressure conditions (Figures 3.6e, 3.7). Carpholite-chloritoid assemblages in our samples recorded a prograde path between 280 and 380°C at 0.9-1.1 GPa.

3.5. Conclusions

Based on a detailed petrographic study of aluminous metapelites, we were able to identify multiple generations of Fe-Mg-carpholite and chloritoid that are texturally and chemically distinct. Chloritoid occurs as low-pressure precursor (inclusions in carpholite), as a breakdown product and in equilibrium with carpholite. Both carpholite and chloritoid may display growth zoning. Only in one quartz phyllite sample, zoned chloritoid has been found, while other samples generally contain homogeneous chloritoid of various compositions. Along a prograde *P-T* path, carpholite and chloritoid compositions evolved towards Mg-richer compositions. Samples described in the present study contain the reactants and products of the prograde reaction Fe-rich carpholite = Fe-Mg-carpholite + Fe-rich chloritoid + quartz. Measured Mg-Fe partitioning coefficients (K_D(Car/Ctd)) can vary largely within samples. Where equilibrium textures are obvious, K_D(Car/Ctd) attains 7-10, i.e., consistent with the values reported by (Theye et al., 1992). In turn, reaction textures consistently provide lower apparent K_D-values (< 5).

The thermodynamic data for ferro-carpholite reported in this study permits to model mineral assemblages and mineral compositions of aluminous metapelites in the FMASH system. With this updated database, thermodynamic modelling is used to better understand the successive mineral

assemblages along a prograde evolution and degenerated parageneses (carpholite-chloritoid without quartz).

Re-inspecting carpholite-chloritoid-bearing rocks from high-pressure units, in which *P-T* conditions were determined from other chemical systems (e.g., metabasites), may help to further refine the thermodynamic data provided in the present study and allow using K_D(Car/Ctd) as an accurate thermometre. However, due to small-scale variations of mineral compositions, exact K_D(Car/Ctd), even for pairs in obvious equilibrium, can hardly be retrieved. This illustrates that, beyond the uncertainties on thermodynamic data, the use of Mg-Fe exchange between ferromagnesian phases as a thermometre (e.g., chlorite-chloritoid, garnet-biotite, garnet-clinopyroxene) requires thorough inspection of petrographic textures and element distribution within minerals.

Final amalgamation of the Anatolian microcontinent: Insight from ^{40}Ar-^{39}Ar geochronology and *P-T* estimation in high-pressure metasediments from Western and Central Anatolia

Abstract

Within the Mediterranean tectonic mosaic, the reconstruction of Anatolia amalgamation remains uncertain due to the doubts on the number and position of former Neotethyan oceanic domains. In western to central Anatolia, widespread high-pressure assemblages were recently reported from continental passive margin metasediments of numerous tectonic zones (namely the Afyon Zone, the Ören Unit and the Menderes Massif), opening new perspectives for the understanding of regional geodynamics between the Late Cretaceous and the Neogene. We provide thermobarometric estimates for the Afyon Zone and ^{40}Ar-^{39}Ar phengite ages for the subduction-related metamorphism of these three tectonic zones. Our results reveal that a) in the Afyon Zone and the Ören Unit early medium-pressure retrograde assemblages formed between 65 and 60 Ma ago, and in the southern Menderes cover b) high-pressure metamorphism occurred about 45 Ma ago and c) post-Barrovian mica cooling about 26 Ma ago. These show that the Ören Unit and Afyon Zone belong to a continuous Maastrichtian high-pressure belt, and the southern Menderes cover represents the eastern ending of the Eocene high-pressure belt exposed in the Aegean. In conclusion, we propose a possible geodynamic scenario for the amalgamation of western Anatolia, which conciliates these new results with previous data.

4.1. Introduction

In the Eastern Mediterranean, the pervasive occurrence of Neotethyan ophiolites obducted on top of non-metamorphosed Mesozoic platforms has long hampered deciphering the position and number of former oceanic branches, and thus reconstructing the progressive amalgamation of Gondwana-derived terranes to southern Eurasia. High-pressure metamorphosed passive margin sediments recently discovered in Anatolia have opened new perspectives in this direction. But the precise metamorphic age of these subduction-related metamorphic rocks remains a key issue to be unravelled.

4.2. Geological setting

4.2.1. Tectonic domains of western Anatolia

Western to Central Anatolia can be subdivided in three tectonic regions regarded as distinct terranes that experienced contrasting tectonic evolutions between Late Cretaceous to Palaeogene times.

1) Northern Anatolia exposes a polystage fold-thrust belt known as the Pontides. A large part of this region is occupied by the Sakarya Zone, which consists of a Precambrian to Palaeozoic

crystalline basement (ascribed to the Variscan orogeny; Okay et al., 1996; Topuz et al., 2007), late Triassic blueschists and eclogites (related to the Cimmerian orogeny; Tekeli, 1981; Okay and Monié, 1997), and unconformably overlying non-metamorphosed Jurassic to Cretaceous sediments and volcanic rocks (Altıner et al., 1991; Yılmaz et al., 1995; Okay and Şahintürk, 1997). The eastern Pontides are covered by a thick upper Cretaceous volcanic arc succession (Dewey et al., 1973; Akın, 1978), while the western Pontides are intruded by Eocene to Oligocene calc-alkaline granitoids (Delaloye and Bingöl, 2000; Okay and Satır, 2006). In the Late Cretaceous, the Pontides were part of the southern composite margin of Eurasia, in upper plate position regarding the accretion of the southerly blocks (Şengör and Yılmaz, 1981; Okay and Satır, 2006).

2) Central Anatolia is composed of the Central Anatolian Crystalline Complex made of late Cretaceous intrusions and Barrovian metamorphic rocks (e.g., Seymen, 1981; Göncüoğlu et al., 1997; Aydın et al., 1998; Whitney et al., 2001). Protolithic ages of these high-temperature, low- to medium-pressure rocks are inferred to be early Palaeozoic to Mesozoic, based on relict fossils (Kocak and Leake, 1994) and correlation with lithostratigraphic similarities to the southerly Anatolide-Tauride Block (Göncüoğlu et al., 1997). In an ophiolitic mélange from the northwestern rim of the Central Anatolian Crystalline Complex, blocks of amphibolites revealed that intra-oceanic subduction in the Neotethys started between 178 and 165 Ma ago (Çelik et al., 2011). Remnants of Cretaceous ophiolites (including middle Turonian to early Santonian pelagic sediments) lying on top of the Central Anatolian Crystalline Complex are related to southward obduction between the Santonian and the Maastrichtian (e.g., Yalınız et al., 1996; Yalınız and Göncüoğlu, 1998; Floyd et al., 2000). The late Cretaceous ophiolites, granitoids and metamorphic rocks from central Anatolia are unconformably covered by non-metamorphosed upper Maastrichtian and younger sediments that postdate the emplacement and unroofing of these units. Between 85 and 75 Ma, Central Anatolia was affected by detachment-controlled extension that led to the exhumation of several metamorphic core complexes (e.g., Gautier et al., 2008; Whitney et al., 2008b; Lefebvre et al., 2011).

3) Western and Southern Anatolia consists of metamorphosed and non-metamorphosed Precambrian to Eocene rocks, known as the Anatolide-Tauride Block (Okay and Tüysüz, 1999). This domain is characterized by a Precambrian crystalline basement of Gondwana affinity (Pan-African orogeny), and late Cretaceous to early Cenozoic high-pressure metamorphism along its northern border (Alpine orogeny) (e.g., Şengör and Yılmaz, 1981).

4.2.2. Anatolide-Tauride units

Following Ketin's (1966) definition the term 'Anatolides' is used to designate the rocks affected by Alpine regional metamorphism, and the term 'Taurides' designates the non-metamorphosed thrust and folded sediments more to the south.

The Taurides encompass various tectonic units of Precambrian to Eocene sedimentary age (e.g., de Graciansky, 1972; Özgül, 1976) that escaped substantial Alpine metamorphism (see Bozkaya and Yalçın, 2000). Multistage deformation between latest Cretaceous and late Miocene times resulted

in forming regional-scale nappe complexes: such as the Lycian Nappes, the Hoyran-Beyşehir-Hadim Nappes and the Aladağ Nappes of the western, central and eastern Taurides, respectively (Figure 4.1) (Özgül, 1976; Gutnic et al., 1979; Andrews and Robertson, 2002; Tekeli et al., 1984). Each includes an obduction complex (ophiolites, 90-Ma-old metamorphic sole, Maastrichtian ophiolitic mélange; for review see Robertson, 2002; Çelik et al., 2011), overlying imbricated sedimentary units (mainly Mesozoic platform carbonates), which are in turn thrust over Cenozoic autochthones formations. In the latest Cretaceous, during the obduction of Neotethyan ophiolites from the north, the three nappe complexes underwent a first common imbrication of platform sediments. In the late Eocene, the Lycian Nappes and the Hoyran-Beyşehir-Hadim Nappes further developed by integrating middle Eocene and older sedimentary formations and attained their present-day position after thrusting over a lower Eocene to Oligocene foredeep sequences, and Burdigalian (> 15 Ma) (more internally) to Tortonian (> 7 Ma) (more externally) autochthonous sediments (Özgül, 1976; Monod, 1977). In the present study, we regard the Taurides as a composite fold-thrust belt in foreland position regarding the Anatolide metamorphic belts.

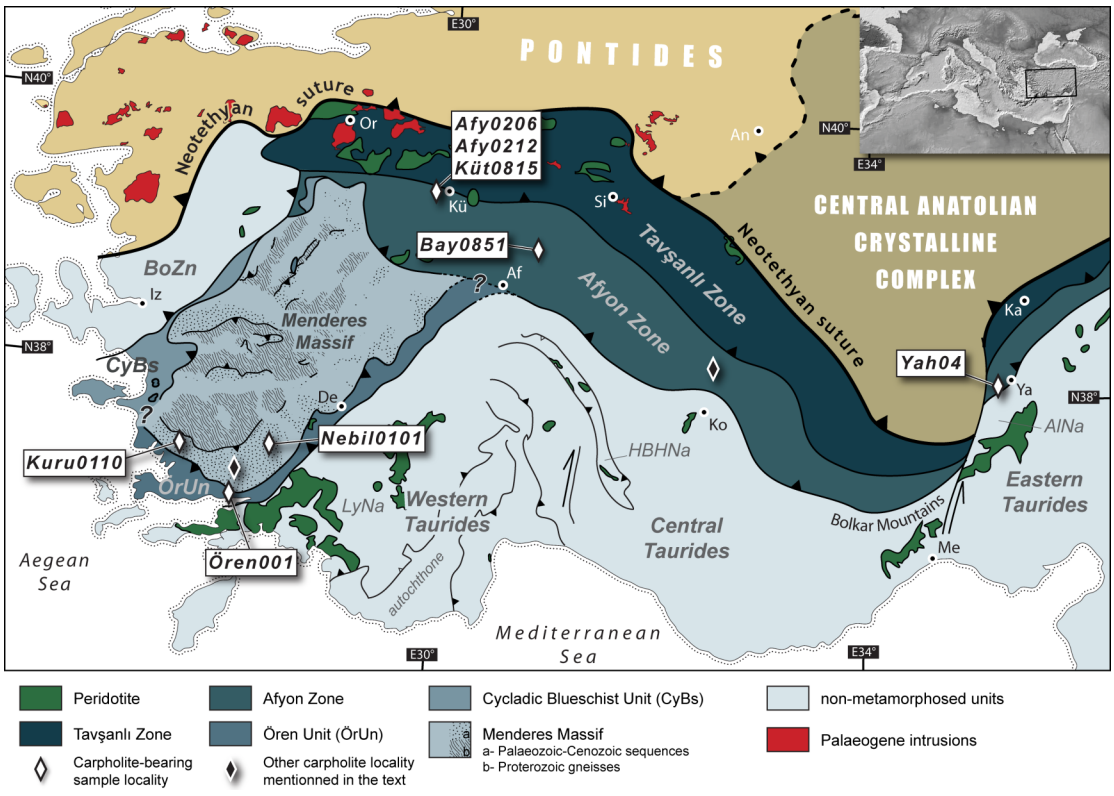

Figure 4.1: Tectonic units of western-central Anatolia and distribution of the carpholite-bearing samples used for Ar-Ar geochronology in the present study. Other carpholite localities discussed in text are Bahçeyaka in the southern Menderes Massif (Rimmelé et al., 2003b), and Konya in the central Afyon Zone (Pourteau et al., 2010). Unit abbreviations are: AlNa, Aladağ Nappes; BoZn, Bornova Zone; CyBs, Cycladic Blueschists; HBHNa, Hoyran-Beyşehir-Hadim Nappes; LyNa, Lycian Nappes; ÖrUn, Ören Unit. Toponymic abbreviations are: Af, Afyonkarahisar; An, Ankara; De, Denizli; Iz, Izmir; Ka, Kayseri; Ko, Konya; Kü, Kütahya; Me, Mersin; Or, Orhaneli; Si, Sivrihisar; Ya, Yahyalı.

Along the westernmost part of the Neotethyan suture, a non-metamorphosed "megaolistostrom", referred to as the Bornova Zone, occurs between the Pontides and the Anatolides

(Figure 4.1). It is made of a highly sheared matrix of Maastrichtian to Danian greywacke and shale, and mappable blocks of neritic limestone and rare mafic volcanic rock, pelagic sediments and serpentinite (Özer and Irtem, 1982; Erdoğan, 1990; Erdoğan et al., 1990; Okay and Siyako, 1993; Robertson et al., 2009), unconformably covered by undeformed Eocene sediments. The Bornova Zone is assumed to have formed along a sinistral transform fault at the edge of the northward-drifting Anatolide-Tauride Block (Okay and Siyako, 1993).

The general lithostratigraphy of the Anatolides consists of an upper Permian to upper Cretaceous sedimentary sequence, and its substratum represented by Precambrian high-grade metamorphic and intrusive rocks and upper Palaeozoic sedimentary formations. The Mesozoic sedimentary sequence generally consists of Triassic clastic sediments with intercalated trachytic to rhyolitic volcanic horizons followed upper Triassic to upper Cretaceous and younger neritic to pelagic marbles and metaolistostroms. This Mesozoic sequence has been interpreted as a continuous record of Triassic rifting above a south-dipping subduction zone (Şengör and Yılmaz, 1981; Akal et al., 2011) and the subsequent development of a carbonate platform, which finally subsided between the late Cretaceous and the early Cenozoic as it approached the trench of the north-dipping Neotethyan subduction zone (Okay et al., 2001b). In this context, the underlying Precambrian and Palaeozoic formations are regarded as the substratum of the Mesozoic continental passive margin. Alpine high-pressure metamorphism was documented from all over the Anatolides as a result of continental margin burial into a subduction zone (Okay et al., 1996; Pourteau et al., 2010).

Among the Anatolides, several tectonic units were defined to account for contrasting metamorphic evolutions (Okay et al., 1996). From north to south, these are: the Tavşanlı Zone, the Afyon Zone, the Menderes Massif, and the Ören Unit. Although it is not part in the "classical" Anatolides, one may include the Cycladic Blueschist Unit (defined in the Aegean region) that crops out in westernmost Anatolia (Figure 4.1). An alternative nomenclature used by Göncüoğlu et al. (1997, 2007, 2011) merges the Tavşanlı Zone, the Afyon Zone and cover series of the Menderes Massif into a single tectonic unit (referred to as the "Kütahya-Bolkardağ Belt"). This classification, however, does not account for variations of the tectonic and metamorphic history within the Anatolides, so we use the nomenclature of Okay.

The Tavşanlı Zone is characterized by high-pressure-blueschist to low-temperature-eclogite facies rocks (Okay, 2002; Davis and Whitney, 2006, 2008; Çetinkaplan et al., 2008). Two subunits are distinguished: a lower coherent Permian to middle Cretaceous stratigraphic sequence, and an upper Cretaceous upper volcano-sedimentary complex. The lower subunit typically contains lawsonite-, jadeite-, and chloritoid-bearing schists interlayered with lawsonite-bearing metabasites of assumedly Permo-Triassic sedimentary age (Okay, 1980; Okay, 1986; Okay and Kelley, 1994; Okay, 2002). These are conformably overlain by a metamorphosed carbonate sequence deposited between early Triassic and middle Cretaceous times, which passes gradually from neritic to pelagic limestone, and alternating basic volcanic, radiolarite and pelagic shale layers (Okay, 1986). Although no aragonite was found in the recrystallized platform carbonates, ubiquitous columnar calcite crystals (away from the intrusions; see below) were interpreted as pseudomorphs after aragonite (Candan et al., 2005; Seaton et al., 2009). This coherent sequence is tectonically overlain by the upper volcano-sedimentary complex,

which consists of tectonic slices of serpentinite, basalts, pelagic shales, pelagic limestone and radiolarian cherts (Okay, 1984). In the western part of the unit, the upper subunit seems unmetamorphosed in the field, but microscopic occurrences of aragonite, jadeite and lawsonite reported from pelagic limestone and mafic volcanic rocks are evidence for incipient blueschist-facies metamorphism (Okay, 1982; Okay et al., 1998; Topuz et al., 2006). In the Sivrihisar area, the lateral equivalent of the upper subunit contains blocks of well-preserved lawsonite blueschists and lawsonite eclogites (Gautier, 1984; Whitney and Davis, 2006; Davis and Whitney, 2006, 2008; Çetinkaplan et al., 2008). In the poorly known Mihaliççık area, the report of eclogite blocks surrounded by serpentinite (Çoğulu, 1967) suggests that the accretionary complex in this area has also been buried to great depths. Farther east, lawsonite-blueschist blocks were scarcely reported from mélange localities in the Konya region, in the Bolkar Mountains, and in the Kayseri region (van der Kaaden, 1966; Droop et al., 2005). They are interpreted as evidence for the eastern continuation of the Tavşanlı Zone until south and east of the Central Anatolian Crystalline Complex (Okay, 1984). Reconstruction of the passive margin palaeogeography places the Tavşanlı Zone in a frontal position (Candan et al., 2005). Tectonic contacts between the coherent blueschists and the overlying sub-ophiolitic mélange and peridotites are sealed by calc-alkaline plutonic rocks, for which 40Ar-39Ar hornblende ages between 53 and 48 Ma were obtained (Harris et al., 1994; Delaloye and Bingöl, 2000). Geochemical features of these intrusives points out the major role of mantle melting, as advective heat source or primary magma (Harris et al., 1994).

The Afyon Zone occurs south of and structurally below the Tavşanlı Zone (Okay, 1984). It is composed of four stratigraphic members: i) Precambrian high-grade schists intruded by leucocratic granites and glaucophane-bearing gabbroic stocks (Candan et al., 2005); ii) pre-Devonian to Permian clastic rocks, lava flows, volcaniclastic rocks, carbonates, and blocky units ("mélanges") (e.g., Demirtaşlı et al., 1984; Ayhan and Lengeranli, 1986; Gençalioglu-Kuşcu et al., 2001; Göncüoğlu et al., 2007; Robertson and Ustaömer, 2009); iii) a continuous sequence of Permo-Triassic clastic sediments (conglomerates, sandstones, siltstones, and phyllites; Candan et al., 2005; Pourteau et al., 2011a) or volcanics (thick trachytic, rhyolitic and dacitic lava flows and volcaniclastics; Akal et al., 2011) that grades into a thick sequence of upper Triassic to upper Jurassic neritic dolomitic limestone followed by lower Cretaceous to Campanian deep-marine sediments (Özcan et al., 1988); and iv) an upper Maastrichtian to lower Palaeocene sedimentary mélange, which notably contains blue-amphibole-bearing mafic blocks (Göncüoğlu et al., 1992). The Triassic-Cretaceous sequence is interpreted as the complete record of a rift to passive margin transition (Okay, 1984; Candan et al., 2005). Fe-Mg-carpholite, glaucophane and calcite pseudomorphs after aragonite documented throughout the Afyon Zone are evidence for Alpine high-pressure, low-temperature metamorphism (Candan et al., 2005; Pourteau et al., 2010). The western part of the Afyon Zone lies structurally over the Menderes Massif (see below), whereas the central part lies on top of Tauride autochthonous late Precambrian to Palaeozoic series (Sandikli and Sultan Dağ units), the upper stratigraphic levels of which are early Cenozoic pelagic limestone passing upwards into middle Eocene turbidites and debris flows (Gutnic, 1977). In the Bolkar Mountains, the Afyon Zone was overthrust by non-metamorphic Permian to

Mesozoic tectonic units derived along post-lower Eocene north-verging faults (Demirtaşlı et al., 1984; Tekeli et al., 1984).

The Menderes Massif, which occurs as a regional tectonic window below the Afyon Zone and the Ören Unit, presents a complicated internal structure (see Şengör et al., 1984; Hetzel et al., 1998; Bozkurt and Oberhänsli, 2001; Okay, 2001; Whitney and Bozkurt, 2002; Régnier et al., 2007). It was classically described as an orogenic dome made of a "gneiss core" overlain by Palaeozoic schists and Mesozoic marbles (Dürr, 1975). The Menderes Massif core is dominantly composed of paragneisses, medium- to high-grade schists and orthogneisses and further contains scarce granulites, migmatites and relict eclogites attributed to the Pan-African orogeny (Oberhänsli et al., 1997; Candan et al., 2001; Oberhänsli et al., 2010b; Candan et al., 2011a). The Menderes gnessic core is unconformably covered by the Palaeozoic cover series that is composed of basal conglomerate, lower to middle grade schists, phyllites and quartzites with black marble (e.g., Dürr, 1975; Akkök, 1983; Şengör et al., 1984; Candan et al., 2011b). A metamorphosed polygenic conglomerate deposited unconformably on top of the Palaeozoic schists represents the lowermost level of the marble sequence (Dürr, 1975). It passes upwards into upper Triassic to upper Cretaceous marbles containing characteristic emery, metabauxite layers and well-preserved rudist fossils (Dürr, 1975; Özer et al., 2001). The top of this thick carbonate sequence consists of latest Cretaceous pelagic marbles intercalated with cherts beds (Özer, 1998). A metamorphosed Palaeocene to middle Eocene olistostrom occurs atop the pelagic marbles. It contains blocks of serpentinite and marbles in a pelitic matrix (Dürr, 1975; Gutnic et al., 1979; Özer et al., 2001) metamorphosed into the greenschist facies (Rimmelé, 2003). The entire Menderes Massif has undergone low-pressure Barrovian metamorphism of increasing grade towards the core (Şengör et al., 1984; Bozkurt, 1996), as notably documented by multiple mineral isograds (including the diaspore-corundum isograds; Rimmelé et al., 2003b and references therein) in the Palaeozoic to earliest Cenozoic sequence of the southern margin. However, in the southern Menderes Massif, Fe-Mg-carpholite, reported as relics from two localities in the diaspore zone, and pseudomorphs from one locality of the corundum zone, occurs in quartz conglomerates at the base of the Mesozoic marble sequence, as evidence for high-pressure low-temperature metamorphism in this part of the unit at least (Rimmelé et al., 2003b; Whitney et al., 2008a).

The Ören Unit (Pourteau et al., 2010), formerly referred to as the metamorphosed part of the Lycian Nappes (Oberhänsli et al., 2001; Rimmelé et al., 2003a), lies structurally over the southern and eastern edges of the Menderes Massif. As pointed out by Pourteau et al. (2010), the contact zone between the Ören Unit and the Lycian Nappes was reworked in the Oligocene by the formation of the Kale-Tavas piggy-back basin (Alçiçek & ten Venn, 2008), rendering their relative structural positions uncertain. Klippen of the Ören Unit atop the Anatolian part of the Cycladic Blueschist Unit and the northern Menderes Massif (Figure 4.1; Rimmelé et al., 2006) support the model that it was transported southwards away from the suture zone over the Menderes Massif (de Graciansky, 1972; Gutnic et al., 1979; Şengör et al., 1984; Güngör and Erdoğan, 2001; Rimmelé et al., 2003a). The Ören Unit consists of upper Permian to lower Triassic reddish metasediments overlain by middle Triassic to middle Jurassic neritic marbles that grade into upper Jurassic to lower Cretaceous micritic limestone containing chert horizons and a metamorphosed upper Cretaceous flysch (Bernoulli et al., 1974;

Rimmelé, 2003). Fe-Mg-carpholite in the lower reddish metasediments and calcite pseudomorphs after aragonite in marbles are widespread evidence for blueschist-facies metamorphism (Oberhänsli et al., 2001; Rimmelé et al., 2003a, 2006).

West to the Menderes Massif, an additional high-pressure unit corresponds to the easternmost extension of the Cycladic Blueschist Unit, defined in the Aegean Domain (Candan et al., 1997; Oberhänsli et al., 1998; Okay, 2001). It is made of two tectonic subunits: a lower succession of metabauxite-bearing marbles with blue amphibole-bearing schists and metabasites intercalations, and an upper "metaolistostrom" made of blueschist and eclogite blocks in a garnet-micaschist matrix (Candan et al., 1997; Çetinkaplan, 2002). High-pressure minerals (including diaspore in metabauxite) in the lower platform sequence are preserved in the western part of the unit, as well as on Samos Island, while only retrograde greenschist assemblages (including corundum) were documented in the eastern part (Candan et al., 1997). The Cycladic Blueschist Unit lies tectonically over micaschists of the Menderes Massif (Okay, 2001). In the Aegean domain, it is thrust over a Variscan crystalline complex that locally contains evidence for high-pressure metamorphism (Bonneau, 1984).

The Anatolide-Tauride Block is topped by widespread ophiolites (Figure 4.1), which typical sequence includes an ophiolitic mélange, a greenschist- to amphibolite-facies metamorphic sole, ultramafic tectonite (mostly serpentinized harzburgite), mafic and ultramafic cumulates and massive gabbros (e.g., Robertson, 2002). Geochemical investigations showed that these ophiolites were generally generated in supra-subduction zone settings, while amphibolites from the metamorphic soles commonly show MORB to OIB affinities (e.g., Çelik et al., 2006). Based on the regional uniformity of ophiolite stratigraphy and metamorphic sole ages (95-90 Ma), all the ophiolite occurrences atop the Anatolides and Taurides units have been interpreted as remnants of a single obducted oceanic slab transported from the north (e.g., Ricou et al., 1986; Robertson, 2002).

4.2.3. Metamorphic PT conditions and ages in the Anatolides

In the Tavşanlı Zone, peak P-T conditions in the lower subunit were estimated to have reached 2.0-2.4 GPa and 430 ± 30°C in schists from the westernmost part of the unit (north and west of Kütahya) (Okay and Kelley, 1994; Okay, 2002), and ca. 1.6 GPa and 520°C in a metabasite from Sivrihisar (Davis and Whitney, 2006). The upper subunit that underwent incipient blueschist-facies metamorphism yielded P-T conditions estimates of 0.5-0.8 GPa and ca. 200°C (Okay, 1982; Topuz et al., 2006). Near Sivrihisar, peak P-T conditions from 2.2 to 2.6 GPa and from 430 to 550°C were calculated from lawsonite-bearing blueschists and eclogites blocks (Davis and Whitney, 2006, 2008; Çetinkaplan et al., 2008). In the region of Konya, lawsonite- and epidote-bearing blueschists blocks from a mélange unit assigned to correlate the upper subunit of the Tavşanlı Zone recorded P-T conditions of 0.9-1.1 GPa and 375-450°C (Droop et al., 2005). Late Cretaceous isotopic ages ranging between 89 and 80 Ma were obtained on blueschists from the Tavşanlı Zone and interpreted as high-pressure metamorphic ages (^{40}Ar-^{39}Ar and Rb-Sr on phengite; Table 4.1 and references therein).

Table 4.1: Summary of the published isotopic ages for high-pressure metamorphism in the Anatolides. Mineral abbreviations: Car, carpholite; Ctd, chloritoid; Ky, kyanite; Phg, phengite; Qz, quartz.

Unit	Locality	Rock type	Method	Age type	Age	Error	Reference
Tavşanlı Zone	Orhaneli	Jadeite schist	Ar-Ar Phg	In-situ ablation (3 spots)	88.4	0.5	Okay and Kelley (1994)
	Orhaneli	Metabasite	Rb-Sr Phg	Isochron	78.5	1.6	Sherlock et al. (1999)
	Sivrihisar	Metabasite	Rb-Sr Phg	Isochron	79.7	1.6	Sherlock et al. (1999)
	Sivrihisar	Impure marble	Ar-Ar Phg	Stepwise heating (plateau)	87.9	0.6	Seaton et al. (2009)
Afyon Zone	Kütahya	Car-Qz vein	Ar-Ar Phg	In-situ ablation (5 spots)	62.8	1.5	this study
	Kütahya	Car-Qz vein	Ar-Ar Phg	Stepwise heating (plateau)	66.0	2.8	this study
	Kütahya	Car-Qz vein	Ar-Ar Phg	Stepwise heating (plateau)	61.5	8.0	this study
	Afyon	Car-bearing phyllite	Ar-Ar Phg	In-situ ablation (3 spots)	74.6	1.1	this study
	Afyon	Car-bearing phyllite	Ar-Ar Phg	In-situ ablation (4 spots)	83.4	0.7	this study
	Yahyalı	Car-Qz vein	Ar-Ar Phg	Stepwise heating (plateau)	65.7	0.2	this study
	Yahyalı	Car-Qz vein	Ar-Ar Phg	Stepwise heating (plateau)	64.8	0.4	this study
	Yahyalı	Car-Qz vein	Ar-Ar Phg	Stepwise heating (plateau)	66.7	0.4	this study
Ören Unit	Milas	Red-green phyllite	Ar-Ar Phg	Stepwise heating	70-90		Ring and Layer (2003)
	Ören	Car-Qz vein	Ar-Ar Phg	Stepwise heating (plateau)	62.6	0.4	this study
	Ören	Car-Qz vein	Ar-Ar Phg	Stepwise heating (plateau)	59.4	0.7	this study
	Ören	Car-Qz vein	Ar-Ar Phg	Stepwise heating (plateau)	60.3	0.3	this study
Menderes Massif	Kurudere	Car-Ky-Qz vein	Ar-Ar Phg	In-situ ablation (5 spots)	45.9	2.0	this study
	Nebiler	Ctd-Ky conglomerate	Ar-Ar Phg	In-situ ablation (5 spots)	26.5	0.8	this study
Dilek-Selçuk Unit	Dilek	Epidote-blueschist	Ar-Ar Phg	Stepwise heating (plateau)	40.1	0.4	Oberhänsli et al. (1998)

Metamorphic conditions undergone by the passive margin sequence of the Afyon Zone were quantified based on carpholite-chloritoid assemblages in metasediments. Carpholite-chloritoid-pyrophyllite assemblage in metasediments from the western Afyon Zone accounts for pressure of 0.7-1.0 GPa and maximal temperatures of 350°C (Candan et al., 2005; Pourteau et al., 2011a). No isotopic age information is available yet for the metamorphic evolution of the Afyon Zone. Stratigraphic relations (i.e., the time gap between the oldest metamorphic rocks and the youngest non-metamorphosed, unconformable cover sediments) leave a possible interval between the Maastrichtian and the Palaeocene for the western (Kütahya-Afyon) and eastern parts (Kayseri) of Afyon Zone (Dirik

et al., 1999; Candan et al., 2005). In between, near the Bolkar Mountains (Figure 4.1), non-metamorphosed Maastrichtian to lowermost Palaeocene sediments are documented to be unconformable on top of an ophiolitic mélange and recrystallized platform carbonates attributed to the Afyon Zone (Oktay, 1982; Demirtaşlı et al., 1984; Clark and Robertson, 2002). This suggests that this part of the Afyon Zone was buried and exhumed before the end of the Cretaceous.

In the Menderes Massif, the Alpine period is characterized by a locally preserved high-pressure low-temperature stage (carpholite-bearing metaconglomerates from the southern marble sequence) and a general Barrovian stage (greenschist and amphibolite assemblages in the entire unit). High-pressure, low-temperature metamorphism was evaluated to be 1.2-1.4 GPa and 470-550°C in Kurudere (carpholite-kyanite-chlorite multi-equilibrium), 0.6-0.8 GPa and 400-450°C in Bahçekaya (carpholite-chloritoid-pyrophyllite equilibrium), and 0.9-1.1 GPa and 380-480°C in Nebiler (chlorite-white mica multi-equilibrium) (Rimmelé et al., 2003b, 2005). On the other hand, the polymetamorphic history of the Menderes "gneiss core" renders difficult deciphering the extent of Barrovian metamorphism during the only Alpine orogeny (see Bozkurt and Oberhänsli, 2001). We thus rely on the estimates concerning the post-Pan-African series (i.e., Palaeozoic schist and Mesozoic schist envelopes). P-T conditions for the Barrovian metamorphism were calculated as 0.4-0.5 GPa and 330-530°C in Palaeozoic schists from the southern Menderes Massif, and 0.4-0.8 GPa and 450-660°C in the central Menderes Massif (Akkök, 1981, 1983; Ashworth and Evirgen, 1984, 1985; Okay, 2001; Whitney and Bozkurt, 2002; Régnier et al., 2003). The timing of the high-pressure metamorphism is not constrained isotopically yet. Although this event was documented from only three localities from a single stratigraphic horizon, one may infer that the entire marble sequence, described as stratigraphically continuous (Dürr, 1975; Özer et al., 2001), was buried into the subduction zone. Thus, Maastrichtian fossils reported from the top of the marble sequence predate this metamorphism. In turn, it is post-dated by the Barrovian metamorphism, which occurred 35 ± 5 Ma ago, as suggested by the average of Rb-Sr mica ages obtained on Palaeozoic schists (ca. 63-27 Ma; Satır and Friedrichsen, 1986; Bozkurt and Satır, 2000). High-pressure metamorphism therefore occurred some time in the Palaeogene.

In the Ören Unit, P-T conditions recorded by the carpholite-bearing metasediments were firstly estimated to be ca. 0.7-0.8 GPa and 350-400°C (carpholite-chloritoid-pyrophyllite equilibrium; Oberhänsli et al., 2001), and later refined to ca. 1.0-1.2 GPa and 400°C (carpholite-chlorite-phengite multi-equilibrium; Rimmelé et al., 2005). According to this latter study, rocks at the base of the Ören Unit (including the klippen) experienced isothermal decompression at ca. 450°C, while at higher tectonostratigraphic positions rocks experienced syn-cooling decompression. This shows that the thermal evolution of high-pressure rocks during their exhumation can significantly vary within a single tectonic unit, poorly constrained ^{40}Ar-^{39}Ar ages between 90 and 70 Ma were obtained on high-Si phengite from metasediments as the only isotopic metamorphic age estimate for the Ören Unit (Ring and Layer, 2003). Stratigraphic relations constrain the high-pressure metamorphic event into a latest Cretaceous to Eocene interval (Rimmelé et al., 2003a).

Peak metamorphic conditions in the Anatolian part of the Cycladic Blueschist Unit were estimated to be ca. 1.1 GPa and 445°C in the epidote-blueschist-facies lower subunit, and ca. 1.2 GPa

and 490°C in the upper eclogite-facies sub-unit (Çetinkaplan, 2002). Isothermal decompression occurred in both subunits through the greenschist facies. ^{40}Ar-^{39}Ar geochronology on retrograde phengite yielded an age of 40.1 ± 0.4 Ma for the epidote blueschists of the lower subunit (Oberhänsli et al., 1998). This data coincides with the retrograde history of the Cycladic Blueschist Unit from the Aegean region, in which abundant isotopic ages have shown that high-pressure metamorphic assemblages formed in the Eocene (peak 53-49 Ma ago, followed by retrograde path until 38 Ma ago) and were retrogressed at low-pressure medium-grade conditions in the Oligocene (22-16 Ma) (e.g.,, Maluski et al., 1981; Wijbrans et al., 1990; Forster and Lister, 2005; Lagos et al., 2007).

The timing of high-P low-T metamorphic event in the Afyon Zone, Menderes Massif cover and Ören Unit thus still needs to be established in order to better understand the amalgamation of the Anatolide-Tauride Block to the Pontides, and correlate Western Anatolia with the Aegean.

4.3. P-T *estimation and ^{40}Ar-^{39}Ar geochronology*

Fe-Mg-carpholite-bearing metasediments are the main, or even the only evidence of Alpine high-pressure metamorphism in the Afyon Zone, the Ören Unit and the Menderes Massif. K-rich white mica (below referred to as phengite), often accompanied by chlorite, commonly occurs in carpholite-bearing rocks, offering the chance to determine the age of metamorphism by using ^{40}Ar-^{39}Ar geochronology. Several studies previously showed that this approach yields reliable metamorphic ages (Jolivet et al., 1996; Agard et al., 2002; Wiederkehr et al., 2009; Oberhänsli et al., 2010a, 2011). In these rocks, phengite may have formed before, during and after carpholite growth, so several generations can coexist in a single sample and thus provide different isotopic ages (Agard et al., 2002; Wiederkehr et al., 2008, 2009). In order to avoid such issues, PT conditions prevailing for phengite growth can be estimated by chlorite-mica thermobarometry (multi-equilibrium approach; see Vidal and Parra, 2000). Therefore, when possible, we combined ^{40}Ar-^{39}Ar age determination with PT estimation from the same samples and decipher the actual significance of isotopic dating results.

4.3.1. Sample selection

4.3.1.1. Selection criteria

For ^{40}Ar-^{39}Ar geochronology, we selected samples, in which: a) white mica is rich in potassium and poor in sodium, b) white mica is obviously of metamorphic origin, c) white mica occurs as large-sized crystals (> 125 μm), d) white mica is not intergrown with chlorite or pyrophyllite, and e) no late fluid circulation is seen (e.g., no fractures, no late calcite crystallization). Bearing in mind that carpholite-bearing quartz vein originates from the crystallization of a fluid phase under high-pressure low-temperature conditions, mica in such rock type is exclusively of metamorphic origin. In order to avoid the risk of the age inheritance of detrital mica recrystallized during metamorphism, we therefore preferentially selected quartz vein samples. Both fine grain size and common intergrowth of white mica with chlorite critically restricted sample selection.

4.3.1.2. Selected samples

The Afyon Zone encompasses a wide variety of carpholite-bearing rocks. In the region of Kütahya (Figure 4.1), carpholite, in quartz veins, is mainly accompanied by chloritoid + pyrophyllite ± chlorite, and more rarely by phengite + chlorite. We retained the samples Afy0206, Afy0212 and Küt0815 from the area of Kütahya. In the sample Afy0206, phengite and chlorite occur as elongated pseudomorphs after carpholite. Intergrowth is frequent, but in some areas pseudomorphs are only composed of phengite. This makes in-situ laser ablation the most appropriate technique for ^{40}Ar-^{39}Ar geochronology. The sample Afy0212 was described by Pourteau et al. (2011a) for remarkable carpholite-chloritoid textures. Pyrophyllite, which occurs as large crystals wrapping carpholite and chloritoid, contains discrete layers of low-Si phengite. In the sample Küt0815, carpholite is rather well preserved but displays evidence for local breakdown into chlorite and pyrophyllite that here again contains thin low-Si phengite interlayers. In the region of Afyon, carpholite-bearing metapelites and metaconglomerates contain abundant, fine-grained phengite, intergrown with pyrophyllite, quartz and iron oxides, but notably no chlorite (Candan et al., 2005; Pourteau et al., 2011a). We retained the sample Bay0851 from a carpholite-bearing silvery phyllite, which was petrographically inspected by Pourteau et al. (2011a). The notable absence of chlorite in this sample, on the one hand, prevents its use for accurate PT estimation, but, on the other hand, indicates that peak mineral assemblage (carpholite and chloritoid) was well preserved. Phengite in Bay0851 commonly contains up to 15% of the celadonite end-member (Table 4.2), which represents among the highest Tschermack substitution found in the Afyon Zone. This suggests that ^{40}Ar-^{39}Ar isotopic dating of mica in this sample might provide near-peak metamorphic ages.

In the Konya region (Figure 4.1), some carpholite-quartz veins also contain white mica, but this contains a significant paragonite component, preventing any accurate PT estimation and, a priori, hampering ^{40}Ar-^{39}Ar geochronologic investigations. We tentatively performed Ar isotope analyses on a sample from the region of Konya, but laser ablation experiments did not release any significant gas amount for Ar isotope analysis.

In the easternmost regions of Yahyalı and Kayseri (Figure 4.1), carpholite was substantially pseudomorphed into phengite and chlorite, locally accompanied by chloritoid. We selected the sample Yah04, in which phengite and chlorite are mostly intergrown, but also occur as isolated crystals, allowing easy mineral separation.

In the Ören Unit, carpholite documented in quartz veins is commonly accompanied by phengite and chlorite (Oberhänsli et al., 2001; Rimmelé et al., 2003a). We selected the sample Ören001 (Figure 4.1) from a quartz vein encompassing well-preserved carpholite needles accompanied by phengite and chlorite (Rimmelé et al., 2003a). Carpholite-chlorite-phengite equilibrium in this sample accounts for *P-T* conditions of 0.8-1.1 GPa and 320-380°C (Rimmelé et al., 2005).

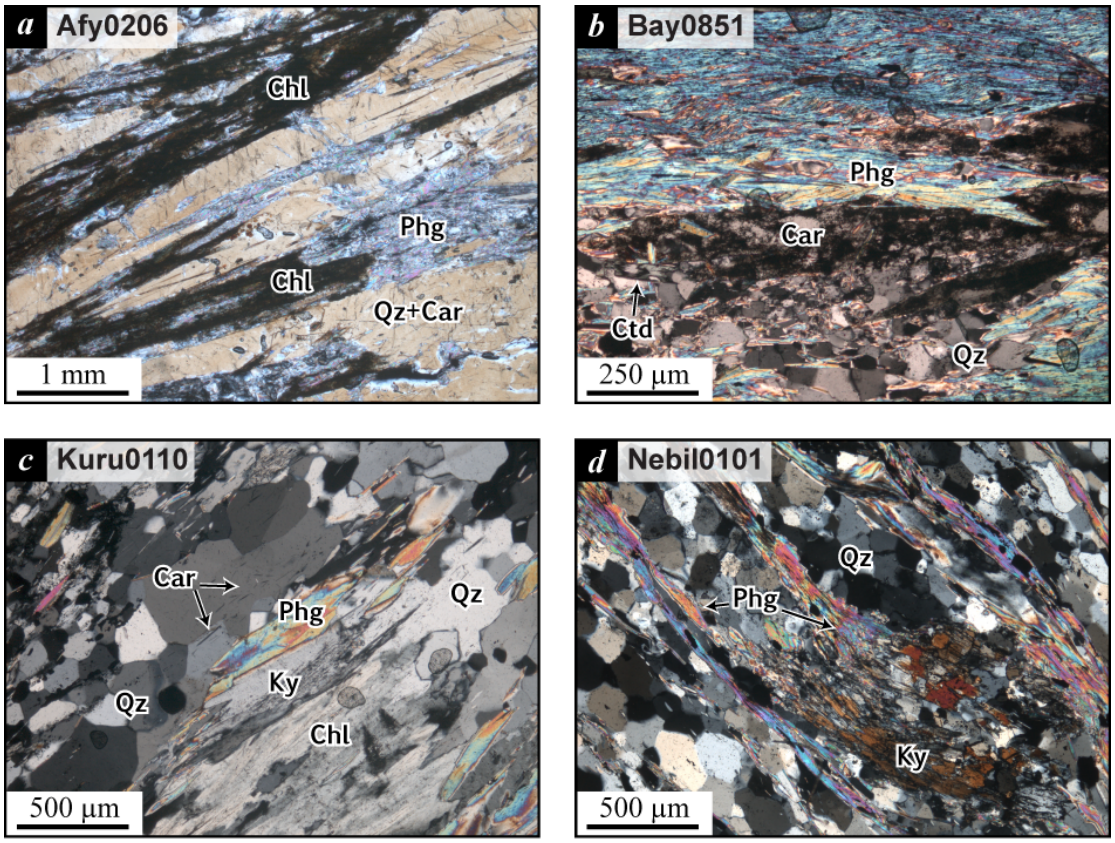

Figure 4.2: Optical microphotographs (cross polars) of the samples investigated by in-situ UV laser ablation. Mineral abbreviations: Car, carpholite; Chl, chlorite, Ctd, chloritoid; Ky, kyanite; Phg, phengite; Qz, quartz.

From the Menderes Massif cover, we retained the samples Kuru0110 (from Kurudere, diaspore zone) and Nebil0101 (from Nebiler, corundum zone), for which PT estimates were already estimated based on carpholite-chlorite-kyanite equilibrium and phengite-chlorite equilibrium, respectively (Rimmelé et al., 2005). The sample Kuru0110 is a quartz vein containing the main assemblage carpholite + kyanite + chlorite + phengite + pyrophyllite. Kyanite, chlorite and phengite obviously grew coevally from the breakdown of carpholite that is only preserved as small fibres in quartz. The easterly sample Nebil0101 is a metamorphosed quartz microconglomerate bearing kyanite + chloritoid + phengite as a main assemblage. Chlorite was reported to be abundant in this sample (Rimmelé et al., 2003b), but was not seen in the sample fragment that we selected. Furthermore, no carpholite relic is observed in this sample, whereas complete kyanite-chlorite pseudomorphs after carpholite were described from the same locality. In the selected sample, white mica obviously formed after kyanite (Figure 4.2d).

Table 4.2: Calculated average compositions of chlorite and mica in Afy0206 and Yah04 samples.

	Afy0206			Yah04		
Chlorite	C1	C2	C3	C1	C2	C3
SiO_2	25.25	26.39	27.51	25.75	26.57	27.93
Al_2O_3	21.88	22.83	22.71	25.68	26.24	27.14
FeO	27.59	26.33	25.06	22.45	21.52	20.06
MnO	0.06	0.06	0.06	0.05	0.05	0.05
MgO	11.55	11.60	11.22	14.59	14.07	13.23
CaO	0.09	0.09	0.09	0.02	0.02	0.02
NaO	0.04	0.04	0.04	0.06	0.13	0.25
K_2O	0.35	0.48	0.69	0.04	0.07	0.14
Atom site distribution (14 anhydrous oxygen basis including Fe3+)						
Si(T1+T2)	2.67	2.74	2.82	2.62	2.68	2.77
Al(T2)	1.33	1.26	1.18	1.38	1.32	1.23
Al(M1)	0.33	0.26	0.18	0.38	0.32	0.23
Mg(M1)	0.23	0.21	0.20	0.25	0.24	0.22
Fe^{2+}(M1)	0.30	0.22	0.18	0.22	0.20	0.18
V(M1)	0.14	0.31	0.44	0.15	0.24	0.37
Mg(M2+M3)	1.59	1.58	1.52	1.96	1.87	1.73
Fe^{2+}(M2+M3)	2.00	1.63	1.37	1.69	1.58	1.39
Al(M2+M3)	0.34	0.69	0.99	0.32	0.51	0.81
Al(M4)	0.85	0.57	0.40	1.00	0.96	0.90
Fe^{3+}(M4)	0.15	0.43	0.60	0.00	0.04	0.10
X(Fe^{3+}) (%)	6	19	28	0	3	6
Temperature (°C)*	351	258	197	384	320	248

*Vidal et al. (2006). initial pressure = 5 kbar

	Afy0206		Yah04	
Mica	M1	M2	M1	M2
SiO_2	48.13	47.19	47.78	47.55
Al_2O_3	32.55	33.60	35.85	36.11
FeO	2.25	2.07	0.40	0.40
MnO	0.01	0.01	0.01	0.01
MgO	0.96	0.84	0.45	0.42
CaO	0.04	0.04	0.03	0.03
NaO	1.05	1.36	1.10	1.31
K_2O	9.21	8.86	8.86	8.39
Atom site distribution (11 anhydrous oxygen basis including Fe3+)				
Si(T1+T2)	3.23	3.17	3.15	3.14
Al(T2)	0.77	0.83	0.85	0.86
V(M1)	0.98	0.97	1.00	0.99
Mg(M1)	0.01	0.01	0.00	0.01
Fe(M1)	0.01	0.02	0.00	0.00
Al(M2+M3)	1.80	1.83	1.94	1.95
Mg(M2+M3)	0.09	0.07	0.04	0.03
Fe(M2+M3)	0.11	0.10	0.02	0.02
K(A)	0.79	0.76	0.75	0.71
Na(A)	0.13	0.17	0.14	0.17
V(A)	0.08	0.07	0.11	0.12
Prp	0.07	0.06	0.11	0.12
Tri	0.02	0.03	0.01	0.01
Prg	0.14	0.18	0.14	0.17
Ms	0.61	0.62	0.70	0.68
Cel	0.16	0.11	0.04	0.02

4.3.2. *P-T* estimation

4.3.2.1. Method

Element mapping combined with spot analyses were performed on an electron microprobe JEOL4500 (Potsdam University), following the procedure described by De Andrade et al. (2006). Areas selected for mapping contain the coarsest grains possible and display sharp grain boundaries (i.e., limited intergrowths). Maps dimensions are 454*206 and 240*79 pixels in Afy0206 and Yah04, respectively. Operating conditions for maps were 15-kV accelerating voltage, 5-µm beam size, 100-nA beam current, for counting times of 20 s on peak and 10 s on background. Spot analyses were acquired with 15-kV accelerating voltage, 5-µm beam size, 10-nA beam current, for counting times of 20 s on peak and 10 s on background. Standards of pyrope for Si, rutile for Ti, pyrope for Al, hyperstene for Fe, fayalite for Mn, diopside for Mg, diopside for Ca, anorthite for Na and microcline for K were used.

Profiles of individual spot quantitative analyses were traced across phengite-chlorite aggregates. Using these profiles as standards, each pixel of the qualitative element maps was quantified into a punctual quantitative analysis (in oxide weight percent). This was done using XMapTools software (Lanari et al., in prep.; http://www.xmaptools.com). In each investigated area, a large number of spot analyses were acquired for each phase in order to ensure the precision of this quantification.

Structural formulae and atom site repartition of chlorites and phengites were calculated following the solid solution models of Vidal and Parra (2000), Vidal et al. (2005) and Dubacq et al. (2010).

The K-means clustering method (Saporta, 1990) was used to distribute chlorite and phengite compositions into various groups. Each group was first considered individually to calculate temperatures using the chlorite-quartz-water equilibrium (at a given pressure) following the method of Vidal et al. (2005, 2006). For phengite, the method of Dubacq et al. (2010) was used to plot a PT line corresponding to the phengite-quartz-water equilibrium, with phengite internal hydration state varying (% of water in interlayer vacancies) along this line. Using chlorite temperature allows us, in this case, estimating a pressure for phengite equilibration. Then, chlorite-mica-quartz-water equilibrium between the various chlorite and mica groups was tested in order to calculate *P-T* conditions by using the multi-equilibrium approach described by Vidal and Parra (2000). The presence of tiny chloritoid in Yah04, albeit not allowing element mapping, provided the possibility to calculated *P-T* conditions prevailing for local chlorite-chloritoid-quartz-water equilibrium. *P-T* estimation was based on the calculation of multi-equilibria by using 'ChlMicaEqui', a Matlab GUI-based software.

4.3.2.2. Mineral analyses

Chlorite and mica analyses from the samples Afy0206 and Yah04 were distributed into three (C1, C2, C3 and c1, c2, c3) and two groups (M1, M2, M+P, and m1, m2, m+p), respectively (Figure 4.3). Average compositions for each of these groups, except the muscovite-paragonite mixtures (M+P and m+p), are shown in the Table 4.2. In both samples, chlorite compositional groups display an increase of the sudoite-content from C1 to C3 and from c1 to c3, while the proportion of the other end-members does not significantly change (Figure 4.3a-a'). Abundance of the sudoite end-member (vacancy on the octahedral site [M1]) decreases with increasing temperature (Cathelineau and Nieva,

1986; Hillier and Velde, 1991; Vidal et al., 2001). Therefore the decrease of sudoite-content from the inner to the outer crystals (Figure 4.3b-b') reflects chlorite growth under decreasing temperature. Many phengite analyses show a significant contribution of paragonite. Phengite groups account for slightly different Si-contents, with Si-content that trend to be higher in M1 and m1 than M2 and m2, respectively (Figure 4.3a-a'). This possibly indicates that the formers formed at slightly higher pressure than the latter. Analysis of chloritoid in Yah04 reveals that X_{Mg} (= $Mg/(Fe^{2+} + Mn + Mg)$) covers a range between 0.12 and 0.15.

4.3.2.3. Thermobarometry

In Afy0206, C1, C2 and C3 chlorite average compositions give temperatures of 351, 258 and 197 ± 50°C and X_{Fe3+} of 6, 19 and 28 % respectively. Mica groups M1 and M2 yield pressures of 6 and <0.3 GPa at 350°C, respectively. Multi-equilibrium calculation revealed that C1 chlorite and M1 mica equilibrated (residual energy of 7200 J) at *P-T* conditions of ca. 0.6 GPa and ca. 350°C (Figure 4.3c), which are very consistent with those determined individually using chlorite-quartz-water and phengite-quartz-water equilibriums.

In Yah04, the chlorite groups c1, c2 and c3 correspond to temperatures of 384, 320 and 248 ± 50°C at 1.0 GPa and X_{Fe3+} of 6, 19 and 28 % respectively. For a temperature set to 380°C, m1 and m2 micas equilibrated at 0.7 and < 0.4 GPa, respectively. On the one hand, no chlorite-mica equilibrium was found among the average compositions calculated, likely due to the use of anhydrous mica end-members in the method of Vidal and Parra (2000). On the other hand, multi-equilibrium calculation shows an equilibrium between the c1 chlorite and average chloritoid composition (X_{Mg} = 0.14) at *P-T* conditions of ca. 0.9 GPa and ca. 380°C (Figure 4.3c). In addition, individual chlorite-chloritoid pairs based on individual spot analyses provide conditions of 390-420°C and 0.9-1.1 GPa (Table 4.3).

These *P-T* estimates out of the stability field of carpholite (Figure 4.3d-d') are consistent with the fact that chlorite and phengite in these samples occur as pseudomorphs after carpholite. No relic of high-pressure phengite (high celadonite content) was found. ^{40}Ar-^{39}Ar geochronology will thus consistently provide retrograde ages.

4.3.3. ^{40}Ar-^{39}Ar geochronology

4.3.3.1. Sample preparation

Phengite were extracted from the samples Afy0212, Küt0815, Yah04 and ÖREN001 in order to perform ^{40}Ar-^{39}Ar dating by stepwise heating on mineral separates with CO_2 laser. Pure phengite grain bunches were obtained by gently scratching the surface of the quartz vein samples followed by enrichment and purification using conventional techniques for mineral separation, including washing, sieving, adherence to paper and handpicking under binoculars.

In order to perform ^{40}Ar-^{39}Ar dating by in-situ UV laser ablation, 1-mm-thick rock chips were prepared from the samples Afy0206, Bay0851, Kuru0110 and Nebil0101.

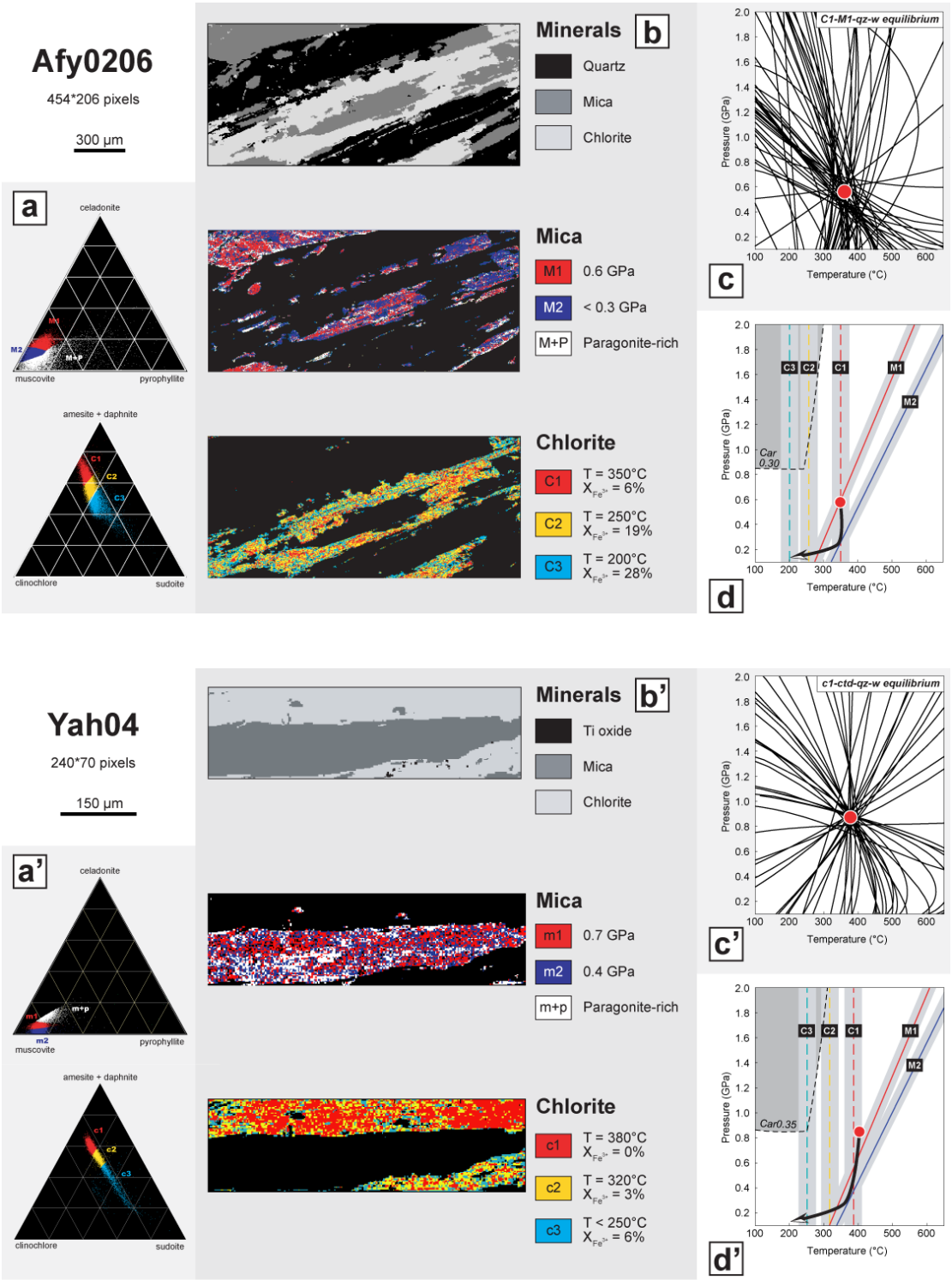

Figure 4.3: Results of multi-equilibrium thermobarometry for the samples Afy0206 and Yah04. a-a') Ternary diagrams for white mica and chlorite compositions. b-b') Map view of mineral distribution, and mica and chlorite chemical groups in the investigated areas. c-c') chlorite-mica-quartz-water (Afy0206) and chlorite-chloritoid-quartz-water (Yah04) multi-equilibrium calculations using average group compositions. d-d') Result summary. Stability fields of carpholite calculated with TheriakDomino (De Capitani and Petrakakis, 2010) following Pourteau et al. (2011a) (Chapter 3). See text for details.

Table 3.3: Chlorite and chloritoid mineral compositions and Chl-Ctd-Qz-w multiequilibrium thermobarometric estimates obtained from pairs in Yah04.

	pair 1		pair 2		pair 3		pair 4	
	Ctd	Chl	Ctd	Chl	Ctd	Chl	Ctd	Chl
SiO_2	24.645	25.462	24.432	29.956	24.579	25.114	24.577	25.162
Al_2O_3	42.154	25.893	41.991	26.045	41.849	25.875	41.640	25.749
FeO	25.389	23.254	25.191	22.044	25.400	22.520	25.779	22.776
MnO	0.291	0.078	0.233	0.071	0.209	0.000	0.212	0.000
MgO	2.309	14.029	2.563	14.471	2.561	14.924	2.427	14.757
CaO	0.010	0.049	0.001	0.017	0.000	0.018	0.000	0.024
Na_2O	0.000	0.058	0.023	0.039	0.000	0.011	0.000	0.020
K_2O	0.029	0.048	0.004	0.030	0.014	0.039	0.002	0.034
Si(T1+T2)	1.99	2.59	1.98	2.63	1.99	2.55	1.99	2.56
Al(T2)	4.01	1.40	4.01	1.37	3.99	1.45	3.98	1.44
Al(M1)		0.40		0.37		0.45		0.44
Mg(M1)	0.28	0.23	0.31	0.23	0.31	0.21	0.29	0.22
Fe^{2+}(M1)	1.71	0.22	1.71	0.20	1.72	0.17	1.75	0.17
V(M1)		0.15		0.20		0.17		0.17
Mg(M2+M3)		1.90		1.95		2.04		2.05
Fe^{2+}(M2+M3)		1.76		1.62		1.60		1.62
Al(M2+M3)		0.31		0.41		0.35		0.35
Al(M4)		1.00		0.95		0.85		0.85
Fe^{3+}(M4)		0.00		0.05		0.15		0.14
Cln		0.23		0.23		0.21		0.22
Daph		0.22		0.20		0.17		0.17
Am		0.40		0.37		0.45		0.44
Sud		0.15		0.20		0.17		0.17
X_{Mg}(Ctd)	0.14		0.15		0.15		0.15	
P (GPa)	**0.82**		**0.89**		**0.95**		**0.96**	
T (°C)	**411**		**400**		**425**		**418**	

	pair 5		pair 6		pair 7	
	Ctd	Chl	Ctd	Chl	Ctd	Chl
SiO_2	24.800	25.611	25.843	25.927	24.263	25.942
Al_2O_3	41.628	25.290	39.713	25.542	41.845	25.127
FeO	25.322	23.212	24.784	22.225	24.690	22.147
MnO	0.328	0.042	0.181	0.021	0.283	0.088
MgO	2.337	14.846	3.631	15.465	2.451	15.598
CaO	0.000	0.023	0.013	0.024	0.004	0.027
Na_2O	0.026	0.015	0.000	0.000	0.012	0.000
K_2O	0.009	0.030	0.020	0.026	0.020	0.020
Si(T1+T2)	2.01	2.59	2.09	2.58	1.98	2.62
Al(T2)	3.97	1.41	3.79	1.42	4.02	1.38
Al(M1)		0.41		0.42		0.38
Mg(M1)	0.28	0.23	0.44	0.18	0.30	0.26
Fe^{2+}(M1)	1.72	0.19	1.68	0.11	1.68	0.19
V(M1)		0.17		0.29		0.17
Mg(M2+M3)		2.01		2.11		2.09
Fe^{2+}(M2+M3)		1.63		1.30		1.56
Al(M2+M3)		0.35		0.58		0.34
Al(M4)		0.85		0.56		0.88
Fe^{3+}(M4)		0.15		0.44		0.12
Cln		0.23		0.18		0.26
Daph		0.19		0.11		0.19
Am		0.41		0.42		0.38
Sud		0.17		0.29		0.17
X_{Mg}(Ctd)	0.14		0.22		0.15	
P (GPa)	**0.95**		**1.13**		**0.96**	
T (°C)	**400**		**383**		**389**	

4.3.3.2. Analytical procedure

Procedure for ^{40}Ar-^{39}Ar analysis in the University of Potsdam is also described in the recent literature (e.g., Wiederkehr et al., 2009; Willner et al., 2009; Vásquez et al., 2010; Wilke et al., 2010). Neutron activation of polished sections and mineral separates was performed at Geesthacht Neutron Facility (GeNF), GKSS research centre in Geesthacht, Germany. The ^{40}Ar-^{39}Ar ages were obtained as the relative age against the age of a neutron flux (or J value) monitoring mineral standard, Fish Canyon tuff sanidine, which was irradiated together with the samples of unknown ages. The Fish Canyon Tuff sanidine used was prepared by the Geological Survey of Japan and the age of 27.5 Ma was obtained and adopted (Uto et al., 1997; Ishizuka, 1998; Ishizuka et al., 2002). Crystals of K_2SO_4 and CaF_2 were also irradiated together in order to correct the interference of Ar isotopes produced by the nuclear reactions of K and Ca in the samples with neutron fluxes. After the irradiation and subsequent cooling down for a month, the samples were brought back to ^{40}Ar-^{39}Ar laboratory in the University of Potsdam for Ar isotope analysis. Analyzed samples were then loaded on a copper disc in the sample chamber and baked at 100°C during pumping for two days for reduction of atmospheric argon contamination.

The Ar isotopic analytical system in the University of Potsdam consists of: (1) a New Wave Gantry Dual Wave laser ablation system with a 50W CO_2 laser (wavelength 10.6 micrometer) and 6 mJ UV pulse laser (wavelength 266 nanometre, frequency-quadrupled) for heating and extracting gas from the samples, (2) an ultra-high vacuum purification line with SAES getters and cold trap with temperature of frozen ethanol, and (3) a Micromass 5400 noble gas mass spectrometer with a high sensitivity and a ultra-low background. The mass spectrometer has adopted a pulse counting system with an electron multiplier, which effectively works for the very small amounts of gas.

Age spectra obtained by stepwise heating of bulk white mica grains were produced from bunches of 3 to 7 grains of size ranging between 125 and 500 μm, which were heated by scanning laser beam with a diameter of 1600 microns for 45 to 90 seconds with 70 μm/sec scan speed. In-situ UV laser ablation was carried out with a beam with a diameter of 50 μm and a 5 μm/sec scan speed. When phengite grains were small, the in-situ ablation was performed following long paths (up to 1500 μm) to release sufficient gas amount. Ar isotope analyses may thus yield average ages for several coexisting generations of white mica. This is evaluated below. Data have been corrected for blank, mass discrimination, decay of radiogenic ^{37}Ar and ^{39}Ar, and interference of Ar isotopes derived from K and Ca.

4.3.3.3. Raw age results

Results of Ar isotope analyses are shown in Appendix 2. Representative age diagrams are presented in the Figure 4.4. A significant plateau age is defined by a series of adjacent steps, which represent individually more than 5 % and in all more than 50 % of the total ^{39}Ar release and contiguously agree within 2-SD error limits as McDougall and Harrison (1999) mentioned. The age spectra obtained fully satisfy these conditions. On the other hand, in-situ age results are displayed in 'pseudo-plateau' diagrams (Figure 4.4b) in order to show the representability of each spot analysis in terms of released ^{39}Ar amount.

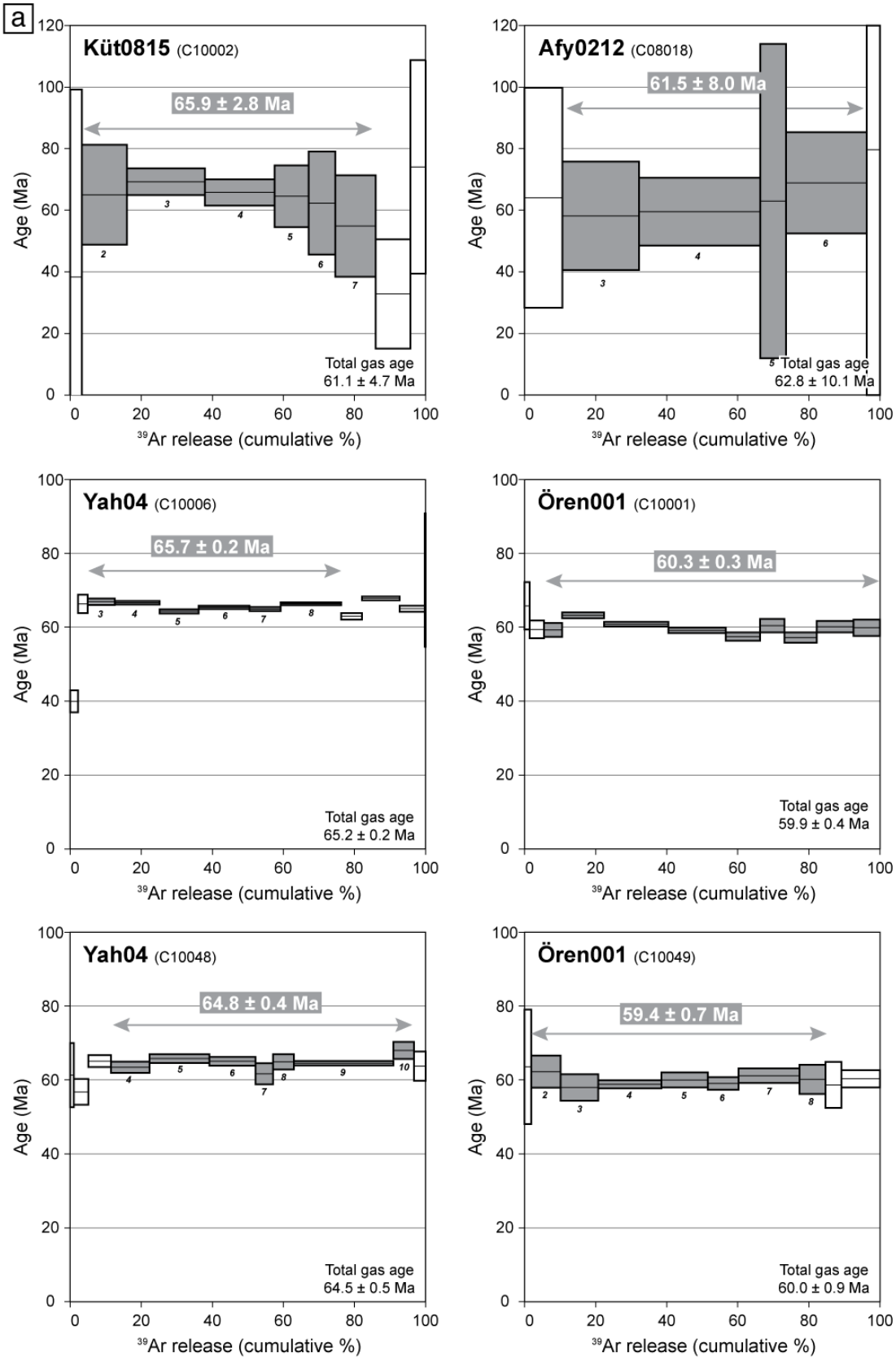
a
Küt0815 (C10002)
65.9 ± 2.8 Ma
Total gas age
61.1 ± 4.7 Ma
Afy0212 (C08018)
61.5 ± 8.0 Ma
Total gas age
62.8 ± 10.1 Ma
Yah04 (C10006)
65.7 ± 0.2 Ma
Total gas age
65.2 ± 0.2 Ma
Ören001 (C10001)
60.3 ± 0.3 Ma
Total gas age
59.9 ± 0.4 Ma
Yah04 (C10048)
64.8 ± 0.4 Ma
Total gas age
64.5 ± 0.5 Ma
Ören001 (C10049)
59.4 ± 0.7 Ma
Total gas age
60.0 ± 0.9 Ma
Age (Ma)
39Ar release (cumulative %)

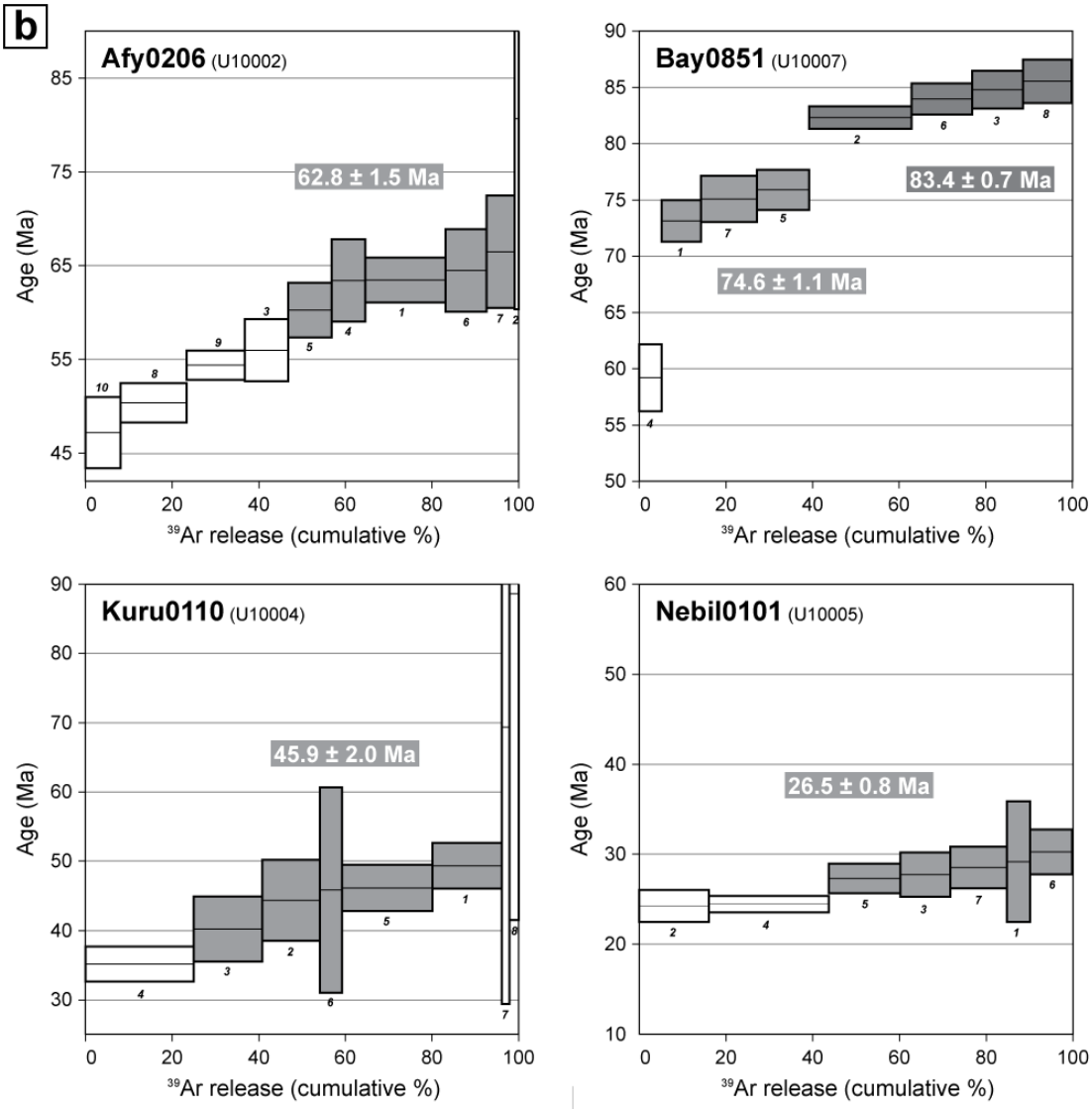

Figure 4.4: Ar-Ar age spectra. a) Representative plateau age diagrams obtained by stepwise heating of mineral separates using a CO_2 laser. b) "Pseudo-plateau" age diagrams for in-situ ablation of rock sections using a UV laser. Box numbers refer to step numbers in the Table A2.4 (Appendix 2).

Afyon Zone. In-situ laser ablation in Afy0206 provided age results scattered between 47.1 ± 3.8 and 66.4 ± 6.1 Ma, without apparent correlation between age, atmospheric Ar content and released-gas amount. Five of the ten steps, representing about 52% of the total ^{39}Ar release, give an average age of 62.8 ± 1.5 Ma (Figure 4.4a). In-situ laser ablation in Bay0851 provided ages results that, except one, are distributed into two groups (Figure 4.5a): one around 83.4 ± 0.7 Ma (4 analyses) and another one 74.6 ± 1.1 Ma (3 analyses). Mineral separates from the sample Yah04 yielded well-defined plateaus (Figure 4.4b), indicating consistent ages of 65.3 ± 0.5 Ma, 65.7 ± 0.2 Ma and 64.8 ± 0.4 Ma. For each separate, isochron and inverted isochron ages, as well as total gas ages, are similar to these plateau ages within the 2-SD analytical uncertainty.

Ören Unit. Mineral separates from the sample Ören001 furnished well-defined plateaus (Figure 4.4b), indicating ages of 60.3 ± 0.3 Ma, 62.6 ± 0.4 Ma and 59.4 ± 0.7 Ma. For each separate,

isochron and inverted isochron ages, as well as total gas ages, are similar to these plateau ages within the 2-SD analytical uncertainty.

Menderes Massif. In-situ laser ablation in Kuru0110 provided age results scattered between 35.0 ± 2.5 and 49.2 ± 3.3 Ma. Five of the eight steps, representing about 71% of the total ^{39}Ar release, give an average age of 45.2 ± 2.0 Ma (Figure 4.4a). In-situ laser ablation in Nebil0101 provided age results scattered between 24.2 ± 1.8 and 30.2 ± 2.5 Ma. Five of the seven steps, representing about 56% of the total ^{39}Ar release, give an average age of 26.5 ± 0.8 Ma (Figure 4.4a).

4.4. Age significance

4.4.1. Argon retention

Although intergranular fluids and lattice deformation play important roles in argon diffusivity, temperature is generally regarded as the predominant external parameter controlling argon exchange between white mica and surroundings (e.g., Villa, 1998). Theoretically, below a certain temperature, referred to as "closure temperature", minerals behave as closed systems, retaining radiogenic isotopes as they form. The closure temperature for Ar diffusion in white mica has been highly debated for the last decades. Following pioneer works of E. Jäger (e.g., Jäger, 1973; Purdy and Jäger, 1976), a value of 350°C was long considered. However, many studies demonstrated that white mica retains argon up to higher temperatures and agreed to reconsider a higher closure temperature (450-500°C) (e.g., Hammerschmidt and Franz, 1991; Di Vincenzo et al., 2001; Balogh and Dunkl, 2005).

Still little is known about the effect of the Tschermak substitution on the diffusivity of argon in white mica. So temperature closure of phengite is commonly considered to be similar to the one of muscovite (Wijbrans and McDougall, 1986; Hames and Bowring, 1994; Reddy et al., 1996). Since phengite that we dated shows low celadonite content (i.e., limited Tschermack substitution), this assumption seems reasonable in the frame of our study. Bearing in mind that temperature in the Afyon Zone and Ören Unit did not exceed 400°C, white mica ^{40}Ar-^{39}Ar ages from these regions represent crystallization ages. By contrast, high-pressure metamorphism in the southern Menderes cover was followed by a temperature increase (Barrovian phase) during the retrograde path, which has erased most of the high-pressure minerals (carpholite in favour of chloritoid, kyanite and chlorite; diaspore in favour of corundum). At the base of the Palaeozoic schists, temperature reached at least 520°C (Whitney and Bozkurt, 2002; Régnier et al., 2003), opening the possibility to partially reset the ^{40}Ar-^{39}Ar isotopic system.

4.4.2. Isotopic ages and petrology

Afyon Zone

In-situ laser ablation in the carpholite-bearing phyllite sample Bay0851 yielded two age trends: around 75 and 83 Ma (Figure 4.4b). Fine grain size of analyzed phengite required laser ablation on relatively large area in order to extract sufficient gas amount, so any textural distinction between

these two age groups is not possible yet. Since, in this sample, prograde and peak minerals (carpholite and chloritoid) are well preserved and retrograde phases (chlorite in particular) are absent and (prograde and peak conditions), phengite, which displays among the highest celadonite content of the region, is likely to represent peak (and even prograde?) conditions. The present ^{40}Ar-^{39}Ar results are therefore assumed to indicate that high-pressure metamorphism in the Afyon Zone occurred before 75 Ma ago.

In the samples Afy0206, Afy0212 and Yah04, phengite obviously formed after carpholite. Accordingly, thermobarometric results from these samples show that ^{40}Ar-^{39}Ar phengite ages concern the retrograde path of the high-pressure loop. Although the two samples investigated for PT estimations (Afy0206 and Yah04) yielded homogeneous phengite composition and temperatures lower than Ar closure in phengite, scattered ^{40}Ar-^{39}Ar ages were obtained (from one spot analysis to the other in Afy0206; from one mineral separate bunch to the other for Yah04; Figure 4.4). Phengite that equilibrated under middle-pressure conditions (0.6-0.7 GPa) provided ^{40}Ar-^{39}Ar ages of about 63 and 65 Ma for the retrograde path of the western and eastern parts of the Afyon Zone, respectively. This is consistent with our assumption that the metamorphic peak occurred ≥ 75 Ma ago.

Ören Unit

According to the PT estimates of Rimmelé et al. (2005), phengite and chlorite from the sample Ören001 formed between 0.8 and 1.0 GPa and 300 and 400°C along a syn-cooling decompression path. The ^{40}Ar-^{39}Ar ages between 60 and 62 Ma obtained for the sample Ören001 therefore prevail for high-pressure retrograde stages in the Ören Unit.

Menderes Massif

For the Menderes Massif cover, we obtained contrasting ages from the two dated localities.

Since petrographic textures in Kuru0110 indicate that white mica formed along with chlorite and kyanite from the breakdown of carpholite, the mean ^{40}Ar-^{39}Ar age of 45.2 ± 2.0 Ma obtained from this sample, represents post-high-pressure retrograde stages. As suggested by the partial preservation of diaspore in metabauxites from area, Barrovian metamorphism did not significantly affected this part of the Menderes marbles.

In the sample Nebil0101, the mean ^{40}Ar-^{39}Ar age 26.5 ± 0.8 Ma obtained on phengite, formed after kyanite and chloritoid, represents late retrograde stage. The total replacement of carpholite by chlorite and kyanite, and of diaspore by corundum in this area suggests a low-pressure overprint of high-pressure minerals stronger than in the locality of Kurudere. We therefore regard the ^{40}Ar-^{39}Ar age obtained on the sample from Nebiler to represent post-Barrovian cooling.

4.5. Discussion: correlations and regional geodynamics

4.5.1. Origin of the Ören Unit

Since high-pressure metamorphism was documented in the Ören Unit (Oberhänsli et al., 2001; Rimmelé et al., 2003a), the geodynamic signification of this unit, previously inferred to be part of the

non-metamorphosed Lycian Nappes, has become a challenging issue. Kinematic indicators documented along the basal thrust and in the lower schists of the Ören Unit recorded non-coaxial deformation oriented top-to-ENE along the southern margin of the Menderes Massif, top-to-SSW in the klippen atop the Cycladic Blueschist Unit, and top-to-ESE in the Borlu klippe, as well as on the eastern margin of the Menderes Massif (Güngör and Erdoğan, 2001; Rimmelé et al., 2003a, 2006). The regional consistency of the kinematic indicators was obviously perturbed by subsequent extensional tectonics from the Oligocene onwards. In late Miocene to early Pliocene times, the central Menderes Massif was exhumed along bivergent detachments (Gessner et al., 2001b) accommodating scissor-like extension around an easterly pivot point that led to a differential rotation of 25-30° counter clockwise of the southern part regarding the northern part of the Menderes Massif (Pourteau et al., 2010; van Hinsbergen et al., 2010). In order to correlate the shear senses documented in the Ören Unit throughout the region, the position of the southern Menderes region needs to be restored of this post-imbrication rotation. This restoration shows that, before the Neogene, extension kinematic indicators were likely of similar orientation in the southern and northern Menderes Massif, i.e., directed approximately top-to-ESE. Kinematic analysis in the klippen atop the Cycladic Blueschist Unit shows shear senses in contrast with those from the other regions. There, top-to-SSW displacement associated to a low-angle tectonic contact with the underlying formations was attributed to normal faulting (Güngör and Erdoğan, 2001), apparently representing the western extension of a top-to-S detachment at the southern edge of the central Menderes Massif (Emre and Sözbilir, 1997; Gessner et al., 2001a). No correlation is therefore to be envisaged between these extensional kinematic indicators and those from the other areas, which are instead related to the exhumation of the high-pressure rocks (Rimmelé et al., 2003a, 2006). We thus argue that during its exhumation the Ören Unit was transported towards the ESE over the Menderes Massif, as already suggested by van Hinsbergen (2010). It therefore originates from the northwestern margin of the Menderes Massif.

On the basis of the following points, we discuss the possible relation between the Afyon Zone and the Ören Unit.

(i) The Ören Unit lies over the Menderes Massif and the Cycladic Blueschist Unit, and below the Lycian Ophiolites and associated mélange. As seen at the northwestern margin of the Menderes Massif, the Afyon Zone lies over a thin tectonic slice of Cycladic Blueschist Unit. It also represents the hanging-wall of a top-to-NNE detachment that accommodated the exhumation of the northern Menderes Massif (Işik and Tekeli, 2001). The Ören Unit and Afyon Zone thus have similar structural positions regarding the adjacent tectonic units. Because the contact between these units does not crop out anywhere, their relative structural position has always remained unknown. Considering them as a single unit allows avoiding this issue.

(ii) Lithostratigraphic correlation, albeit not strictly required for connecting tectonic units, is often used to test the possibility for units to stem from a similar palaeogeographic domain. Beyond the fact that the Ören Unit and the western Afyon Zone display similar Mesozoic lithostratigraphies, reddish metasediments containing carpholite-bearing quartz veins characteristic of the Ören Unit (Rimmelé et al., 2003a) are also common near Kütahya, in the western Afyon Zone (Pourteau et al., 2010). The lack of conglomerate levels at the base of the metapelitic sediments suggests that lower

Triassic schist layers were used as main décollement horizon. Moreover, in both units, the Mesozoic carbonates are topped by a weakly metamorphosed Maastrichtian wildflysch, which contains blocks of neritic and pink pelagic limestones, mafic volcanic rocks, radiolarite and blue-amphibole-bearing schists (Bernoulli et al., 1974; Rimmelé, 2003; Göncüoğlu et al., 1992; Robertson et al., 2009).

(iii) Carpholite-bearing rocks in the Ören Unit and Afyon Zone attest for similar metamorphic grade in the lower blueschist facies. The fact that carpholite is little replaced by chloritoid, and never accompanied by kyanite, shows that these units both staid in the pyrophyllite stability field, i.e., temperature < ca. 400-450°C. Although some parts of the Ören Unit were shown to have followed a syn-cooling decompression path (Rimmelé al., 2005), others obviously experienced relatively isothermal decompression like evidenced in the Afyon Zone (this study).

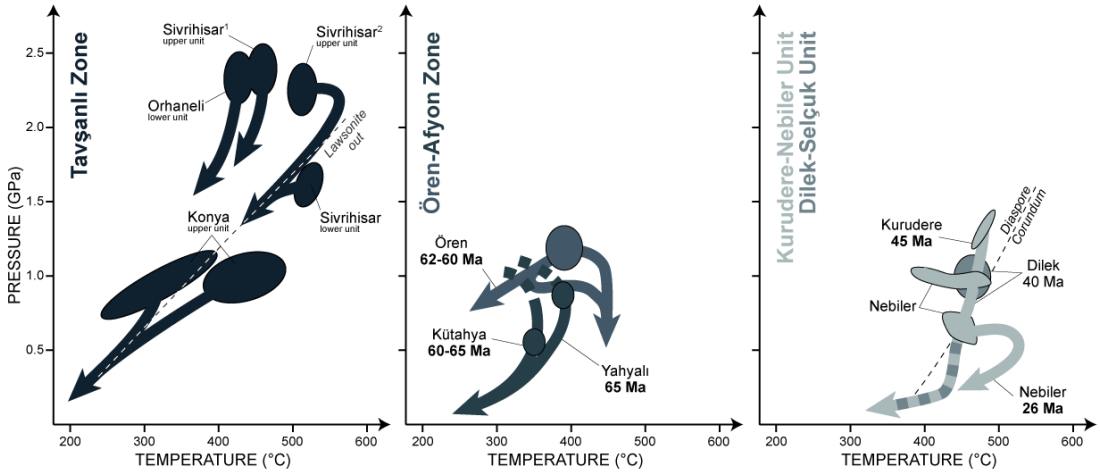

Figure 4.5: Synthetic *P-T-t* paths for the three Anatolide high-pressure belts. Ages in bold characters refer to ^{40}Ar-^{39}Ar geochronologic results from the present study. "Dilek" refers to the Anatolian part of the Cycladic Blueschist Unit; "Sivrihisar[1]" after Davis and Whitney (2008); "Sivrihisar[2]" after Çetinkaplan et al. (2008). Other references in text.

(iv) Isotopic age results show that retrogression subsequent to high-pressure metamorphism occurred slightly later in the Ören Unit (62-60 Ma ago) than in the Afyon Zone (63-65 Ma ago). Such little lateral variations of metamorphic age, which are common thing in high-pressure metamorphic belts, are here regarding as insignificant. The evolution of these units appears thus commonly distinct from those of the Tavşanlı Zone on the one hand, and the Cycladic Blueschist Unit and the Menderes Massif on the other hand (Figure 4.5).

We therefore argue that, before it was transported on top of the Menderes Massif, the Ören Unit represented the western continuation of the Afyon Zone. We thus merge these units as the Ören-Afyon Zone.

4.5.2. A new tectonic unit: the Kurudere-Nebiler Unit

4.5.2.1. Extent of the high-pressure metamorphism at the southern margin of the Menderes Massif

Evidence for Cenozoic high-pressure, low-temperature metamorphism in the Menderes Massif are strictly restricted to the relics and ghosts (pseudomorphs) of carpholite reported from three localities of metamorphosed lower Triassic conglomerates at the base of the southern Menderes marble sequence (Rimmelé et al., 2003b). The Precambrian gneissic core, the Palaeozoic schist cover, as well as the other parts of the Mesozoic marble cover are completely free of high-pressure minerals related to the Alpine orogeny (Candan et al., 2011a). The occurrence of diaspore in metabauxites intercalated with Jurassic to lower Cretaceous marbles is limited to the southern margin. Corundum is consistently reported anywhere else (Dürr, 1975). In the southern Menderes marble sequence, carpholite relics were reported where diaspore was preserved (Kurudere and Bahçeyaka localities), while only textural pseudomorphs after carpholite were documented from one locality in the diaspore-free corundum zone (Nebiler) (Rimmelé et al., 2003b). The preservation of diaspore and high-pressure minerals thus coincides in the Menderes Massif, like in the platform unit of the Anatolian part of the Cycladic Blueschist Unit (Candan et al., 1997). In our opinion, the fact that, except in those three localities, the southern Menderes marble sequence does itself lack evidence of high-pressure minerals prevents any clear distinction between a "high-pressure zone" and a "low-pressure zone". The intensity of the Barrovian overprint apparently controlled the preservation of the high-pressure assemblage in this sector.

The regional extent of the Eocene high-pressure metamorphism in the Menderes Massif therefore constitutes a key issue. We envisage and evaluate two models for the basal boundary of this high-pressure tectonic unit, which we refer to as the Kurudere-Nebiler Unit (from carpholite localities).

1) Because the Palaeozoic to early Cenozoic sedimentary sequence at the southern margin of the Menderes Massif was described as stratigraphically continuous (Dürr, 1975; Şengör et al., 1984; Konak et al., 1987) and the core-cover unconformity was reworked as a multistage fault (see e.g., Régnier et al., 2003; Bozkurt, 2007), the entire Menderes cover might be assumed to have undergone high-pressure metamorphism. Following this model, the absence of high-pressure minerals in the Palaeozoic schists would be attributed to complete retrogression of the early blueschist- by upper-greenschist- to amphibolite-facies assemblages (Barrovian type metamorphism). However, fossil-rich (e.g., crinoids, corals) Palaeozoic metasediments and basic volcanic lenses exposed east of the well-preserved carpholite locality of Bahçeyaka (Rimmelé et al., 2003b) are free of any high-pressure mineral whereas they exhibit only low-grade metamorphism (chlorite zone) (Schuiling, 1962). This disproves the assumption of a total erasure of the Eocene high-pressure assemblages during the Oligocene Barrovian metamorphism.

2) The alternative model, which we favour, considers that only the southern Menderes marble sequence underwent high-pressure metamorphism, and not the underlying Palaeozoic schist cover and Precambrian gneiss core (Menderes Massif *sensu stricto*), which only exhibit Barrovian-type assemblages. This view partly follows the model of Ring et al. (1999), based on lithostratigraphic

similarities. Ring and co-worker claim that western Anatolia consists of a stack of three tectonic nappes, in which the Alpine orogeny did not imply any internal imbrication. These nappes are from bottom to top: i) the "Menderes Nappes" that consist of the Precambrian core and the Palaeozoic cover of the Menderes Massif, ii) the Cycladic Blueschist Unit that includes the Mesozoic marble sequence from the entire Menderes Massif, and iii) the Lycian Nappes (including the Ören Unit) (Gessner et al., 2001c). However, platform-type marbles containing rudist fossils and metabauxite layer, characteristic of the Menderes Mesozoic marble cover, are exposed, in a valley on the southern flank of the central Menderes sub-massif, as the lowermost unit of a tectonic stack implying mainly Palaeozoic metasediments (Okay, 2001). This shows that the Menderes Massif was internally imbricated during the Alpine orogeny. Moreover, including in the Cycladic Blueschist Unit Mesozoic marbles sequences of the central Menderes submassif where any relic of Alpine high-pressure metamorphism was never found seems very speculative.

Given the restriction of high-pressure index minerals to the southern Menderes margin, we suggest that the Eocene high-pressure unit is restricted to the Kurudere-Nebiler sector and that the rest of the Menderes Massif, including Mesozoic marbles from the central and northern submassifs, only underwent Barrovian metamorphism. We assumed that the metamorphic gap between the Mesozoic sequence and the underlying Palaeozoic is accommodated by a major thrust, although it was not mentioned by early works in the region. Regarding the fact that the Barrovian metamorphic zones crosscut the folded Palaeozoic-Mesozoic sequences, this thrust was active after the blueschist-facies metamorphism but before the greenschist- to amphibolite-facies overprint. It therefore is related to the exhumation of the Kurudere-Nebiler Unit during the underplating of the Menderes Massif *sensu stricto*.

4.5.2.2. Aegean-Anatolian Eocene high-pressure belt

Isotopic age results indicate that the Kurudere-Nebiler Unit (ca. 45 Ma ago; this study) underwent high-pressure metamorphism coevally with the Cycladic Blueschist Unit (e.g., Altherr et al., 1979; Maluski et al., 1981; Wijbrans et al., 1990; Oberhänsli et al., 1998; Putlitz et al., 2005). The units have moreover similar Mesozoic lithostratigraphies and similar structural positions (below the Ören-Afyon Zone). Heterogeneous metamorphic conditions were estimated throughout the Cycladic Blueschist Unit

Bearing in mind obviously differences in terms of metamorphic rock type and pressure-temperature conditions between and within these units, the Kurudere-Nebiler Unit and the Cycladic Blueschist Unit cannot be considered to strictly belong any single tectonic unit. But we propose that they form a continuous Eocene high-pressure metamorphic belt, as envisaged by Gutnic et al. (1979), Dercourt et al. (1993), Barrier and Vrielynck (2008) and Schmid et al. (2011).

Metabauxites, intercalated in Jurassic to lower Cretaceous marbles as evidence for emersion periods, are characteristic of the Menderes Massif sensu lato (i.e., including the Kurudere-Nebiler Unit) and the southwestern Cyclades, but absent from the northwestern part of the Aegean archipelago (e.g., Syros, Tinos, Andros; Feenstra, 1997). There, the Cycladic Blueschist Unit is rather composed of outer-shelf carbonate facies, manganese-rich pelites and abundant basalts (Reinecke et al., 1985). Lateral stratigraphic variations in the platform sequence of Eocene high-pressure belt depict a

palaeogeographic gradient from proximal in southwestern Anatolia to distal facies in the northwestern Cyclades. This gradient might partly be responsible for contrasting rock types found in the either regions.

In the Kurudere-Nebiler Unit, the greenschist-facies metamorphosed Palaeogene olistostrom, which occurs pinched between the southern Menderes Mesozoic marbles and the tectonically overlying Ören Unit, constitutes a lower-grade equivalent of the high-pressure metamorphosed mélange of the Cycladic Blueschist Unit (Anatolia: Candan et al., 1997; Çetinkaplan, 2002; Aegean: Dürr, 1975; Bröcker and Enders, 2001). We regard the blocks of eclogitic late Cretaceous mafic rocks (metabasalts, metagabbros) and meta-serpentinite (e.g., Bröcker and Enders, 2001; Bulle et al., 2010; Çetinkaplan, 2002) included in this formation as relics of the Neotethyan oceanic crust (referred in the Aegean to as the Pindos Ocean; e.g., Papanikolaou, 2009), which extended once north of the Cyclades-Menderes platform, and therefore south of the Ören-Afyon Zone. The consumption by subduction of this oceanic domain provides the most likely explanation for the burial of the Kurudere-Nebiler Unit down to a depth of about 40 km (1.2-1.4 GPa; Rimmelé et al., 2005) at least 20 Ma later than the Ören-Afyon Zone (this study). The absence of Eocene high-pressure metamorphic rocks between in the central Anatolides and Taurides indicates that the subduction zone, and in consequent the Pindos Ocean, terminated not farther east than the Menderes Massif.

4.5.3. Origin of the Lycian Nappes

Although the internal imbrication of the Lycian Nappes was since long deciphered as a succession of distinct tectonic stages in the latest Cretaceous, the late Eocene and the Miocene (de Graciansky, 1972; Gutnic et al., 1979), the palaeogeographic origin of the stacked sedimentary units still remains debated, and represents a critical point to be addressed when reconstructing the geodynamic history of the region. The most accepted view restores the Lycian Nappes to the northern edge of the Menderes Massif (de Gracianski, 1972; Brunn et al., 1976; Robertson and Dixon, 1984; Collins and Robertson, 1999; Okay and Altıner, 2007, van Hinsbergen, 2010). This seems to us rather unlikely since supposedly-Lycian leftovers atop the Menderes Massif and Cycladic Blueschist Unit all underwent high-pressure metamorphism and therefore belong to the Ören Unit (Rimmelé et al., 2006). Based on this argument, we favour an alternative model that assumes a more external origin of the Lycian Nappes (Poisson, 1977, 1984; Gutnic et al., 1979; Özkaya, 1990, 1991; Şenel, 1991).

Until recently, based on the common Triassic to Upper Cretaceous lithostratigraphies, the Ören Unit was considered as the continuation of the upper (sedimentary) nappe of the Lycian Nappes (e.g., Bernoulli et al., 1974; Collins and Roberston, 1998). However, sedimentation in the upper Lycian nappe was maintained until the Maastrichtian (71-65 Ma) (planktonic foraminifera; de Graciansky, 1972), while the Ören Unit was at lower crustal depths (this study). We therefore regard the Ören Unit as a tectonic unit distinct from the upper Lycian nappe, but possibly derived from the same palaeogeographic domain (platform).

While the southern Menderes cover was suffering high-pressure metamorphism and later uplifted to middle crustal levels (Oberhänsli et al., 1998; this study), pelagic sedimentation in the intermediate Lycian nappe locally persisted without any break until the Lutetian (49-40 Ma) (Şenel,

1991; Collins and Robertson, 1998, 1999). We therefore assumed that the intermediate Lycian nappe escaped pre-Upper Eocene tectonics because it was located externally to the Menderes Massif.

Based on common occurrence of Permian fusulinid limestones and lower Triassic shale and arenite (Özer, 1998; Collins and Robertson, 1999), we restore the lower Lycian nappe to the same late Palaeozoic to early Mesozoic palaeogeographic domain as the Menderes Massif sensu stricto, whereas they represent distinct Alpine tectonic units.

In summary, the Lycian Nappes constitute a composite stack of sedimentary units from various palaeogeographic domains. Stepwise imbrication, in the latest Cretaceous, the late Eocene and the Oligo-Miocene, is related to the successive incorporations of the upper, the intermediate and the lower Lycian nappes, respectively.

4.5.4. Central Anatolia

In the western and southern part of the Central Anatolian Crystalline Complex, the exhumation of high-grade metamorphic rocks in core-complex took place between 85 and 70 Ma (Gautier et al., 2008; Whitney et al., 2008b; Lefebvre et al., 2011), i.e., coevally with the uplift of the Tavşanlı Zone towards middle crustal depths. Although in this period these terranes were separated by an oceanic strand (root of the obducted ophiolites north of Mersin), exhumation of high-pressure rocks along the subduction interface and substantial extension in the upper plate seem to be related to tectonic processes and not just pure coincidence. Our present results show that these tectonic events occurred while subduction was still active, dragging the Afyon Zone down to lower crustal depth. This suits to the syn-cooling decompression path of the Tavşanlı Zone inferred from the good preservation of lawsonite-bearing assemblages.

Amalgamation of the Anatolide-Tauride Block with the Central Anatolian Crystalline therefore consisted in a rather simple succession of events: (i) onset of intra-oceanic subduction around 93-90 Ma ago, (ii) fast burial of the most distal part of the Anatolide-Tauride passive continental margin (Tavşanlı Zone) until metamorphic peak by 88-80 Ma ago, (iii) exhumation of the Tavşanlı Zone during the burial of more proximal parts of the margin (Afyon Zone), (iv) exhumation of both high-pressure units across crustal depths coevally with obduction of ophiolites on external platforms (Taurides). An identical geodynamic scenario is assumed for the central and western Anatolides-Taurides in the latest Cretaceous to Palaeocene.

4.6. Conclusions: Regional geodynamics

The Anatolides were affected by three successive high-pressure, low-temperature metamorphisms: the Tavşanlı Zone into high-pressure blueschist- to low-temperature eclogite-facies conditions in the middle Upper Cretaceous, the Afyon Zone and its derivative, the Ören Unit, into low-grade blueschist-facies conditions in the late Maastrichtian, and the southern Menderes cover, connected westwards to the Cycladic Blueschist Unit, into epidote-blueschist-facies conditions in early

Eocene. Any reliable geodynamic reconstruction must thus account for the formation of these three successive metamorphic belts.

Despite these obvious contrasting metamorphic evolutions, the Anatolide units were correlated stratigraphically into a single palaeogeographic domain (i.e., a Triassic to early Cenozoic north-facing carbonate passive margin). We propose a revised geodynamic evolution of western Anatolia that takes account of the new results provided in this study.

4.6.1. From 95 to 75 Ma ago

A north-dipping intra-oceanic subduction zone, running from the Izmir-Ankara into the Inner-Tauride segments of the Neotethys, was created offshore of the Anatolides around 93-90 Ma (for review see, Robertson, 2002; Çelik et al., 2006). Shortly after subduction initiation, likely around 85 Ma ago, the rocks of the Tavşanlı Zone, which represent the most distal parts of a continental passive margin, attained the deepest burial levels (ca. 75 km or 2.5 GPa). Very-low-temperature high-pressure metamorphic conditions recorded throughout the Tavşanlı Zone indicate very rapid burial, in accord with the short time gap between subduction onset and high-pressure metamorphism. In this period, Central Anatolia was affected by detachment-controlled extension and sedimentation was persisting in the other Anatolide units and the Taurides.

Then, blueschists and eclogites of the Tavşanlı Zone were exhumed along a very-low apparent geothermal gradient, accounting for the good preservation of lawsonite along the retrograde path. Such syn-decompression cooling is clear evidence for exhumation during continuous subduction, i.e., during the transport of the Afyon Zone down to depth.

4.6.2. From 75 to 55 Ma ago

The Ören-Afyon Zone, including a carbonate platform and its Precambrian-Palaeozoic substratum, was metamorphosed in low-grade high-pressure conditions around 75 Ma ago (Middle-Late Campanian), while Central Anatolia was hosting abundant calc-alkaline magmas and the more external carbonate platform of the southern Menderes cover subsided to pelagic environments.

Coevally with the Tavşanlı Zone, the Ören-Afyon Zone was then exhumed up to upper crustal levels from the Maastrichtian to the Palaeocene. In the Afyon Zone, the common occurrence of pre-Mesozoic rocks (substratum of the Mesozoic passive margin sequence) suggests that uplift of high-pressure rocks may have been triggered by the underplating of the rather buoyant material. Coevally, the ophiolites from the Izmir-Ankara and Inner-Tauride oceanic branches were thrust southwards onto Mesozoic platform sediments (formation of Maastrichtian to early Palaeocene ophiolitic mélanges). The obduction initiated the formation of the nappe complexes in the Western, Central and Eastern Taurides.

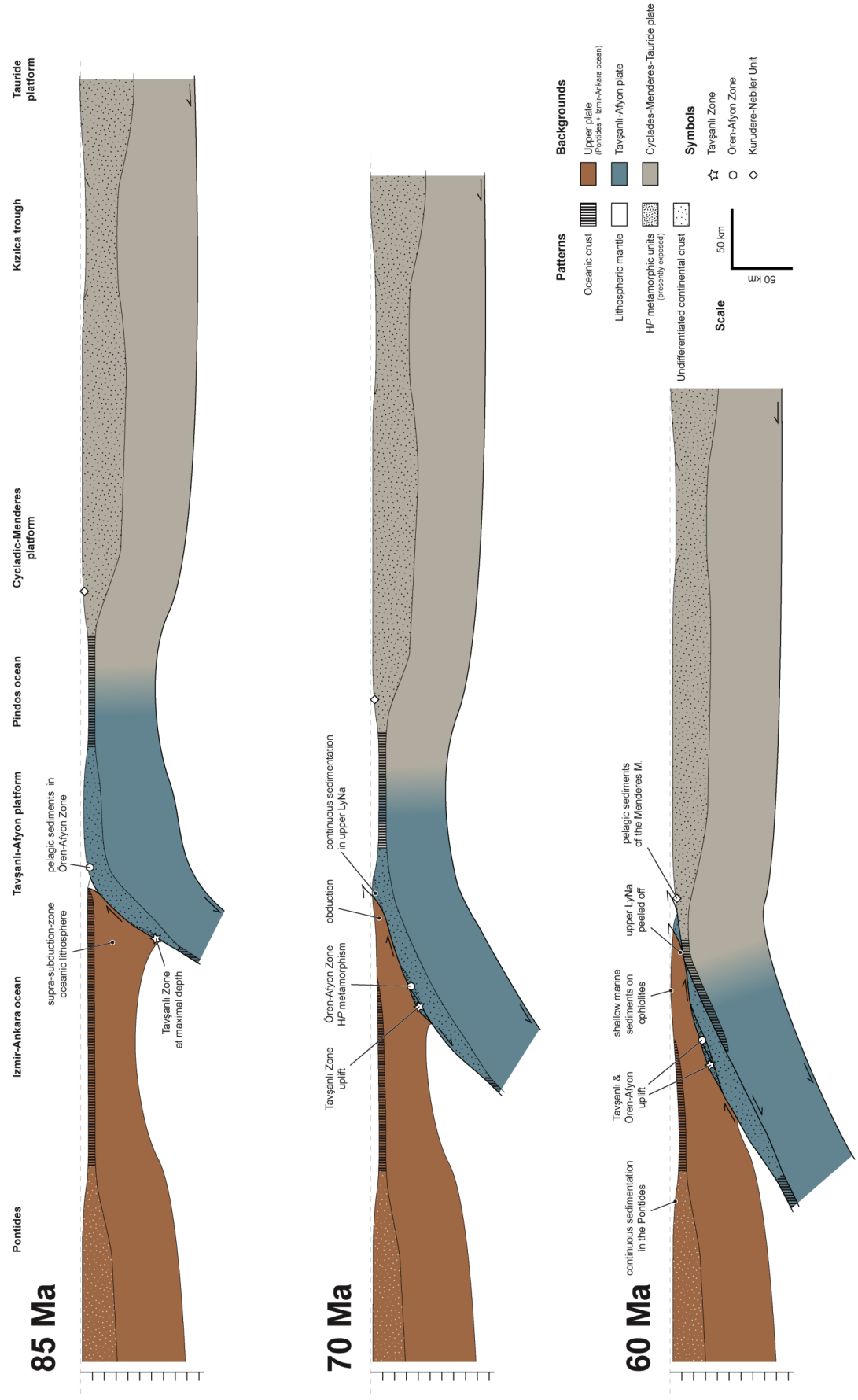

Figure 4.6: Schematic reconstruction of the geodynamic evolution of western Anatolia from the Late Cretaceous to the Neogene.

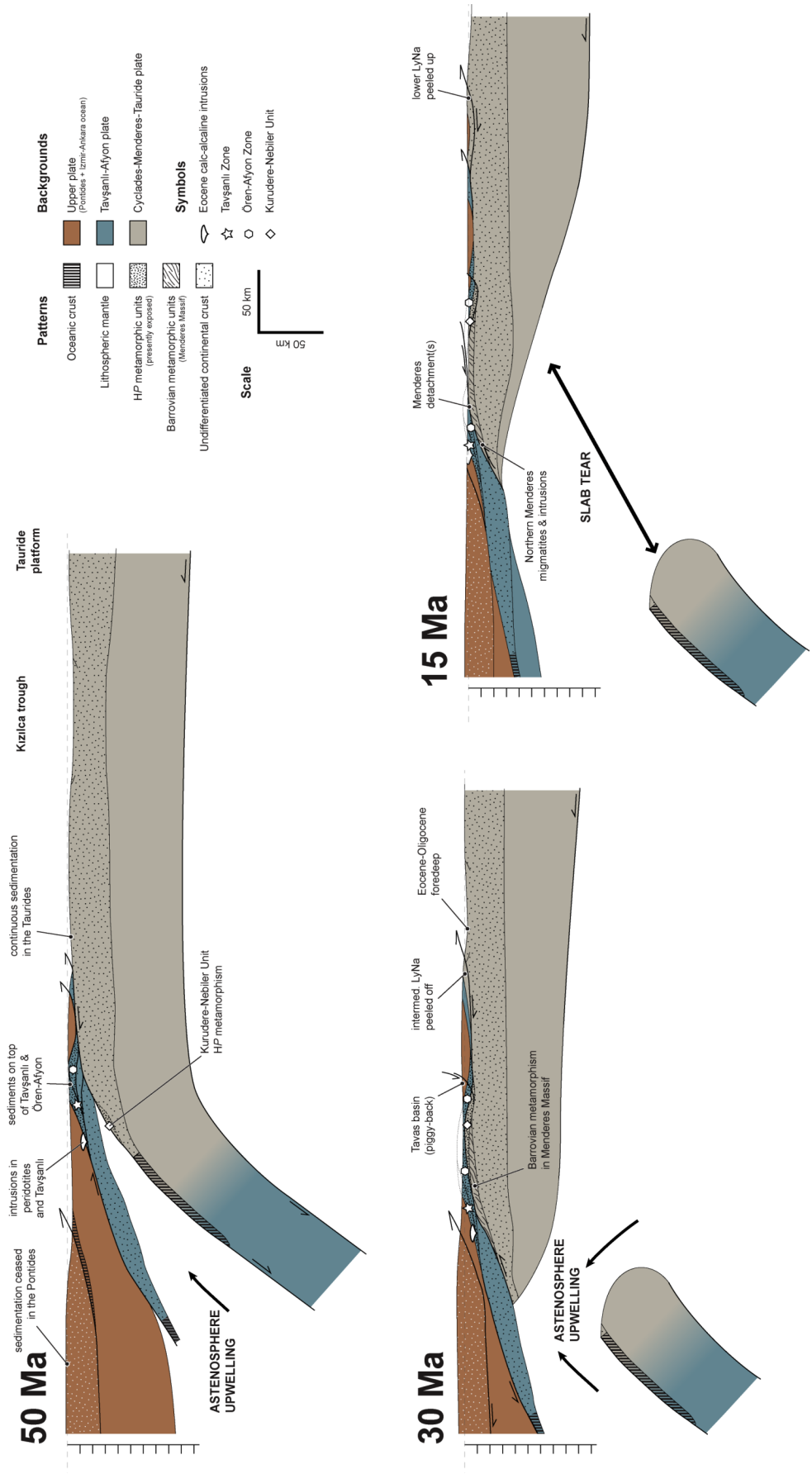

Figure 4.6 (continued).

Under continuous regional compressional strain, a northward subduction zone was created within the Pindos Ocean sometime in the Palaeocene. We envisage that the southward transfer of the active subduction zone was accommodated by a décollement along either a weak surface separating an upper from a lower crust (as proposed for the Aegean Domain; Jolivet et al., 2003), or the crust-mantle interface ("rheological Moho"). For simplicity, the latter scenario was depicted in the geodynamic sketch (Figure 4.6).

Subduction within the Pindos Ocean likely started between the latest Cretaceous and the Palaeocene.

4.6.3. From 55 to 35 Ma ago

The northern edge of the Menderes-Tauride continent was dragged down to high-pressure conditions in the Early Eocene. The entry of the buoyant continental margin stuffed the subduction zone, leading to the retreat of the Pindos slab. The mantle wedge thus was invaded by hot material ("asthenosphere upwelling"; Figure 4.6) that provoked partial melting of mantle rocks. This is recorded by the calc-alkaline intrusion that emplaced in the Tavşanlı Zone and overlying peridotites between 53 and 48 Ma ago. In this period, while these magmas intruded parts of the Tavşanlı Zone and the ophiolites hence still lying at a depth of ca. 10 km (Harris et al., 1994), other parts of the Tavşanlı Zone, as well as the Afyon Zone, were already exposed at the Earth's surface and unconformably covered by shallow-marine sediments.

The early Eocene high-pressure belt (southern Menderes cover in western Anatolia) was then exhumed during the middle and late Eocene, while the Lycian Nappes and the Hoyran-Beyşehir-Hadim Nappes experienced a second tectonic stage, consisting of the incorporation of platform sequences up to Eocene in age.

The oblique accretion of the Menderes Massif to the Ören-Afyon Zone led to detach and transport the westernmost part of the latter (Ören Unit) towards the ESE, and to rework tectonically the olistostromal Bornova Zone under sinistral transpressional strain.

4.6.4. Since 35 Ma onwards

In the Oligocene, the frontal part of the external terrane, including the Menderes Massif, collided the late Cretaceous-Palaeocene accretionary complex. This is recorded by Barrovian metamorphism in the Kurudere-Nebiler Unit (Figure 4.5) and the Menderes Massif s.s. and the general sedimentary hiatus and local continental sedimentation (orogeny).

The presence of a slab tear at depths from < 80 to ca. 200 km and the absence of a seismogenic Benioff surface below present-day western Anatolia (Rayleigh-wave tomographic imaging; Salaün et al., 2011) suggests that subduction below this region ceased sometime by the end of the Oligocene. In contrast, subduction continued in the Aegean Domain, after the subduction zone was transferred externally, as recorded in particular by early Miocene high-pressure metasediments in Crete. We propose that such a transfer in western Anatolia required decoupling along a too long

distance to be possible. The Oligocene collision therefore engendered the break off of the oceanic slab, asthenosphere upwelling and exhumation of the Menderes Massif along detachment faults in the Miocene. Compression however persisted in the Taurides leading to the inversion of an intra-platform pelagic basin (Kizilca trough of Poisson, 1977, 1984) and the final emplacement of the Lycian Nappes onto an Eocene-Oligocene foredeep and the external autochthonous platforms.

Conclusion

The present work is based on the inspection (or re-inspection) of the metamorphic evolution of metasediments from a Mesozoic continental passive margin, the Afyon Zone in Western and Central Anatolia. Such an approach can greatly help to reconstruct palaeotectonic and palaeogeographic domains in regions where the position of former plate boundaries are debated, as the Eastern Mediterranean.

Index minerals of the blueschist facies (Fe-Mg-carpholite and glaucophane) are documented throughout the Afyon Zone, in a specific stratigraphic interval ascribed to the Lower Triassic (Chapter 2). Studying the well-preserved carpholite-chloritoid-bearing assemblages of the western Afyon Zone offers the opportunity to improve our understanding of phase relations and Mg-Fe partitioning within the (K)FMASH system, and to estimate *P-T* conditions experienced by these metamorphic rocks. As presented in Chapter 3, a detailed inspection of prograde textures and Mg-Fe distribution within and among minerals reveals: • multistage growth of carpholite and chloritoid, • progressive increase of Mg content in minerals, • continuous replacement of Fe-rich carpholite by Fe-Mg-carpholite and Fe-rich chloritoid, and • strong Mg-Fe partitioning between carpholite and chloritoid. Thermodynamic modelling using new data for ferro-carpholite permits deciphering phase relations in the FMASH system and unravelling the significance of Mg-Fe distribution among and within carpholite and chloritoid. In particular, it is predicted that Mg-Fe exchange between carpholite and chloritoid can be used as a sensitive geothermometer. Based on this model, textural and chemical observations in carpholite-bearing rocks from the western Afyon Zone account for a temperature increase from ca. 280 to 380°C at 0.9-1.1 GPa, indicating that the Afyon Zone was subducted along a low thermal gradient (< 10°C/km).

In order to further constrain regional geodynamics, thermobarometric estimates (using a multi-equilibrium approach based on quartz-chlorite-mica and quartz-chlorite-chloritoid assemblages) were combined with ^{40}Ar-^{39}Ar geochronology (on white mica) in carpholite-bearing samples of the Afyon Zone, as well as of the Ören and Kurudere-Nebiler Units (SW Anatolia; Figure 5.1). This combination allows deciphering the significance of the calculated ages in terms of metamorphic conditions (Chapter 4). Based on these thermobarometric and geochronologic results and literature, it is shown that: • the Ören Unit corresponds to the westernmost extension of the Afyon Zone that was transported towards the southeast away from the suture zone after suffering low-temperature, high-pressure metamorphism in the latest Cretaceous (Campanian?-Maastrichtian); • the Kurudere-Nebiler Unit is an early Eocene high-pressure unit distinct from the underlying low- to moderate-pressure Menderes Massif. Around the Oligo-Miocene boundary, Eocene high-pressure mineral assemblages were overprinted during

Barrovian-type metamorphism, which decreases in intensity from the core of the Menderes Massif to the lowermost levels of the Kurudure-Nebiler Unit, i.e., upwards in the tectonic pile.

In summary, no less than three contiguous, but distinct high-pressure metamorphic belts are recognized in Western Anatolia: • the lawsonite blueschists and eclogites of the Tavşanlı Zone (88-80 Ma, Coniacian-Santonian), • the carpholite-chloritoid-pyrophyllite metasediments of the Ören-Afyon Zone (Campanian?-Maastrichtian) and • the carpholite-kyanite metasediments of the Kurudere-Nebiler Unit (Lutetian).

In Figure 5.1, I propose a revised version of the tectonic map of Western and Central Anatolia, which takes account of these new considerations: • distinguishing the Ören Unit (H*P*) from the rest of the Lycian Nappes (not metamorphosed); • merging the Ören Unit and the Afyon Zone as a single metamorphic belt; • distinguishing the Kurudere-Nebiler Unit (H*P* + Barrovian overprint) from the rest of the Menderes Massif (only Barrovian metamorphism); • merging the Kurudere-Nebiler Unit with the Cycladic Blueschist Unit as a single metamorphic belt.

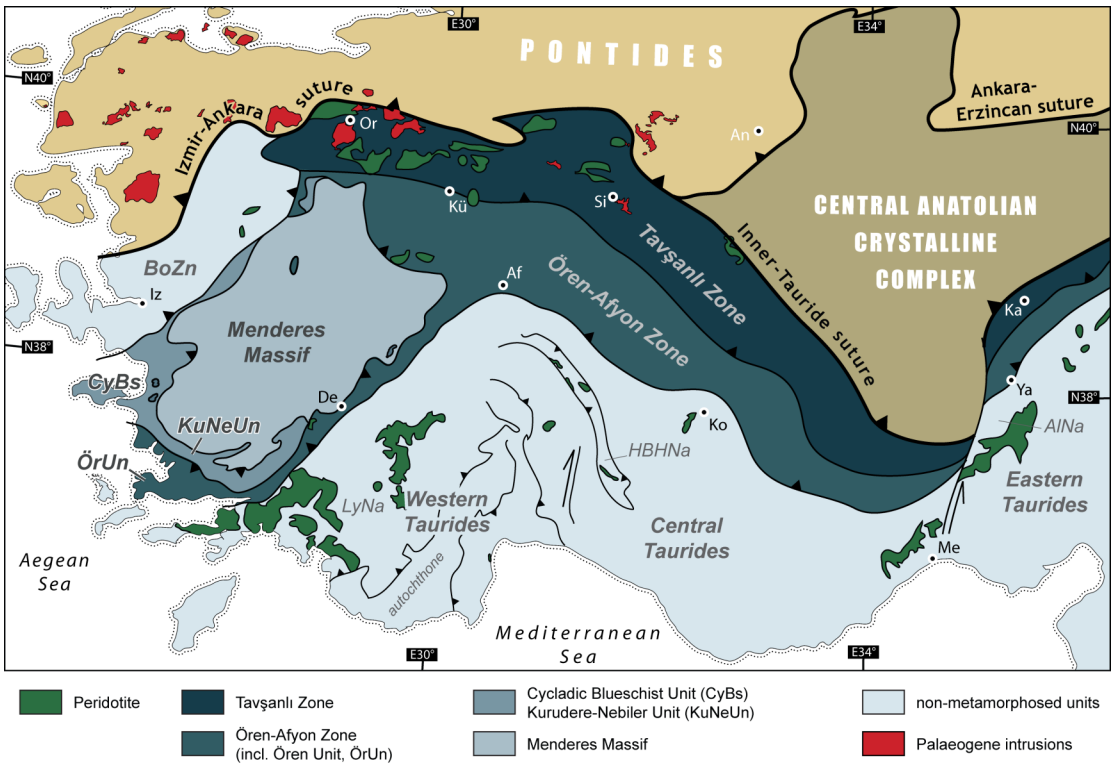

Figure 5.1: Tectonic map of Western and Central Anatolia. Abbreviations as in Figure 4.1.

Based on the results provided in the present study and from the literature, I review the geodynamic evolution of Anatolia since the Late Cretaceous.

- The lateral continuity of the Afyon Zone, representing a high-pressure metamorphic belt, confirms the existence of a Neotethyan oceanic suture (named the Inner Tauride suture) in southern

Central Anatolia, which previous geological, sedimentological, geochemical and geophysical studies in the region could support but not verify (see Chapter 2).

- By restoring the post-accretionary deformation in the Anatolide accretionary zone, kinematic indicators related to nappe stacking are interpreted at a regional scale (Chapters 2 and 4). It is demonstrated that: • extensional tectonics in Western Anatolia led to rotation of the southern margin of the Menderes Massif with respect to the northern margin, and thus to largely amplified the apparent distance over which the Ören Unit was transported; • the bending of the eastern Anatolides-Taurides results from the indentation of either the Central Anatolia Crystalline Complex in the Eocene, or the Arabian plate in the Oligo-Miocene.
- The present study consistently supports the existence of several branches of the Neotethys in Anatolia. In the Early Cretaceous, the Central Anatolian Crystalline Complex was separated from the Pontides in the north by the Ankara-Erzincan Ocean and from the Anatolide-Tauride Block in the south by the Inner Tauride Ocean. These two oceanic strands used to merges westwards into the Izmir-Ankara Ocean. The Ören-Afyon Zone was once separated from the underlying Kurudere-Nebiler Unit by the eastern termination of the Pindos Ocean, defined in the Aegean Domain.
- Based on the Oligo-Miocene continental collision in Western Anatolia (Barrovian metamorphism in the Kururdere-Nebiler Unit and Menderes Massif), it is assumed that subduction in this area ceased after the Eocene high-pressure metamorphic event. For comparison, in the adjacent Aegean Domain, subduction has persisted until the present despite the accretion of continental units throughout the Cenozoic. I therefore envisage that the continental fragment encompassing the Kurudere-Nebiler Unit, the Menderes Massif and the Taurides was too large to allow tectonic decoupling between the accreted continental crust and the lithospheric mantle. In contrast, its continuation in the Aegean Domain was separated into two parts by the Ionian trough, which closed in the early Miocene. Therefore, I suggest that rather than lithospheric delamination having occurred beneath the Menderes Massif, there was a slab break-off event, as suggested by recent tomographic imaging.

Chapter 6

Perspectives

Although the new structural, petrologic and geochronologic results provided in this thesis contribute to better constraining the tectonic assembly of Anatolia since the Late Cretaceous, major questions remain to be answered.

Continental accretion in Central Anatolia could be better understood thanks to additional constraints on the exact pressure-temperature metamorphic history of the Afyon Zone, and its possible lateral variations from NW to Central Anatolia. For this purpose, thermodynamic data for ferro-carpholite and likely for other phases of the FMASH system (likely ferro-chloritoid) should be further refined so that Mg-Fe partitioning between carpholite and chloritoid can be used as a precise geothermometer. However, this method cannot provide accurate pressure estimates. As shown by recent works (e.g., Yamato et al., 2007), reliable thermobarometric estimates can be obtained by multi-equilibrium calculation on chloritoid-chlorite-mica assemblages. Refined thermodynamic data for ferro-carpholite could therefore be used for thermobarometric estimates in carpholite-mica±chlorite assemblages and thus investigation of the earliest high-pressure stages of the prograde metamorphic path.

Tectonic stacking of the Anatolide metamorphic zones seems now rather well constrained in time, but poorly in space. Several structural studies at the southern margin of the Menderes Massif (including the Kurudere-Nebiler and Ören Units) have clarified the emplacement of the metamorphic tectonic units in South-western Anatolia, but deformation coeval to the high-pressure metamorphism of the Afyon Zone still needs to be investigated. Furthermore, mineral lineations in the high-pressure rocks of the Tavşanlı Zone strike roughly east-west (Okay et al., 1998), i.e., parallel to the Izmir-Ankara suture. This indicates that the common assumption of a continental accretion perpendicular to the present-day suture (i.e., northwards) neglects the transform component that only detailed field-based structural work can elucidate.

The evolution of the eastern Anatolide-Tauride Block is also uncertain. Published geological maps suggest that the metamorphosed northern edge of the Anatolide-Tauride Block is mostly concealed under Neogene sediments and volcanic rocks. Nevertheless, the sporadic occurrence of an ophiolitic mélange along the assumed suture strike may allow this issue to be addressed by field investigations. If lawsonite-bearing blueschist blocks can be found in this ophiolitic mélange, it could correlated with the upper unit of the Tavşanlı Zone, and thus represents the easternmost segment of the Inner Tauride suture (Figure 2.1). In the Bolkar Mountains and the Aladağ Nappes (Figure 4.1), the southern edge of the Afyon Zone is tectonically overlain by non-metamorphosed Tauride sediments (Demirtaşlı et al., 1984; Tekeli et al., 1984). In the present study, it is assumed that north-verging faults at the base of the Tauride units are back-thrusts formed during the closure of another Neotethyan branch to the south (Chapter 2). However, there is little published information in this respect, so this

constitutes another key challenge for deciphering the deformation of continental regions pinched between two accretionary zones.

References

Agard P., Monié P., Jolivet L. and Goffé B., 2002. Exhumation of the Schistes Lustrés complex: in situ laser probe $^{40}Ar/^{39}Ar$ constraints and implications for the Western Alps. Journal of Metamorphic Geology, 20(6): 599-618.

Akal C., Candan O., Koralay O. E. and Oberhänsi R., 2007. Geochemistry, geochronology and tectonic setting of Early Triassic metavolcanics of the Afyon Zone, Turkey. Project No 103Y011, Tübitak.

Akal C., Candan O., Koralay E., Oberhänsli R., Chen F. and Prelevic D., 2011. Early Triassic potassic volcanism in the Afyon Zone of the Anatolides/Turkey: implications for the rifting of the Neo-Tethys. International Journal of Earth Sciences.

Akıman O., Erler A., Göncüoğlu M. C., Güleç N., Geven A., Türeli T. K. and Kadioğlu Y. K., 1993. Geochemical Characteristics of Granitoids Along the Western Margin of the Central Anatolian Crystalline Complex and Their Tectonic Implications. Geological Journal, 28(3-4): 371-382.

Akın H., 1978. Geologie, Magmatismus und Lagerstättenbildung im ostpontischen Gebirge-Türkei aus der Sicht der Plattentektonik. Geologische Rundschau, 68: 253-283.

Akkök R., 1981. Metamorphic conditions of gneisses and schists in the Menderes Massif, Alaşehir-Manisa. Bulletin of the Geological Society of Turkey, 24: 11-20.

Akkök R., 1983. Structural and metamorphic evolution of the northern part of the Menderes Massif - New data from the Derbent area and their implication for the tectonics of the massif. Journal of Geology, 91(3): 342-350.

Altherr R., Schliestedt M., Okrusch M., Seidel E., Kreuzer H., Harre W., Lenz H., Wendt I. and Wagner G. A., 1979. Geochronology of High-Pressure Rocks on Sifnos (Cyclades, Greece). Contributions to Mineralogy and Petrology, 70(3): 245-255.

Altiner D., Koçyiğit A., Farinacci A., Nicosia. U. and Conti M. A., 1991. Jurassic-Lower Cretaceous stratigraphy and paleogeographic evolution of the southern part of north-western Anatolia. Geologica Romana, 27: 13-80.

Andrew T. and Robertson A. H. F., 2002. The Beysehir-Hoyran-Hadim Nappes: genesis and emplacement of Mesozoic marginal and oceanic units of the northern Neotethys in southern Turkey. Journal of the Geological Society, London, 159: 529-543.

Armijo R., Meyer B., Hubert A. and Barka A., 1999. Westward propagation of the North Anatolian fault into the northern Aegean: Timing and kinematics. Geology, 27(3): 267-270.

Ashworth J. R. and Evirgen M. M., 1984. Mineral chemistry of regional chloritoid assemblages in the chlorite zone; Lycian Nappes, Southwest Turkey. Mineralogical Magazine, 48: 159-165.

Ashworth J. R. and Evirgen M. M., 1985. Plagioclase relations in pelites, central Menderes Massif, Turkey .2. Perturbation of garnet-plagioclase geobarometers. Journal of Metamorphic Geology, 3(3): 219-229.

Ateş A., Kearey P. and Tufan S., 1999. New gravity and magnetic anomaly maps of Turkey. Geophysical Journal International, 136: 499-502.

Aydın N. S., Göncüoğlu M. C. and Erler A., 1998. Latest Cretaceous Magmatism in the Central Anatolian Crystalline Complex: Review of Field, Petrographic and Geochemical Features. Turkish Journal of Earth Sciences, 7: 259-268.

Ayhan A. and Lengeranli Y., 1986. Tectonostratigraphic Characteristics of the Area between Yahyali and Demirkazik (Aladağlar Region). Jeoloji Mühendisliği, 27: 31-45.

Azañón J. M. and Goffé B., 1997. Ferro- and magnesiocarpholite assemblages as record of high-P, low-T metamorphism in the Central Alpujarrides, Betic Cordillera (SE Spain). European Journal of Mineralogy, 9: 1035-1051.

Azañón J. M., Garcia-Dueñas V. and Goffé B., 1998. Exhumation of high-pressure metapelites and coeval crustal extension in the Alpujarride Complex (Betic Cordillera). Tectonophysics, 285: 231-252.

Balogh K. and Dunkl I., 2005. Argon and fission track dating of Alpine metamorphism and basement exhumation in the Sopron Mts. (Eastern Alps, Hungary): thermochronology or mineral growth? Mineralogy and Petrology, 83(3-4): 191-218.

Barrier E. and Vrielinck B., 2008. Palaeotectonic maps of the Middle East. Commision for the Geological Map of the World, Paris.

Bayiç A., 1968. On Metaporphyrites of the Sizma Region-Province of Konya. Bulletin of the Mineral Research and Exploration Institute of Turkey, 70.

Ben-Avraham Z., Garfunkel Z. and Lazar M., 2008. Geology and evolution of the southern dead sea fault with emphasis on subsurface structure. Annual Review of Earth and Planetary Sciences, 36: 357-387.

Berman R. G. and Brown T. H., 1985. Heat-capacity of minerals in the system Na2O-K2O-CaO-MgO-FeO-Fe2O3-Al2O3-SiO2-TiO2-H2O-CO2 - Representation, estimation, and high-temperature extrapolation. Contributions to Mineralogy and Petrology, 89(2-3): 168-183.

Berman R. G., 1988. Internally-Consistent Thermodynamic Data for Minerals in the system Na_2O-K_2O-CaO-MgO-FeO-Fe_2O_3-Al_2O_3-SiO_2-TiO_2-H_2O-CO_2. Journal of Petrology, 29(2): 445-522.

Bernoulli D., de Graciansky P.-C. and Monod O., 1974. The Extension of the Lycian Nappes (SW Turkey) into the Southeastern Aegean Islands. Eclogae Geologicae Helvetiae, 67(1): 39-90.

Bingöl E., 1974. Discussions on the Metamorphic Map of Turkey in A Scale of 1:2,500,000 And Geotectonic Evolution of Some Metamorphic Belts. Bulletin of the Mineral Research and Exploration Institute of Turkey, 83: 119-131.

Blumenthal M., 1955. Yüksek Bolkardağın Kuzey Kenarı Bölgelerinin ve Batı Uzantılarının Jeolojisi (Güney Anadolu Torosları), Serie D. Mineral Research and Exploration Institute of Turkey (MTA), 153 pp.

Blumenthal M., 1963. Le système structural du Taurus sud-anatolien, Livre à la mémoire du Professeur P. Fallot. Mémoire de la Société Géologique de France, pp. 611-662.

Bonneau M., 1984. Correlation of the Hellenide nappes in the south-east Aegean and their recontruction. In: Dixon J. E. and Robertson A. H. F. (Editors), The Geological Evolution of the Eastern Mediterranean. Geological Society, London, Special Publications, pp. 517-527.

Bousquet R., Oberhänsli R., Goffé B., Jolivet L. and Vidal O., 1998. High pressure-low temperature metamorphism and deformation in the Bündnerschiefer of the Engadine window: implications for the regional evolution of the eastern Central Alps. Journal of Metamorphic Geology, 16: 657-674.

Bousquet R., Goffé B., Vidal O., Oberhänsli R. and Patriat M., 2002. The tectono-metamorphic history of the Valaisan domain from the Western to the Central Alps: New constraints on the evolution of the Alps. Geological Society of America Bulletin, 114(2): 207-225.

Bouybaouene M. L., Goffé B. and Michard A., 1995. High-pressure, low-temperature metamorphism in teh Sebtides nappes, northern Rif, Morocco. Geogaceta, 17: 117-119.

Bozkaya O. and Yalcin H., 2000. Very low grade metamorphism of Upper Paleozoic-Lower Mesozoic sedimentary rocks related to burial and thrusting in the Central Taurus Belt, Konya, Turkey. International Geology Review, 42(4): 353-367.

Bozkurt E., Park R. G. and Winchester J. A., 1993. Evidence against the core/cover interpretation of the southern section of the Menderes Massif, west Turkey. Terra Nova, 5(445-451).

Bozkurt E. and Park R. G., 1994. Southern Menderes Massif: an icipient metamorphic core complex in western Anatolia, Turkey. Journal of the Geological Society, London, 151: 213-216.

Bozkurt E., 1996. Metamorphism of Palaeozoic Schists in the Southern Menderes Massif: Field, Petrographic, Textural and Microstructural Evidence. Turkish Journal of Earth Sciences, 5: 105-121.

Bozkurt E. and Park R. G., 1997. Microstructures of deformed grains in the augen gneisses of southern Menderes Massif (western Turkey) and their tectonic significance. Geologische Rundschau, 86(1): 103-119.

Bozkurt E., 2000. Timing of extension on the Büyük Menderes Graben, western Turkey, and its tectonic implications. In: Bozkurt E., Winchester J. A. and Piper J. D. A. (Editors), Tectonics and Magmatism in Turkey and the Surrounding Area. Geological Society, London, Special Publication, 173, pp. 385-404.

Bozkurt E. and Satır M., 2000. The southern Menderes Massif (western Turkey): geochronology and exhumation history. Geological Journal, 35(3-4): 285-296.

Bozkurt E. and Oberhänsli R., 2001. Menderes Massif (Western Turkey): structural, metamorphic and magmatic evolution - a synthesis. International Journal of Earth Sciences, 89(4): 679-708.

Bozkurt E., 2004. Granitoid rocks of the southern Menderes Massif (southwestern Turkey): field evidence for Tertiary magmatism in an extensional shear zone. International Journal of Earth Sciences, 93(1): 52-71.

Bozkurt E., 2007. Extensional vs. contractional origin for the southern Menderes shear zone, SW Turkey: tectonic and metamorphic implications. Geological Magazine, 144(1): 191-210.

Boztuğ D., 1998. Post-Collisional Central Anatolian Alkaline Plutonism, Turkey. Turkish Journal of Earth Sciences, 7: 145-165.

Boztuğ D., 2000. S-I-A type intrusive associations: geodynamics significance of synchronism between metamorphism and magmatism in Central Anatolia, Turkey. In: Bozkurt E., Winchester J. A. and Piper J. D. A. (Editors), Tectonics and Magmatism in Turkey and the Surrounding Area. Geological Society, London, Special Publication, 173, pp. 441-458.

Boztuğ D., Harlavan Y., Arehart G. B., Satır M. and Avci N., 2007. K-Ar age, whole-rock and isotope geochemistry of A-type granitoids in the Divrigi-Sivas region, eastern-central Anatolia, Turkey. Lithos, 97(1-2): 193-218.

Bröcker M. and Enders M., 2001. Unusual bulk-rock compositions in eclogite-facies rocks from Syros and Tinos (Cyclades, Greece): implications for U-Pb zircon geochronology. Chemical Geology, 175(3-4): 581-603.

Brunn J. H., Argyriadis I., Ricou L. E., Poisson A., Marcoux J. and de Graciansky P.-C., 1976. Eléments majeurs de liaison entre Taurides et Hellénides. Bulletin de la Société géologique de France, 7(2): 481-497.

Bulle F., Bröcker M., Gaertner C. and Keasling A., 2010. Geochemistry and geochronology of HP melanges from Tinos and Andros, cycladic blueschist belt, Greece. Lithos, 117(1-4): 61-81.

Candan O., Dora O. Ö., Oberhänsi R., Oelsner F. and Dürr S., 1997a. Blueschist relics in the Mesozoic cover series of the Menderes Massif and correlations with Samos Islan, Cyclades. Schweizerische Mineralogische und Petrographische Mitteilungen, 77: 95-99.

Candan O., Dora O. Ö., Oberhänsli R., Oelsner F. and Durr S., 1997b. Blueschist relics in the Mesozoic cover series of the Menderes Massif and correlations with Samos Island, Cyclades. Schweizerische Mineralogische und Petrographische Mitteilungen, 77(1): 95-99.

Candan O., Dora Ö. O., Oberhänsli R., Çetinkaplan M., Partzsch J. H., Warkus F. C. and Dürr S., 2001. Pan-African high-pressure metamorphism in the Precambrian basement of the Menderes Massif, western Anatolia, turkey. International Journal of Earth Sciences, 89(4): 793-811.

Candan O., Çetinkaplan M., Oberhänsli R., Rimmelé G. and Akal C., 2005. Alpine high-P/low-T metamorphism of the Afyon Zone and implications for the metamorphic evolution of Western Anatolia, Turkey. Lithos, 84(1-2): 102-124.

Candan O., Dora O. Ö., Oberhänsli R., Koralay E., Çetinkaplan M., Akal C., Satır M., Chen F. and Kaya O., 2011a. Stratigraphy of the Pan-African basement of the Menderes Massif and the relationship with late Neoproterozoic/Cambrian evolution of the Gondwana. Bulletin of the Mineral Research and Exploration Institute of Turkey, 142: 25-68.

Candan O., Koralay O. E., Akal C., Kaya O., Oberhänsli R., Dora O. Ö., Konak N. and Chen F., 2011b. Supra-Pan-African unconformity between core and cover series of the Menderes Massif/Turkey and its geological implications. Precambrian Research, 184(1-4): 1-23.

Cathelineau M. and Nieva D., 1985. A chlorite solid-solution geothermometer - The Los-Azufres (mexico) geothermal system. Contributions to Mineralogy and Petrology, 91(3): 235-244.

Çelik Ö. F., Delaloye M. and Feraud G., 2006. Precise Ar-40-Ar-39 ages from the metamorphic sole rocks of the Tauride Belt Ophiolites, southern Turkey: implications for the rapid cooling history. Geological Magazine, 143(2): 213-227.

Çemen I., Göncüoğlu M. C. and Dirik K., 1999. Structural evolution of the Tuzgolu basin in Central Anatolia, Turkey. Journal of Geology, 107(6): 693-706.

Çetinkaplan M., 2002. Tertiary High-Pressure / Low-Temperature Metamorphism in the Mesozoic Cover Series of the Menderes Massif and Correlation with the Cycladic Crystalline Complex. PhD Thesis, Universitesi Izmir, 47 pp.

Çetinkaplan M., Candan O., Oberhänsli R. and Bousquet R., 2008. Pressure-temperature evolution of lawsonite eclogite in Sivriihisar; Tavsanli Zone-Turkey. Lithos, 104(1-4): 12-32.

Chopin C. and Schreyer W., 1983. Magnesiocarpholite and magnesiochloritoid: two index minerals of pelitic blueschists and their preliminary phase relations in tne system MgO-Al_2O_3-SiO_2-H_2O. American Journal of Science, 283-A: 72-96.

Chopin C., Seidel E., Theye T., Ferraris G., Ivaldi G. and Catti M., 1992. Magnesiochloritoid, and the Fe-Mg series in the chloritoid group. European Journal of Mineralogy, 4: 67-76.

Çiftçi N. B. and Bozkurt E., 2009. Evolution of the Miocene sedimentary fill of the Gediz Graben, SW Turkey. Sedimentary Geology, 216(3-4): 49-79.

Clark M. and Robertson A. H. F., 2002. The role of the Early Tertiary Ulukişla Basin, southern Turkey, in suturing of the Mesozoic Tethys ocean. Journal of the Geological Society, London, 159: 673-690.

Çoğulu E., 1967. Etude pétrographique de la région de Mihaliçcik. Schweizerische Mineralogische und Petrographische Mitteilungen, 47: 683-824.

Collins A. S. and Robertson A. H. F., 1998. Processes of Late Cretaceous to Late Miocene episodic thrust-sheet translation in the Lycian Taurides, SW turkey. Journal of the Geological Society, London, 155: 759-772.

Collins A. S. and Robertson A. H. F., 1999. Evolution of the Lycian Allochthon, western Turkey, as a north-facing Late Palaeozoic to Mesozoic rift and passive continental margin. Geological Journal, 34(1-2): 107-138.

Davis P. B. and Whitney D. L., 2006. Petrogenesis of lawsonite and epidote eclogite and blueschist, Sivrihisar Massif, Turkey. Journal of Metamorphic Geology, 24(9): 823-849.

Davis P. B. and Whitney D. L., 2008. Petrogenesis and structural petrology of high-pressure metabasalt pods, Sivrihisar, Turkey. Contributions to Mineralogy and Petrology, 156(2): 217-241.

De Andrade V., Vidal O., Lewin E., O'Brien P. and Agard P., 2006. Quantification of electron microprobe compositional maps of rock thin sections: an optimized method and examples. Journal of Metamorphic Geology, 24(7): 655-668.

De Capitani C. and Brown T. H., 1987. The computation of chemical equilibrium in complex systems containing non-ideal solutions. Geochimica Et Cosmochimica Acta, 51: 2639-2652.

De Capitani C. and Petrakakis K., 2010. The computation of equilibrium assemblage diagrams with Theriak/Domino software. American Mineralogist, 95(7): 1006-1016.

de Graciansky P.-C., 1972. Recherches Géologiques dans le Taurus Lycien Occidental. PhD Thesis, Université de Paris-Sud, Paris.

de Roever E. W. F., 1977. Chloritoid-bearing metapelites associated with glaucophane rocks in W crete. Contributions to Mineralogy and Petrology, 60(3): 317-319.

Delaloye M. and Bingol E., 2000. Granitoids from Western and Northwestern Anatolia: Geochemistry and modeling of geodynamic evolution. International Geology Review, 42(3): 241-268.

Demirtaşlı E., Turhan N., Bilgin A. Z. and Selim M., 1984. Geology of the Bolkar Mountains. In: Tekili O. and Göncüoğlu M. C. (Editors), Proceedings of the International Symposium on the Geology of the Taurus Belt. Mineral Research and Exploration Intitute of Turkey (MTA), Ankara, Turkey, pp. 125-141.

Dercourt J., Ricou L. E. and Vrielinck B., 1993. Atlas Tethys, paleoenvironmental maps. Gauthier-Villars, Paris, 307 pp.

Dercourt J., Gaetani M., Vrielynck B., Barrier E., Biju-Duval B., Brunet M.-F., Cadet J.-P., Crasquin-Soleau S. and Sandulescu M., 2000. Peri-Tethys Paleogeographical Atlas. CCGM, Paris.

Dewey J. F., Pitman W. C., Ryan W. B. F. and Bonnin J., 1973. Plate tectonics and evolution of Alpine system. Geological Society of America Bulletin, 84(10): 3137-3180.

Di Vincenzo G., Ghiribelli B., Giorgetti G. and Palmeri R., 2001. Evidence of a close link between petrology and isotope records: constraints from SEM, EMP, TEM and in situ Ar-40-Ar-39 laser analyses on multiple generations of white micas (Lanterman Range, Antarctica). Earth and Planetary Science Letters, 192(3): 389-405.

Dilek Y. and Whitney D. L., 1997. Counterclockwise P-T-t trajectory from the metamorphic sole of a Neo-Tethyan ophiolite (Turkey). Tectonophysics, 280(3-4): 295-310.

Dirik K., Göncüoğlu M. C. and Kozlu H., 1999. Stratigraphy and pre-Miocene tectonic evolution of the southwestern part of the Sivas Basin, Central Anatolia, Turkey. Geological Journal, 34(3): 303-319.

Droop G. T. R., Karakaya M. Q., Eren Y. and Karakaya N., 2005. Metamorphic evolution of blueschists of the Altinekin Complex, Konya area, south central Turkey. Geological Journal, 40(2): 127-153.

Dubacq B., Vidal O. and De Andrade V., 2010. Dehydration of dioctahedral aluminous phyllosilicates: thermodynamic modelling and implications for thermobarometric estimates. Contributions to Mineralogy and Petrology, 159(2): 159-174.

Dubertret L., 1932. Les formes structurales de la Syrie et de la Palestine: leur origine. Comptes Rendus de l'Académie des Sciences de Paris, 195: 65-66.

Dürr S., 1975. Über Alter und geotektonische Stellung des Menderes-Kristallins/SW-Anatolien und seine Äquivalente in der mittleren Aegaeis. Habilitation Thesis, Uni Marburg/Lahn, 107 pp.

El-Shazly A. K., 1995. Petrology of Fe-Mg-carpholite-bearing metasediments from NE Oman. Journal of Metamorphic Geology, 13: 379-396.

Elitok O. and Drüppel K., 2008. Geochemistry and tectonic significance of metamorphic sole rocks beneath the Beysehir-Hoyran ophiolite (SW-Turkey). Lithos, 100(1-4): 322-353.

Ellis D. J. and Green D. H., 1979. Experimental-study of the effect of Ca upon garnet-clinopyroxene Fe-Mg exchange equilibria. Contributions to Mineralogy and Petrology, 71(1): 13-22.

Emre T. and Sözbilir H., 1997. Field evidence for metamorphic core complex, detachment faulting and accommodation faults in the Gediz and Büyük Menderes Grabens, Western Anatolia. In: Pişkin Ö., Ergün M., Savaşcın M. Y. and Tarcan G. (Editors), International Earth Sciences Colloquium on the Aegean Region, Izmir-Güllük, Turkey), pp. 73-93.

Erdoğan B., 1990. Tectonic relations between Izmir-Ankara Zone and Karaburun belt. Bulletin of the Mineral Research and Exploration Institute of Turkey, 110: 1-15.

Erdoğan B., Altıner D., Güngör T. and Özer S., 1990. Stratigraphy of Karaburun Peninsula. Bulletin of the Mineral Research and Exploration Institute of Turkey, 111: 1-20.

Erdoğan B., Akay E. and Uğur S. M., 1996. Geology of the Yozgat region and evolution of the collision Çankırı Basin. International Geology Review, 38: 788-806.

Erkan E., Özer S., Sümengen M. and Terlemez I., 1978. Sarız-Şarkışla-Gemerek-Tomarza Arasının Temel Jeolojisi, Mineral Research and Exploration Institute of Turkey (MTA) Report No. 5646.

Eskola P., 1921. The mineral facies of rocks. Norsk Geologisk Tidskrift, 6: 143-194.

Evans B. W., 1990. Phase relation of epidote blueschists. Lithos, 25: 3-23.

Feenstra A., 1997. Zincohogbomite and gahnite in a diaspore-bearing metabauxite from eastern Samos (Greece): Mineral chemistry, element partitioning and reaction relations. Schweizerische Mineralogische und Petrographische Mitteilungen, 77(1): 73-93.

Ferry J. M. and Spear F. S., 1978. Experimental calibration of partitioning of Fe and Mg between biotite and garnet. Contributions to Mineralogy and Petrology, 66(2): 113-117.

Floyd P. A., Yalınız M. K. and Göncüoğlu M. C., 1998. Geochemistry and petrogenesis of intrusive and extrusive ophiolitic plagiogranites, Central Anatolian Crystalline Complex, Turkey. Lithos, 42: 225-241.

Floyd P. A., Göncüoğlu M. C., Winchester J. A. and Yalınız M. K., 2000. Geochemical character and tectonic environment of Neotethyan ophiolitic fragments and metabasites in the Central Anatolian Crystalline Complex, Turkey. In: Bozkurt E., Winchester J. A. and Piper J. D. A. (Editors), Tectonics and Magmatism in Turkey and the Surrounding Area. Geological Society, London, Special Publications, pp. 183-202.

Forster M. A. and Lister G. S., 2005. Several distinct tectono-metamorphic slices in the Cycladic eclogite-blueschist belt, Greece. Contributions to Mineralogy and Petrology, 150(5): 523-545.

Freund R., Zak I. and Garfunkel Z., 1968. Age and rate of sinistral movement along Dead Sea Rift. Nature, 220(5164): 253-255.

Gautier P., Bozkurt E., Hallot E. and Dirik K., 2002. Dating the exhumation of a metamorphic dome: geological evidence for pre-Eocene unroofing of the Nigde Massif (Central Anatolia, Turkey). Geological Magazine, 139(5): 559-576.

Gautier P., Bozkurt E., Bosse V., Hallot E. and Dirik K., 2008. Coeval extensional shearing and lateral underflow during Late Cretaceous core complex development in the Nigde Massif, Central Anatolia, Turkey. Tectonics, 27(TC1003).

Gautier Y., 1984. Deformations et métamorphisme associés à la suture téthysienne en Anatolie Centrale (Région de Sivrihisar, Turquie). PhD Thesis, Paris-Sud Orsay, 236 pp.

Gençalioğlu-Kuşcu G., Göncüoğlu M. C. and Kuşçu G. G., 2001. Post-Collisional Magmatism on the Northern Margin of the Taurides and its Geological Implications: Geology and Petrology of the Yahyalı-Karamadazı Granitoid. Turkish Journal of Earth Sciences, 10: 103-119.

Gessner K., Piazolo S., Güngör T., Ring U., Kröner A. and Passchier C. W., 2001a. Tectonic significance of deformation patterns in granitoid rocks of the Menderes nappes, Anatolide belt, southwest Turkey. International Journal of Earth Sciences, 89(4): 766-780.

Gessner K., Ring U., Johnson C., Hetzel R., Passchier C. W. and Güngör T., 2001b. An active bivergent rolling-hinge detachment system: Central Menderes metamorphic core complex in western Turkey. Geology, 29(7): 611-614.

Gessner K., Ring U., Passchier C. W. and Güngör T., 2001c. How to resist subduction: evidence for large-scale out-of-sequence thrusting during Eocene collision in western Turkey. Journal of the Geological Society, London, 158: 769-784.

Glodny J. and Hetzel R., 2007. Precise U-Pb ages of syn-extensional Miocene intrusions in the central Menderes Massif, western Turkey. Geological Magazine, 144(2): 235-246.

Goffe B., Azanon J. M., Bouybaouene M. L. and Jullien M., 1996. Metamorphic cookeite in Alpine metapelites from Rif, northern Morocco, and the Betic Chain, southern Spain. European Journal of Mineralogy, 8(2): 335-348.

Goffé B., Goffé-Urbano G. and Saliot P., 1973. Sur la présence d'une variété magnésienne de la ferrocarpholite en Vanoise (Alpes françaises) : sa signification probable dans le métamorphisme alpin. Comptes Rendus de l'Académie des Sciences Paris, 277: 1965-1968.

Goffé B., 1982. Définition du faciès à Fe,Mg-carpholite-chloritoide, un marqueur du métamorphisme de HP-BT dans les métasédiments alumineux, Paris, Université P. et M. Curie.

Goffé B. and Chopin C., 1986. High-pressure metamorphism in the Western Alps: zoneography of metapelites, chronology and consequences. Schweizerische Mineralogische und Petrographische Mitteilungen, 66: 41-52.

Goffé B., Michard A., Kienast J.-R. and Le Mer O., 1988. A case study of obduction-related high pressure, low temperature metamorphism in the upper crustal nappes, Arabian continental margin, Oman: P-T paths and kinematic interpretation. Tectonophysics, 151: 363-386.

Goffé B. and Oberhänsli R., 1992. Ferro- and magnesiocarpholite in the "Bündnerschiefer" of the eastern Central Alps (Grisons and Engadine Window). European Journal of Mineralogy, 4: 835-838.

Goffé B. and Bousquet R., 1997. Ferrocarpholite, chloritoïde et lawsonite dans les métapelites des unités du Versoyen et du Petit St Bernard (zone valaisanne, Alpes occidentales). Schweizerische Mineralogische und Petrographische Mitteilungen, 77: 137-147.

Gökten E. and Floyd P. A., 1987. Geochemistry and tectonic environment of the Şarkışla area volcanic rocks in Central Anatolia, Turkey. Mineralogical Magazine, 51: 553-559.

Gökten E., 1993. Geology of the Southern Boundary of the Sivas Basin in the East of Ulaş (Sivas - Central Anatolia); Tectonics Development Related to the Closure of Inner Tauride Ocean. Turkish Association of Petroleum Geologists Bulletin, 5(1): 35-55.

Göncüoğlu M. C., 1986. Geochronological data from the southern part (Niğde Area) of the Central Anatolian Massif. Bulletin of the Mineral Research and Exploration Institute of Turkey, 105-106: 83-96.

Göncüoğlu M. C., Özcan A., Turhan N. and Işık A., 1992. Stratigraphy of Kütahya region, ISGB-92 Field Guide Book. MTA, Ankara, pp. 3-11.

Göncüoğlu M. C., Dirik K. and Kozlu H., 1997. General Characteristics of pre-Alpine and Alpine Terranes in Turkey: Explanatory notes to the terrane map of Turkey. Annales Géologiques des Pays Helleniques, 37: 515-536.

Göncüoğlu M. C., Çapkinoğlu Ş., Gürsu S., Noble P., Turhan N., Tekin U. K., Okuyucu C. and Göncüoğlu Y., 2007. The Mississippian in the Central and Eastern Taurides (Turkey): constraints on the tectonic setting of the Tauride-Anatolide Platform. Geologica Carpathica, 58(5): 427-442.

Göncüoğlu M. C., 2011. Geology of the Kütahya-Bolkardağ Belt. Bulletin of the Mineral Research and Exploration Institute of Turkey, 142: 223-277.

Görür N., Oktay F. Y., Seymen I. and Şengör A. M. C., 1984. Palaeotectonic evolution of the Tuzgölü basin complex, Central Turkey: sedimentary record of a Neo-Tethyan closure. In: Dixon J. E. and Robertson A. H. F. (Editors), The Geological Evolution of the Eastern Mediterranean. Geological Society, London, Special Publication, 17.

Görür N., Tüysüz O. and Şengör A. M. C., 1998. Tectonic Evolution of the Central Anatolian Basins. International Geology Review, 40: 831-850.

Güngör T. and Erdoğan B., 2001. Emplacement age and direction of the Lycian nappes in the Soke-Selçuk region, western Turkey. International Journal of Earth Sciences, 89(4): 874-882.

Gürsu S., Göncüoğlu M. C. and Bayhan H., 2004. Geology and geochemistry of the pre-Early Cambrian rocks in the Sandikli area: Implications for the Pan-African evolution of NW Gondwanaland. Gondwana Research, 7(4): 923-935.

Gutnic M., 1977. Géologie du Taurus Pisidien au Nord d'Isparta (Turquie). PhD thesis Thesis, Université de Paris-Sud, Orsay.

Gutnic M., Monod O., Poisson A. and Dumont J.-F., 1979. Géologie des Taurides occidentales (Turquie). Nouvelle Série, 137. Société Géologiques de France, Paris, 112 pp.

Hames W. E. and Bowring S. A., 1994. An empirical-evaluation of the argon diffusion geometry in muscovite. Earth and Planetary Science Letters, 124(1-4): 161-167.

Hamilton W. J., 1842. Researches in Asia Minor, Pontus and Armenia. John Murray, London, 544 pp.

Hammerschmidt K. and Frank E., 1991. Relics of high-pressure metamorphism in the Lepontinde Alps (Switzerland) - 40Ar/39Ar and microprobe analyses on white K-micas. Schweizerische Mineralogische und Petrographische Mitteilungen, 71: 261-274.

Harris N. B. W., Kelley S. and Okay A. I., 1994. Postcollision Magmatism and Tectonics in Northwest Anatolia. Contributions to Mineralogy and Petrology, 117(3): 241-252.

Hempton M. R., 1987. Constraints on Arabian Plate motion and extensional history of the Red Sea. Tectonics, 6(6): 687-705.

Henry C., Burkhard M. and Goffé B., 1996. Evolution of synmetamorphic veins and their wall rocks through a Western Alps transect: no evidence for a large-scale fluid flow. Stable isotope, major- and trace-element systematics. Chemical Geology, 127: 81-109.

Hetzel R., Passchier C. W., Ring U. and Dora O. Ö., 1995a. Bivergent Extension in Orogenic Belts - the Menderes Massif (Southwestern Turkey). Geology, 23(5): 455-458.

Hetzel R., Ring U., Akal C. and Troesch M., 1995b. Miocene NNE-directed extensional unroofing in the Menderes-Massif, southwestern Turkey. Journal of the Geological Society, London, 152(4): 639.

Hetzel R. and Reischmann T., 1996. Intrusion age of Pan-African augen gneisses in the southern Menderes Massif and the age of cooling after Alpine ductile extensional deformation. Geological Magazine, 133: 565-572.

Hetzel R., Romer R. L., Candan O. and Passchier C. W., 1998. Geology of the Bozdag area, central Menderes massif, SW Turkey: Pan-African basement and Alpine deformation. Geologische Rundschau, 87(3): 394-406.

Hillier S. and Velde B., 1991. Octahedral occupancy and the chemical-composition of diagenetic (low-temperature) chlorites. Clay Minerals, 26(2): 149-168.

Holland T. J. B., 1989. Dependence of entropy on volume for silicate and oxide minerals - a review and a predictive model. American Mineralogist, 74(1-2): 5-13.

Hubert-Ferrari A., Armijo R., King G., Meyer B. and Barka A., 2002. Morphology, displacement, and slip rates along the North Anatolian Fault, Turkey. Journal of Geophysical Research-Solid Earth, 107(B10).

Ilbeyli N., Pearce J. A., Thirlwall M. F. and Mitchell J. G., 2004. Petrogenesis of collision-related plutonics in Central Anatolia, Turkey. Lithos, 72(3-4): 163-182.

Ilbeyli N., 2005. Mineralogical–geochemical constraints on intrusives in central Anatolia, Turkey: tectono-magmatic evolution and characteristics of mantle source. Geological Magazine, 142(2): 187-207.

Ishizuka O., 1998. Vertical and horizontal variation of the fast neutron flux in a single irradiation capsule and their significance in the laser-heating 40Ar/39Ar analysis: Case study for the hydraulic rabbit facility of the JMTR reactor, Japan. Geochemical Journal, 32(4): 243-252.

Ishizuka O., Yuasa M. and Uto K., 2002. Evidence of porphyry copper-type hydrothermal activity from a submerged remnant back-arc volcano of the Izu-Bonin arc - Implications for the volcanotectonic history of back-arc seamounts. Earth and Planetary Science Letters, 198(3-4): 381-399.

Işık V. and Tekeli O., 2001. Late orogenic crustal extension in the northern Menderes massif (western Turkey): evidence for metamorphic core complex formation. International Journal of Earth Sciences, 89(4): 757-765.

Işık V., Seyitoğlu G. and Çemen I., 2003. Ductile-brittle transition along the Alasehir detachment fault and its structural relationship with the Simav detachment fault, Menderes massif, western Turkey. Tectonophysics, 374(1-2): 1-18.

Işık V., Tekeli O. and Seyitoğlu G., 2004. The 40Ar/39Ar age of extensional ductile deformation and granitoid intrusion in the northern Menderes core complex: implications for the initiation of extensional tectonics in western Turkey. Journal of Asian Earth Sciences, 23(4): 555-566.

Jaffey N. and Robertson A. H. F., 2001. New sedimentological and structural data from the Ecemis Fault Zone, southern Turkey: implications for its timing and offset and the Cenozoic tectonic escape of Anatolia. Journal of the Geological Society, London, 158: 367-378.

Jäger E., 1973. Die alpine Orogenese im Lichte der radiometrischen Altersbestimmung. Eclogae Geologicae Helvetiae, 66: 11-21.

Jolivet L., Goffé B., Monié P., Truffert-Luxey C., Patriat M. and Bonneau M., 1996. Miocene detachment in Crete and exhumation P-T-t paths of high-pressure metamorphic rocks. Tectonics, 15(6): 1129-1153.

Jullien M. and Goffé B., 1993. Occurrences de cookeite et de pyrophyllite dans les schistes du Dauphinois (Isère, France): Conséquences sur la répartition du métamorphisme dans les zones externes alpines. Schweizerische Mineralogische und Petrographische Mitteilungen, 73: 357-363.

Jullien M., Baronnet A. and Goffé B., 1996. Ordering of the stacking sequence in cookeite with increasing pressure: An HRTEM study. American Mineralogist, 81: 67-78.

Juteau T., 1980. Ophiolites of Turkey. Ofioliti, 2: 199-235.

Kadioğlu Y. K., Ateş A. and Güleç N., 1998. Structural interpretation of gabbroic rocks in Ağaçören Granitoid, central Turkey: field observations and aeromagnetic data. Geological Magazine, 135(2): 245-254.

Kadioğlu Y. K., Dilek Y., Güleç N. and Foland K. A., 2003. Tectonomagmatic evolution of bimodal plutons in the central Anatolian crystalline complex, Turkey. Journal of Geology, 111(6): 671-690.

Ketin I., 1966. Tectonic units of Anatolia. Maden Tetkik ve Arama Bulletin, 66: 23-34.

Kissel C. and Poisson A., 1987. Etude paléomagnétique préliminaire des formations cénozoiques des Bey Dağları (Taurides occidentales, Turquie). Comptes Rendus de l'Académie des Sciences de Paris, 304(8): 343-348.

Kissel C., Averbuch O., Delamotte D. F., Monod O. and Allerton S., 1993. 1st Paleomagnetic Evidence for a Posteocene Clockwise Rotation of the Western Taurides Thrust Belt East of the Isparta Reentrant (Southwestern Turkey). Earth and Planetary Science Letters, 117(1-2): 1-14.

Kissel C., Laj C., Poisson A. and Görür N., 2003. Paleomagnetic reconstruction of the Cenozoic evolution of the Eastern Mediterranean. Tectonophysics, 362(1-4): 199-217.

Knipper A., Ricou L. E. and Dercourt J., 1986. Ophiolites as indicators of the geodynamic evolution of the Tethyan Ocean. Tectonophysics, 123(1-4): 213-240.

Kocak K. and Leake B. E., 1994. The petrology of the Ortaköy district and its ophiolite at the western edge of the Middle Anatolian Massif, Turkey. Journal of African Earth Sciences, 18(2): 163-174.

Koçyiğit A., 1989. Susehri Basin - an Active Fault-Wedge Basin on the North Anatolian Fault Zone, Turkey. Tectonophysics, 167(1): 13-29.

Koçyiğit A. and Beyhan A., 1998. A new intracontinental transcurrent structure: the Central Anatolian Fault Zone, Turkey. Tectonophysics, 284(3-4): 317-336.

Koçyiğit A. and Beyhan A., 1999. Reply to Rob Westaway's comment on 'A new intracontinental transcurrent structure: the Central Anatolian Fault Zone, Turkey'. Tectonophysics, 314(4): 481-496.

Koçyiğit A., Yusufoglu H. and Bozkurt E., 1999. Evidence from the Gediz graben for episodic two-stage extension in western Turkey. Journal of the Geological Society, London, 156: 605-616.

Koçyiğit A., Ünay E. and Saraç G., 2000. Episodic graben formation and extensional neotectonic regime in west Central Anatolia and the Isparta Angle: a case study in the Aksehir-Afyon Graben, Turkey. Tectonics and Magmatism in Turkey and the Surrounding Area(173): 405-421.

Köksal S., Romer R. L., Göncüoğlu M. and Toksoy-Köksal F., 2004. Timing of post-collisional H-type to A-type granitic magmatism: U-Pb titanite ages from the Alpine central Anatolian granitoids (Turkey). International Journal of Earth Sciences, 93(6): 974-989.

Koons P. O. and Thompson A. B., 1985. No-mafic rocks in the greenschist, blueschist and eclogite facies. Chemical Geology, 50: 3-30.

Kurt H., 1996. Geochemical Characteristics of the Meta-igneaous Rocks Nea Kadinhani (Konya), Turkey. Geosound, 28: 1-21.

Lagos M., Scherer E. E., Tomaschek F., Muenker C., Keiter M., Berndt J. and Ballhaus C., 2007. High precision lu-hf geochronology of eocene eclogite-facies rocks from syros, cyclades, Greece. Chemical Geology, 243(1-2): 16-35.

Le Pichon X., Needham H. D. and Renard V., 1973. Traits structuraux de la fosse Nord-égéenne, 1re Réunion Annuelles de Sciences de la Terre. Société Géologique de France, Paris.

Lefebvre C., Barnhoorn A., van Hinsbergen D. J. J., Kaymakcı N. and Vissers R. L. M., 2011. Late Cretaceous extensional denudation along a marble detachment fault zone in the Kırşehir massif near Kaman, central Turkey. Journal of Structural Geology, 33: 1220-1236.

Leoni L., Sartori F. and Tamponi M., 1998. Composition variation in K-white micas and chlorites coexisting in Al- saturated metapelites under late diagenetic to low-grade metamorphic conditions (Internal Liguride Units, Northern Apennines, Italy). European Journal of Mineralogy, 10(6): 1321-1339.

Lips A. L. W., Cassard D., Sözbilir H., Yılmaz H. and Wijbrans J. R., 2001. Multistage exhumation of the Menderes Massif, western Anatolia (Turkey). International Journal of Earth Sciences, 89(4): 781-792.

Loos S. and Reischmann T., 1999. The evolution of the souhern Menderes Massif in SW Turkey as revealed by zircon dating. Journal of the Geological Society, London, 156: 1021-1030.

Lytwyn J. N. and Casey J. F., 1995. The Geochemistry of Postkinematic Mafic Dike Swarms and Subophiolitic Metabasites, Pozanti-Karsanti Ophiolite, Turkey - Evidence for Ridge Subduction. Geological Society of America Bulletin, 107(7): 830-850.

Maluski H., Vergely P., Bavay D., Bavay P. and Katsikatsos G., 1981. 39Ar/40Ar Dating of glaucophanes and phengites in Southern Euboa (Greece) geodynamic implications. Bulletin de la Société géologique de France, 23(5): 469-476.

McClusky S. et al.,, 2000. Global Positioning System constraints on plate kinematics and dynamics in the eastern Mediterranean and Caucasus. Journal of Geophysical Research-Solid Earth, 105(B3): 5695-5719.

McDade P. and Harley S. L., 2001. A petrogenetic grid for aluminous granulite facies metapelites in the KFMASH system. Journal of Metamorphic Geology, 19(1): 45-60.

McDougall I. and Harrison T. M., 1999. Geochronology and thermochronology by the 40Ar/39Ar method. Oxford University Press, New York Oxford.

McKenzie D. P., Davies D. and Molnar P., 1970. Plate tectonics of Red Sea and East Africa. Nature, 226(5242): 243-248.

Miyashiro A. and Banno S., 1958. Nature of glaucophanitic metamorphism. American Journal of Science, 256(2): 97-110.

Miyashiro A., 1973. Metamorphism and metamorphic belts. Allen & Unwin, London.

Moix P., Beccaletto L., Kozur H. W., Hochard C., Rosselet F. and Stampfli G. M., 2008. A new classification of the Turkish terranes and sutures and its implication for the paleotectonic history of the region. Tectonophysics, 451(1-4): 7-39.

Monod O., 1977. Recherches géologiques dans le Taurus Occidental au Sud de Beyşehir (Turquie). Thèse de Doctorat Thesis, Univ. Paris-Sud, Orsay.

MTA, 2002. Geological Map of Turkey, 1:500,000. MTA, Ankara.

MTA, 2007. Aeromagnetic map (Total Intensity) of Turkey. MTA, Ankara.

Oberhänsli R., Candan O., Dora O. Ö. and Dürr S. H., 1997. Eclogites within the Menderes Massif western Turkey. Lithos, 41(1-3): 135-150.

Oberhänsli R., Monié P., Candan O., Warkus F. C., Partzsch J. H. and Dora O. Ö., 1998. The age of blueschist metamorphism in the Mesozoic cover series of the Menderes Massif. Schweizerische Mineralogische und Petrographische Mitteilungen, 78(2): 309-316.

Oberhänsli R., Partzsch J., Candan O. and Cetinkaplan M., 2001. First occurrence of Fe-Mg-carpholite documenting a high-pressure metamorphism in metasediments of the Lycian Nappes, SW Turkey. International Journal of Earth Sciences, 89(4): 867-873.

Oberhänsli R., Candan O., Bousquet R., Rimmelé G., Okay A. I. and Goff J., 2010a. Alpine HP evolution of the eastern Bitlis complex, SE Turkey. In: Sosson M., Kaymakci N., Stephenson R., Bergerat F. and Starostenko V. (Editors), Sedimentary Basin Tectonics from the Black Sea and Caucasus to the Arabian Platform. Geological Society, London, Special Publication, pp. 461-483.

Oberhänsli R., Candan O. and Wilke F., 2010b. Geochronological evidence of Pan-African eclogites from the Central Menderes Massif, Turkey. Turkish Journal of Earth Sciences, in press.

Oberhänsli R., Bousquet R., Candan O. and Okay A., 2011. Dating subduction events in East Anatolia, Turkey. Turkish Journal of Earth Sciences, in press.

Okay A. and Siyako M., 1993. The new position of the Izmir-Ankara Neo-Tethyan suture between Izmir and Balikesir. In: Turgut S. (Editor), Ozan Sungurlu Symposium Proceedings, November 1991. Association of Turkish Petroleum Geologists, Ankara.

Okay A. I., 1980a. Lawsonite Zone Blueschists and a Sodic Amphibole Producing Reaction in the Tavsanli Region, Northwest Turkey. Contributions to Mineralogy and Petrology, 75(3): 179-186.

Okay A. I., 1980b. Mineralogy, Petrology, and Phase-Relations of Glaucophane-Lawsonite Zone Blue Schists from the Tavsanli Region, Northwest Turkey. Contributions to Mineralogy and Petrology, 72(3): 243-255.

Okay A. I., 1982. Incipient Blueschist Metamorphism and Metasomatism in the Tavşanlı Region, Northwest Turkey. Contributions to Mineralogy and Petrology, 79: 361-367.

Okay A. I., 1984. Distribution and characteristics of the north-west Turkish blueschists. In: Dixon J. E. and Robertson A. H. F. (Editors), The Geological Evolution of the Eastern Mediterranean. Geological Society, London, Special Publications, pp. 455-466.

Okay A. I., 1986. High-pressure/low-temperature metamorphic rocks of Turkey. In: Evans B. W. and Brown E. H. (Editors), Blueschists and eclogites. Geological Society of America Memoir 164, pp. 333-347.

Okay A. I. and Kelley S. P., 1994. Tectonic Setting, Petrology and Geochronology of Jadeite Plus Glaucophane and Chloritoid Plus Glaucophane Schists from North-West Turkey. Journal of Metamorphic Geology, 12(4): 455-466.

Okay A. I., Satır M., Maluski H., Siyako M., Monié P., Metzger R. and Akyüz S., 1996. Paleo- and Neo-Tethyan events in northwestern Turkey: Geologic and geochronologic constraints. In: Yin A. and Harrison T. M. (Editors), The Tectonic Evolution of Asia. University Press, Cambridge, pp. 420-441.

Okay A. I. and Monié P., 1997. Early Mesozoic subduction in the Eastern Mediterranean: Evidence from Triassic eclogite in northwest Turkey. Geology, 25(7): 595-598.

Okay A. I. and Sahinturk O., 1997. Geology of the Eastern Pontides. In: Robinson A. G. (Editor), Regional and Petroleum Geology of the Black Sea and Surrounding Region. AAPG Memoir, pp. 291-311.

Okay A. I., Harris N. B. W. and Kelley S. P., 1998. Exhumation of blueschists along a Tethyan suture in northwest Turkey. Tectonophysics, 285(3-4): 275-299.

Okay A. I. and Tüysüz O., 1999. Tethyan sutures of northern Turkey. In: Durand B., Jolivet L., Horváth F. and Séranne M. (Editors), The Mediterranean Basins: Tertiary Extension within the Alpine Orogen. Geological Society, London, Special Publications, pp. 475-515.

Okay A. I., 2001. Stratigraphic and metamorphic inversions in the central Menderes Massif: a new structural model. International Journal of Earth Sciences, 89(4): 709-727.

Okay A. I., Tansel I. and Tüysüz O., 2001. Obduction, subduction and collision as reflected in the Upper Cretaceous-Lower Eocene sedimentary record of western Turkey. Geological Magazine, 138(2): 117-142.

Okay A. I., 2002. Jadeite-chloritoid-glaucophane-lawsonite blueschists in northwest Turkey: unusually high P/T ratios in continental crust. Journal of Metamorphic Geology, 20(8): 757-768.

Okay A. I. and Satır M., 2006. Geochronology of Eocene plutonism and metamorphism in northwest Turkey: evidence for a possible magmatic arc. Geodinamica Acta, 19(5): 251-266.

Okay A. I., Tüysüz O., Satır M., Ozkan-Altıner S., Altıner D., Sherlock S. and Eren R. H., 2006. Cretaceous and Triassic subduction-accretion, high-pressure-low-temperature metamorphism, and continental growth in the Central Pontides, Turkey. Geological Society of America Bulletin, 118(9-10): 1247-1269.

Okay A. I. and Altıner D., 2007. A condensed mesozoic succession north of Izmir: A fragment of the anatolide-tauride platform in the Bornova Flysch zone. Turkish Journal of Earth Sciences, 16: 257-279.

Oktay F. Y., 1982. Ulukışla ve çevresinin stratigrafisi ve jeolijik evrimi. Bulletin of the Geological Society of Turkey, 25: 1-23.

Önen A. P. and Hall R., 2000. Sub-ophiolite metamorphic rocks from NW Anatolia, Turkey. Journal of Metamorphic Geology, 18(5): 483-495.

Önen A. P., 2003. Neotethyan ophiolitic rocks of the Anatolides of NW Turkey and comparison with Tauride ophiolites. Journal of the Geological Society, London, 160: 947-962.

Özcan A., Göncüoğlu M., Turan N., Uysal Ş., Senturk K. and Işık V., 1988. Late Paleozoic Evolution of the Kütahya-Bolkardağ Belt. METU Journal of Pure and Applied Sciences, 21(1-3): 211-220.

Özer S. and Irtem O., 1982. Geologial setting, stratigraphy and facies characteristics of the Upper Cretaceous limestones in the Işıldar - Altınadağ (Bornova - Izmir) area. Bulletin of the Geological Society of Turkey, 25: 41-47.

Özer S., Sözbilir H., Özkar I., Toker V. and Sari B., 2001. Stratigraphy of Upper Cretaceous-Palaeogene sequences in the southern and eastern Menderes Massif (western Turkey). International Journal of Earth Sciences, 89(4): 852-866.

Özgül N., 1976. Some geological aspects of the Taurus orogenic belt (Turkey). Bulletin of the Geological Society of Turkey, 19: 65-78.

Özgül N., 1984. Stratigraphy and tectonic evolution of the Central Taurides. In: Tekeli O. and Göncüoğlu M. C. (Editors), Proceedings of the International Symposium on the Geology of the Taurus Belt. Mineral Research and Exploration Intitute of Turkey (MTA), Ankara, Turkey, pp. 77-90.

Ozkaya I., 1991. Evolution of a tertiary volcanogenic trough in SW Turkey - The Alakaya basins of the Lycien belt. Geologische Rundschau, 80(3): 657-668.

Özkaya I., 1990. Origin of the Allochthons in the Lycien Belt, Southwest Turkey. Tectonophysics, 177(4): 367-379.

Papanikolaou D., 2009. Timing of tectonic emplacement of the ophiolites and terrane paleogeography in the Hellenides. Lithos, 108(1-4): 262-280.

Paréjas E., 1940. La tectonique transversale de la Turquie. Istanbul Universitesi Fen Fakültesi Mecmuasi, série B, tome V(fasc. 3-4): 133-244.

Parlak O., Delaloye M. and Bingol E., 1996. Mineral chemistry of ultramafic and mafic cumulates an indicator of the arc-related origin of Mersin ophiolite (southern Turkey). Geologische Rundschau, 85(4): 647-661.

Parlak O. and Delaloye M., 1999. Precise 40Ar/39Ar ages from the metamorphic sole of the Mersin ophiolite (southern Turkey). Tectonophysics, 301(1-2): 145-158.

Parlak O., Hock V. and Delaloye M., 2002. The supra-subduction zone Pozanti-Karsanti ophiolite, southern Turkey: evidence for high-pressure crystal fractionation of ultramafic cumulates. Lithos, 65(1-2): 205-224.

Pearce J. A., Harris N. B. W. and Tindle A. G., 1984. Trace element discrimination diagrams for the tectonic interpretation of granitic rocks. Journal of Petrology, 25: 956-983.

Philipson A., 1911-1915. Reisen und Forschungen im westilchen Kleinasien., Gotha.

Platzman E. S., Tapirdamaz C. and Sanver M., 1998. Neogene anticlockwise rotation of central Anatolia (Turkey): preliminary palaeomagnetic and geochronological results. Tectonophysics, 299(1-3): 175-189.

Poinssot C., Goffe B. and Toulhoat P., 1997. Geochemistry of the Triassic-Jurassic Alpine continental deposits: Origin and geodynamic implications. Bulletin de la Société géologique de France, 168(3): 287-300.

Poisson A., 1977. Recherches géologiques dans les Taurus occidentales, Turquie. PhD Thesis, Université de Paris-Sud, Orsay.

Poisson A., 1984. The extension of the Ionian trough into southwestern Turkey. In: Dixon J. E. and Robertson A. H. F. (Editors), The Geological Evolution of the Eastern Mediterranean. Geological Society, London, Special Publications, pp. 241-249.

Pourteau A., Candan O. and Oberhänsli R., 2010. High-Pressure metasediments in central Turkey: constraints on the Neotethyan closure history. Tectonics, 29(TC5004).

Pourteau A., Bousquet R., Vidal O., Oberhänsli R. and Candan O., 2011a. Multistage growth of Fe-Mg-carpholite and chloritoid, from field evidence to thermodynamic modelling. Journal of Petrology, submitted.

Pourteau A., Sudo M., Candan O., Lanari P., Vidal O. and Oberhänsli R., 2011b. Final amalgamation of the Anatolian microcontinent: insight from 40Ar-39Ar geochronology and P-T estimation in high-pressure metasediments from Western and Central Anatolia. Journal of Metamorphic Geology, submitted.

Purdy J. W. and Jäger E., 1976. K-Ar ages on rock-forming minerals from the Central Alps, Mem Ist Geol Mineral Univ Padova, pp. 31pp.

Purvis M. and Robertson A. H. F., 2004. A pulsed extension model for the Neogene-Recent E-W-trending Alasehir Graben and the NE-SW-trending Selendi and Gordes Basins, western Turkey. Tectonophysics, 391(1-4): 171-201.

Putlitz B., Cosca M. A. and Schumacher J. C., 2005. Prograde mica 40Ar/39Ar growth ages recorded in high pressure rocks (Syros, Cyclades, Greece). Chemical Geology, 214(1-2): 79-98.

Quennell A. M., 1958. The structural and geomorphic evolution of the Dead Sea Rift. Quaterly Journal of the Geological Society of London, 114: 1-24.

Reddy S. M., Kelley S. P. and Wheeler J., 1996. A 40Ar/39Ar laser probe study of micas from the Sesia Zone, Italian Alps: Implications for metamorphic and deformation histories. Journal of Metamorphic Geology, 14(4): 493-508.

Régnier J. L., Ring U., Passchier C. W., Gessner K. and Güngör T., 2003. Contrasting metamorphic evolution of metasedimentary rocks from the Cine and Selimiye nappes in the Anatolide belt, western Turkey. Journal of Metamorphic Geology, 21(7): 699-721.

Régnier J. L., Mezger J. E. and Passchier C. W., 2007. Metamorphism of Precambrian-Palaeozoic schists of the Menderes core series and contact relationships with Proterozoic orthogneisses of the western Cine Massif, Anatolide belt, western Turkey. Geological Magazine, 144(1): 67-104.

Reinecke T., Okrusch M. and Richter P., 1985. Geochemistry of ferromanganoan metasediments from the island-of-Andros, Cycladic Blueschist Belt, Greece. Chemical Geology, 53(3-4): 249-278.

Rice S. P., Robertson A. H. F. and Ustaömer T., 2006. Late Cretaceous-Early Cenozoic tectonic evolution of the Eurasian active margin in the Central and Eastern Pontides, northern Turkey. In: Robertson A. H. F. and Mountrakis D. (Editors), Tectonic Development of the Eastern Mediterranean Region. Geological Society, London, Special Publication, 260, pp. 413-445.

Ricou L. E., Dercourt J., Geyssant J., Grandjacquet C., Lepvrier C. and Bijuduval B., 1986. Geological Constraints on the Alpine Evolution of the Mediterranean Tethys. Tectonophysics, 123(1-4): 83-122.

Rimmelé G., 2003. Structural and metamorphic evolution of the Lycian Nappes and the Menderes Massif (Southwest Turkey): Geodynamic implications and correlations with the Aegean Domain. PhD thesis Thesis, Universität Potsdam/Université d'Orsay-Paris Sud, 243 pp.

Rimmelé G., Jolivet L., Oberhänsli R. and Goffé B., 2003a. Deformation history of the high-pressure Lycian Nappes and implications for tectonic evolution of SW Turkey. Tectonics, 22(TC1007).

Rimmelé G., Oberhänsli R., Goffé B., Jolivet L., Candan O. and Çetinkaplan M., 2003b. First evidence of high-pressure metamorphism in the "Cover Series" of the southern Menderes Massif. Tectonic and metamorphic implications for the evolution of SW Turkey. Lithos, 71(1): 19-46.

Rimmelé G., Parra T., Goffé B., Oberhänsli R., Jolivet L. and Candan O., 2005. Exhumation paths of high-pressure-low-temperature metamorphic rocks from the Lycian Nappes and the Menderes Massif (SW Turkey): a multi-equilibrium approach. Journal of Petrology, 46(3): 641-669.

Rimmelé G., Oberhänsli R., Candan O., Goffé B. and Jolivet L., 2006. The wide distribution of HP-LT rocks in the Lycian Belt (Western Turkey): implications for accretionary wedge geometry In: Robertson A. H. F. and Mountrakis D. (Editors), Tectonic Development of the Eastern Mediterranean Region. Geological Society, London, Special Publications, pp. 447-466.

Ring U., Gessner K., Güngör T. and Passchier C. W., 1999. The Menderes Massif of western Turkey and the Cycladic Massif in the Aegean - do they really correlate? Journal of the Geological Society, London, 156: 3-6.

Ring U., Johnson C., Hetzel R. and Gessner K., 2003. Tectonic denudation of a Late Cretaceous-Tertiary collisional belt: regionally symmetric cooling patterns and their relation to extensional faults in the Anatolide belt of western Turkey. Geological Magazine, 140(4): 421-441.

Ring U. and Layer P. W., 2003. High-pressure metamorphism in the Aegean, eastern Mediterranean: Underplating and exhumation from the Late Cretaceous until the Miocene to Recent above the retreating Hellenic subduction zone. Tectonics, 22(TC1022).

Ring U. and Collins A. S., 2005. U-Pb SIMS dating of synkinematic granites: timing of core-complex formation in the northern Anatolide belt of western Turkey. Journal of the Geological Society, London, 162: 289-298.

Robertson A., Parlak O. and Ustaömer T., 2009. Melange genesis and ophiolites emplacement related to subduction of the northern margin of the Tauride-Anatolide continent, central and western Turkey. In: van Hinsbergen D. J. J., Edwards M. A. and Govers R. (Editors), Collision and Collapse at the Africa-Arabia-Eurasia Subduction Zone. Geological Society, London, Special Publications, pp. 9-66.

Robertson A. H. F. and Dixon J. E., 1984. Introduction: aspects of the geological evolution of the Eastern Mediterranean. In: Dixon J. E. and Robertson A. H. F. (Editors), The Geological Evolution of the Eastern Mediterranean. Geological Society, London, Special Publications, pp. 1-74.

Robertson A. H. F., 2002. Overview of the genesis and emplacement of Mesozoic ophiolites in the Eastern Mediterranean Tethyan region. Lithos, 65(1-2): 1-67.

Robertson A. H. F., Poisson A. and Ankıncı Ö., 2003. Developments in research concerning Mesozoic-Tertiary Tethys and neotectonics in the Isparta Angle, SW Turkey. Geological Journal, 38(3-4): 195-234.

Robertson A. H. F., Ustaömer T., Parlak O., Unlügenç U. C., Taşli K. and Inan N., 2006. The Berit transect of the Tauride thrust belt, S Turkey: Late Cretaceous-Early Cenozoic accretionary/collisional processes related to closure of the Southern Neotethys. Journal of Asian Earth Sciences, 27(1): 108-145.

Robertson A. H. F. and Ustaömer T., 2009. Formation of the Palaeozoic Konya Complex and comparable units in southern Turkey by subduction-accretion processes: Implications for the tectonic development of Tethys in the Eastern Mediterranean region. Tectonophysics, 473: 113-148.

Salaün G. et al.,, 2011. High-Resolution Surface Wave Tomography beneath the Aegean-Anatolia region – II. 3-D constraints on the upper mantle structure. Journal of Geophysical Research-Solid Earth, submitted.

Saporta G., 1990. Probabilités, analyse des données et statistique. , 388 pp.

Satır M. and Friedrichsen H., 1986. The origin and evolution of the Menderes Massif, W-Turkey: A rubidium/strontium and oxygen isotop study. Geologische Rundschau, 75(3): 703-714.

Schmid S. M., Bernoulli D., Fügenschuh B., Matenco L., Schefer S., Oberhänsli R. and Ustaszewski K., 2011. Tracing the closure of Neotethys from the Alps to Western Turkey II: Similarities and differences between Dinarides, Hellenides and Anatolides-Taurides. In: Abstracts G. R. (Editor), EGU General Assembly, Vienna, Austria, pp. EGU2011-4000.

Schuiling R. D., 1962. On petrology, age and structure of the Menderes migmatite complex (SW-Turkey). Bulletin of the Mineral Research and Exploration Institute of Turkey, 58: 71-84.

Seaton N. C. A., Whitney D. L., Teyssier C., Toraman E. and Heizler M. T., 2009. Recrystallization of high-pressure marble (Sivrihisar, Turkey). Tectonophysics, 479(3-4): 241-253.

Şenel M., 1991. Paleocene-Eocene sediments interbedded with volcanics within the Lycian Nappes: Faralya formations. Bulletin of the Mineral Research and Exploration Institute of Turkey, 113: 1-14.

Şengör A. M. C. and Yılmaz Y., 1981. Tethyan Evolution of Turkey - a Plate Tectonic Approach. Tectonophysics, 75(3-4): 181-241.

Şengör A. M. C., Satır M. and Akkok R., 1984. Timing of tectonic events in the Menderes Massif, Western Turkey - Implications for tectonic evolution and evidence for Pan-African basement in Turkey. Tectonics, 3(7): 693-707.

Şengör A. M. C., Görür N. and Şaroğlu F., 1985. Strike-slip faulting and related basin formation in zones of tectonic escape: Turkey as a case study. In: Biddle K. T. and Christie-Blick N. (Editors), Strike-Slip Faulting and Basin Formation. Special Publication of the Society of Economic Paleontologists and Mineralogists, pp. 227-267.

Şengör A. M. C., 1990. Plate-Tectonics and Orogenic Research after 25 Years - a Tethyan Perspective. Earth-Science Reviews, 27(1-2): 1-201.

Şengün M., 2006. A critical review of the Anatolian geology: a dialectic to sutures and evolution of the Anatolian Tethys and Neotethys. Bulletin of the Mineral Research and Exploration Institute of Turkey, 133: 1-29.

Seyitoğlu G. and Scott B. C., 1992. The Age of the Buyuk Menderes Graben (West Turkey) and Its Tectonic Implications. Geological Magazine, 129(2): 239-242.

Seyitoğlu G., Tekeli O., Çemen I., Şen S. and Işık V., 2002. The role of the flexural rotation/rolling hinge model in the tectonic evolution of the Alasehir graben, western Turkey. Geological Magazine, 139(1): 15-26.

Seyitoğlu G., Işık V. and Çemen I., 2004. Complete Tertiary exhumation history of the Menderes massif, western Turkey: an alternative working hypothesis. Terra Nova, 16: 358-364.

Seymen I., 1981. Stratigraphy and metamorphism of the Kırşehir Massif around Kaman (Kırşehir - Turkey). Bulletin of the Geological Society of Turkey, 24: 7-14.

Sherlock S., Kelley S., Inger S., Harris N. B. W. and Okay A. I., 1999. 40Ar-39Ar and Rb-Sr geochronology of high-pressure metamorphism and exhumation history of the Tavsanli Zone, NW Turkey. Contributions to Mineralogy and Petrology, 137(1-2): 46-58.

Spear F. S., 1993. Metamorphic Phase Equilibria and Pressure-Temperature-Time Paths. Mineralogical Society of America, Washington, D. C, 799 pp.

Stampfli G. M. and Borel G. D., 2002. A plate tectonic model for the Paleozoic and Mesozoic constrained by dynamic plate boundaries and restored synthetic oceanic isochrons. Earth and Planetary Science Letters, 196(1-2): 17-33.

Tekeli O., 1981. Subduction complex of pre-Jurassic age, northern Anatolia, Turkey. Geology, 9(2): 68-72.

Tekeli O., Aksay A., Ürgün B. M. and Işık A., 1984. Geology of the Aladağ Mountains. In: Tekili O. and Göncüoğlu M. C. (Editors), Proceedings of the International Symposium on the Geology of the Taurus Belt. Mineral Research and Exploration Intitute of Turkey (MTA), Ankara, Turkey, pp. 125-141.

Theye T., Seidel E. and Vidal O., 1992. Carpholite, sudoite, and chloritoid in low-grade high-pressure metapelites from Crete and the Peloponnese, Greece. European Journal of Mineralogy, 4(3): 487-507.

Theye T., Reinhardt J., Goffé B., Jolivet L. and Brunet C., 1997. Ferro- and magnesiocarpholite from the Monte Argentario (Italy): First evidence for high-pressure metamorphism of the metasedimentary Verrucano sequence, and significance for P-T path reconstruction. European Journal of Mineralogy, 9: 859-873.

Thomson S. N. and Ring U., 2006. Thermochronologic evaluation of postcollision extension in the Anatolide orogen, western Turkey. Tectonics, 25(3).

Thuizat R., Whitechurch H., Montigny R. and Juteau T., 1981. K-Ar dating of some infra-ophiolitic metamorphic soles from the eastern Mediterranean: New evidence for oceanic thrustings before obduction. Earth and Planetary Science Letters, 52(2): 302-310.

Tolluoğlu Ü., Erkan Y., Sümer E. Ö., Boyacı M. and Yavaş F., 1997. The Pre-Mesozoic metamorphic evolution of the Afyon Metasedimentary Group. Geological Bulletin of Turkey, 40(1): 1-17.

Topuz G., Okay A. I., Altherr R., Meyer H. P. and Nasdala L., 2006. Partial high-pressure aragonitization of micritic limestones in an accretionary complex, Tavsanli Zone, NW Turkey. Journal of Metamorphic Geology, 24(7): 603-613.

Topuz G., Altherr R., Schwarz W. H., Dokuz A. and Meyer H. P., 2007. Variscan amphibolite-facies rocks from the Kurtoglu metamorphic complex (Gumushane area, Eastern Pontides, Turkey). International Journal of Earth Sciences, 96: 861-873.

Trotet F., Goffé B., Vidal O. and Jolivet L., 2006. Evidence of retrograde Mg-carpholite in the Phyllite-Quartzite nappe of Peloponnese from thermobarometric modelisation - geodynamic implications. Geodynamica Acta, 19(5): 323-343.

Turner F. J., 1981. Metamorphic Petrology. McGraw-Hill, New York, 403 pp.

Umhoefer P. J., Whitney D. L., Teyssier C., Fayon A. K., Casale G. and Heizler M. T., 2007. Yo-yo tectonic in a wrench zone, Central Anatolian fault zone, Turkey. In: Till A. B., Roeske S. M., Sample J. C. and Foster D. A. (Editors), Exhumation Associated with Continental Strike-Slip Fault Systems. Geological Society of America Special Paper, pp. 35-57.

Uto K., Ishizuka O., Matsumoto A., Kamioka H. and Togashi S., 1997. Laser-heating 40Ar/39Ar dating system of the Geological Survey of Japan: System outline and preliminary results. Bulletin of the Geological Society of Japan, 48: 23-46.

van der Kaaden G., 1966. The significance and distribution of glaucophane rocks in Turkey. Bulletin of the Mineral Research and Exploration Institute of Turkey, 67: 37-67.

van Hinsbergen D. J. J., 2010. A key extensional metamorphic complex reviewed and restored: The Menderes Massif of western Turkey. Earth-Science Reviews, 102(1-2): 60-76.

van Hinsbergen D. J. J., Dekkers M. J., Bozkurt E. and Koopman M., 2010. Exhumation with a twist: Paleomagnetic constraints on the evolution of the Menderes metamorphic core complex, western Turkey. Tectonics, 29(TC3009).

Verlaguet A., Goffe B., Brunet F., Poinssot C., Vidal O., Findling N. and Menut D., 2011. Metamorphic veining and mass transfer in a chemically closed system: a case study in Alpine metabauxites (western Vanoise). Journal of Metamorphic Geology, 29(3): 275-300.

Vidal O., 1991. Etude expérimentale des relations de phase des chlorites di/trioctaédriques dans les systèmes Li_2O-Al_2O_3-SiO_2-H_2O et MgO-Al_2O_3-SiO_2-H_2O. Application aux métapélites et métabauxites de haute pression-basse température., Paris VI, 224 pp.

Vidal O. and Goffé B., 1991. Cookeite $LiAl_4(Si_3Al)O_{10}(OH)_8$: Experimental study and thermodynamical analysis of its compatibility relations in the LiO_2-Al_4O_3-SiO_2-H_2O system. Contributions to Mineralogy and Petrology, 108: 72-81.

Vidal O., Goffé B. and Theye T., 1992. Experimental study of the stability of sudoite and magnesiocarpholite and calculation of a new petrogenetic grid for the system FeO-MgO-Al_2O_3-SiO_2-H_2O. Journal of Metamorphic Geology, 10: 603-614.

Vidal O., Theye T. and Chopin C., 1994. Experimental study of chloritoid stability at high pressure and various fO_2 conditions. Contributions to Mineralogy and Petrology, 118: 256-270.

Vidal O. and Theye T., 1996. Comment on "Petrology of Fe-Mg-carpholite-bearing metasediments from NE Oman". Journal of Metamorphic Geology, 14: 381-386.

Vidal O., Goffé B., Bousquet R. and Parra T., 1999. Calibration and testing of an empirical chloritoid-chlorite exchange thermometer and thermodynamic data for daphnite. Journal of Metamorphic Geology, 17(1): 25-39.

Vidal O. and Parra T., 2000. Exhumation paths of high pressure metapelites obtained from local equilibria for chlorite-phengite assemblages. Geological Journal, 35(3-4): 139-161.

Vidal O., Parra T. and Trotet F., 2001. A thermodynamic model for Fe-Mg aluminous chlorite using data from phase equilibrium experiments and natural pelitic assemblages in the 100-600°C, 1-25 kbar range. American Journal of Science, 301: 557-592.

Vidal O., Parra T. and Vieillard P., 2005. Thermodynamic properties of the Tschermak solid solution in Fe-chlorite: Application to natural examples and possible role of oxidation. American Mineralogist, 90(2-3): 347-358.

Vidal O., De Andrade V., Lewin E., Munoz M., Parra T. and Pascarelli S., 2006. P-T-deformation-Fe3+/Fe2+ mapping at the thin section scale and comparison with XANES mapping: application to a garnet-bearing metapelite from the Sambagawa metamorphic belt (Japan). Journal of Metamorphic Geology, 24(7): 669-683.

Villa I. M., 1998. Isotopic closure. Terra Nova, 10(1): 42-47.

Wei C. J., Powell R. and Clarke G. L., 2004. Calculated phase equilibria for low- and medium-pressure metapelites in the KFMASH and KMnFMASH systems. Journal of Metamorphic Geology, 22(5): 495-508.

Westaway R., 1994. Present-Day Kinematics of the Middle-East and Eastern Mediterranean. Journal of Geophysical Research-Solid Earth, 99(B6): 12071-12090.

Westaway R., 1999. Comment on "A new intracontinental transcurrent structure: the Central Anatolian Fault Zone, Turkey" by A. Koçyiğit and A. Beyhan. Tectonophysics, 314(4): 469-479.

Westaway R., Pringle M., Yurtmen S., Demir T., Bridgland D., Rowbotham G. and Maddy D., 2004. Pliocene and Quaternary regional uplift in western Turkey: the Gediz River terrace staircase and the volcanism at Kula. Tectonophysics, 391: 121-169.

Whitney D. L., Teyssier C., Dilek Y. and Fayon A. K., 2001. Metamorphism of the Central Anatolian Crystalline Complex, Turkey: influence of orogen-normal collision vs, wrench-dominated tectonics on P-T-t paths. Journal of Metamorphic Geology, 19(4): 411-432.

Whitney D. L. and Bozkurt E., 2002. Metamorphic history of the southern Menderes massif, western Turkey. Geological Society of America Bulletin, 114(7): 829-838.

Whitney D. L., Teyssier C., Fayon A. K., Hamilton M. A. and Heizler M., 2003. Tectonic controls on metamorphism, partial melting, and intrusion: timing and duration of regional metamorphism and magmatism in the Nigde Massif, Turkey. Tectonophysics, 376(1-2): 37-60.

Whitney D. L. and Hamilton M. A., 2004. Timing of high-grade metamorphism in central Turkey and the assembly of Anatolia. Journal of the Geological Society, London, 161: 823-828.

Whitney D. L. and Davis P. B., 2006. Why is lawsonite eclogite so rare? Metamorphism and preservation of lawsonite eclogite, Sivrihisar, Turkey. Geology, 34(6): 473-476.

Whitney D. L., Teyssier C., Kruckenberg S. C., Morgan V. L. and Iredale L. J., 2008a. High-pressure-low-temperature metamorphism of metasedimentary rocks, southern Menderes Massif, westem Turkey. Lithos, 101(3-4): 218-232.

Whitney D. L., Umhoefer P. J., Teyssier C. and Fayon A. K., 2008b. Yo-yo tectonics of the Nigde Massif during wrenching in Central Anatolia. Turkish Journal of Earth Sciences, 17(2): 209-217.

Wiederkehr M., Bousquet R., Schmid S. M. and Berger A., 2008. From subduction to collision: Thermal overprint of HP/LT meta-sediments in the north-eastern Lepontine Dome (Swiss

Alps) and consequences regarding the tectono-metamorphic evolution of the Alpine orogenic wedge. Swiss Journal of Geosciences, 101: 127-155.

Wiederkehr M., Sudo M., Bousquet R., Berger A. and Schmid S. M., 2009. Alpine orogenic evolution from subduction to collisional thermal overprint: The (40)Ar/(39)Ar age constraints from the Valaisan Ocean, central Alps. Tectonics, 28(TC6009).

Wijbrans J. R. and McDougall I., 1986. $^{40}Ar/^{39}Ar$ Dating of White Micas from an Alpine High-Pressure Metamorphic Belt on Naxos (Greece) - the Resetting of the Argon Isotopic System. Contributions to Mineralogy and Petrology, 93(2): 187-194.

Wijbrans J. R., Schliestedt M. and York D., 1990. Single Grain Argon-Laser Probe Dating of Phengites from the Blueschist to Greenschist Transition on Sifnos (Cyclades, Greece). Contributions to Mineralogy and Petrology, 104(5): 582-593.

Winkler H. G. F., 1974. Petrogenesis of metamorphic rocks. Springer, Berlin.

Yalınız M. K., Floyd P. A. and Göncüoğlu M. C., 1996. Supra-subduction zone ophiolites of Central Anatolia: Geochemical evidence from the Sarikaraman Ophiolite, Aksaray, Turkey. Mineralogical Magazine, 60(402): 697-710.

Yalınız M. K. and Göncüoğlu M. C., 1998. General geological characteristics and distribution of the Central Anatolian Ophiolites. Yerbilimleri, 20: 19-30.

Yalınız M. K., Floyd P. A. and Göncüoğlu M. C., 2000a. Geochemistry of volcanic rocks from the Cicekdag Ophiolite, Central Anatolia, Turkey, and their inferred tectonic setting within the northern branch of the Neotethyan Ocean. Tectonics and Magmatism in Turkey and the Surrounding Area(173): 203-218.

Yalınız M. K., Göncüoğlu M. C. and Ozkan-Altıner S., 2000b. Formation and emplacement ages of the SSZ-type Neotethyan ophiolites in Central Anatolia, Turkey: palaeotectonic implications. Geological Journal, 35(2): 53-68.

Yamato P., Agard P., Goffe B., De Andrade V., Vidal O. and Jolivet L., 2007. New, high-precision P-T estimates for Oman blueschists: implications for obduction, nappe stacking and exhumation processes. Journal of Metamorphic Geology, 25(6): 657-682.

Yetiş C., 1984. New observations on the age of the Ecemiş Fault. In: Tekeli O. and Göncüoğlu M. C. (Editors), Proceedings of the International Symposium on the Geology of the Taurus Belt. Mineral Research and Exploration Intitute of Turkey (MTA), Ankara, Turkey, pp. 159-164.

Yılmaz Y., Genç S. C., Yiğitbaş E., Bozcu M. and Yılmaz K., 1995. Geological Evolution of the Late Mesozoic Continental-Margin of Northwestern Anatolia. Tectonophysics, 243(1-2): 155-171.

Yılmaz Y., Genç S. C., Gürer F., Bozcu M., Yılmaz K., Karacık K., Altunkaynak S. and Elmas A., 2000. When did the western Anatolian grabens begin to develop? In: Bozkurt E., Winchester J. A. and Piper J. D. A. (Editors), Tectonics and Magmatism in Turkey and the Surrounding Area. Geological Society, London, Special Publication, 173, pp. 353-384.

Appendix 1

Beyond Mg-Fe^{2+} zoning

Variations of major elements contents of carpholite and chloritoid

As presented in Chapter 3, carpholite and chloritoid in the Afyon Zone commonly display a consistent increase of their Mg-content with time, related to the continuous reaction: Fe-rich carpholite = Fe-Mg-carpholite + ferro-chloritoid. Compositional changes were only discussed in terms of Fe-Mg distribution within and partitioning between carpholite and chloritoid. However, electron microprobe analyses reveal variations of the contents in other elements.

This appendix shows the complete set of element maps of chloritoid that were performed, and present a short discussion on the amount Fe^{3+} in chloritoid, as well as carpholite.

A.1.1. Elements maps of chloritoid

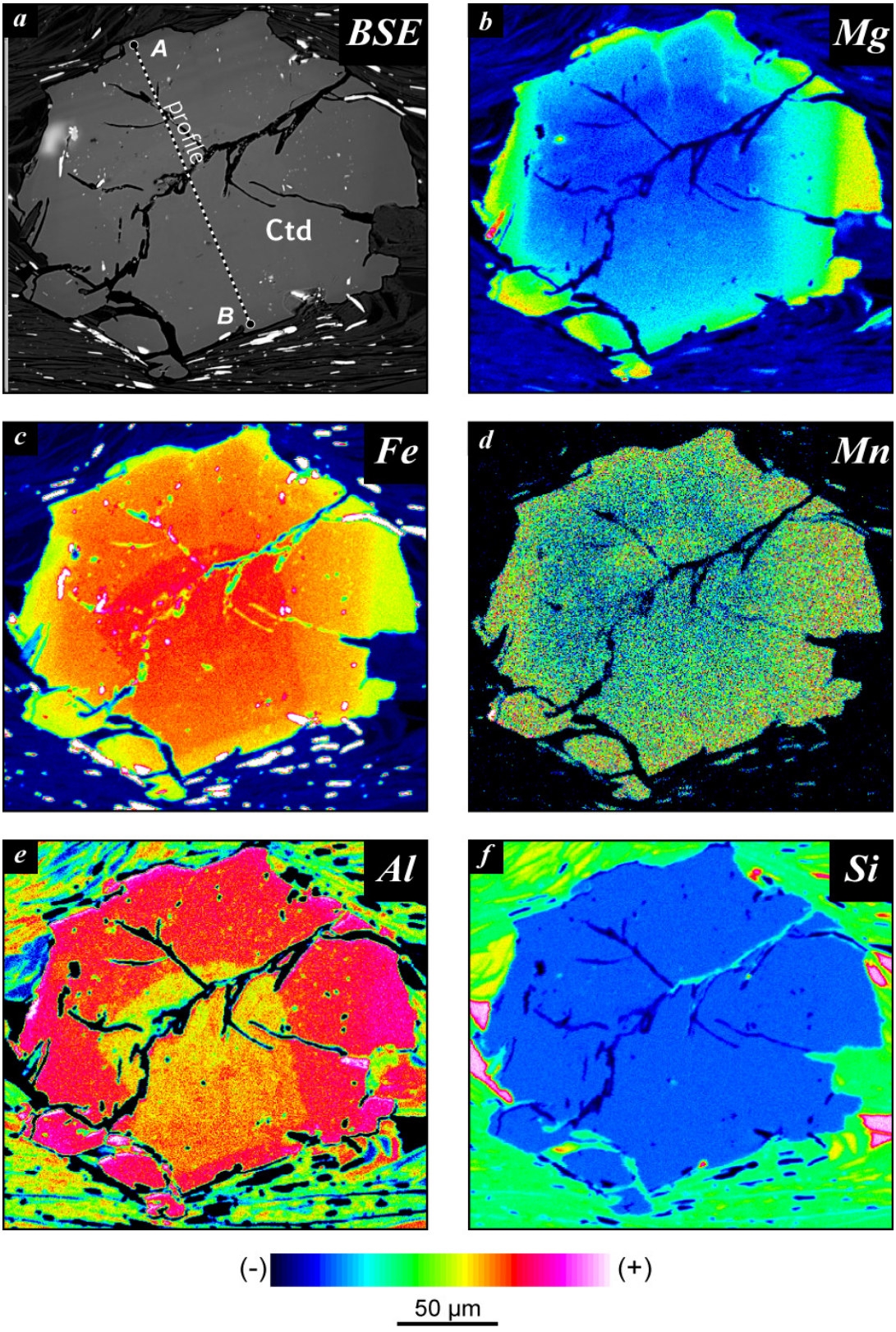

Figure A1.1: Element maps of a chloritoid crystal in beige phyllite (Bay0851).

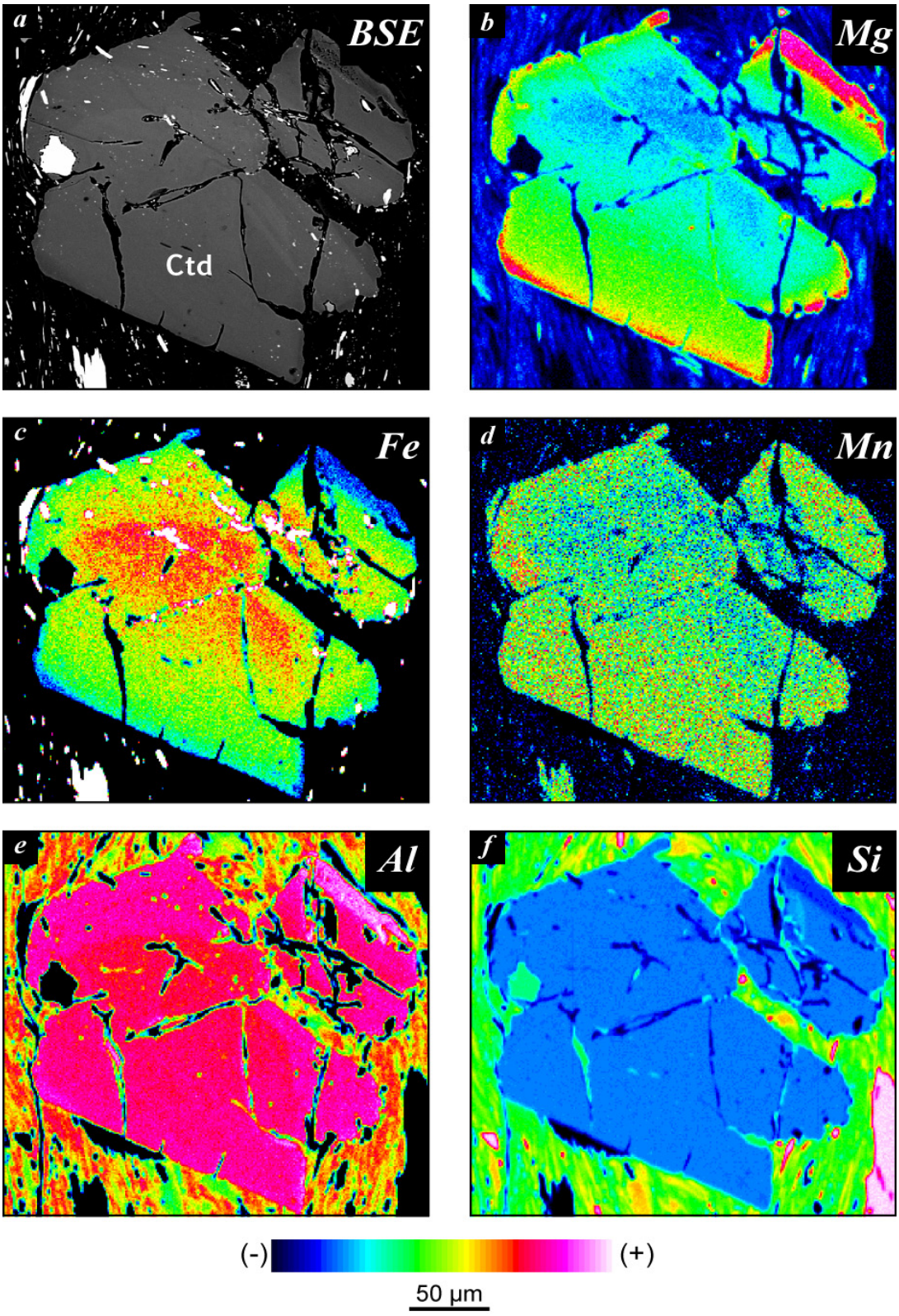

Figure A1.2: Element maps of a chloritoid crystal in beige phyllite (Bay0851).

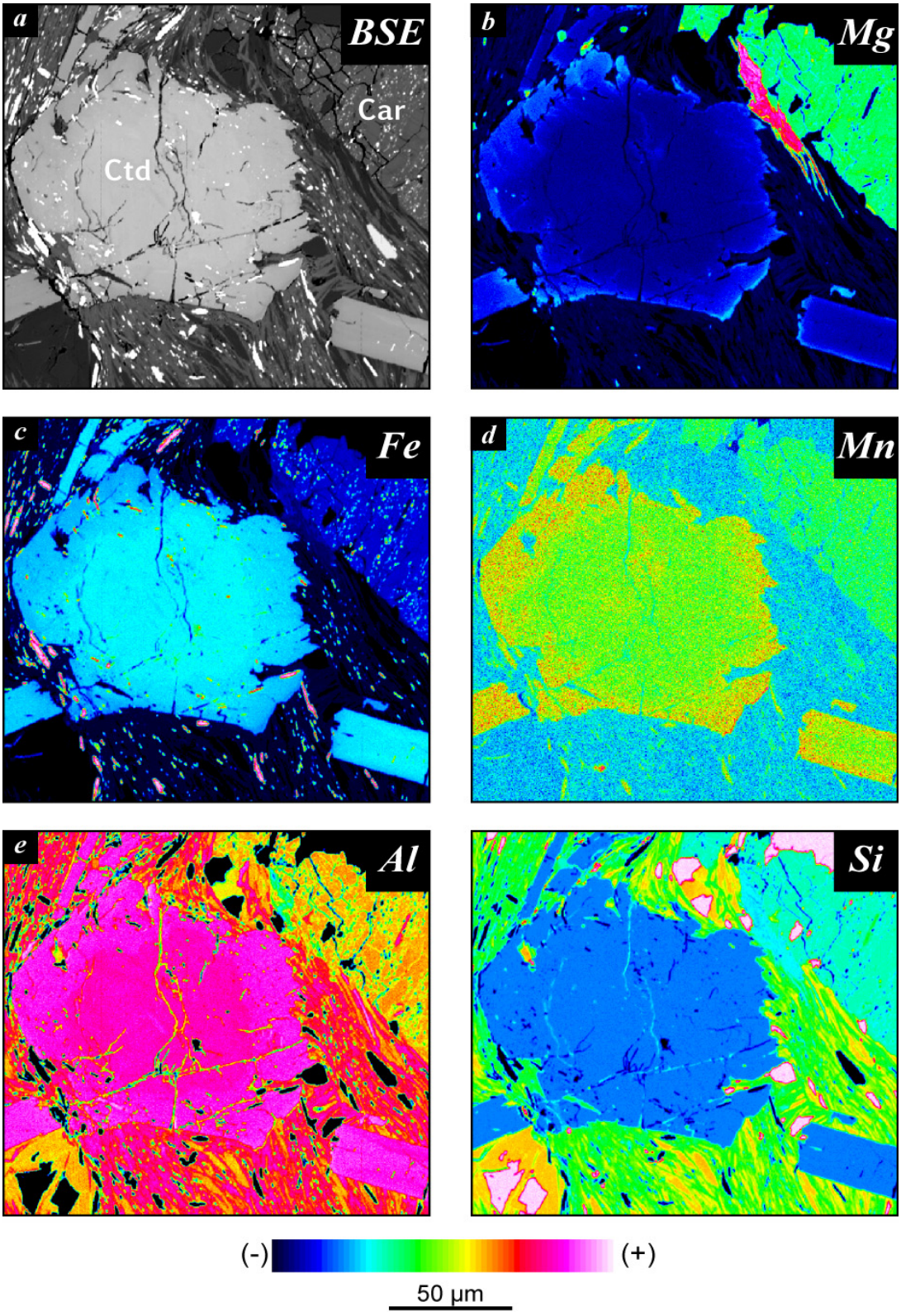

Figure A1.2: Element maps of a chloritoid crystal in beige phyllite (Bay0851).

A.1.2. Ferric iron

Fe^{3+}-content of chloritoid

Element maps of chloritoid from the silvery phyllite sample Bay0851 reveal that Mg and Fe zoning may not strictly overlap (Figures A1.1, A1.2). In Figure A1.1, Fe is more concentrated in a toast-shaped area that does not appear on Mg map. This suggests that Fe zoning does not only depends on the (Mg,Fe) substitution, but also to variations in Fe^{3+}-content.

Plotting the amount of Fe *vs.* Mg in chloritoid from the samples investigated in Chapter 3 (Figure A1.4) shows shift from the ideal chloritoid composition (Fe^{3+}-free). This shift indicates a minimal content in Fe^{3+}, which might be slightly attenuated by the presence of vacancies on the (Fe,Mg) site.

Beside Mg and Fe, Mn and Al also are zoned, while Si is clearly homogeneously distributed (Figures A1.1, A1.2, A1.3). Mn-content, albeit in consistently very low, consistently increases from core to rim following a gradient apparently overlapping Mg zoning. According to profile analyses, this increase of Mg . Al maps show increasing contents from core to rim. Al zoning obviously overlap Fe zoning (Figures A1.1, A1.2), which confirms the existence of the (Al, Fe^{3+}) substitution. Increase of Al-content can be interpreted as a decrease of the substitution of Fe^{3+} for Al. The decrease of Fe-content in chloritoid therefore appears to affect both ferrous and ferric iron.

In all, chloritoid zoning seems to be controlled by the progressive depletion in Fe that controls the increases of the Mg-, Mn- and Al-contents.

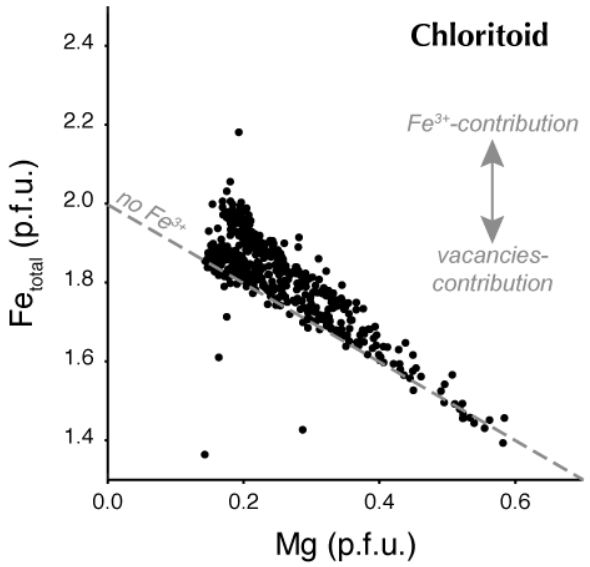

Figure A1.4: Relation between Fe- and Mg-contents in chloritoids from the Afyon Zone.

Fe^{3+}-content of carpholite

In structural formula of carpholite, $(Fe,Mg)Al_2Si_2O_6(OH)_4$, the contents in ferric iron (Fe^{3+}) and site vacancies ($v = 1 - (Fe^{2+} + Mn + Mg)$) cannot be measured by electron microprobe and therefore must be estimated from site occupancy. On Figure A1.5, I plotted the amount of Fe_{total} *vs.* Mg and Si *vs.* Al measured in carpholite of the samples investigated in Chapter 3. The Fe_{total} *vs.* Mg plot indicates that Fe_{total}+Mg is generally close to one. Like in chloritoid (see section A1.2), the presence of Fe^{3+} contributes to increase the sum Fe^{3+}+Mg, while Mn and vacancies on the M2 site (host of Fe^{2+}, Mn and Mg) balance the sum to lower values.

Following Goffé and Oberhänsli (1992), Fe^{3+}-content is calculated so to respect to the total occupancy of the Al octahedral site with the equation $Fe^{3+} = 2 - Al$ and Fe^{2+}-content follows as $Fe^{2+} = Fe_{total} - Fe^{3+}$. In my samples, this method of calculation results in M2 site occupancy of 91-99%. For comparison, the calculated cation sum (= 5 in theory) provides the amount of vacancies that can be expected throughout the various sites. Overall, the cation sum in carpholite ranges between 4.97 and 5.00, indicating that the amount of vacancies on the M2 site that attained up to 9% is overestimated.

Measured Al-content in carpholite (= 2 p.f.u. in theory) ranges between 1.93 and 1.99 pf.u.. while Si-content (= 2 p.f.u. in theory) ranges between 2.00 and 2.04 p.f.u.. Given the large grain size of analysed carpholite and the fact that identical values are obtained from quartz-free samples, any quartz contamination is precluded. Plotting Si *vs.* Al (Figure A1.5) shows that Si-content trends to decrease with increasing Al-content, suggesting substitution of Si for Al on the M1 octahedral site.

In consequence, I propose an alternative method to estimate the abundance of ferric iron that takes into account this substitution. Fe^{3+}-content is now calculated using as $Fe^{3+} = 4 - (Si + Al)$. This method leads to vacancy-contents on the M2 site comparable with the deficiency on the total cation sum (0-4 %).

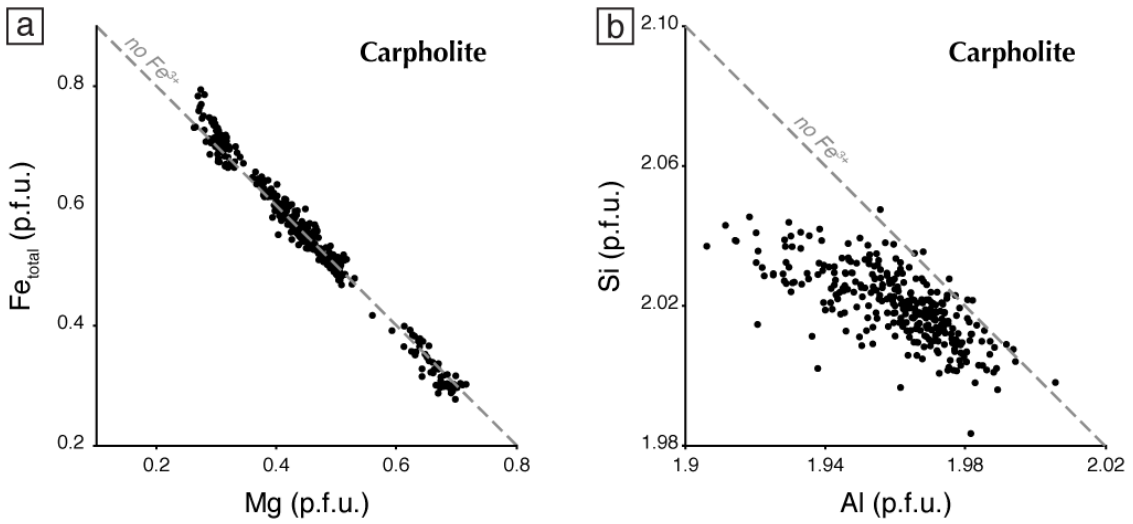

Figure A1.5: Relation between amount of Fe_{total} and Mg (a), and Si and Al (b) in carpholites from the Afyon Zone.

Appendix 2

^{40}Ar-^{39}Ar geochronology data

Table A2.1: CO_2 laser stepwise heating on grain samples

Küt0815 (C10002)

#	Laser output (%)	$^{40}Ar/^{39}Ar$			$^{37}Ar/^{39}Ar$			$^{36}Ar/^{39}Ar$ ($x10^{-3}$)			K/Ca	$^{40}Ar^*$ (%)	^{39}ArK (%)	$^{40}Ar^*/^{39}ArK$			Age (±1s) (Ma)		
		J= 0.00210																	
1	1.4	211.09	±	4.61	33.574	±	15.689	694.85	±	55.55	1.70	4.70	3.33	10.23	±	16.46	38.3	±	61.0
2	1.6	70.49	±	0.96	13.981	±	3.850	185.93	±	14.85	0.04	24.52	12.67	17.50	±	4.45	65.1	±	16.2
3	1.8	25.81	±	0.26	0.258	±	1.576	24.25	±	3.90	2.28	72.35	21.89	18.68	±	1.19	69.3	±	4.3
4	2.0	19.70	±	0.26	3.458	±	2.434	8.33	±	3.73	0.17	89.69	19.65	17.72	±	1.17	65.9	±	4.3
5	2.2	24.86	±	0.88	17.742	±	3.192	33.74	±	8.92	0.03	68.75	9.53	17.37	±	2.77	64.6	±	10.1
6	2.4	21.62	±	0.32	15.467	±	5.151	23.73	±	15.13	0.04	76.44	7.54	16.76	±	4.59	62.4	±	16.8
7	2.6	16.48	±	0.39	4.677	±	4.715	8.14	±	14.91	0.13	88.93	11.34	14.72	±	4.48	54.9	±	16.4
8	2.8	18.55	±	0.32	18.144	±	4.610	41.29	±	15.80	0.03	46.38	9.75	8.75	±	4.78	32.8	±	17.8
9	3.0	26.66	±	0.56	19.205	±	9.647	31.81	±	31.39	0.03	73.68	4.30	19.99	±	9.53	74.1	±	34.6
													Plateau age				**65.9**	±	**2.8**
													Total gas age				61.1	±	4.7

Afy0212 (C08018)

#	Laser output (%)	$^{40}Ar/^{39}Ar$			$^{37}Ar/^{39}Ar$			$^{36}Ar/^{39}Ar$ ($x10^{-3}$)			K/Ca	$^{40}Ar^*$ (%)	^{39}ArK (%)	$^{40}Ar^*/^{39}ArK$			Age (±1s) (Ma)		
		J= 0.00177																	
1	1.4	0.01	±	68.94	41.923	±	41922	79.38	±	239.42	0.01	<0	0.02	<0	±	<0	-60.7	±	-18758
2	1.6	46.39	±	1.49	0.088	±	88.289	87.73	±	2.59	6.66	44.14	10.65	20.48	±	11.62	64.1	±	35.7
3	1.8	26.38	±	0.54	0.044	±	43.593	26.43	±	0.63	13.49	70.41	21.58	18.57	±	5.71	58.2	±	17.6
4	2.0	22.33	±	0.52	0.027	±	27.094	11.33	±	0.28	21.71	85.03	34.06	18.99	±	3.57	59.5	±	11.0
5	2.2	24.35	±	0.97	0.127	±	126.607	14.38	±	1.06	4.65	82.61	7.29	20.12	±	16.59	63.0	±	51.0
6	2.4	26.56	±	0.61	0.041	±	40.741	15.24	±	0.54	14.44	83.06	22.67	22.06	±	5.37	68.9	±	16.5
7	2.8	40.76	±	1.40	0.247	±	246.972	51.49	±	3.18	2.38	62.75	3.74	25.58	±	32.54	79.7	±	99.1
													Plateau age				**61.5**	±	**8.0**
													Total gas age				62.8	±	10.1

Yah04 (C10003)

#	Laser output (%)	$^{40}Ar/^{39}Ar$			$^{37}Ar/^{39}Ar$			$^{36}Ar/^{39}Ar$ ($x10^{-3}$)			K/Ca	$^{40}Ar^*$ (%)	^{39}ArK (%)	$^{40}Ar^*/^{39}ArK$			Age (±1s) (Ma)		
		J= 0.00210																	
1	1.4	152.06	±	2.22	1.722	±	0.867	508.55	±	11.19	0.34	1.31	2.75	2.00	±	2.51	7.5	±	9.4
2	1.6	36.57	±	0.32	0.586	±	0.717	61.43	±	2.07	1.00	50.57	6.77	18.50	±	0.64	68.6	±	2.3
3	1.8	24.65	±	0.20	0.306	±	0.487	23.16	±	0.69	1.92	72.39	14.68	17.85	±	0.27	66.2	±	1.0
4	2.0	20.22	±	0.11	0.138	±	0.338	8.66	±	0.66	4.27	87.43	18.25	17.68	±	0.22	65.6	±	0.8
5	2.2	19.56	±	0.07	0.448	±	0.260	7.45	±	0.65	1.31	89.03	16.29	17.42	±	0.20	64.7	±	0.8
6	2.4	19.54	±	0.27	0.293	±	2.696	10.80	±	4.84	2.00	83.85	1.56	16.39	±	1.49	60.9	±	5.4
7	2.6	19.20	±	0.08	1.676	±	0.722	2.42	±	1.34	0.35	97.36	7.73	18.72	±	0.41	69.4	±	1.5
8	2.8	18.76	±	0.13	0.817	±	0.581	3.71	±	1.00	0.72	94.69	10.45	17.78	±	0.33	66.0	±	1.2
9	3.0	18.84	±	0.09	0.037	±	0.578	0.07	±	0.62	16.09	99.91	12.58	18.82	±	0.21	69.8	±	0.8
10	3.2	18.57	±	0.18	0.114	±	1.751	0.22	±	2.08	5.15	99.73	4.03	18.52	±	0.68	68.7	±	2.5
11	3.4	18.82	±	0.25	0.094	±	1.423	0.18	±	1.64	6.27	99.78	4.91	18.78	±	0.57	69.6	±	2.1
													Plateau age				**66.7**	±	**0.4**
													Total gas age				65.3	±	0.5

Yah04 (C10006)

#	Laser output (%)	$^{40}Ar/^{39}Ar$			$^{37}Ar/^{39}Ar$			$^{36}Ar/^{39}Ar$ ($x10^{-3}$)			K/Ca	$^{40}Ar^*$ (%)	^{39}ArK (%)	$^{40}Ar^*/^{39}ArK$			Age (±1s) (Ma)		
		J= 0.00208																	
1	1.4	59.76	±	0.42	0.215	±	1.800	166.00	±	2.83	2.73	17.97	2.24	10.74	±	0.81	39.9	±	3.0
2	1.6	23.22	±	0.53	0.420	±	2.122	17.95	±	1.44	1.40	77.37	2.74	17.97	±	0.68	66.3	±	2.5
3	1.8	22.16	±	0.18	0.151	±	0.528	13.69	±	0.51	3.88	81.83	7.61	18.14	±	0.22	66.9	±	0.9
4	2.0	22.44	±	0.09	0.091	±	0.450	14.86	±	0.24	6.45	80.48	12.63	18.06	±	0.12	66.6	±	0.5
5	2.2	22.17	±	0.04	0.105	±	0.661	16.16	±	0.37	5.59	78.52	10.95	17.41	±	0.14	64.3	±	0.6
6	2.4	19.50	±	0.06	0.081	±	0.406	6.06	±	0.24	7.30	90.87	14.33	17.72	±	0.10	65.4	±	0.4
7	2.6	19.32	±	0.03	0.132	±	0.957	5.91	±	0.21	4.45	91.04	8.73	17.59	±	0.14	65.0	±	0.6
8	2.8	19.72	±	0.02	0.068	±	0.485	5.94	±	0.21	8.67	91.14	17.02	17.98	±	0.09	66.3	±	0.4
9	3.0	18.08	±	0.13	0.196	±	1.473	3.62	±	0.30	3.00	94.23	5.88	17.04	±	0.24	63.0	±	0.9
10	3.2	19.94	±	0.04	0.771	±	0.540	5.61	±	0.26	0.76	92.17	10.59	18.39	±	0.11	67.8	±	0.5
11	3.4	18.98	±	0.15	1.362	±	0.883	5.23	±	0.41	0.43	92.74	7.05	17.63	±	0.22	65.1	±	0.8
12	3.6	19.80	±	0.57	47.086	±	30.035	5.01	±	9.83	0.01	95.48	0.22	19.75	±	5.00	72.8	±	18.1
													Plateau age				**65.7**	±	**0.2**
													Total gas age				65.2	±	0.2

Yah04 (C10048)

#	Laser output (%)	$^{40}Ar/^{39}Ar$			$^{37}Ar/^{39}Ar$			$^{36}Ar/^{39}Ar$ ($x10^{-3}$)			K/Ca	$^{40}Ar^*$ (%)	^{39}ArK (%)	$^{40}Ar^*/^{39}ArK$			Age (±1s) (Ma)		
	J= 0.00208																		
1	1.2	1803.8	±	421.62	249.42	±	995.75	5720.1	±	1400.5	0.00	8.01	0.01	186.4	±	317	592	±	860.2
2	1.4	98.02	±	1.19	39.481	±	13.141	294.12	±	6.42	1.44	16.33	1.03	16.60	±	2.39	61.3	±	8.7
3	1.6	26.92	±	0.33	0.967	±	4.281	39.63	±	2.59	0.61	56.95	4.07	15.35	±	0.95	56.8	±	3.5
4	1.8	23.42	±	0.19	0.616	±	2.678	19.88	±	0.82	0.95	75.24	6.40	17.63	±	0.44	65.1	±	1.6
5	2.0	22.94	±	0.29	0.957	±	2.295	19.96	±	0.57	0.61	74.80	10.85	17.18	±	0.42	63.4	±	1.5
6	2.2	20.33	±	0.28	1.688	±	1.393	9.26	±	0.22	0.35	87.57	16.87	17.83	±	0.32	65.8	±	1.2
7	2.4	18.92	±	0.21	1.943	±	1.682	5.30	±	0.43	0.30	93.00	12.94	17.63	±	0.32	65.1	±	1.2
8	2.6	18.45	±	0.27	0.801	±	5.854	6.33	±	0.42	0.73	90.40	4.93	16.69	±	0.78	61.7	±	2.9
9	2.8	19.54	±	0.23	0.679	±	3.877	6.95	±	0.68	0.87	89.92	5.82	17.58	±	0.57	64.9	±	2.1
10	3.0	19.37	±	0.07	0.141	±	0.840	6.45	±	0.22	4.17	90.25	28.01	17.49	±	0.14	64.6	±	0.6
11	3.2	20.63	±	0.09	0.679	±	4.746	7.72	±	0.70	0.87	89.35	5.82	18.44	±	0.64	68.0	±	2.3
12	3.4	19.92	±	0.38	1.218	±	7.723	9.56	±	1.32	0.48	86.58	3.25	17.27	±	1.10	63.8	±	4.0
													Plateau age				**64.8**	±	**0.4**
													Total gas age				64.5	±	0.5

Ören001 (C10001)

#	Laser output (%)	$^{40}Ar/^{39}Ar$			$^{37}Ar/^{39}Ar$			$^{36}Ar/^{39}Ar$ ($x10^{-3}$)			K/Ca	$^{40}Ar^*$ (%)	^{39}ArK (%)	$^{40}Ar^*/^{39}ArK$			Age (±1s) (Ma)		
	J= 0.00208																		
1	1.4	130.57	±	0.88	4.158	±	1.857	383.40	±	6.40	0.14	13.63	1.39	17.86	±	1.77	65.8	±	6.4
2	1.6	20.33	±	0.23	1.633	±	0.488	15.09	±	2.09	0.36	79.06	4.09	16.09	±	0.65	59.4	±	2.4
3	1.8	20.92	±	0.37	2.357	±	0.511	17.52	±	1.37	0.25	76.65	5.07	16.07	±	0.52	59.3	±	1.9
4	2.0	18.78	±	0.11	0.813	±	0.268	5.88	±	0.55	0.72	91.29	11.77	17.15	±	0.19	63.2	±	0.7
5	2.2	16.70	±	0.10	0.522	±	0.157	1.04	±	0.46	1.13	98.55	18.14	16.47	±	0.17	60.8	±	0.7
6	2.4	16.57	±	0.07	0.266	±	0.271	2.00	±	0.58	2.21	96.64	16.12	16.02	±	0.19	59.1	±	0.7
7	2.6	16.60	±	0.07	0.598	±	0.464	3.76	±	0.95	0.98	93.75	9.70	15.57	±	0.29	57.5	±	1.1
8	2.8	17.12	±	0.12	1.907	±	0.468	3.49	±	1.75	0.31	95.36	6.81	16.36	±	0.54	60.4	±	2.0
9	3.0	17.11	±	0.11	1.370	±	0.366	6.02	±	1.33	0.43	90.60	9.08	15.52	±	0.41	57.3	±	1.5
10	3.2	17.20	±	0.13	0.031	±	0.689	3.15	±	1.40	18.98	94.61	10.37	16.28	±	0.44	60.1	±	1.6
11	3.4	16.25	±	0.11	0.043	±	0.953	0.09	±	1.93	13.64	99.88	7.46	16.23	±	0.59	59.9	±	2.2
													Plateau age				**60.3**	±	**0.3**
													Total gas age				59.9	±	0.4

Ören001 (C10005)

#	Laser output (%)	$^{40}Ar/^{39}Ar$			$^{37}Ar/^{39}Ar$			$^{36}Ar/^{39}Ar$ ($x10^{-3}$)			K/Ca	$^{40}Ar^*$ (%)	^{39}ArK (%)	$^{40}Ar^*/^{39}ArK$			Age (±1s) (Ma)		
		J= 0.00207																	
1	1.6	23.97	±	0.26	0.635	±	0.411	23.55	±	1.30	0.93	71.29	9.01	17.09	±	0.43	62.6	±	1.6
2	1.8	18.18	±	0.15	0.298	±	0.254	3.35	±	0.56	1.97	94.76	10.19	17.23	±	0.22	63.1	±	0.8
3	2.0	18.31	±	0.14	0.766	±	0.302	3.23	±	0.50	0.77	95.31	12.26	17.46	±	0.21	63.9	±	0.8
4	2.2	17.14	±	0.14	0.185	±	0.201	1.18	±	0.37	3.18	98.09	15.19	16.82	±	0.17	61.6	±	0.7
5	2.4	16.71	±	0.06	0.036	±	0.512	0.07	±	1.17	16.49	99.91	15.12	16.70	±	0.36	61.2	±	1.3
6	2.6	16.86	±	0.12	0.511	±	0.941	0.12	±	2.04	1.15	99.79	8.45	16.83	±	0.63	61.6	±	2.3
7	2.8	17.47	±	0.17	0.280	±	0.741	0.10	±	1.75	2.10	99.83	10.25	17.44	±	0.55	63.8	±	2.0
8	3.0	17.20	±	0.12	1.018	±	0.766	0.10	±	1.71	0.58	99.83	10.45	17.19	±	0.53	62.9	±	1.9
9	3.2	16.76	±	0.28	0.059	±	0.823	0.11	±	1.91	9.90	99.85	9.09	16.73	±	0.64	61.3	±	2.3
													Plateau age				**62.6**	±	**0.4**
													Total gas age				62.4	±	0.5

Ören001 (C10049)

#	Laser output (%)	$^{40}Ar/^{39}Ar$			$^{37}Ar/^{39}Ar$			$^{36}Ar/^{39}Ar$ ($x10^{-3}$)			K/Ca	$^{40}Ar^*$ (%)	^{39}ArK (%)	$^{40}Ar^*/^{39}ArK$			Age (±1s) (Ma)		
		J= 0.00207																	
1	1.4	30.07	±	0.89	24.718	±	29.725	54.67	±	6.55	0.02	56.47	1.89	17.37	±	4.30	63.6	±	15.5
2	1.6	19.79	±	0.34	10.232	±	8.243	14.25	±	1.81	0.06	85.14	8.24	17.01	±	1.21	62.3	±	4.4
3	1.8	17.90	±	0.61	1.171	±	5.154	7.59	±	1.62	0.50	88.28	10.57	15.82	±	0.99	58.0	±	3.6
4	2.0	16.72	±	0.23	0.556	±	0.799	2.52	±	0.49	1.06	95.95	17.84	16.05	±	0.29	58.8	±	1.1
5	2.2	16.76	±	0.19	3.216	±	4.023	2.81	±	0.49	0.18	97.43	12.99	16.38	±	0.56	60.0	±	2.0
6	2.4	17.61	±	0.22	1.143	±	2.154	5.59	±	1.03	0.51	91.43	8.67	16.11	±	0.46	59.1	±	1.7
7	2.6	18.74	±	0.15	1.946	±	3.212	7.82	±	1.16	0.30	88.96	17.14	16.70	±	0.55	61.2	±	2.0
8	2.8	16.64	±	0.13	5.029	±	8.414	3.05	±	0.78	0.12	98.34	7.34	16.44	±	1.09	60.2	±	3.9
9	3.0	16.07	±	0.17	2.239	±	12.708	1.25	±	2.19	0.26	99.44	4.43	16.01	±	1.73	58.7	±	6.2
10	3.2	16.70	±	0.33	5.587	±	4.056	3.37	±	0.73	0.10	98.19	10.90	16.48	±	0.64	60.4	±	2.3
													Plateau age				**59.4**	±	**0.7**
													Total gas age				60.0	±	0.9

Table A2.2: In-situ UV laser ablation on rock samples

Afy0206 (U10002)

#	Laser output (%)	$^{40}Ar/^{39}Ar$			$^{37}Ar/^{39}Ar$			$^{36}Ar/^{39}Ar$ ($x10^{-3}$)			K/Ca	$^{40}Ar^*$ (%)	^{39}ArK (%)	$^{40}Ar^*/^{39}ArK$			Age (±1s) (Ma)		
		J= 0.00195																	
1	80	27.34	±	0.25	0.329	±	2.564	30.62	±	2.03	1.79	67.06	18.45	18.34	±	0.70	63.4	±	2.4
2	80	23.34	±	1.27	6.745	±	38.139	2.99	±	12.27	0.09	99.80	0.89	23.44	±	6.19	80.6	±	20.8
3	80	34.01	±	0.51	0.610	±	4.083	60.76	±	2.72	0.96	47.43	9.96	16.14	±	0.96	55.9	±	3.3
4	80	25.47	±	0.49	3.272	±	3.716	25.73	±	3.87	0.18	71.74	7.75	18.33	±	1.29	63.3	±	4.4
5	80	26.84	±	0.25	1.155	±	2.506	32.51	±	2.61	0.51	64.74	10.06	17.40	±	0.85	60.2	±	2.9
6	80	35.27	±	0.30	0.641	±	3.357	56.59	±	4.13	0.92	52.82	9.49	18.64	±	1.30	64.4	±	4.4
7	80	74.22	±	0.81	0.970	±	5.443	186.50	±	5.93	0.61	25.91	6.35	19.24	±	1.81	66.4	±	6.1
8	80	51.90	±	0.43	0.402	±	2.121	126.74	±	2.04	1.46	27.93	15.32	14.50	±	0.61	50.3	±	2.1
9	80	41.44	±	0.37	0.457	±	2.186	87.43	±	1.29	1.29	37.80	13.49	15.67	±	0.46	54.3	±	1.6
10	80	56.59	±	1.17	0.748	±	3.202	145.95	±	4.14	0.79	23.95	8.25	13.56	±	1.11	47.1	±	3.8
													Deduced age				**62.8**	±	**1.5**

Kuru0110 (U10004)

#	Laser output (%)	$^{40}Ar/^{39}Ar$			$^{37}Ar/^{39}Ar$			$^{36}Ar/^{39}Ar$ ($x10^{-3}$)			K/Ca	$^{40}Ar^*$ (%)	^{39}ArK (%)	$^{40}Ar^*/^{39}ArK$			Age (±1s) (Ma)		
		J= 0.00193																	
1	80	21.21	±	0.23	0.995	±	4.248	23.70	±	2.71	0.59	67.56	16.09	14.34	±	0.97	49.2	±	3.3
2	80	23.64	±	0.30	1.200	±	7.434	37.04	±	4.90	0.49	54.32	13.35	12.85	±	1.72	44.2	±	5.9
3	80	4075	±	894.1	73.93	±	349.90	13441	±	2964.7	0.01	2.78	0.20	121.3	±	122	379	±	346.1
4	80	23.35	±	0.24	1.019	±	7.429	40.09	±	3.44	0.58	49.81	15.75	11.64	±	1.38	40.1	±	4.7
5	80	15.22	±	0.13	2.519	±	4.035	18.27	±	1.81	0.23	66.58	25.22	10.15	±	0.74	35.0	±	2.5
6	80	26.18	±	0.24	0.284	±	5.870	43.43	±	2.22	2.07	51.12	20.86	13.39	±	0.99	46.0	±	3.4
7	80	71.99	±	3.70	3.215	±	14.947	200.09	±	16.38	0.18	18.43	5.08	13.31	±	4.37	45.7	±	14.8
8	80	315.8	±	4.62	9.232	±	39.071	1005	±	38.46	0.06	6.37	1.76	20.28	±	11.92	69.2	±	39.9
9	80	422.9	±	11.34	9.644	±	58.571	1348	±	53.35	0.06	6.11	1.69	26.06	±	14.22	88.5	±	47.1
													Deduced age				**26.4**	±	**0.8**

Nebil0101 (U10005)

#	Laser output (%)	$^{40}Ar/^{39}Ar$			$^{37}Ar/^{39}Ar$			$^{36}Ar/^{39}Ar$ ($x10^{-3}$)			K/Ca	$^{40}Ar^*$ (%)	^{39}ArK (%)	$^{40}Ar^*/^{39}ArK$			Age (±1s) (Ma)		
	J= 0.00194																		
1	80	8.75	±	0.19	7.749	±	11.84	4.65	±	4.21	0.08	95.30	5.30	8.40	±	1.95	29.1	±	6.7
2	80	11.00	±	0.14	0.470	±	2.556	13.84	±	1.32	1.25	63.36	16.26	6.97	±	0.51	24.2	±	1.8
3	80	11.41	±	0.10	0.668	±	3.646	11.90	±	1.84	0.88	69.91	11.44	7.98	±	0.71	27.7	±	2.5
4	80	10.67	±	0.06	0.277	±	1.460	12.44	±	0.64	2.12	65.87	27.60	7.03	±	0.27	24.4	±	0.9
5	80	12.22	±	0.15	0.667	±	2.682	15.09	±	1.11	0.88	64.20	16.61	7.85	±	0.47	27.3	±	1.6
6	80	11.97	±	0.29	0.796	±	3.265	11.39	±	1.90	0.74	72.72	9.72	8.71	±	0.72	30.2	±	2.5
7	80	11.08	±	0.10	0.593	±	2.978	9.99	±	1.88	0.99	74.01	13.06	8.21	±	0.67	28.5	±	2.3
														Deduced age			**62.8**	±	**1.5**

Bay0851 (U10007)

#	Laser output (%)	$^{40}Ar/^{39}Ar$			$^{37}Ar/^{39}Ar$			$^{36}Ar/^{39}Ar$ ($x10^{-3}$)			K/Ca	$^{40}Ar^*$ (%)	^{39}ArK (%)	$^{40}Ar^*/^{39}ArK$			Age (±1s) (Ma)		
	J= 0.00193																		
1	80	22.06	±	0.24	0.666	±	2.669	2.66	±	1.23	0.88	96.81	9.09	21.37	±	0.55	73.1	±	1.9
2	80	25.98	±	0.23	0.278	±	1.286	6.44	±	0.27	2.11	92.80	23.69	24.11	±	0.28	82.2	±	1.0
3	80	26.78	±	0.26	1.393	±	2.375	7.18	±	1.02	0.42	92.72	11.69	24.86	±	0.49	84.7	±	1.7
4	80	23.33	±	0.26	1.237	±	4.386	21.23	±	2.22	0.48	73.77	5.33	17.23	±	0.88	59.1	±	3.0
5	80	25.04	±	0.26	0.552	±	2.364	9.89	±	1.24	1.06	88.60	11.96	22.19	±	0.52	75.8	±	1.8
6	80	27.67	±	0.19	0.476	±	1.602	10.60	±	1.03	1.24	88.89	14.02	24.61	±	0.40	83.9	±	1.4
7	80	24.14	±	0.39	0.515	±	2.274	7.66	±	1.35	1.14	90.88	12.97	21.95	±	0.61	75.0	±	2.1
8	80	27.88	±	0.26	0.594	±	1.622	9.75	±	1.64	0.99	89.93	11.25	25.08	±	0.58	85.5	±	1.9
														Deduced ages			**74.6**	±	**1.1**
																	83.4	±	**0.7**